# A Morphological and Morphometric Investigation into the Morphogenesis of the Crocodilian Lung

by

Deran Reddy

A thesis submitted in fulfilment of the requirements for the degree of Doctor of Philosophy


School of Anatomical Sciences

University of the Witwatersrand

Johannesburg, South Africa

October, 2013

**"… all matter is subject to the same spatial constraints, regardless of scale or position. Thus given these constraints, tensegrity is the most economical and efficient way to build at the molecular scale, at the macroscopic scale and all scales in between … tensegrity structures may have been selected through evolution because of their efficiency-their high mechanical strength using minimum of materials" Ingber (1998).**

**DECLARATION**

I declare that this thesis is my own unaided work. It is being submitted for the Degree of Doctor of Philosophy at the University of the Witwatersrand, Johannesburg, South Africa. It has not been submitted before for any degree or examination in any other University.

_____

Deran Reddy

(Signature of candidate)

Signed at the University of the Witwatersrand, Johannesburg, South Africa on the 22nd day of October 2013.

# Dedication

This work is dedicated to my parents, Babs and Veni Reddy,

For giving me all the strength, support and tools

To allow me to reach all my goals

Had it not been for your wisdom, guidance and intellectual capacities

This work would've been a feat I would have never accomplished.

All your sacrifices to ensure I received the best possible education have not and never will be forgotten

Thanks for the inspiration to extract the maximum out of what life has to offer

My brother, Donovan,

For all your motivation and being there every step of the way

Your help, in every aspect of life, has been invaluable

Standing by me, from trying to show me the angles in mathematics,

To plain moral support in the academic disciplines I decided to pursue

It means a lot to me and has been a contributing factor in the completion of this work

Thank You

# Publications and Presentations Arising from this Study

**Publications:**

To date, no publications have arisen from the data collected from this project however two manuscripts are in preparation and will be submitted to ISI accredited journals for review.

Presentations:

**Presentations:**

**2009:**

International Federation of Association of Anatomists, Cape Town, South Africa.

**2010:**

Biodiversity Symposium, University of the Witwatersrand, Johannesburg, South Africa.

**2010:**

Postgraduate Cross – Faculty Symposium of the University of the Witwatersrand, Johannesburg, South Africa.

**2011:**

Second Mediterranean Congress of Herpetology, Marrakech, Morocco.

**2012:**

7th World Congress of Herpetology, Vancouver, Canada.

# Abstract

The reptilian lung has been well documented, morphologically and morphometrically, across the spectrum. Models on the different structural types and correlations to lifestyles have been made from these. Interestingly, very few studies have been conducted on the Nile crocodilian lung given its evolutionary significance. The previously conducted studies were limited to narrow scales of examination and used few techniques to develop hypotheses and reach conclusions. Furthermore, none of the studies conducted examined the Nile crocodile lung at various life stages, given their ecology. This study examined the lung morphology of the Nile crocodiles of different ages at various scales. The structural components that comprise the respective age groups were also quantified. This was done to conceptualise the full functionality of the lung and the effects on its lifestyle. It also served to examine and create new hypotheses on the actual mechanisms that the lung employs for direct and indirect functions, based on its structure. Latex casting, light microscopy, scanning electron microscopy, 3 dimensional serial section computer reconstruction, transmission electron microscopy and confocal microscopy were used to document the morphology of the Nile crocodile lung from macroscopic to ultrastructural scales respectively. Stereology was used to morphometrically quantify the structural components that comprise the lung. At a macroscopic scale the lungs were observed to be conically shaped with broad base decreasing to an apex cranially. Moving to microscopic scales, cranial regions of the lung were found to be more subdivided than the middle and caudal regions of the lung respectively. All of the respective ventral regions of the lung were discovered to be more subdivided than their dorsal counterparts. The presence of smooth muscle was also markedly observed in the middle to caudal regions of the lung. Upon examination of the ultrastructural composition of the lung, various septa were observed which facilitated the subdivision of the lung into favourable gas exchange units, mainly in the cranial regions of the lung. Interfaveolar pores, stereocilia and

microvilli were also observed, the former two never documented in the scientific literature previously. It is hypothesised that these structures are integrally involved in ensuring efficient gas exchange occurs to suit particular behaviours. Stereological analyses confirmed the morphological observations. Interestingly it showed that the various regions of the young age groups had more highly subdivided lungs than the older age groups. Apart from degrees of subdivision, which has notable impacts on respiration, and allometric size scaling, the lungs of the various age groups were similar. All morphological and morphometric evidence illustrate that the ventral cranial region of the lungs is the most gas efficient region with the highest surface area to volume ratio. This is followed by the dorsal cranial region, ventral middle region, dorsal middle region, ventral caudal region and the dorsal caudal region of the lungs. Due to the arrangement and different levels of efficiency of the various regions of the lung, normal tidal ventilation doesn't seem feasible. Instead of this, unidirectional airflow with a mechanism, made of the various structural components, rationing air usage for optimal gas exchange for particular activities is more plausible. This hypothesis strengthens the currently envisaged reptile – avian pulmonary evolutionary theory due to the similar nature of their respiratory systems.

# Acknowledgements

I would like to extend my gratitude to my supervisor, Professor Margot Hosie, for her invaluable input, support and guidance throughout the course of my PhD.

I wish to thank Professor Paul Manger, for helping me acquire the specimens for my PhD and furthermore for all the other administrative help rendered.

I would like to thank my parents, Mr and Mrs L. Reddy, for their financial assistance. Apart from that, thank you for everything in life. You guys truly have spoilt me and just so you know, you'll have to constantly do so but on a more serious note – I'll be forever indebted to you. Just so you know your omnipotent presence and moral support is more than anyone can ask for.

The NRF is highly acknowledged for their funding of this project - NRF Rated Researchers Grant: Allocated to Professor M. J. Hosie, School of Anatomical Sciences, University of the Witwatersrand.

My brother and sister in law, Mr and Mrs D. Reddy, thanks for the good old campus day's guys. Don, your support throughout my life and this venture, Don; Vandana; Shivan and Nivan, has really made an impact and serves as a motivation for me to strive for excellence.

To my girlfriend, Kaajal Makka, thank you for your unwavering support and for being ever present. Your motivation and selfless aid has helped me finish my PhD, more than you know.

To my dearest friend, Monica Gomes, thank you so much for the fun times and lunch breaks. Your advice has and always will be treasured. On the academic front, thank you for proof reading aspects of this this thesis and help with all my molecular work. If there are mistakes –

everyone knows who to point fingers at, just kidding. I have no doubt that this thesis is better than it would be thanks to your editorial “machete” skills.

To Mrs Hasiena Ali, thanks for the entertaining lunches and random chats. In terms of the work for this thesis, thank you for the help with all my solutions and protocols. Your magic touch really helped me with my light microscopy work.

To Mrs Alison Mortimer, thank you for teaching me solid basic histology techniques – I could never have done anything without these.

To Professor Alexander Ziegler, Mr Jacques Gerber, Ms Pamela Sharp, Ms Caroline Lalkhan, and the late Mr Abe Ramebele of the Microscopy and Microanalysis Unit of the University of the Witwatersrand, thank you for all your help and guidance with regard to electron microscopy.

I would like to thank the CSIR, Pretoria, South Africa for allowing me to use their Scanning Electron Microscope. To Shannon, thank you for all your help operating the microscope and getting “pretty” pictures.

To Mr J. Woodward, your help with the 3 Dimensional reconstructions, in development of algorithms and the knowledge thereof, has been vital in the context of my research.

To the School of Anatomical Sciences, its members and anyone that I have not mentioned; thank you from the bottom of my heart for allowing and helping me to complete all the work I needed to do in order to complete my PhD.

# Table of Contents



## Chapter 1: Introduction

## Chapter 2: Materials and Methods

## Chapter 3: Results

# List of Figures

**Chapter 1: Introduction**



**Chapter 2: Materials and Methods**

**Chapter 3: Results**

**Appendix C**

# List of Tables

**Chapter 2: Materials and Methods**



**Chapter 3: Results**



**Appendix D**

# Introduction

## 1.1.1. Study Animal: The Nile crocodile*, Crocodylus niloticus niloticus*,

### An overview

The first appearance of crocodiles in human history was the Nile crocodile, originally documented by the Greek writer Herotodus in the 5$^{th}$ century B.C. (Dodson, 2003). With regards to scientific nomenclature, the Nile crocodile belongs to the class Reptilia, order Crocodylia and family Crocodylidae (Janke *et al.,* 2005, Kyalo, 2008; Martin, 2008). Phylogenetically, Nile crocodiles belong to the great group called archosaurs which includes many extinct clades, namely the pterosaurs and dinosaurs (Blake, 1982; Buffetaud, 1982; Taplin, 1984; Taplin and Grigg, 1989). Being one of the largest extant reptile species and the last of the archosaurs (Grigg *et al*., 1998) it is understandable why the Nile crocodile is referred to as a living dinosaur.

The origin of its scientific name is from the Greek word *Krokodeilos*, which is literally translated to 'pebble worm' (due to its appearance) and *niloticus*, meaning 'of the Nile'. Their common names include Mamba (Swahili), Garwe (Shona), Ngwenya (Ndebele), Voay (Malagasy), Kwena (Tswana), Crocodilo (Portuguese), Crocodil du Nil (French), Temsah (Arabic) and Denkyem (Twi), (Kyalo, 2008; Fergusson, 2010).

Amongst the crocodilians, the Nile crocodile is one of the largest and is biologically well recognised (Fergusson, 2010). They have a delayed rate of maturation, a great longevity and are semi – aquatic (Garrick and Lang, 1977). Adults achieve an average length of 5 metres (m) and may exceed lengths of 5.5 m (Cott, 1961; Ross and Magnusson, 1989; Grenard, 1991; Branch, 1998; Jones, 1998). Dorsally, adult Nile crocodiles have a constant blotched olive or grey coloration whilst the juveniles are olive brown to green with

prominent black cross bands across the body and tail (Branch, 1993, 1998; Ross and Magnusson, 1989).

Ventrally, the coloration is typically straw – yellow. Illustrations of these features are highlighted by Neill (1971), Guggisberg (1972), Ross and Magnusson (1989), Graham (1990), Branch (1993, 1998) and Lamar (1997).

### 1.1.2. Distribution and Habitat of the Nile crocodile

Their native distribution spans Sub-Saharan Africa inclusive of Madagascar (Cansdale, 1955; Groombridge, 1987; King, 1989; Ross and Magnusson, 1989; Grenard, 1991; Branch, 1993, 1998; Dodson, 2003; Martin, 2008; Fergusson, 2010). Historical evidence shows that the range of the Nile crocodile once included Israel, Syria, Comoros and the Seychelles (King, 1989; Ross and Magnusson, 1989).

The habitats that the Nile crocodile occupies are primarily aquatic and located mainly in tropical and subtropical regions (Garrick and Lang, 1977; Martin, 2008). These habitats include freshwater wetlands, lakes, rivers, fresh water swamps, marshes and dams (Kyola, 2008; Martin, 2008; Fergusson, 2010). Arguably, according to Martin (2008) Nile crocodiles are the largest fresh water dwellers. Despite their affinity for freshwater habitats they have been documented to inhabit salty / brackish water environments (mangroves or estuaries), (Dunson, 1982; Pooley, 1982; Mazzotti and Dunson, 1984, Pauwels *et al.,* 2004; Fergusson, 2010). Nile crocodiles have also been documented to inhabit extremely dry habitats; an example is a small population in the Mauritanian Sahara (Gans, 1976; Shine *et al*., 2001). During prolonged periods of drought they either migrate until they find new water spots (Martin, 2008), survive by means of aestivation and or occupy mud burrow retreats until more favourable conditions arise (Cott, 1961; Martin, 2008).

Figure 1.1: A map illustrating the current native distribution of the Nile crocodile. (From Fergusson, 2010).


Egypt
Mauritania
Mali
Niger
Chad
Sudan
Eritrea
Senegal
Gambia
Guinea-
Bissau
Guinea
Sierra Leone
Liberia
Cote d'Ivoire
Ghana
Togo
Benin
Burkina Faso
Nigeria
Cameroon
Central
African Republic
Ethiopia
Kenya
Somalia
Gabon
Equatorial Guinea
Republic of Congo
Democratic
Republic
of Congo
Uganda
Rwanda
Burundi
Tanzania
Mozambique
Angola
Zambia
Zimbabwe
Namibia
Botswana
Swaziland
Madagascar
South
Africa

### 1.1.3. Thermoregulatory Behaviour

Being ectotherms, Nile crocodiles actively thermoregulate to attain set body temperatures which average at 25.6$^{o}$ C, (Cott, 1961, Grigg *et al.,* 1998). In order to do this they have varying interactions with their environment and practice various behaviours (Modha, 1968; Loveridge, 1984). Heat exchange between their bodies and the substratum, governed by its conductivity index, generally determines where individuals will reside in the habitat over short and large temporal scales (Cott, 1961).

Nile crocodiles generally bask through the day to replace heat lost during the night (Cott, 1961). Diurnal movement studies indicate that they hardly move and if they do the distances are minimal (Hutton 1989). It is assumed that they bask until they reach the upper limit of their normal activity range (Cott, 1961). This could be attributed to the fact that it takes them a long period of time to heat up as they have a low surface area to volume ratio (Cott, 1961). Upon reaching this temperature they dissipate heat by either crawling to the shade, lying at the water's edge or going into the water (Cott, 1961).

Nile crocodiles also thermoregulate by mouth gapping (Cott, 1961; Grigg *et al.,* 1998). Exposure of the moist buccal mucosa results in evaporation which in turn provides a cooling mechanism (Cott, 1961). It has been shown that the proportion with which the jaws open is proportional to the amount of heat being dissipated (Cott, 1961). An interesting observation is that Nile crocodiles often submerge their body or tails in the water while mouth gaping in order to replenish lost water by absorption (Cott, 1961; Diefenbach, 1973). Thermoregulation is important in these animals as it dictates their pace of life and assimilation efficiency (Hutton, 1987).

### 1.1.4. Locomotion: Terrestrial and Aquatic

Approximately half of a Nile crocodile's life is spent on shore where it remains inert (Cott, 1961). Terrestrial labour is one only undertaken in case of emergencies and or to thermoregulate (Cott, 1961; Parrish, 1987). When travelling on land, Nile crocodiles utilise three gaits namely; the high walk, the belly run and the gallop (Schaeffer, 1941; Cott, 1961; Parrish, 1987; Brinkman, 1980). This basically requires an erect posture due to active movement (Zug, 1974; Webb and Gans, 1982).

The high walk is considered to be the normal gait which is a method of progression in moving up river banks and onto rocks (Cott, 1961). The high walk is also used for casual overland travel; for example when returning from basking to water (Cott, 1961). This gait involves the legs moving beneath the body keeping the belly off the ground (Cott, 1961; Parrish, 1987). The belly run, faster than the high walk, is generally used in response to escape a disturbance (Cott, 1961). The crocodile assumes a crawling posture and with intense motile power heads to water for safety (Cott, 1961; Parrish, 1987). The gallop is a gait generally observed in juveniles (Cott, 1961; Parrish, 1987) and hardly observed in adults (Cott, 1961). This gait employs the same mechanism of a galloping horse and is used to escape danger when an individual is far away from a water source (Cott, 1961, Parrish, 1987).

The dexterity and proficiency of terrestrial locomotion in the Nile crocodile has no comparison to the grace and ease of movement in water, which can be described as their real environment – both as a feeding ground and place of refuge (Cott, 1961). They have mastered the art of aquatic locomotion. Within its freshwater habitat the crocodiles hardly exert themselves (Cott, 1961). They either float idly at the surface in lagoons and still

waters or keep their position in rivers by means of relaxed gentle tail strokes (Cott, 1961). Active swimming involves undulations of the tail while the body is in a sprawled posture (Cott, 1961; Parrish, 1987). These undulations are slow for general swimming speed however when hunting or injured, they may dart with a spurt of energy; sometimes leaping out of the water (Cott, 1961; Parrish, 1987).

In undisturbed waters, which they often reside in, Nile crocodiles float with just the nasal disc, eyes and occiput above the water (Cott, 1961). Before diving, they close their nares and sink, presumably by increasing their specific gravity by the contraction of the abdomen and thorax (Cott, 1961). Stomach stones have been hypothesised to play a role in this (Brander, 1925) but there is no clear evidence to confirm or reject this. The mechanism, if the aforementioned hypothesis holds, by which they operate is to aid in stability once the animal has submerged, aid in drowning prey and also to act as ballast (Cott, 1961).

Stomach stones have also been hypothesised to also aid in digestion and relieve pangs of hunger (Cott, 1961). Both of these hypotheses are unrealistic as Nile crocodiles swallow their food as a whole and secondly reside in areas of high prey density or practice aestivation if prey is scarce (Cott, 1961). It is not clear where the stomach stones are derived from however three hypotheses exist; they are that they are deliberately ingested, that they are advantageously derived from stomachs of prey or that they are deliberately swallowed (Cott, 1961). According to a model by Henderson (2003), stomach stones are inconsequential for buoyancy and stability in aquatic tetrapods but that lungs are the principle agent for hydrostatic buoyancy control. Graham *et al.,* (1975) hypothesised that

the lung of the Nile crocodile influences its buoyancy but to date this has not empirically been proven.

While submerged, Nile crocodiles can hold their breath for lengthy periods of time, depending on the size of the crocodile, stress condition, the temperature and composition of the air breathed in (Cott, 1961; Glass and Joahnsen, 1979). During a normal undisturbed ventilatory cycle, at 25$^{o}$ C, it is documented that they hold their breaths for 80% of the time (Glass and Johansen, 1979). When they require a fresh bolus of air, the crocodile breaks the water surface with its nasal disc, or snout in turbulent water, and exhales (Cott, 1961). Following this they inspire a new bolus of air and submerge again (Cott, 1961).

### 1.1.5. Growth

According to Peters and Wassenberg (1983) life history phenomena are scaled according to body size. In the Nile crocodile, growth appears to be intermediate (Graham, 1968) growth rates are variable (Cott, 1961; Graham, 1968, Blake and Loveridge, 1975) and survival is size related. According to Hutton (1987) climate (temperature) is the most important factor governing growth, feeding behaviour, and physical condition in the Nile crocodiles. Hatchlings grow throughout their first year and then growth slows down significantly as they approach their first cool-dry season of life (Hutton, 1987). Correlatively, their mean relative condition and feeding frequency decline as the cool-dry season approaches. In the cool-dry season larger older juveniles stop growing and their condition deteriorates with some individual declining in length (Hutton, 1987). As individuals grow older, the rate at which they grow declines (Cott, 1961), females having a slower rate than that of males (Hutton, 1987).

### 1.1.6. Reproduction

The Nile crocodile is an egg laying reptilian species (Kyalo, 2008) and is sexually dimorphic, with the males being up to 30% larger than the females (Kyalo, 2008; Fergusson, 2010). The males are territorial, with the size of their territories varying proportionally according to the size and health of an individual (basically factors governing dominance), (Garrick and Lang, 1977; Hutton 1989). Aspects of territoriality in the Nile crocodile has been described (Modha, 1967) but no data exists describing the spatial and social behaviour of either younger animals or adults out of the breeding season (Hutton, 1989). According to Owen-Smith (1977) "territoriality is a strategy used by individuals to secure a disproportionate share of each resource of potential significance to genetic success". Combat for dominance between males precedes the establishment of mating territories (Garrick and Lang, 1977) and becomes particularly defensive during the reproductive season (Pooley, 1977). Out of the breeding season, males are territorial over basking and feeding grounds (Cott, 1961). A variety of territorial behaviours, apart from aggressive behaviour resulting in serve injuries, are observed during defence of a territory.

Garrick and Lang (1977) identify these as follows:

- Territorial males approach intruder males after displaying a head emergent, tail arched posture which apparently signifies alertness.
- Exchanges in the form of chases, lunges and mock or real biting are made between the territorial male and the intruder.
- After a chase most territorial males will inflate their posture to show dominance. According to Modha (1967) they also snap their jaws after successfully maintaining their territory.

- Territorial males and intruder males will have open jaw contact. If no outcome follows, other behaviours to assert dominance are practiced.
- Territorial males actively patrol their territories.
- Nasal geysering (water spouts rising from the nares) occurs between a territorial male and intruder as warming signals and as a show of strength.

Submissive behaviours are also observed. Females and intruder male Nile crocodiles' snout lift which is appeasement behaviour (Garrick and Lang, 1977).

Courtship behaviour is observed between dominant males and females (Garrick and Lang, 1977). It is often lengthy, extending over a period of 6 – 8 weeks (Garrick and Lang, 1977). Cott (1975) describes courtship displays as quite "leisurely" and observed that it may range from approximately several minutes to an hour. According to Garrick and Lang (1977) courtship is divided into three phases, the attraction and advertisement signals, pair formation and copulation. Territorial male crocodiles roar, bark and cough to attract females, (Cott, 1961). In the presence of females they provide a "courtship splash display" (Modha, 1967) and or a "fountain display" / nasal geysering (Cott, 1975). Other behaviours such as bubbling and submergence, mutual head contact and riding occurs (Garrick and Lang, 1977). A prenuptial display by females is the lifting of their snouts and arching of their tails out of the water (Garrick and Lang, 1977). After this signal, the pair circles each other, the males mount the female and they copulate. After copulation and egg laying, males and females form a pair bond (Pooley, 1977).

Reproductive males are identified by grossly enlarged and distended testis that have a smooth texture and are bluish – white in colour (Cott, 1961). The immature male testis is relatively small in size with an attenuated shape, has a granular texture and is generally

"liver coloured" (Cott, 1961). Breeding females are recognised according to the following: (1) individuals ovulating with ova ranging from 2mm in diameter upward, (2) those with oviduct eggs, unshelled or shelled and (3) spent females, whose ovaries undergoing resorption are flaccid granular and discoloured while the oviducts remain distended and have prominent vascularisation (Cott, 1961).

Reproduction occurs within the broader habitat where adequate nest material, shade and water are available (Garrick and Lang, 1977). Nest sites are made in the dry season, usually in the coarse sands of spits, riverside mud-flats, low lying islets, lake-side beaches or in the bed of a dried watercourse (Cansdale, 1955; Cott, 1961; Pooley, 1977; Lang, 1987; Magnusson *et al*., 1989; Branch, 1993, 1998; Allen, 1998). Anecdotal evidence shows that the nests are dug up to approximately 50cm in depth. In the case of rocky habitats, eggs are laid in shallow gravel beds (Cott, 1961). After eggs are laid they are covered with surrounding substrate (Cott, 1961). As the eggs are cleidoic, the eggshell and its membranes are resistant to water and gas exchange between the egg and the nest environment (Lutz et al., 1980).

Females actively nest guard during the whole incubation period (Cott, 1961, Pooley, 1977). This is done by either lying over the nest using the lower throat / thorax or by visual means throughout the day and night (Cott, 1961). Their visual system is adapted for nocturnality (Walls, 1942) so they are well equipped to nest guard at night. In response to threats females growl, splash water with their tails and as a last resort actively chase off predators (Garrick and Lang, 1977).It should be noted that during this period the female does not feed (Pooley, 1977).

Males lie vigilantly on banks close to the nest actively monitoring the surrounding area and respond to any potential threats (Pooley, 1977). This allows females the opportunity to watch over her eggs with less physiological stress. Water availability is integral to nest selection for two reasons, first crocodilian eggs are sensitive to moisture (Voeltzkow, 1893) and secondly to allow easy access of hatchlings from land to water (Cott, 1961).

Prior to hatching, the young begin to vocalise a bark, croak and or vibrate even prior to pipping (Cott, 1961; Garrick and Lang, 1977; Pooley, 1977). In response to the vocal and or vibrating cues (Pooley, 1962, 1969) the female exhumes the eggs from the nest. Partially hatched eggs are cracked open, using her palate and teeth, and the young are transported in her buccal pouch into the water (Garrick and Lang, 1977; Pooley, 1977). Transport of hatchlings from nest to water is a behaviour that is practised by all crocodilians (Ogden and Singletary, 1973; Hunt, 1974; Toro, 1969; Kushlan, 1973). All empty egg shells, membranes and remaining yolk are swallowed (Pooley, 1977). Transport of hatchlings from the nest to water and consuming the remnants of eggs is also practiced by males (Pooley, 1977). It is hypothesised that egg shell, membrane and yolk swallowing is an anti-predatory behaviour that removes evidence of hatchlings in an area (Pooley, 1977).

Fecundity in the Nile crocodile is high with clutch sizes of 35 – 50 eggs, which may vary markedly amongst populations (Fergusson, 2010) attributed mainly to the size of the female (Blake and Loveridge, 1975; Pooley and Gans, 1976; Leslie, 1997). Some discrepancies regarding the incubation time of the eggs exists. According to Pitman (1936) and Pooley (1969) the incubation period of the eggs lasts for about 84 – 96 days, however, Garrick and Lang (1977) state that it is 49 – 84 days. Anecdotal accounts from the

crocodile farmer at Thaba Kwena Crocodile Farm (Bela Bela, Limpopo Province, South Africa) concur with the finding of Pitman (1936) and Pooley (1969). Breeding begins in the dry season and the eggs hatch during the wet season (Cott, 1961; Garrick and Lang, 1977). This timing affords optimum conditions for the hatchlings as they have a medium of dispersal from water to land and an abundance of insect food (Cott, 1961).

Eggs of the Nile crocodile are generally predated upon by the Nile monitor lizard, baboons, honey badgers, spotted hyenas and the Marabou Stork (Cott, 1961; Blake and Loveridge, 1975). The eggs are Temperature Sex Dependent (TSD) i.e. gender of hatchling is determined by the heat of the sun warmed nest (Branch, 1998). Low temperatures produce females and high temperatures males (Branch, 1998). Great amounts of parental care is exhibited by adult Nile crocodiles, from transport of juveniles to water through to actively defending the brood from predators (Hadley, 1969; Pooley, 1974a, 1974b; Pooley and Gans, 1976; Pooley 1977; Lang, 1987, 1989; Magnusson *et al*., 1989; Branch, 1993, 1998). This visible form of parental care has been recognised since the days of Aristotle and Pliny the Elder (Shine, 1988).

### 1.1.7. Parental Care

Parental care is markedly exhibited by Nile crocodiles. Crèche formation for hatchlings is a very well documented phenomenon (Magnusson, 1980; Hutton, 1989). Each crèche is uniquely designed for the protection of hatchlings (Magnusson, 1980). Mothers become bold in their defence of their young and will attack any predators (Cott, 1961). The hatchlings are guarded against natural predators (Garrick and Lang, 1977) and even older Nile crocodile juveniles (Hutton, 1989), where cannibalism is common (Hippel, 1946,

Cott, 1961; Pooley, 1969; Stanton and Dixon, 1975; Messel and Vorlicek, 1987). Whenever hatchlings vocalise a stress call, the mother and or father always respond (Cott, 1961; Kushlan, 1973; Pooley, 1974; Modha, 1967; Garrick and Lang, 1977; Pooley 1977; Stanton, 1978).

After approximately 3 months they young begin to move away from the parents individually or in small groups (Garrick and Lang, 1977). Cott (1961) documented that the juveniles are generally gregarious and disperse whenever a threat arises but regroup after the threat subsides. Post-copulatory contact amongst breeding individuals involves the use of appeasement signals so as to reduce aggression (Garrick and Lang, 1977). This is important as gravid females or females tending to young could be injured and endangers all reproductive efforts (Garrick and Lang, 1977).

### 1.1.8. Prey and Hunting Methods

The Nile crocodile is classified as an omnicarnivorous, primarily aquatic predator whose prey consists of fish, turtles and other reptiles, small and large mammals (including zebra, buffalo, and even juvenile hippo), birds, carrion, invertebrates and any other animal it can overpower, swallow whole or rip apart, and ingest (Roosevelt, 1909; Cansdale, 1955; Cott, 1961; Grenard, 1991; Branch, 1993, 1998; Lamar, 1997). In order to capture terrestrial prey they utilise binocular vision, aerial focusing (Fleishman *et al.,* 1988) and acceleration thrust provided by the tail and hind limbs from a cryptic floating posture (Davenport *et al.*, 1990; Busbey, 2005). In order to capture aquatic prey tactile senses are used to trigger a snapping behaviour (Davenport *et al.*, 1990) with rapid lateral movements of the head (Busbey, 2005). This method of hunting reinforces the fact that the crocodiles are unable

to focus underwater (Fleishman *et al.,* 1988). When they don't actively hunt, crocodiles have also been known to scavenge, filling the same niche as hyenas and vultures (Cott, 1961).

After killing their prey, the crocodiles swallow their prey using inertial feeding (Gans, 1969; Busbey, 2005). This involves puncturing the integumentary envelope of prey (Davenport *et al.*, 1990) which may even help in digestion (Jackson and Ryan, 1986). The dorsal and ventral components of the gular valve create an efficient seal which is consistent with the natural behaviour and feeding habits of the crocodile (Putteril and Soley, 2006). In addition to this, taste and pressure receptors are evenly distributed throughout the epithelium of the gingivae and palate (Putteril and Soley, 2003).

An ontogenetic shift in the diet of the Nile crocodile exists (Cott, 1954, 1961; Corbett, 1959a, 1959b; Modha, 1967; Taylor, 1973; Blomberg, 1976; Pooley and Gans, 1976; Whitfield and Blaber, 1979; Hutton, 1987; Kyola, 2008; Wallace and Leslie, 2008). The diet of juveniles consists mainly of invertebrates including arachnids, crustaceans and amphibians (Cott, 1961; Kyola, 2008). With maturity, their diet changes to include fish (Corbett, 1959a; Cott, 1961; Graham, 1968; Blomberg, 1976). The diet of adults consists of large vertebrates (Pitman, 1936, 1949; Owen, 1951; Cott, 1961; Kyola, 2008). The main shifts in their diet can be attributed to the changes in the allometric dimensions of their heads as they age (Hutton, 1987). Not surprisingly, fatal attacks and preying on humans have been well documented in numerous parts of Africa (Cansdale, 1955; Guggisberg, 1972; Pooley *et al*., 1989; Graham, 1990; Allen, 1998; Branch, 1998). Magnuson *et al.,* (1987) describes Nile crocodiles as nocturnal carnivorous opportunistic predators, whose diet depends on their developmental stage and potential prey diversity.

### 1.1.9. Enemies / Predators of the Nile crocodile

Despite the fact that the Nile crocodile is an apex predator, it also has enemies. Juveniles are predated upon by larger crocodiles, Nile monitor lizard, Thirse turtles, catfish, fish eagles and hornbills (Cott, 1961).

In general, the Nile crocodile plays an important role in the environment by regulating the ecosystem it resides in. It does this mainly through the intricate web of the food chain where the Nile crocodile is a "master predator, cannibal, and scavenger" (Cott, 1961). Juveniles feed on belostomatid bugs, dragonflies, dytiscid and hydrophilid beetles and crabs – all of which feed on a multitude of fish fry (Cott, 1961). Adults maintain population dynamics by regulating fish and large vertebrate population sizes (Cott 1961). Lastly, they have symbiotic relationships with birds, e.g. the *Zic Zac* (H. *spinosus*), who get food by removing scraps and leeches from the crocodile's mouth thereby leaving the crocodile with a "clean" oral cavity (Cott, 1961).

## 1.2. The Vertebrate Gas Exchanger

Throughout evolution, an important and fundamental challenge animals have faced is the acquisition of molecular oxygen for aerobic metabolism (Maina, 2002a). Kleiber (1961) called oxygen '***fire of life***' whilst Krogh (1941) stated that the fundamental necessity for oxygen was '***the call for oxygen***'. Laitman *et al.,* (1996) reinforced that "the acquisition and processing of oxygen and its by-products is the primary vision of any air breathing vertebrate".

Preceding the discovery of oxygen in 1771 by J. Priestly and subsequently the description of the chemical composition of air three years later by A. Lavoisier, it was well understood that respiration, a conspicuous mechanical process, was essential for life (Maina, 2002a).

Respiration is the process whereby molecular oxygen is acquired from an external fluid medium of an organism and distributed to its tissues and cells for energy production (Maina, 2000a, 2002a, 2002b). This process may also be referred to as gas exchange. To perform gas exchange, an intricate and sophisticated assembly of structural components and co-ordinated physiological, biochemical and behavioural processes is required (Maina, 2002b). The specific functional designs exhibited by respiratory organs generally correlate with the metabolic requirements of animals including factors such as body mass, habitat occupied, sex, age and lifestyle (Maina, 2002c; Torday *et al.,* 2007). As one of the integral factors governing metabolism, the respiratory rate of animals often predicts their pace of life (Maina 2000a). Those animals which maintain high oxygen to carbon dioxide ratios, allometrically, are generally the most successful (Maina, 2000a).

The efficiency of gas exchange is governed by the morphological assembly of the respiratory organ as a whole but not mutually exclusive of other aspects of an animal's physiology, e.g. feeding, circulation or locomotion (Klein and Codd, 2010). The correlation of an animal's habitat and the animal itself is the best method to conceptualise the essence of the morphology of a gas exchanger (Maina, 2002b). According to Maina (2000a) whether by default or design, morphological plasticity is a key factor in allowing the adaptive radiation of animal species.

Respiratory organs are the primary boundary between an organism and the external environment (Maina 2003). In its simplest form, a gas exchanger is basically a tissue barrier across which diffusion of oxygen and carbon dioxide occurs under a partial pressure gradient (Maina 2002b; Torday *et al.*, 2007). All gas exchange organs share a multitude of structural and functional properties however they are not identical, which in part can only be explained by historical, evolutionary biology or through comparative and or developmental studies (Torday *et al.,* 2007). It is important to recognise that throughout

the evolutionary continuum various gas exchange designs have been created and transformed while being rigorously tested (Maina, 2002a). Deficient features and aspects have been discarded and the optimal ones conserved (Maina, 2002a).This leads to the conclusion that the relationship between form and function of respiratory organs is an intimate one. This kindred relationship for dextrous performance is termed symmorphosis (Weibel, 2000). According to Taylor and Weibel (1981), symmorphosis is defined as "a state of structural design commensurate to functional needs resulting from regulated morphogenesis, whereby the formation … of structural elements is regulated to satisfy but not exceed the requirements of the functional system".

The geometric arrangement of the constituent structural components of gas exchangers determines the direction and presentations of the respiratory media across the gas exchanger for efficient gas exchange to occur (Maina, 2003). If the external (ventilating media, water or air) and the internal (perfusing medium, blood) flow in the same direction, the arrangement is concurrent, alternatively counter-current if they run in opposite directions (Maina, 2002a). As a result, the physical properties of the gas exchanger as a whole are consistent with the optimisation of prevailing conditions for diffusion to occur (Torday *et al.,* 2007). In addition they reflect the physical properties of water and or air, the only two naturally occurring respiratory media (Torday *et al.,* 2007). In comparison to other organs and organ systems, respiratory structures are distinctive in that no structural elements are ubiquitous to them (Maina, 2002a).

Maina (2000a, 2002b) states that the optimal design of the gas exchanger for particular phylogenetic levels of development, habitat and lifestyle have developed only so far as to satisfy prescribed needs. Surpassing the basic design, all gas exchangers display the following morphological features:

1) Evagination or invagination from the surface of the body.
2) Stratification or compartmentalisation.
3) Partitioning between internal and external compartments to promote a flux of respiratory gases.
4) Vascularisation.
5) Various geometric organisations of structural components (Maina, 2002b).

Respiratory organs need to be actively ventilated to constantly provide oxygen at the gas exchange surface and also to remove carbon dioxide. This maintains a concentration gradient between the animal and its environment which results in facilitating the diffusion of respiratory gases in and out of the gas exchanger (Klein and Codd, 2010). In order to do this, contraction of muscles are required, which are often involved in other functions e.g. feeding (Klein and Codd, 2010). This 'potential conflict' sparks functional trade-offs between the respiratory system and other physiological requirements (Klein and Codd, 2010). Despite their primary function of gas exchange, respiratory organs also have numerous auxiliary functions (Bakhle, 1975; Neckvasil and Olson, 1986). These functions include synthesis, metabolism, the regulation of concentrations of pharmacologically active agents and lipids etc., (Bakhle, 1975). Maina (2003) summarises the importance of the auxiliary functions of gas exchangers by stating "the morphologies and physiologies of the respiratory organs should be examined judiciously from a holistic perspective: from their inclusive functions and not from the better known, narrow aspect merely of gas exchange". Even though a spectrum of gas exchangers exist, at the most elementary level of operation, the structure and function of vertebrate lungs are amazingly similar (Maina, 2003).

Life undoubtedly originated in water, where unsophisticated fragile life forms were given a stable environment and essential support (Maina 2002a). With regard to the vertebrate gas

exchangers, gills (evaginated respiratory organs) are the primordial respiratory organs (Maina, 2002a, 2002b; Duncker, 2004). Interestingly, more than one half of the living vertebrates have arisen directly from lineages that still persist and inhabit water (Maina, 2002a). In combination with simplicity of design and functional complexity, gills occur in different sizes, forms and locations (Maina, 2002b). Gills were developed for water breathing, with different geometric configurations, so as to provide a highly proficient respiratory design (Maina, 2002a). Gas exchange in most aquatic lower vertebrates is through gills or gills and skin (cutaneous respiration), both dependent on allometry and the prevailing environmental conditions (Duncker, 2004).

During the transition from water to land cutaneous respiration played an important linking role (Maina, 2002a). In comparison to ventilated gas exchangers, cutaneous respiration is a energy expensive mode of acquiring oxygen (Maina, 2002a). This compensates for its structural and functional limitations (Maina, 2002a). The water / air blood barrier of the skin is however exceptionally thick resulting in a poor diffusing capacity (Maina, 2002a). By virtue of this, animals, predominantly aquatic species (amphibians in particular), who utilise cutaneous respiration are constrained to wet or humid, non-desiccating habitats (Maina 2002a).

Cutaneous respiration prevents very few possibilities for innovatory change and as a result the skin has been dismissed as an evolutionary “dead end” (Maina, 2002a). The relinquishment of skin as respiratory organ was a necessary trade – off by amphibious vertebrates in the pursuit for colonisation of the terra firma (Maina, 2002a).

Historically early fishes developed lungs (invaginated respiratory organs) as a supplementary air breathing organ (Duncker, 2004). In the Osteichthyes, this occurred in the Actinopterygians with “bony fish” and in the Sarcopterygians with the lung fishes

(Duncker, 2004). In most of the bony fishes the lungs were reduced to swimbladders and in some species the swimbladders became part of a sound production apparatus (Rauther, 1937; Ihle *et al*., 1971). Interestingly, only the African lungfishes utilise lungs as their dominant gas exchanger during survival in dry mud cocoons, often spanning several years (Duncker, 2004). These animals who can breathe in both water and on air are termed bimodal breathers, e.g. African lungfishes and amphibians.

Particular respiratory designs have been perpetuated under a variety of adaptive pressures that different animal lineages have withstood during their evolutionary histories (Maina, 2000a). Wagner (1998) called these conserved features 'the frozen core' (the Bauer plan). However, evolution from one major animal group to another requires a multitude of changes of traits which range from structural, physiological to behavioural ones (Maina 2002a, 2002b). The transition from water to land, an event crucial in the evolution of animal life, illustrates an exemplary event for understanding intricate transactions in the change from gill to pulmonary respiration (Maina, 2003). The ability to breathe in air and clean it, restrict gas exchange to a specific site where it could be controlled, reduce water loss and prevent trauma to a gas exchanger was instrumental in calculated pre-adaptations for terrestrial habitation (Maina, 2002b; Maina, 2003). As the Greek philosopher Aristotle (322 B. C) said "nature does nothing to no purpose".

The first land vertebrates, Stegocephalia, had variable broad and long ribs to support the construction of their trunks (Carroll, 1988). The integration of rib movements then provided a good mechanism for the ventilation of lungs and was the probable precursor in the development of aspiration breathing which substituted buccal pumping (Duncker, 2004). On the other hand, an extreme reduction in the size of the ribs of recent amphibians, urodeles and anurans, has forced them to utilise buccal pumping for lung inflation (Duncker, 2004).

Even though the lung has a passive appearance, intrinsically it's not an inert organ (Maina, 2002a). It is highly metabolically active and provides an interface between respiratory media and blood, which are biophysically significant (Maina, 2002a). The lung is also the only organ that transmits the entire volume of blood in the systemic circulation and submits to ventilatory rhythms under movements of the ribs and diaphragm (Maina, 2002a).In almost all lungs, blood capillaries bulge from the respiratory surface as a result of intramural (hydrodynamic) pressure and from the compaction of red blood cells, which enhances the exposure of blood to air (Maina, 2002b).

In lungs, a large surface area is created by the internal subdivision of the parenchyma which gives rise to terminal gas exchange units (Maina, 2002b). In vertebrates, the degree of internal subdivision of lung parenchyma increases from amphibian, reptilian, mammalian to avian lungs (Maina, 2002b). Limitations to the degree of internal subdivision of the lung to increase the gas exchange surface area are governed by the structural and functional integrity of the organ (Maina, 2002b). The highly varying degree of lung exchange surface area is due to the variations in the amount of gas exchange performed by an individual species (Duncker, 2004).

"The modern gas exchangers are products of a long evolutionary process. The present designs have been reached through a fierce cost-benefit analysis. Despite the many forms that have developed, in certain regards, the structure of the gas exchangers has largely been refractory" (Maina, 2002b).

Figure 1.2: A phylogenetic tree illustrating the relationship between different vertebrate orders. The multitude of structural types are demonstrated by schematic drawings (From Duncker, 1991).

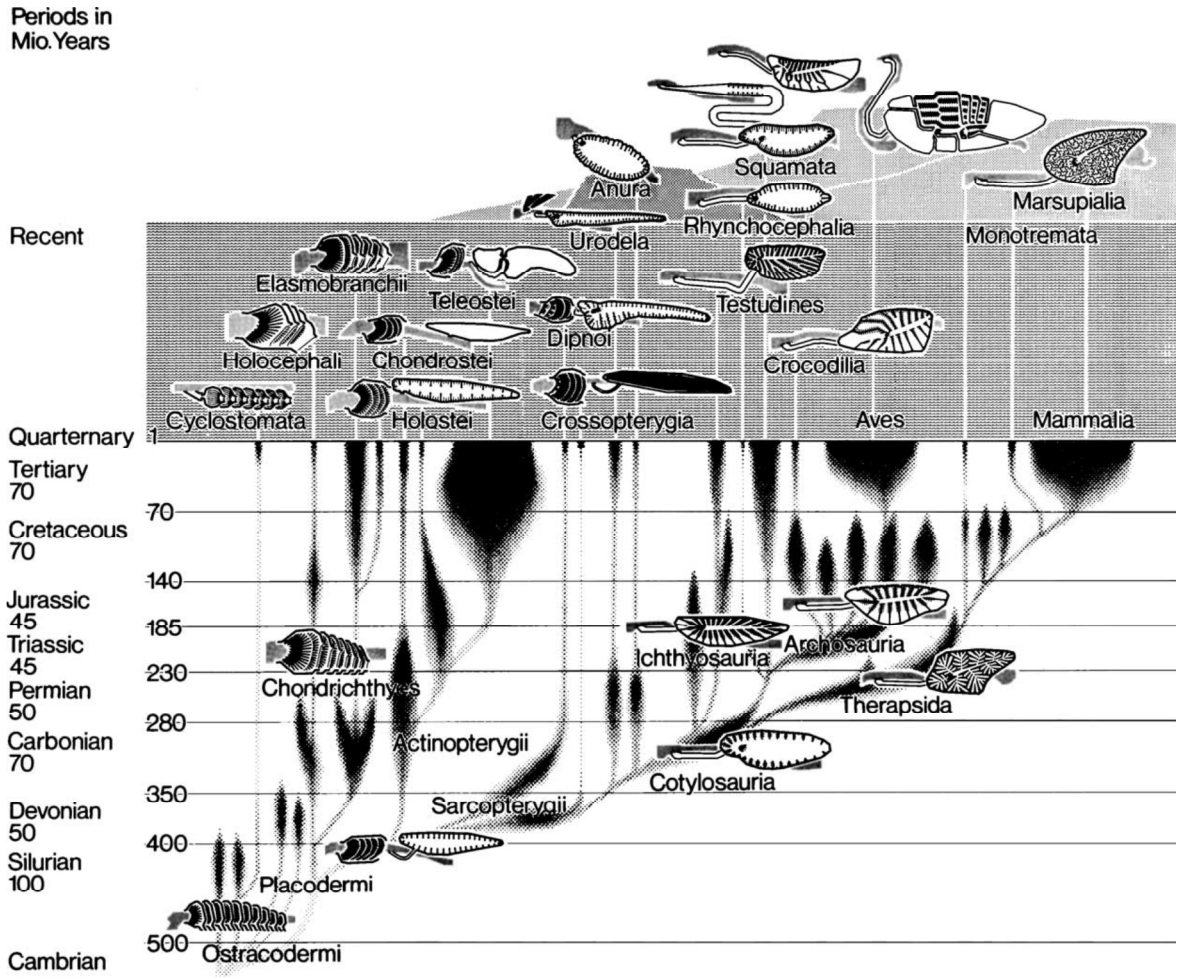
Periods in
Mio. Years
Recent
Quarternary
Tertiary
70
Cretaceous
70
Jurassic
45
Triassic
45
Permian
50
Carbonian
70
Devonian
50
Silurian
100
Cambrian
1
70
140
185
230
280
350
400
500
Squamata
Anura
Urodela
Rhynchocephalia
Marsupialia
Monotremata
Elasmobranchii
Teleostei
Testudines
Dipnoi
Holocephali
Chondrostei
Crocodilia
Cyclostomata
Holostei
Crossopterygia
Aves
Mammalia
Ichthyosauria
Archosauria
Chondrichthyes
Therapsida
Actinopterygii
Cotylosauria
Sarcopterygii
Placodermi
Ostracodermi

## 1.3. The Reptilian Lung

Reptiles are characterised by the great diversity of their pulmonary structure (Cope, 1894; Perry, 1989a, 1989b; 1998). They were the first vertebrates that were sufficiently adapted for terrestrial habitation and pulmonary respiration (Perry, 1989b). In a trade-off, reptiles became lung (= air) breathers by abandoning the skin as a respiratory pathway (Maina, 2003). Amongst reptiles, a great diversity in the respiratory system exists, particularly with regard to lung morphology and the mechanisms of ventilation (Klein and Codd, 2010). This diversity of structures and mechanisms is a result of, at least partially, overcoming the constraints between locomotion and breathing (Klein and Codd, 2010).

The lungs possessed by reptiles are structurally diverse (Milani, 1894; Perry, 1989a, 1989b, 1990), which correlates well with the lifestyle and multiplicity of the habitats that they occupy (Maina, 2003). No single model reptilian lung exists (Maina, 2002a). Reptilian lungs display numerous degrees of internal subdivision, which has resulted in a multitude of morphological patterns of lung subdivision being proposed (Duncker, 1978; Hlastala *et al.*, 1985; Perry 1989a, 1998).

These forms of reptilian lungs range from unicameral lungs (simple, single chambered, saccular, smooth walled and transparent), paucicameral lungs (less elaborate division) and multicameral lungs (highly subdivided and multichambered), (Duncker, 1978; Perry 1989a, 1998). Generally oval shaped lungs are unicameral, i.e. containing only one chamber (Duncker, 1978). The lung wall is developed into an extremely specialised gas exchange formation that is regularly partitioned into long, narrow, thin walled tubes which are orientated perpendicularly forming ediculae, terminal gas exchange units (Duncker, 1978). Smooth muscle networks hold ediculae open during the various stages of respiration so as to allow the parenchyma access to air (Duncker, 1978). This arrangement

is generally observed in lizard families and snakes (Duncker, 1978). Paucicameral lungs retain all the structural properties of unicameral lungs with the exception of septa that protrude into the lumen of the lung subdividing it into smaller chambers (Duncker, 1978). These lungs are more freely movable in the pleuro – peritoneal cavity and are found mostly in in animals such as the chameleon (Duncker, 1978). Following this transitional lung type are multicameral lungs. They are found in monitor lizards, turtles and crocodiles (Duncker, 1978; Perry, 1988). The lumen and subsequently parenchyma of the lung is subdivided into numerous chambers / faveoli, terminal gas exchange units, by an increase in septation (Duncker, 1978). Concurrent with the development of the numerous chambers, an intrapulmonary bronchus is created to maintain communication of the all the chambers with the extrapulmonary bronchus in all respiratory phases (Duncker, 1978). In order to prevent any collapse, the intrapulmonary bronchus is supported by cartilaginous plates or rings (Duncker, 1978).

It must be noted that parallel with the development of the multicameral lung, the vascular system changed, distinctly, by incorporating the pulmonary artery and vein (inclusive of their branches) into the lung (Duncker, 1978). While the aforementioned classifications provide a useful guideline they are thought to be “overly simplistic” because transitional forms and gradations occur (Maina, 1998).

Figure 1.3: Line diagrams of the different reptilian lungs. They illustrate the wide range of lungs from the relatively complex multicameral lungs (A) to paucicameral (B and C) to the simple unicameral lungs (D) which are all partitioned heterogeneously. Multicameral lungs (A) have a highly subdivided parenchyma and a marked heterogeneous architecture. The paucicameral lungs (B and C) are less elaborately divided than the multicameral lungs but still display a heterogeneous division pattern. Unicameral lungs (D) are considerably less divided in comparison to (A) (B) and (C) but structural heterogeneity is still clearly evident. A: Crocodile, *Caiman crocodilus*; B: Varanid lizard, *Varanus exanthematicus*; C: Turtle, *Pseudemys scripta*; D: Teju lizard, *Tupinambis nigtopunctatus*. (From Duncker, 1978).

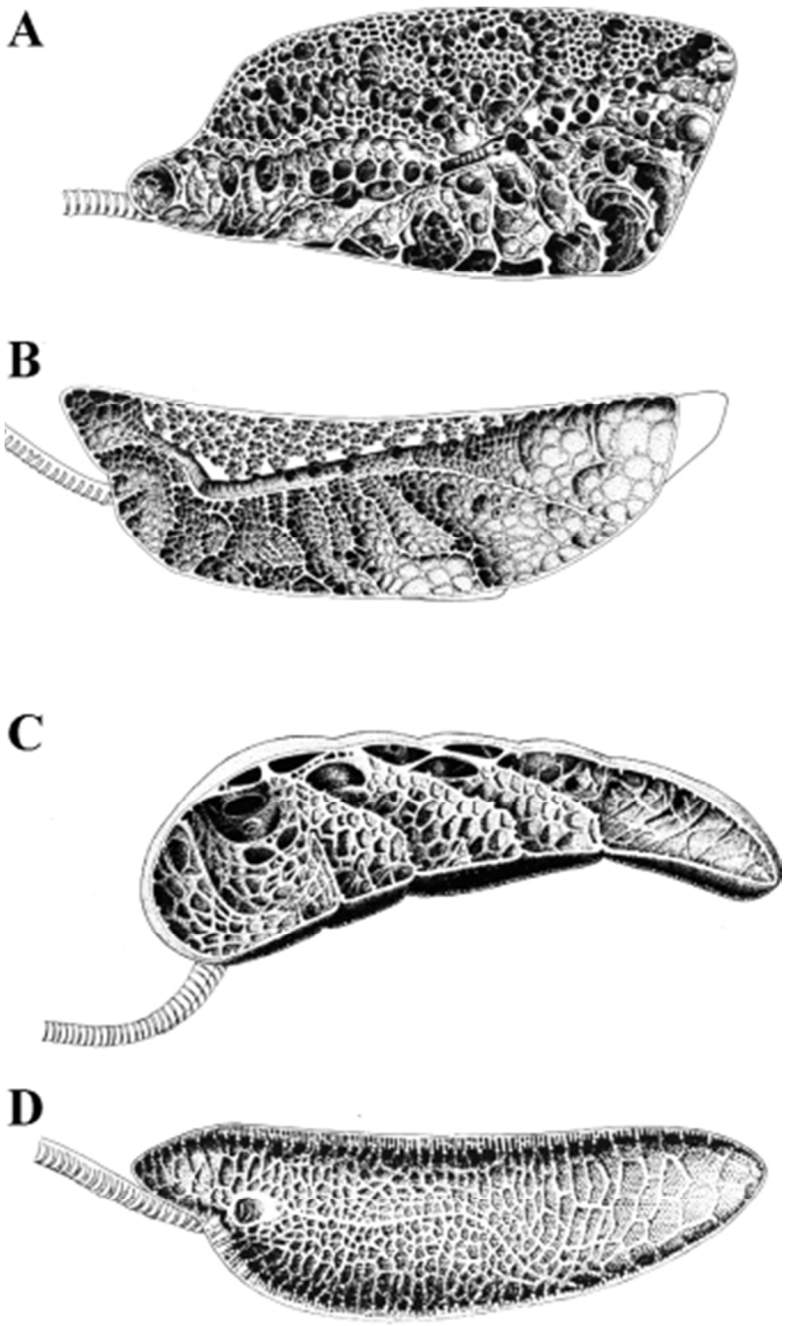
A
B
C
D

Reptilian lungs supply air directly to its terminal gas exchange units, ediculae (unicameral lungs) / faveoli (multicameral lungs), via a large central lumen during breathing episodes (Torday *et al.,* 2007). The term ediculae is derived from Latin meaning small wall recess and faveoli meaning honeycomb, both aptly applicable (Perry, 1998). The lungs of reptiles contain copious amounts of smooth muscle on septa (Perry, 1998), which is hypothesised to promote intrapulmonary convective movements (Perry and Duncker, 1980; Carrier, 1984) by contraction and relaxation. Delivery of oxygen to tissue cells is further aided by the reduction of oxygen consumption by the respiratory organ itself and the development of a thin blood-gas barrier (Maina, 2003). In combination with characteristic irregular breathing patterns and contractile properties, the reptilian lung may constitute an energy saving system (Milsom, 1984).

For animals that are of equivalent body mass, a reptile has a lung volume approximately seven times greater than that of a mammal (Crawford *et al.,* 1976; Glass and Johansen, 1981) however its diffusing capacity for oxygen is relatively low (Crawford *et al*., 1976). This leads to low lung compliance and results in increased rates of breathing when placed under metabolic stress (Perry, 1998). Reptiles also typically have lower metabolic rates (~10-fold) compared with birds and mammals of the same size but they have varying oxygen demands and so their lung structure has evolved accordingly (Powell and Hopkins, 2004) It has been speculated that due to structural shortfalls in the design of reptilian lungs endothermy – homeothermy failed to evolve (Maina, 2003).

Reptilian lungs, like all other vertebrate lungs, have auxiliary functions. These include being a hydrostatic organ (turtles and speculated in crocodiles), gular pumping to supplement normal costal breathing (Saalfeld, 1934a, 1934b; Owerkowicz and Brainerd, 1997), sound production for communication or as threat displays (Gans and Maderson,

1973; Marcellini, 1977) and lastly silent displays, e.g. chameleons which straighten their ribs for camouflage (Marcus, 1937).

## 1.4. The Crocodilian Lung

Crocodiles possess a multicameral lung that is characterised by numerous rows of tubular chambers, which are saccular, with caudal non respiratory dilations (Duncker, 1978, 2004; Perry, 1988, 1990). Generally, they are developed in three rows with at least four chambers in each row (Duncker, 2004). Faveoli which often have perforated capillary bearing walls, enhance the inner respiratory surface area of the air space (Perry, 1988). The lungs are sandwiched between the ribs and are also attached to the parietal pleura (Perry, 1988). The pleural cleft may be partially or totally absent but all lungs fuse with the post-pulmonary septum (Duncker, 1978; 2004) (as crocodiles don't have a diaphragm). The lungs generally fill the entire cranial body cavity, as far as the ribs support the body wall, and are separated from the viscera by means of the aforementioned post-pulmonary septum (Duncker, 1978; 2004).

Crocodiles enhance costal respiration using a muscle called the diaphragmaticus (Gans and Clark, 1976; Claessens, 2004; Farmer, 2006). The diaphragmaticus muscle originates from the pelvis and the posterior row of gastralia and inserts on a fascia surrounding the liver (Claessens, 2004). During inspiration, the muscle contracts which pulls the liver and lungs caudally (Claessens, 2004; Farmer, 2006). Simultaneously, the abdominal volume increases (Claessens, 2002, 2004; Farmer, 2006) due to the contraction of the ischiopubic and ischiotruncus muscles which rotate the pubes and gastralia ventrocaudally (Farmer and Carrier, 2000). Expiration occurs via intercostal musculature and by the contraction of the transversus abdominis and the rectus abdominis which pushes the liver forward and pulls the gastralia and pubes dorsocranially (Farmer and Carrier, 2000).

Figure 1.4: Line drawings of the ventral musculature of both the pelvis and abdomen of the American alligator (*Alligator mississippiensis*). A: an illustrated view of the ventral aspect of the abdomen and gastralia. Cartilage comprises the cranial halves of the pubic plates in juvenile alligators. By means of a collagenous sheet (anteriorly) and a lateral ligament, the pubic plates are attached to the last gastalium. B: The rectus abdominis and ischiocaudalis muscles. C: Ischiopubis muscle. D: An illustration in which the bottom half depicts the truncocaudalis muscle and the ischiotruncus muscle above it. The top half of the illustration, the truncocaudalis muscle has been removed so as show the ischiotruncus muscle. (From Farmer and Carrier, 2000).

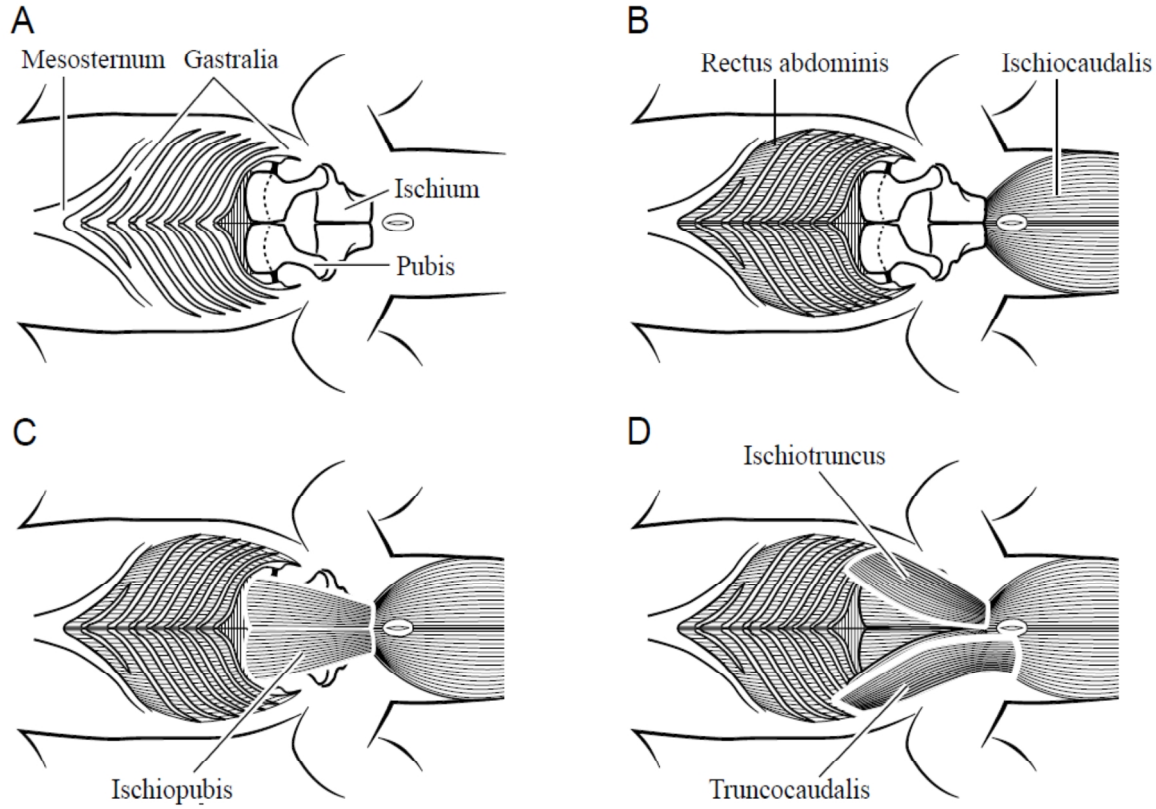
A
Mesosternum
Gastralia
Ischium
Pubis
B
Rectus abdominis
Ischiocaudalis
C
Ischiopubis
D
Ischiotruncus
Truncocaudalis

In the crocodilian lung, the anterior two thirds of the lung generally contain the bulk of the gaseous exchange tissue, defined as parenchyma (Perry, 1988). Smooth and poorly vascularised, the posterior third is hypothesised to store air (Heatwole, 1981), have a hydrostatic role (Graham *et al.*, 1975), and may mechanically ventilate the anteriorly located parenchyma (Maina *et al.,* 1989a). Even though the crocodilian lung appears to be capable of very efficient gas exchange, extant crocodilians appear to use only a fraction of the gas exchange potential of their respiratory system (Carrier 1987; Perry 1990).

According to Walker (1972) and Carroll (1988) birds are regarded as the closest extant relatives of the crocodilians, attributed to embryological evidence and certain unique archosaurian features which characterise both birds and crocodiles. One of these is the very similar pathway of lung evolution observed between crocodiles and birds (Torday *et al.,* 2007). This warrants a kaleidoscope of studies to observe the relationship between the two taxa so as to better understand the "story" of their evolutionary divergence and also that of their predecessors.

## 1.5. The Avian Lung

The evolution of the vertebrate respiratory system attained its highest state in birds with their volume constant parabronchial lungs and highly compliant air sacs (Scheid, 1979; Duncker, 2004). Mclelland (1989) describes the lung air sac system as "the most elaborate gas exchange design to have evolved among air breathing vertebrates and probably in the whole of the Animal Kingdom". Birds are understood to have evolved such an efficient gas exchanger in order to procure oxygen for flight at high speeds, over immense distances, and at great heights (Scheid and Piiper, 1985; Maina, 2003). The lung-air sac system, is unique to the class Aves (Maina, 1988) and is both a structurally complex (Duncker, 1978) and a functionally efficient one (Scheid 1979). The avian lung differs in

many aspects to other vertebrate lungs, e.g. to that of the branchioalveolar lungs of mammals and the faveolar lungs of reptiles, from which the mammalian and avian lung evolved from at different time intervals (Duncker, 1978; Perry, 1989a).

The avian lung is very compact and in addition is virtually nonexpansile (Jones et al., 1985; Maina 2003). It has a high respiratory surface area, which is generated via the intense partitioning of the parenchymal tissue, facilitated by the rigidity of the lungs (Maina, 2000b). This is despite the fact that in comparison to non-flying mammals, birds have smaller lungs per unit body mass (Maina, 1989). Within birds though, the degree of development of lungs vary, e.g. passerines operate at a higher body temperature (41$^{o}$C) than nonpasserine species (39$^{o}$C), (King and Farner, 1969) and have more specialized lungs (Maina, 1984).

The lungs are situated in the dorsal part of the thoracic cavity (Mclelland, 1989). They are flattened quadrilateral or triangular in shape, and generally extend to the first cervical rib and terminate close to the cranial margin of the ilium in most birds (Mclelland, 1989). The gas exchange efficiency of the avian lung can be accounted for due to the spatial organization, morphometric specialization of airways, and the vascular components of the pulmonary system (Maina, 1988). Maina (2003) describes the avian lung as “an elaborate, topographically stratified, contiguous, anastomosing system of air conduits”.

Parabronchi supply the air capillaries, terminal gas exchange units, with fresh air by means of the intricately arranged airways comprising the avian lung (Scheid, 1979; Fedde, 1980). Air sacs are the vital components of the respiratory system which ventilates the lung continuously, consistently and unidirectionally in a synchronized bellows manner (Maina, 2003). They are avascular and play no direct part in gas exchange itself (Magnussen *et al.,* 1976; Maina, 2003). As the avian lung has a limitation of inexspansibility, the air sacs

form the volume compliant element and generate the tidal flow of air in the respiratory tract (Mclelland, 1989).

During inspiration via the inflation of the air sacs, a pressure reduction occurs in the cranial air sacs with their connections to ventrobronchi inducing airflow out of parabronchi into the cranial air sacs (Scheid and Piiper, 1989; Powell, 2000; Duncker, 2004). The reduction of pressure in the cranial air sacs is compensated for by air flow through the dorsobronchi into the parabronchi, which is supplied by the inspiratory air flow through the primary bronchus into the posterior air sacs (Scheid and Piiper, 1989; Powell, 2000; Duncker, 2004). During expiration, air compression in the air sacs guides the air flow out of the posterior air sacs into the posteriorly oriented openings of the dorso - and laterobronchi, causing air to move through the parabronchi into the ventrobronchi and into the primary bronchus (Scheid and Piiper, 1989; Powell, 2000; Duncker, 2004).

This unique unidirectional ventilation of the lung during inspiration and expiration is the foundation for the highly efficient parabronchi cross current gas exchange (Powell and Scheid, 1989) which allows some birds active flight at heights of up to 10km and oxygen pressures as low as 35 mmHg (Scheid and Shams, 1995).

## 1.6. Unidirectional Air Flow

Until recently unidirectional air flow in the vertebrate lung was believed to be exclusive to the avian lung. This is the hypothesised reason for birds being able to meet the oxygen requirements of a high metabolism in order to fly (Maina, 2003). Air flow in the lungs of other vertebrates was believed to be tidal, in and out of the terminal gas exchange units (Farmer and Sanders, 2010). Farmer and Sanders (2010) recently changed this paradigm when they illustrated that unidirectional air flow occurs in the lung of the American alligator.

According to Farmer and Sanders (2010) important features of the avian aerodynamic valve are apparent in the alligator lung. They include:

- The cervical ventral bronchus (CVB) which is similar to the avian ventral bronchus, that connects the with the cervical air sacs
- The small ostium to the CVB which opens into a funnel shaped vestibule that is sharply angled with the intrapulmonary bronchus (IPB) such that the bronchus makes a "hairpin" turn ventrocranially before it moves cranially to the apex of the lung.
- Distal to the CVB ostium, the diameter of the IPB increases and to some extent becomes enclosed as it bends caudally and laterally. This gives rise to a pair of small medial paracardiac bronchi, a large individual dorsolateral bronchus and three caudal bronchi which originate from a common terminal intrabronchial chamber. The orifices of the bronchial branches are larger than the CVB orifice and are better aligned with the IPB. Most of these bronchial passages spiral dorsolaterally in the direction of the apex of the lung in a manner that is comparable to the avian dorsal bronchi.
- The dorsal bronchi connect to each other and the CVB via an abundance of anastomosing parabronchi.
- Small ostia to caudoventral bronchi occur opposite the ostia of the dorsal bronchi, as observed in the class aves. (Farmer and Sanders, 2010).

Perry (1988, 1990) postulated that unidirectional air flow could be viable in the crocodilian lung but conformed to the idea that it was tidal. Also, for typical avian respiration to occur, abdominal air sacs are considered a prerequisite (O'Connor and Claessens, 2005) and the hepatic piston system of crocodilians has to be presumed as discordant (Ruben *et al.,*

1999). Due to this scientific breakthrough, the notion of unidirectional airflow in the crocodilian lung posed by Perry (1988, 1990) has become a viable one. This is due to the fact that alligators and crocodiles are closely related and they would be expected to have similar organ systems, both structure and function. Whilst it has been established that unidirectional airflow occurs in the lung of the alligator, the mechanism by which it operates is still uncertain. Until such time that this is resolved, the evolution of the lung of can't be understood completely.

### 1.7.1. Aims and Objectives

Morphological and morphometric studies of the mature reptilian lung, in general, are to an extent well-documented (Tenney and Tenney, 1970; Perry, 1978; Meban, 1977, 1978; Perry and Duncker, 1978; Klemm *et al.,* 1979; Lutchtel and Kardong, 1981; Perry, 1981). However the only morphometric studies conducted on the mature crocodilian lung are those by Perry (1988, 1990) and furthermore no research, morphological or morphometric, has been conducted on the hatchling / young juvenile crocodilian lung.

The aims of the current research are to help understand the architecture of the crocodilian lung. This in turn should allow for a better understanding of the mechanisms and functions of the components of the lung and the lung as a whole. These findings can in turn be applied to better understand the behaviour and physiological processes of the crocodile and help ecologists in the environmental management and conservation of these organisms. This will help prevent the loss of mature breeding crocodiles and the development of healthier younger populations.

The objectives of this research were prompted by the scarcity of comprehensive morphological and morphometric data on the morphogenesis of crocodilian lungs. They are as follows:

- To conduct morphometric and morphological investigations into the morphogenesis of the crocodilian lung. This will entail:
    1. Obtaining comprehensive and complete data sets, morphological and morphometric, on juvenile and mature adult crocodilian lungs in order to acquire a pragmatic understanding of their lung structure and function.
    2. Combining the acquired morphological and morphometric data, from the juvenile and mature adult lungs. This will be done in order to illustrate how the respective lung morphologies are affected by the contributions of their constituent structural parameters during the course of their development from hatchlings to maturity.

### 1.7.2. Evolutionary Contribution of the Data from this Research

The data from this thesis will add vital information to the currently postulated reptile – avian pulmonary evolutionary theory, which basically hypothesises the evolution of the avian lung from the reptilian lung. As no comprehensive holistic studies have been conducted on the anatomical structures of the crocodilian lung, not enough evidence is present to correlate to the avian lung. This has resulted in multiple speculations and as a result left the theory vulnerable. Eventually, once all the missing pieces of this theory are filled in, Schied's (1990) question "*has the lung structure of birds evolved out of functional needs or simply out of structural constraints with no significance for the higher efficiency"* can be answered.

# Materials and Methods

## 2.1. Study Animals

All the samples, gathered and analysed, were from specimens of the Nile crocodile, *Crocodylus niloticus niloticus*. The crocodiles were obtained from Thaba Kwena Crocodile Farm (Bela Bela, Limpopo Province, South Africa) via the Central Animal Services (CAS) of the University of the Witwatersrand (Animal Ethics Clearance Number: 2011/14/2B). For the experiments carried out, 4 age categories were sampled, with 5 animals in each giving a total of 20 crocodiles. The ages sampled were:

- 2 – 3 months
- 6 months
- 12 months
- 24 months

## 2.2. Euthanasia, Intra-tracheal Instillation and Latex Casting

All the crocodiles were euthanised using an overdose of Sodium Pentobarbitione (Kyron, Johannesburg, South Africa) via an intraperitoneal injection (SANS:2008, 2008). For each age category, the lungs of 4 crocodiles were intra-tracheally instilled and the lungs of 1 crocodile cast using latex, both techniques were done *in situ*.

### 2.2.1. Intra-tracheal Instillation

Lungs were intratracheally instilled with 2.5% glutaraldehyde (Merck KGaA, Damstadt, Germany) buffered in a 0.1M sodium phosphate buffer (pH 7.4) (Appendix A). This was achieved by inserting a cannula, attached to a funnel, into the trachea. Fixative was then

poured down the funnel to the lungs at a pressure of 30cm of water. Once the lungs and all extrapulmonary airways were completely filled with fixative, the tracheae were ligated using twine. Subsequently, the lungs and extrapulmonary airways were carefully dissected out of the crocodiles' peritoneal cavities and immersed in 2.5% glutaraldehyde (Merck KGaA, Damstadt, Germany) buffered in a 0.1M sodium phosphate buffer (pH 7.4) (Appendix A), the same fixative they were instilled with, for 3 months. After this period, all extraneous connective tissue attached to the lung was trimmed away and sampling of the tissue commenced.

### 2.2.2. Latex Casting

Making latex casts of the lungs involved a process similar to the intra-tracheal instillation with a fixative (Adapted from Maina, *pers comm*). An apparatus (Figure 2.1) that has 2 independent closure valves (with attachments for disposable syringes) which attaches to a single cannula was used to achieve this. The first step was to insert the cannula into the trachea. A ligature was then loosely tied around the trachea to secure the cannula in place and prevent unnecessary air flow. An empty syringe was inserted into the valve closest to the attachment of the cannula to the apparatus. The other syringe was filled with a stock solution of 60% liquid latex (NJC Adhesive and Sealant Distributors, Industria West, South Africa) and attached to the other valve.

With the valve housing the latex syringe closed and the other open, the lungs were aspirated by extracting the air in the lungs. This was accomplished by the suction created by pulling the plunger of an empty syringe. This was repeated until as much air could be extracted as possible. Aspiration of the lungs is important as it allows the latex to occupy the full volume of the lung. The presence of air would also form air bubbles in the latex which would obscure the results.

After the aspiration of the lung, the first valve was closed and the valve housing the latex syringe opened. Latex was then injected into the lung until pressure was perceived. A good indicator of this was when the liquid latex started a backflow and the resistance on the syringe plunger increased. At that point, the tracheae were ligated and the lungs left *in situ* for the latex to set. Thereafter they were dissected out and immersed in water and housed in a fridge at ≈ 6 $^{o}$C. After a week, the casts were removed and all surrounding connective tissue dissected away. The rationale for creating latex casts was to encapsulate the gross morphology of the crocodilian lung as best as possible, with minimal or no damage to its naturally occurring structure.

Figure 2.1: A photograph of the apparatus used for latex casting.

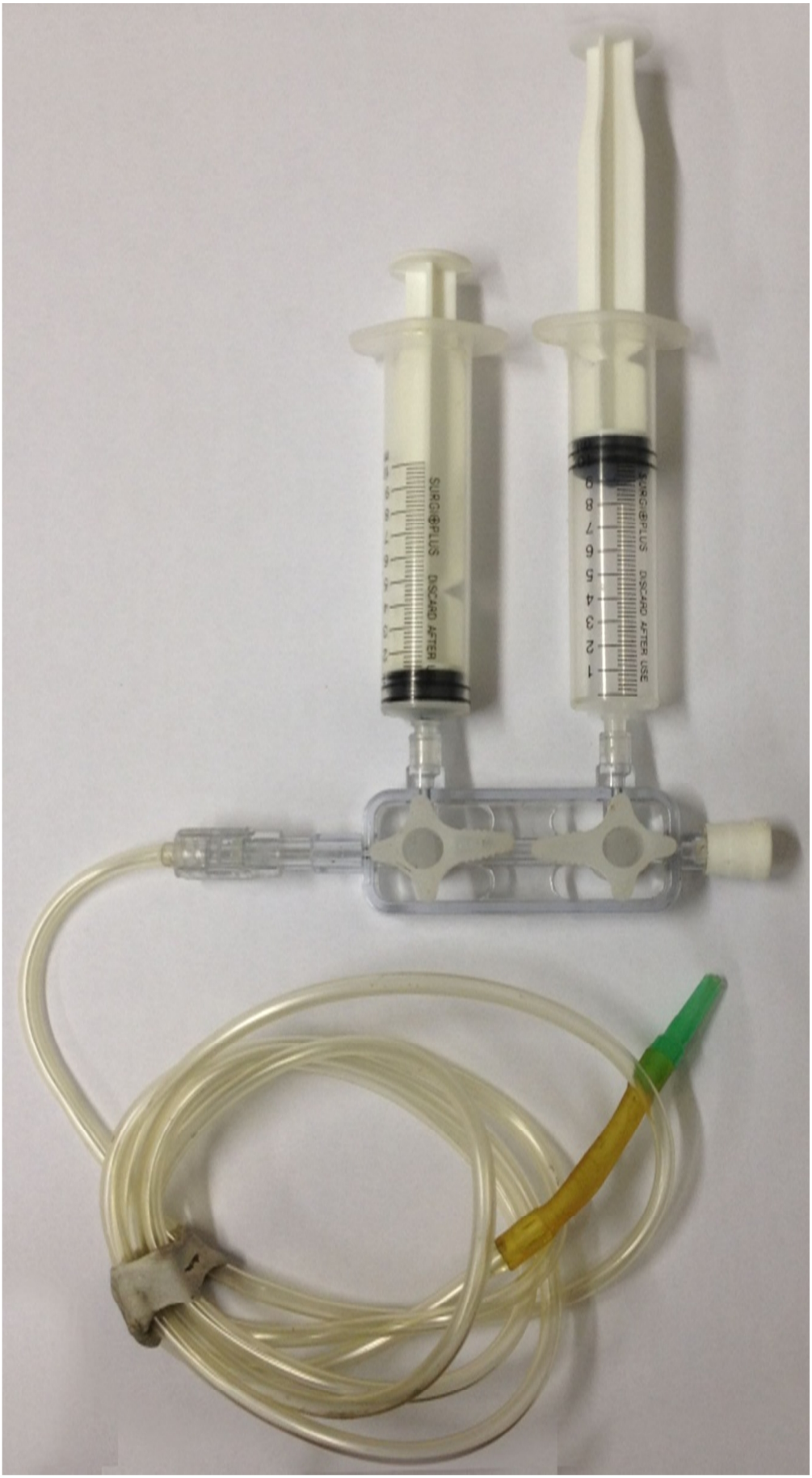
SURG@PLUS DISCARD AFTER USE
SURG@PLUS DISCARD AFTER USE

## 2.3. Volume Determination

The volume of 2 pairs of lungs that were intra-tracheally instilled with 2.5% glutaraldehyde (Merck KGaA, Damstadt, Germany) buffered in a 0.1M sodium phosphate buffer (pH 7.4) (Appendix A) was determined before sampling. This was done using Scherle's Method (Scherle, 1970), which is based on Archimedes principle. Briefly, this technique determines the volume of a structure by weight displacement. For the purposes of this study an Adams PGW 753e weigh balance (Adams equipment, Kempton Park, South Africa) was used to measure the displacement to two decimal points. Prior to the volume determination procedure, each lung was individually ligated at the extrapulmonary primary bronchus (EPPB) being very careful not to let any fixative leak out. Once this was successfully done, the extrapulmonary airways were trimmed away. The rationale for keeping the fixative in the lung is that the fixative occupies space that air would normally and that the true volume of the lung can be determined whilst its structural integrity is preserved.

Before any measurements were conducted, at normal room temperature, the weight balance was calibrated to account for the beaker and fixative in which the lung would be immersed in. It is important to note that during this procedure the lung can't float, sink or touch the sides of the beaker. In order to ensure this happens a coil attached to a string is used to position the lung in the middle of the beaker being totally submerged in the fixative. The weight of the coil and thread was also included into the calibration of the weight balance. Fixative was used as the medium of immersion as it would prevent any diffusion between the lung and immersion medium and also counter any effects that specific gravity of different media would impose. Also, because the specific gravity of 2.5% glutaraldehyde buffered in 0.1M sodium phosphate buffer (pH 7.4) (Appendix A) is

≈1.13, the measurements obtained were as accurate and precise as possible due to the effects of gravity were negligible. Three measures for an individual sample were taken with the average of these measurements being taken as the volume of the lung ($cm^3$).

The lungs that had their volumes determined were then prepared for light microscopy and serial sections were cut (Chapter 2.4.2). The cut sections were then used in a morphometric analysis (Chapter 2.5)

Figure 2.2: A line diagram illustrating the procedure used to determine lung volume using Scherle's method (From Scherle, 1970). (A) Illustrates the calibration procedure, where the beaker filled with fixative and the apparatus used to keep the lung immersed in the middle of the fluid filled beaker is tared to 0. (B) Demonstrates weight displacement of the lung, and thus its volume, after it's been immersed into the fixative as previously described.

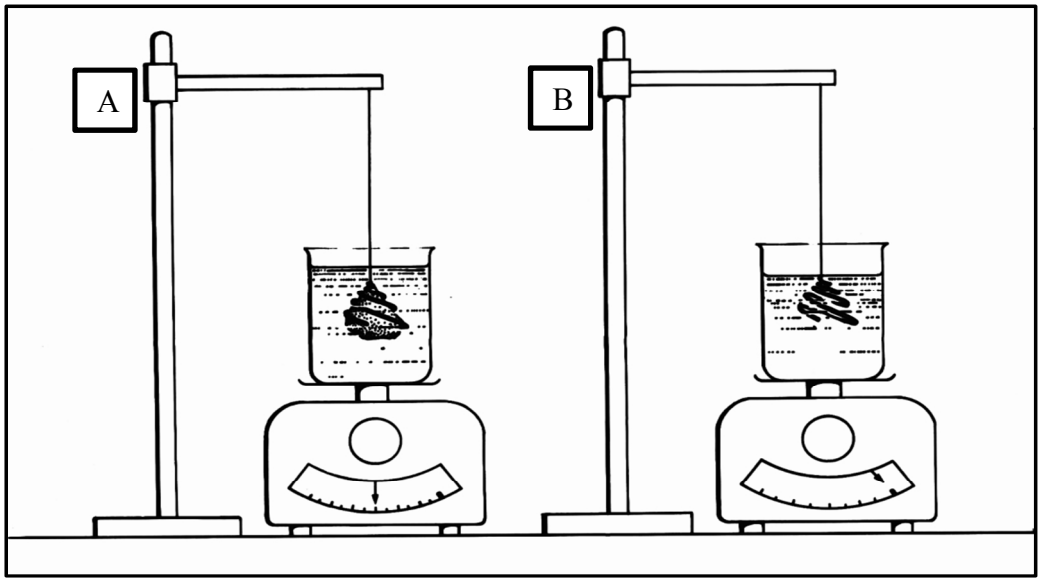
A
B

## 2.4. Morphology

### 2.4.1. Gross Morphology

After all the latex cast samples were set and all surrounding connective tissue removed, they were photographed using a Canon EOS 400D camera (Canon, Japan) with a Canon 70 – 300mm lens (Canon, Japan) attached to a Canon ring-flash (Canon, Japan). They were then dissected into dorsal and ventral halves and the inner surfaces of the respective halves were then photographed.

### 2.4.2. Light Microscopy

#### 2.4.2.1. Sampling of Lung Tissue

2 pairs of the 5 pairs of lungs, for each age category, were used for light microscopy (LM). Owing to the heterogeneity exhibited by the crocodilian lung, the lung was sampled using a systematic region sampling technique (Figure 2.3). First the lung was cut into dorsal and ventral halves (Figure 2.3A). From the dorsal and ventral halves, cranial (Cr), middle (M) and caudal (Ca) samples (ranging from 2 $mm^3$ in the 2 youngest age categories to 5 $mm^3$ in the two older age categories) were taken. The centre points of these sampling regions were defined by measuring the length of the lung and dividing it by 3 (Figure 2.3B). These points were then the defining point to measure the breadth of the respective regions (Figure 2.3C). The breadth of each of these regions were measured and divided by 2 to define a midpoint at which the respective samples would be taken (Figure 2.3C)

Figure 2.3: A flow diagram illustrating the systematic sampling procedure to obtain samples from the crocodile lungs. (A) Illustrates the division of the lung into dorsal and ventral halves. (B) demonstrates how the 3 defining regions are identified and (C) shows how the midpoints of these regions are calculated. Cr = Cranial, M = Middle, Ca = Caudal.

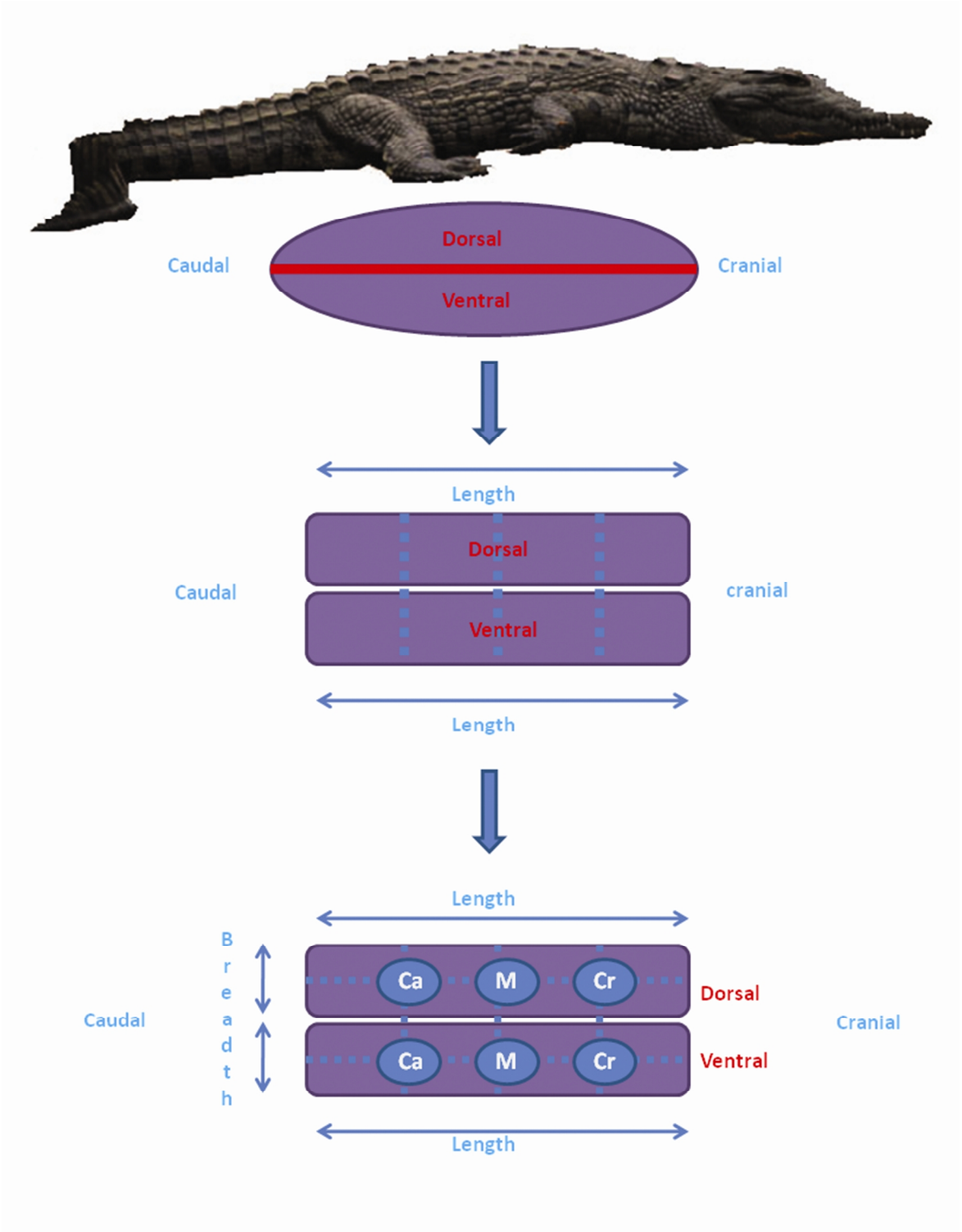
Dorsal
Caudal
Cranial
Ventral
Length
Dorsal
Caudal
cranial
Ventral
Length
Length
Breadth
Ca
M
Cr
Dorsal
Caudal
Cranial
Ca
M
Cr
Ventral
Length

2.4.2.2. Processing and Sectioning of the Sampled Lung Tissue

All processing was conducted at room temperature. The method of preparing the tissue is adapted from Anderson and Bancroft (2002). The tissue samples that were fixed in 2.5% glutaraldehyde (Merck KGaA, Damstadt, Germany) buffered in a 0.1M sodium phosphate buffer (pH 7.4) (Appendix A), for three months, were first washed in three changes of 0.1M sodium phosphate buffer (pH 7.4) (Appendix A) before being introduced into a Shanon Citadel ™ 1000 automated tissue processor (Thermo Scientific, USA). The processor dehydrated the samples in 70% alcohol for an hour, followed by three changes in 95% alcohol, the first change being after two hours and the following two after 1.5 hours. The samples were further dehydrated in three changes of absolute alcohol for an hour, 2 hours and an hour respectively. Once the samples had been dehydrated in the graded series of alcohols, they were processed through two changes of chloroform, the first for an hour and the second for two hours. On completion of the chloroform processing, the samples were transferred into two changes of liquid wax, where the time between the wax changes was 2 hours.

The lungs were then embedded in paraffin wax (VWR International LTD, Dublin, Ireland) on a Miles Scientific Tissue Tec® Cryo-console (Miles Scientific, Princeton, Minnesota, USA) and left to harden. Serial sections were cut on a Leica 2035 Biocut rotary microtome (Leica Instruments GmbH, Germany) at 5 µm using Feather S35 disposable microtome blades (FEATHER Safety Razor Co., Ltd, Japan). The cut sections were routinely stained (Appendix A) using haematoxylin (Merck KGaA, Darmstadt, Germany) and counter stained with eosin (Merck KGaA, Darmstadt, Germany), (H&E, Appendix A) (Anderson and Bancroft, 2002). Thereafter they were cover slipped with Entellan mounting medium (Merck KGaA, Darmstadt, Germany) and dried at room temperature.

All the sections were examined using a Zeiss Montagesatz T-UL research microscope (Zeiss Instruments, Jena, Germany) and photographed using a Zeiss AXIOSKOP 2 plus microscope (Zeiss Instruments, Jena, Germany) with a camera attached to it (Zeiss AxioCam HRc, Carl Zeiss, Oberkochen, Germany). The images were captured using the AxioVision software 40 v 4.8.0.0 (Carl Zeiss Imaging Solution GmbH, Carl Zeiss, Oberkochen, Germany) at dimensions of 1388 x 1040 and at a resolution of 150 DPI.

### 2.4.3. Scanning Electron Microscopy

Another 2 pairs of the 5 pairs of lungs, for each age category, were used for scanning electron microscopy (SEM). The lung was systematically sampled in the same manner as that for light microscopy (chapter 2.4.2.1). After tissue samples were obtained, they were washed in three changes of 0.1M sodium phosphate buffer (pH 7.4) (Appendix A). They were then placed into a fresh solution of 2.5% glutaraldehyde (Merck KgaA, Damstadt, Germany) buffered in a 0.1M sodium phosphate buffer (pH 7.4) (Appendix A), for a minimum of 1 week, before being processed for viewing on the microscope. Due to the delicate nature and limited number of samples available, a pilot study testing for the optimal tissue preparation, for viewing and ultrastructural preservation, was conducted. See Appendix C for a summary of the results of this study. Samples for these tests were taken randomly from lung tissue that had already been systematically sampled. 2 processing methodologies and 2 drying methods were tested in combination. The OTO method and drying samples using hexamethyldisilazane yielded the best results and was thus used to prepare samples for viewing.

#### 2.4.3.1. The “OTO method”

This method is adapted from Kelly *et al*. (1973). Samples were incubated, at room temperature, in a 1% aqueous osmium tetroxide (Agar Scientific Ltd., Essex, England)

solution (Appendix A) for an hour. This was followed by 5 washes with double distilled water ($ddH_2O$) over 10 minutes. Following this, the samples were incubated (at normal room temperature) in a 1% aqueous thiosemicarbazide (The British Drug Houses Ltd., Poole, England) solution (Appendix A) for 10 minutes. This was followed by a further 5 washes of the samples with $ddH_2O$ over 10 minutes. The samples were again incubated (at room temperature) in a 1% osmium tetroxide aqueous solution (Agar Scientific Ltd., Essex, England) (Appendix A) and washed in $ddH_2O$, as in the first step of this method.

#### 2.4.3.2. Dehydration of the Processed Samples

All the samples prepared by the respective techniques were then dehydrated in an ascending series of ethanol, 20 minutes each (50%, 70%, 90%, 95% and two changes of 100%). The samples were then immersed in 100% hexamethyldisilazane (HMDS) (Sigma-Aldrich CHEMIE, GmbH, Germany) for 3 minutes and quickly removed to a desiccator containing silica gel for 24 hours to allow for further drying and to prevent water contamination.

#### 2.4.3.3. Mounting, Sputter Coating and Viewing of Samples

Following the drying procedures, the samples were mounted onto aluminium stubs under a Leica Wild M3B dissecting microscope (Leica, Heerbrugg, Switzerland) using double sided carbon tape. All the samples were sputter coated with gold palladium using an EMITECH K550 X (Emitech Ltd., Kent, England) sputter coater to a thickness of 15 nm. The samples were then examined and photographed using three scanning electron microscopes namely, FEI QUANTA 400 E SEM (FEI Company, USA), and a ZEISS, FIB / SEM cross beam, Auriga (Zeiss, Oberkoden, Germany). Both the FEI microscopes were used for the pilot study.

## 2.4.4. Transmission Electron Microscopy

Tissue that was trimmed off blocks in the preparation of SEM samples, fixed in 2.5% glutaraldehyde (Merck KgaA, Damstadt, Germany) buffered in a 0.1M sodium phosphate buffer (pH 7.4) (Appendix A), for the various age categories, was used for transmission electron microscopy. Samples were processed at room temperature unless otherwise stated.

After tissue samples were obtained, they were washed in three changes of 0.1M sodium phosphate buffer (pH 7.4) (Appendix A) for 5 minutes. Subsequently, the tissue was post fixed in an aqueous solution of 1% osmium tetroxide (Agar Scientific Ltd., Essex, England) in 0.1M sodium phosphate buffer (pH 7.4) (Appendix A) for an hour. All the samples were then dehydrated in an ascending series of ethanol, 10 minutes each (50%, 70%, 90%, 95% and two changes of 100%). Using propylene oxide (Merck KgaA, Damstadt, Germany), two changes at 10 minutes each, clearing of the tissue was conducted. An Embed – 812 Araldite resin (Electron Microscopy Sciences, Hatfield, Pennsylvania, USA) activated with DMP – 30 (Agar Scientific Ltd., Essex, England) was used to infiltrate the tissue samples.

In order to do this, samples were passed through three increasing concentrations of the embedding resin made up with propylene oxide (Merck KgaA, Damstadt, Germany) (Appendix A), each for an hour. The three ratios used (resin: propylene oxide (Merck KgaA, Damstadt, Germany)) were 25:75, 50:50 and 75:25. The tissues were then embedded in pure embedding medium for 24 hours in a Memmert 854 resin oven (Memmert, Schwabach, West Germany) at 60$^{o}$C. Semi thin sections (1µm) of tissue sample blocks were cut using a Leica Ultracut UCT ultra-microtome (Leica Microsystems, Bannockburn, Illinois, USA) and stained with 0.5% toluidine blue (SPI – Chem, West Chester, Pennsylvania, USA)

(Appendix A) in order to orientate the block for gold sections to be cut. Ultrathin sections were cut using glass knives made using on a LKB knife maker Type7801A (LKB produkter, Stockholm, Sweden). These sections were picked up onto 200 mesh copper grids (Ted Pella, Redding, California, USA). The grids were stained with a 5% aqueous uranyl acetate (Electron Microscopy Sciences, Hatfield, Pennsylvania, USA) solution (Appendix A) for 3 minutes, rinsed in three changes of 50% methanol and allowed to dry for 10 minutes before being stained for a further 2 minutes in a 1% aqueous lead citrate (Electron Microscopy Sciences, Hatfield, Pennsylvania, USA) solution in 4% concentrated sodium hydroxide (Merck KgaA, Damstadt, Germany) (Appendix A). The grids were then rinsed in diluted sodium hydroxide followed by three changes of distilled water. They were allowed to dry before transferring them to a grid boxe for storage. Sections were viewed and photographed on a Jeol JEM – 100S transmission electron microscope (Jeol, Tokyo, Japan) at an accelerated voltage of 80kV.

### 2.4.5. Confocal Microscopy

The method used for this research was adapted from the protocols and support product inserts from Lonza (Lonza Walkersville Inc, Walkersville, Maryland, USA). All tissue preparation occurred at room temperature. Sections were cut from light microscopy blocks (Chapter 2.4.2) and placed onto slides. The slides containing the sections were de-waxed using two changes of xylene, 10 minutes each and then dipped 10 times in two changes of 100% alcohol and a further 10 times in two changes of 95% alcohol. After this procedure they were washed with two changes of phosphate buffer saline (PBS) (Appendix A), 5 minutes each, and then placed into a 0.1% Triton ® X – 100 (Sigma-Aldrich Chemie, GmbH, Germany) in 0.1% bovine serum albumin (BSA) (Sigma-Aldrich, St Louis, Missouri, USA)/PBS solution (Appendix A) for a further 5 minutes to permeabilise the

sections. Subsequently, the sections were washed in two changes of PBS (Appendix A). The sections were covered with a 2.5% Phalloidin, Alexa Fluor® 488 Conjugate (Cambrex Bio Science Walkersville Inc, Walkersville, Maryland, USA) / PBS staining solution (Appendix A) for 20 minutes and thereafter washed in three changes of PBS (Appendix A), 5 minutes each. The stained sections were then mounted with an anti – fade mountant, Sigma Fluromont F – 4680 (Sigma-Aldrich Chemie, GmbH, Germany) and stored in the dark before being viewed on a Zeiss LSM 780 confocal microscope (Zeiss, Heidelberg, Germany).

### 2.4.6. 3 Dimensional Serial Section Computer Reconstruction

Multiple series of serial images, for each sampled region for each age category, were photographed using a Zeiss AXIOSKOP 2 plus microscope (Zeiss Instruments, Jena, Germany) with a camera attached to it (Zeiss AxioCam HRc, Carl Zeiss, Oberkochen, Germany). All the pictures were taken at a magnification of 50x. Images were collected in a Jpeg (Joint Photographic Experts Group) image format with dimensions of 1388 x 1040 pixels and at a resolution of 150 DPI.

The captured images were then down-sampled to 5 μm per pixel (equal to the z – dimension / section thickness) and with the use of Adobe Photoshop® CS5, Version 12.1 x64 (1990 – 2011, Adobe Systems Incorporated) balanced. Subsequently the images were converted to grey scale and exported to raw file format with the use of IrfanView, Version 4.20 (1996 – 2008, Irfan Skiljan©). These images were imported into Spider, Version UNIX 17.05 (Spider© Health Research Inc.) (Frank *et al*., 1996) and then normalised to a mean of 0 and a standard deviation of 1. To select areas of interest BOXER (1999, Boxer©, Steve Ludke) was used (Ludke *et al*., 1999). Areas of interest were selected at specific dimensions and cropped.

Using the methods of Woodward and Maina (2008), images were aligned and segmented by means of algorithms. This basic premise involved aligning images by maximising the normalised correlation coefficient (Maina and Woodward, 2009). This encompassed the rotation of the search window through a range of $-30^{o}$ to $+30^{o}$, at $1^{o}$ increments.

The coefficient with the highest value is representative of the best alignment between the active search window and the following image (Roseman, 2003). After the respective images were aligned they were observed individually to check that the alignment process was unremitting and that no erratic alignment errors occurred. Once these precautionary checks were conducted, the aligned images were combined into volumes and Fourier filtered using Spider, Version UNIX 17.05 (Spider© Health Research Inc.).

In order to view the 3D constructions, copies of the aligned and filtered volumes were contrast-inverted and opened simultaneously in UCSF Chimera package (Resource for Biocomputing, Visualization and Informatics at the University of California supported by NIH P41 RR-01081), Version 1.3 (build 5277) (Regents of the University of California©) (Pettersen *et al.,* 2004). Two threshold levels were selected, voxels failing to meet the lower threshold were assigned to the class of septa / blood vessels and those above the higher threshold were assigned to the class of airways.

Voxels (the smallest distinguishable box-shaped part of a three-dimensional space) in between the lower and higher thresholds were not assigned to any of the respective classes. In order to determine the optimal thresholding and filtering parameters, comparisons were conducted between the profiles of the structures of interest with the original histological sections (Woodward and Maina, 2008).

The rotation and viewing manipulations conducted on the 3D reconstructions were done interactively. The parenchyma (septa and blood vessels) and non – parenchyma (airways)

were isolated from one another and merged to determine the exact architectures of the respective component interactions throughout the entire reconstruction of the respective sampled areas of the lungs. Rendering and volume manipulations conducted on the 3D reconstructions were completed by means of the UCSF Chimera package (Resource for Biocomputing, Visualization and Informatics at the University of California supported by NIH P41 RR-01081), Version 1.3 (build 5277) (Regents of the University of California©) (Pettersen *et al.,* 2004). Computation of the reconstructions were conducted using a Intel® Duo™ 2 Core processor, CPU E8400 with 2GB RAM at 3.00 GHz (Model No: Hp Compaq dx 7400 Microtower) under the Ubuntu Linux, Version 8.10 operating system (open source license).

Figure 2.4: A summarised graphical representation of the algorithms that were used to align sections for the 3D serial section computer reconstructions. This is then padded and aligned with the next image in the sequence (image 2). The peak correlation value, which is representative of the x and y translations and in plane rotations required to optimally align the area of interest in the next micrograph, is identified. These values are utilised to window the image thus producing a new search window (image 2). This process is repeated for every image in the micrograph stack with a resultant aligned image stack being produced.

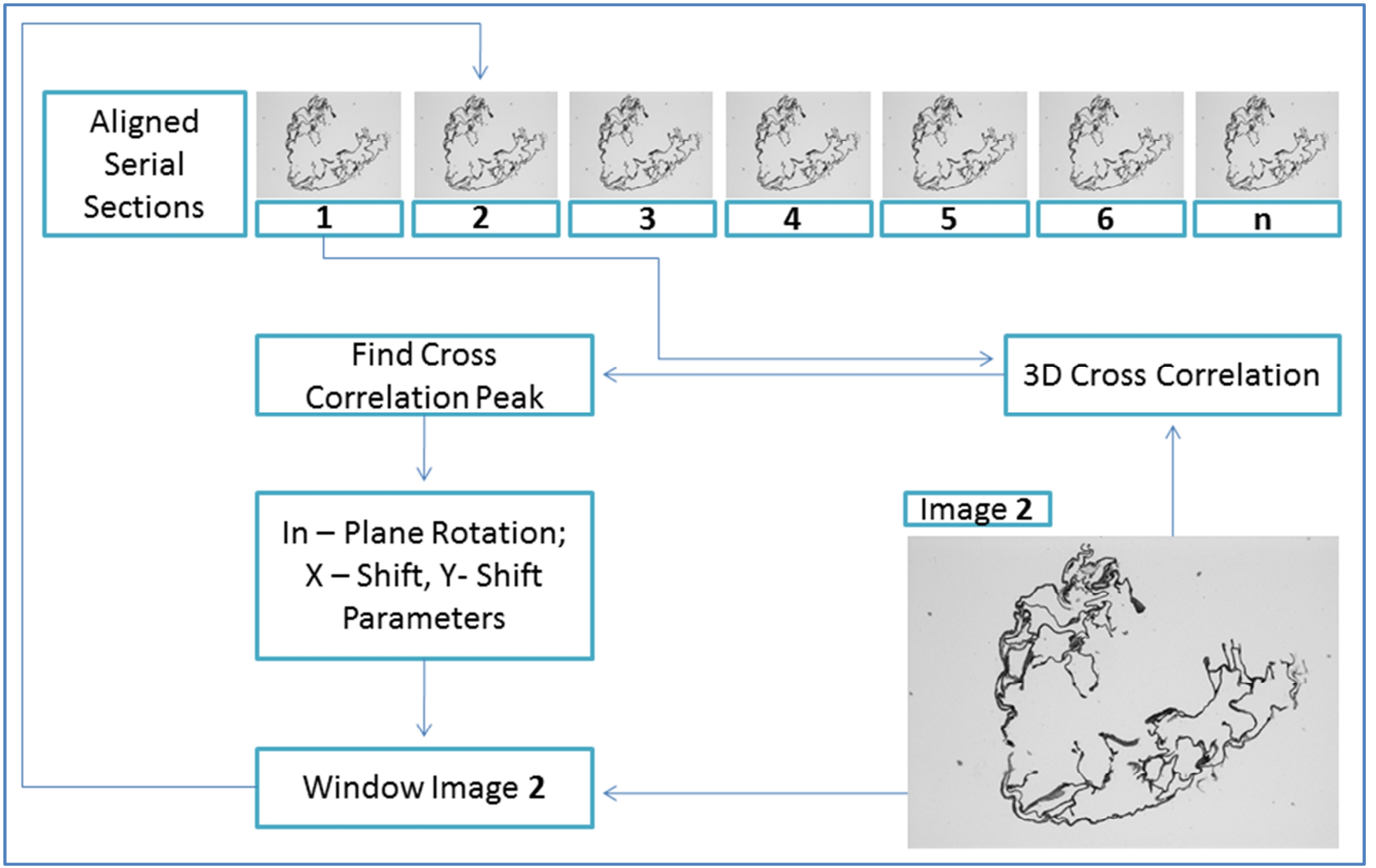
Aligned Serial Sections
1
2
3
4
5
6
n
Find Cross Correlation Peak
3D Cross Correlation
In – Plane Rotation; X – Shift, Y- Shift Parameters
Image 2
Window Image 2

## 2.5. Morphometry

### 2.5.1. Techniques, Parameters and Processes

Serial sections (from 2 age group categories), stained with H&E, of the systematically sampled regions of the various age group categories were used for this analysis (Chapter 2.4.2). Stereology (Weibel, 1979) was used as the technique to quantify the lung. Two parameters were quantified namely, parenchyma and non- parenchyma. Table 2.1 gives a detailed breakdown of what parenchyma and non-parenchyma are comprised of.

Table 2.1: A systematic breakdown of the components that constitute the parenchyma and non-parenchyma of the crocodilian lung.

| **Parenchyma** | **Non-Parenchyma** |
|---|---|
| Faveoli (Terminal Gas Exchange Units) | Central Air Duct and Large Airways |
| Interfaveolar Septa | Cartilage, Large Trabecuale and Smooth Muscle |
| Small Blood Vessels | Large Blood Vessels |

This analysis was conducted at a magnification of 100x on a Zeiss Montagesatz T-UL research microscope (Zeiss Instruments, Jena, Germany) using a 100 point quadratic lattice integrating graticule (Zeiss Instruments, Jena, Germany) which was inserted into an interchangeable graticule holder eye piece (Zeiss Instruments, Jena, Germany). By means of systematic point counting the sections were fully analysed to calculate the volume density (Vv) (the volume proportion of the different structural components of the lung expressed as a perecentage) of the parenchyma ($Vv_{par}$) and non-parenchyma ($Vv_{non\text{-}par}$).

Point-counting involves placing sections under a microscope, fitted with the aforementioned graticule, and counting the number of points that bisect each of the individual components (Pc). Points are defined as the intersection of horizontal and vertical lines in the test or reference system (the quadratic lattice of the graticule). The total number of points that bisect a component (Pc) are then divided by the number of points in the test system (PT) in order to determine its volume density ($Vv_c$): $Vv_c$ = (Pc / PT) x 100. This was done for each field of view of the analysed sections and an average $Vv_c$ per section calculated. An average of the section averages were calculated and used in absolute volume calculations (Av). The Av that a component would occupy, if it occupied the entire lung, is calculated by multiplying the (average $Vv_c$/100) by the volume of the lung, (Vl): $Av_c$ = (average $Vv_c$/100) x Vl. This is important to note as regional samples were analysed and not the entire lung. The Av results displayed for each sampled region is indicative of what $Av_c$ would be if it occupied the entire lung.

The sufficiency of the number of sections to be analysed was be ascertained by plotting cumulative summation average graphs of data acquired from stratified sections (Weibel, 1979). The sufficiency of the number of points counted for the aforementioned components was determined by means of a standard nomogram given by Weibel (1979) (Figure 2.6). The number of points counted for the structural components gave an expected relative standard error (in percentage of mean) of below 2%.

Figure 2.5 A: A low power (50x magnification) light microscope micrograph of a crocodilian lung with a quadratic lattice overlaying a field of view. The micrograph shows the definition of a point (circles, parenchyma = orange circles and non-parenchyma = blue circles) bisecting a component in a test or reference system (square). As observed in the micrograph the reference system must lie completely within a field of view. At higher magnifications and on larger sections more fields of view will be obtained.

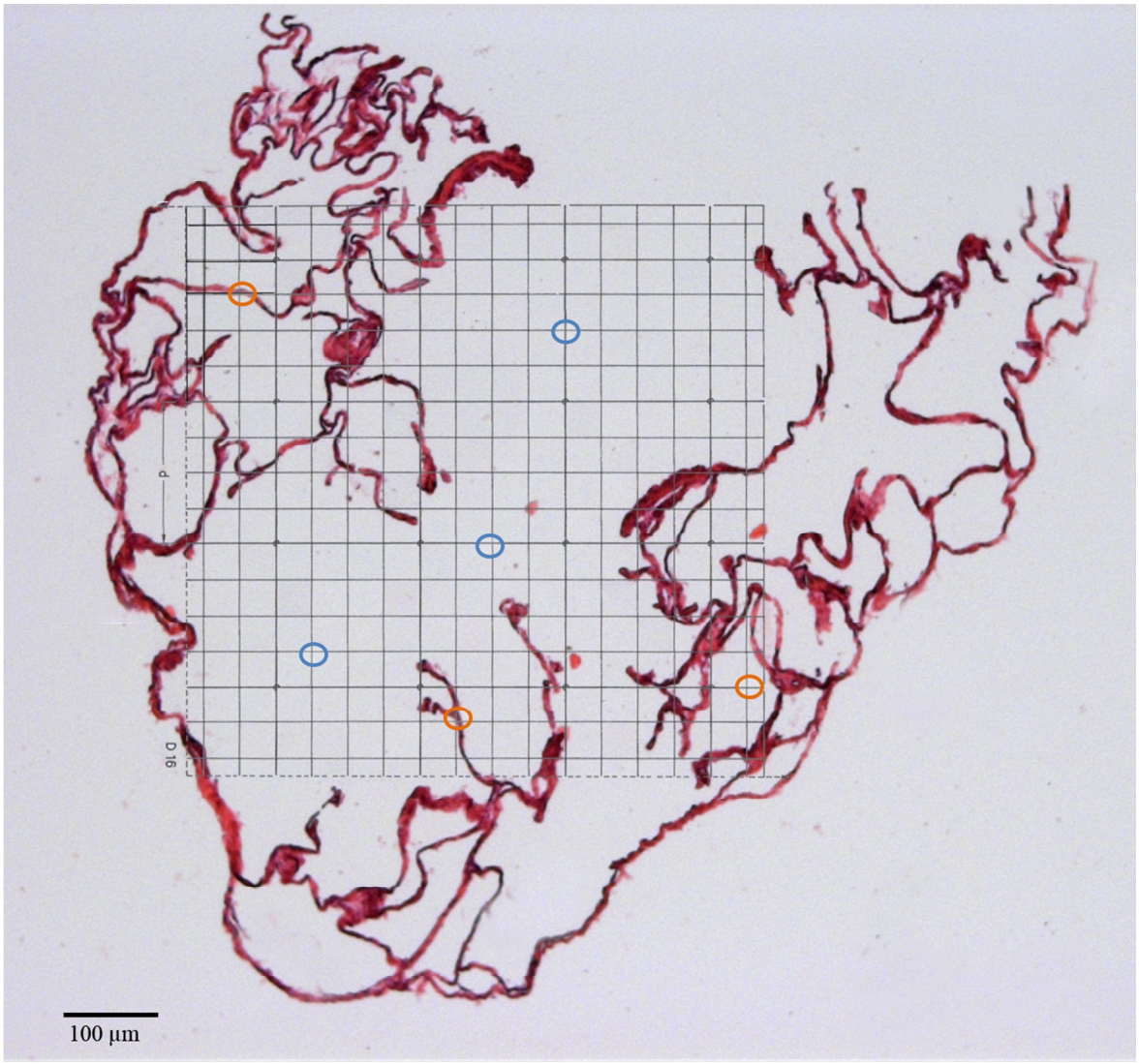
100 µm

Figure 2.5 B: A flow diagram showing the acquisition of data and accompanying calculations.

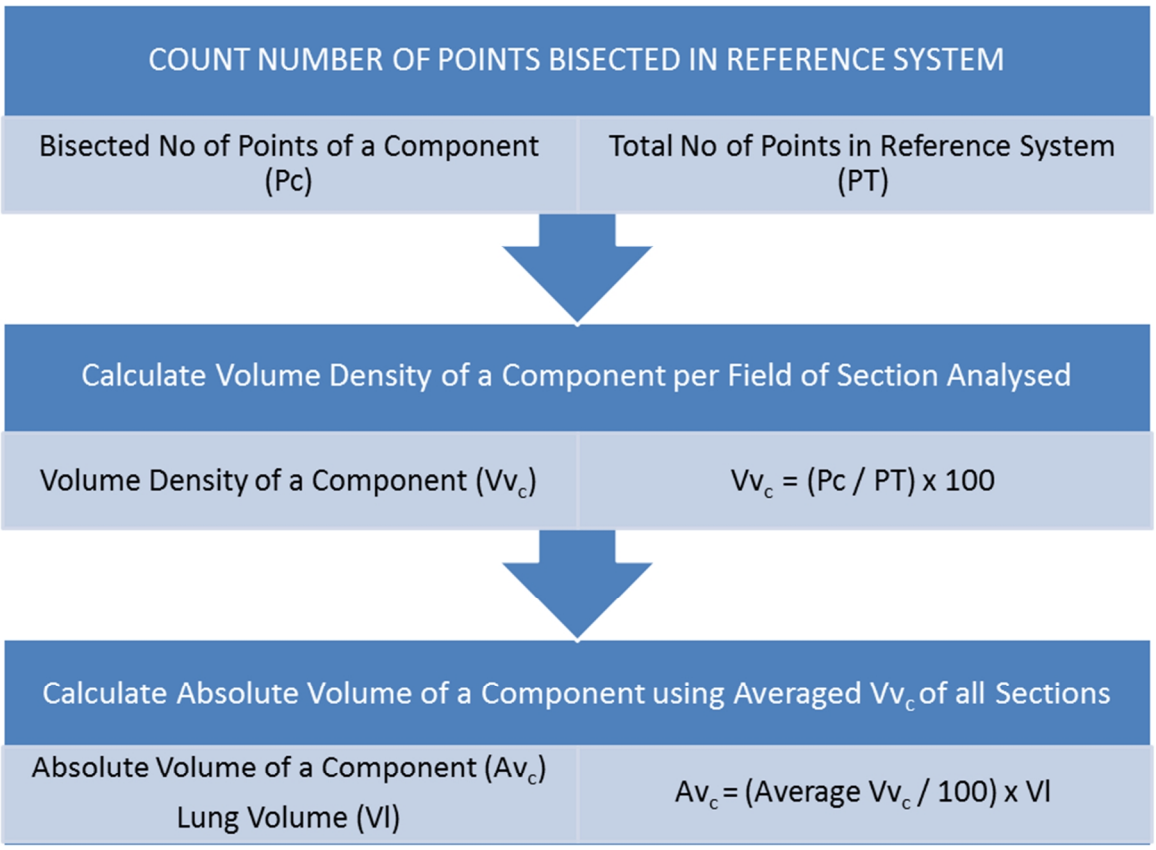
COUNT NUMBER OF POINTS BISECTED IN REFERENCE SYSTEM
Bisected No of Points of a Component (Pc)
Total No of Points in Reference System (PT)
Calculate Volume Density of a Component per Field of Section Analysed
Volume Density of a Component ($Vv_c$)
$Vv_c = (Pc / PT) \times 100$
Calculate Absolute Volume of a Component using Averaged $Vv_c$ of all Sections
Absolute Volume of a Component ($Av_c$)
Lung Volume (Vl)
$Av_c = (\text{Average } Vv_c / 100) \times Vl$

Figure 2.6: A nomogram used to determine the sufficiency of the number of points counted (From Weibel, 1979). The nomogram relates test point number to Vv and expected relative standard error (in percentage of mean).

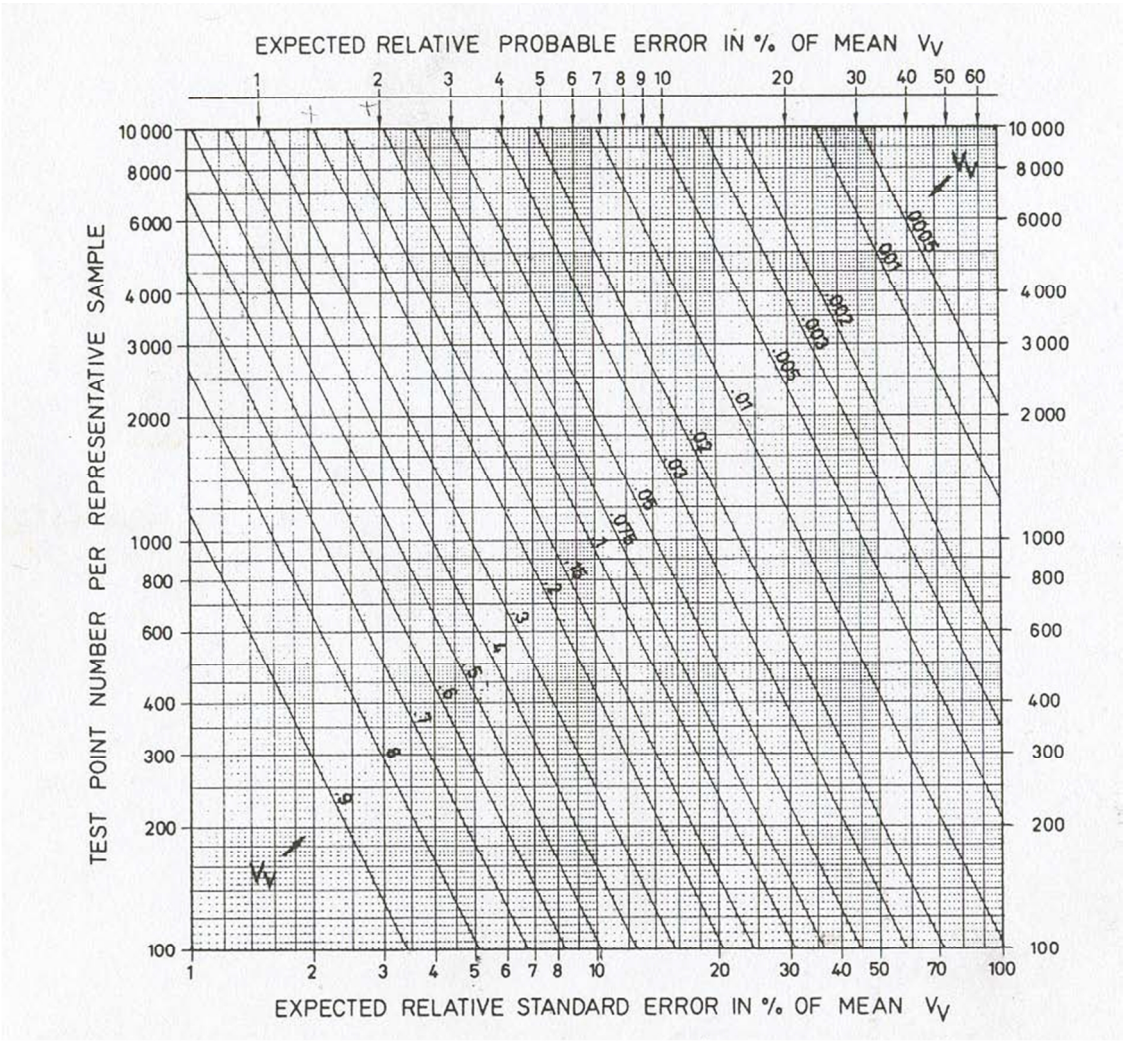
EXPECTED RELATIVE PROBABLE ERROR IN % OF MEAN $V_V$
1 2 3 4 5 6 7 8 9 10 20 30 40 50 60
TEST POINT NUMBER PER REPRESENTATIVE SAMPLE
10 000 8000 6000 4 000 3000 2000 1000 800 600 400 300 200 100
$V_V$
.0005 .001 .002 .003 .005 .01 .02 .03 .05 .075 .1 .15 .2 .3 .4 .5 .6 .7 .8 .9
1 2 3 4 5 6 7 8 10 20 30 40 50 70 100
EXPECTED RELATIVE STANDARD ERROR IN % OF MEAN $V_V$

### 2.5.2. Statistical Analyses

Point count data for the various age group categories was captured using Microsoft Excel 2010 (2011, Microsoft Corporation©). This data was exported into JMP® 10.0.0 (2012, SAS Institute Inc.©). Linear graphs of volume density (parenchyma versus non-parenchyma) and absolute volume (parenchyma versus non-parenchyma) of the systematically sampled regions of the lungs across the age group categories were plotted.

One way ANOVA's were conducted to ascertain if there was a difference between the parenchyma and non –parenchyma of the systematically sampled regions between the age group categories. All statistical analyses conducted were at a 5% level of significance.

Table 2.2: A breakdown of statistical tests conducted

| TEST | PARAMETERS TESTED |
|---|---|
| One way ANOVA | Parenchyma of respective systematically sampled regions between all age group categories |
| One way ANOVA | Non - parenchyma of respective systematically sampled regions between all age group categories |

# Results

## 3.1. Morphology

### 3.1.1. Latex Casting

Latex casting has been used successfully and commendably in pulmonary studies (Frasca *et al*., 1978; Guntheroth *et al*., 1982; Maina, 1982, 1987, 1988; Maina *et al.*, 1989b, 1999). The only major shortcoming of this technique is that artefacts may by generated from extravasates if the pressure of injection of latex is too high or too low (Maina, 1988). No extravasates were observed in the latex cast preparations in this study. This is indicative that the aspiration and injection of latex into the lungs were done at the correct pressure.

Lungs were cast in latex in order to conceptualise its gross morphology as close to its naturally occurring state as possible. From observations of latex cast lungs, the latex doesn't shrink / shrinks minimally and binds to tissue very well. This makes it an ideal casting material for the crocodilian lung. Due to these properties the arrangement of structures aren't obscured as opposed to fixed tissue which is vulnerable to shrinkage and as a result loss of structural integrity. Furthermore latex casts are pliable (Maina, 1988) which make specimens more versatile and easier to study with less risk of damage to the lung.

Lung specimens, for the various age categories, allocated to pulmonary latex casting were all aptly set. The liquid latex filled the entire lung before solidifying into a solid pliable coagulum. Upon dissection of casts, the latex was found to be evenly distributed through the entire lung.

All the cast samples from the various age group categories displayed similar morphological characteristics, both on external surfaces and internal surfaces (Figures 3.1.1 – 3.1.4). For each of the age categories the lungs were enantiomers of each other in (Figures 3.1.1 – 3.1.4). An exception with regard to length was observed in the 3 month and 6 month age categories. The variation in lengths between the right and left lungs were clearly evident (Figures 3.1.1 and 3.1.2). The variation in lung length observed in these two age group categories conforms with the findings of Schachner *et al*., (2013) however, the length of the right and left lungs of the 12 month and 24 month age categories were fairly congruent (Figures 3.1.3 and 3.1.4).

Each lung has a conical shape. The caudal region of the lungs, which are attached to the liver, is broad and sac-like (Figures 3.1.1 – 3.1.4). The middle region of the lungs is smaller in diameter than the caudal region and continually decreases in diameter in a cranial direction (Figures 3.1.1 – 3.1.4). The cranial region of the lungs has the smallest diameter of all the regions. It terminates in an apex which extends to the base of the neck between the shoulder girdle and oesophagus.

The external dorsal surface view of all the cast specimens illustrated a smooth surface (Figures 3.1.1 A, 3.1.2 A, 3.1.3 A and 3.1.4 A) whilst the external ventral surfaces exhibited a granular partitioned surface (Figures 3.1.1 B, 3.1.2 B, 3.1.3 B and 3.1.4 B). Each lung has an extrapulmonary primary bronchus (EPPB), derived from the bifurcation of the trachea (Tr) (Figures 3.1.1 B, 3.1.2 A and B, 3.3.1 A and B and 3.4.1 A and B). The EPPB enters the lung at a hilum located along the medial side of the middle region of the ventral half of the lung (Figures 3.1.1 B, 3.1.2 B, 3.1.3 B and 3.1.4 B). Upon entering the lung the EPPB is called the intrapulmonary primary bronchus (IPPB), not shown here.

When the lung casts were dissected into dorsal and ventral halves the inner surface views illustrated clearly defining borders of the conical shape of the lung (Figures 3.1.1 C and D, 3.1.2 C and D, 3.1.3 C and D and 3.1.4 C and D). The interstitium appeared as a homogenous mass due to the set latex. All the small airways were filled and thus not visible however some borders and spaces of larger airways were observable Figures 3.1.1 C and D, 3.1.2 C and D, 3.1.3 C and D and 3.1.4 C and D). The majority of these airways were apparent in the middle regions of the respective halves of all cast specimens (Figures 3.1.1 C and D, 3.1.2 C and D, 3.1.3 C and D and 3.1.4 C and D).

In summary the latex casts show that throughout the age group categories, the conical shape of the lung remains constant even though the size of the lungs increase with age. The cranial regions of the lung are the narrowest regions of the lung with the caudal regions of the lung being the broadest (sac like). In all age group categories, the EPPB enters the lung at a hilum located on the ventral middle region of the lung and originates from a trachea that bifurcates.

The length and spacing of the trachea and EPPB (external airways) from each other increased with an increase in age, most probably due to allometric scaling. The 3 and 6 month age group categories displayed similar patterns of external airway spacing, likewise the 12 and 24 month age group categories displayed a similar pattern of external airway spacing. The 3 and 6 month age group categories had their external airways and the lung in close proximity of one another (Figures 3.1.1 A and B and 3.1.2 A and B) as opposed to the 12 and 24 month age group categories (Figures 3.1.3 A and B and 3.1.4 A and B). In all the casts, the internal surfaces exhibited cast airways predominantly in the middle regions of the lung (Figures 3.1.1 C and D - 3.1.4 C and D).

Figure 3.1.1: Photographs of the external and internal surfaces of a 3 month old crocodile lung cast. (A) Is an external dorsal view of a pair of cast lungs. (B) is an external ventral view of a pair of cast lungs. (C) Is an internal dorsal view of a cast lung. (D) is an internal ventral view of a cast lung. Tr = Trachea, EPPB = Extrapulmonary primary bronchus, Arrow heads (>) = Airways.

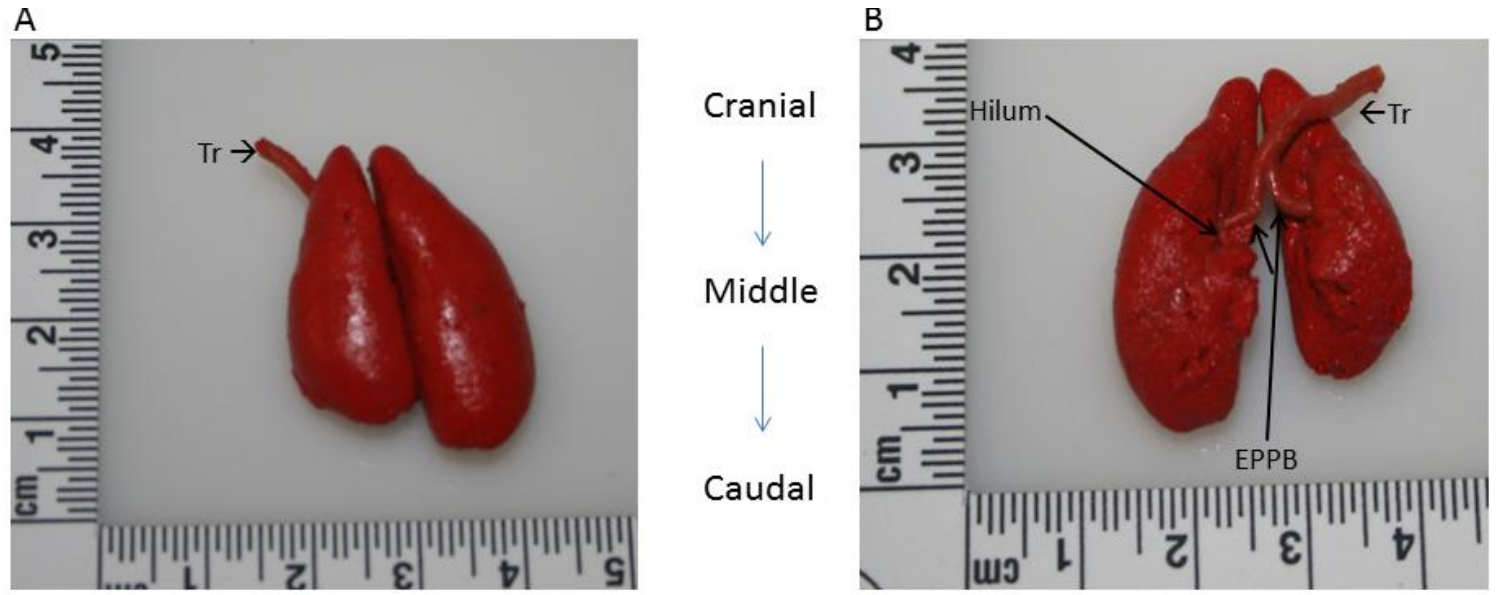
A
Tr
Cranial
Middle
Caudal
B
Hilum
Tr
EPPB
C
Cranial
Middle
Caudal
D

Figure 3.1.2: Photographs of the external and internal surfaces of a 6 month old crocodile lung cast. (A) Is an external dorsal view of a pair of cast lungs. (B) is an external ventral view of a pair of cast lungs. (C) Is an internal dorsal view of a cast lung. (D) is an internal ventral view of a cast lung. Tr = Trachea, EPPB = Extrapulmonary primary bronchus, Arrow heads (>) = Airways.

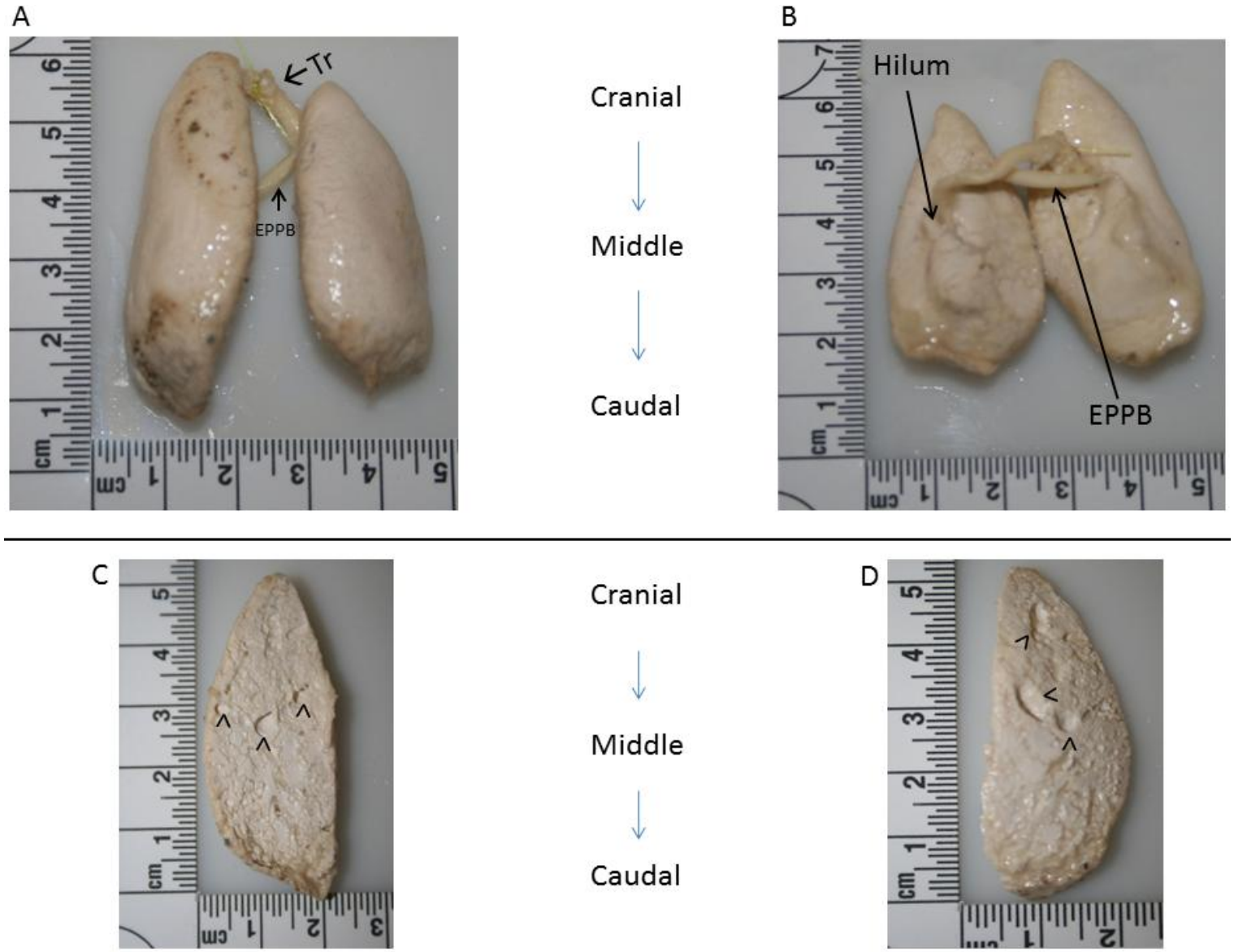
A
Tr
EPPB
Cranial
Middle
Caudal
B
Hilum
EPPB
C
Cranial
Middle
Caudal
D

Figure 3.1.3: Photographs of the external and internal surfaces of a 12 month old crocodile lung cast. (A) Is an external dorsal view of a pair of cast lungs. (B) is an external ventral view of a pair of cast lungs. (C) Is an internal dorsal view of a cast lung. (D) is an internal ventral view of a cast lung. Tr = Trachea, EPPB = Extrapulmonary primary bronchus, Arrow heads (>) = Airways.

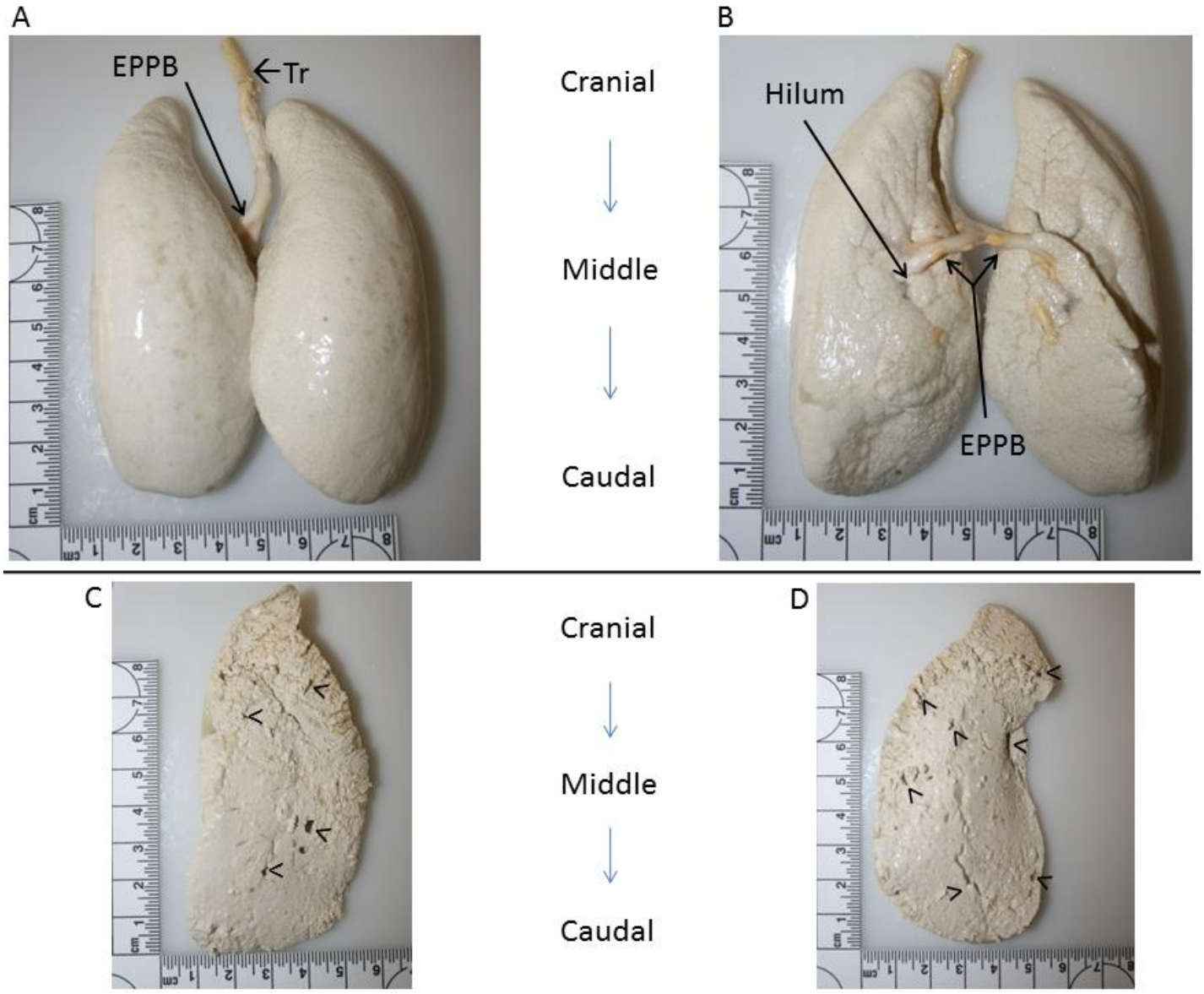
A
EPPB
Tr
Cranial
Middle
Caudal
B
Hilum
EPPB
C
Cranial
Middle
Caudal
D

Figure 3.1.4: Photographs of the external and internal surfaces of a 24 month old crocodile lung cast. (A) Is an external dorsal view of a pair of cast lungs. (B) is an external ventral view of a pair of cast lungs. (C) Is an internal dorsal view of a cast lung. (D) is an internal ventral view of a cast lung. Tr = Trachea, EPPB = Extrapulmonary primary bronchus, Arrow heads (>) = Airways.

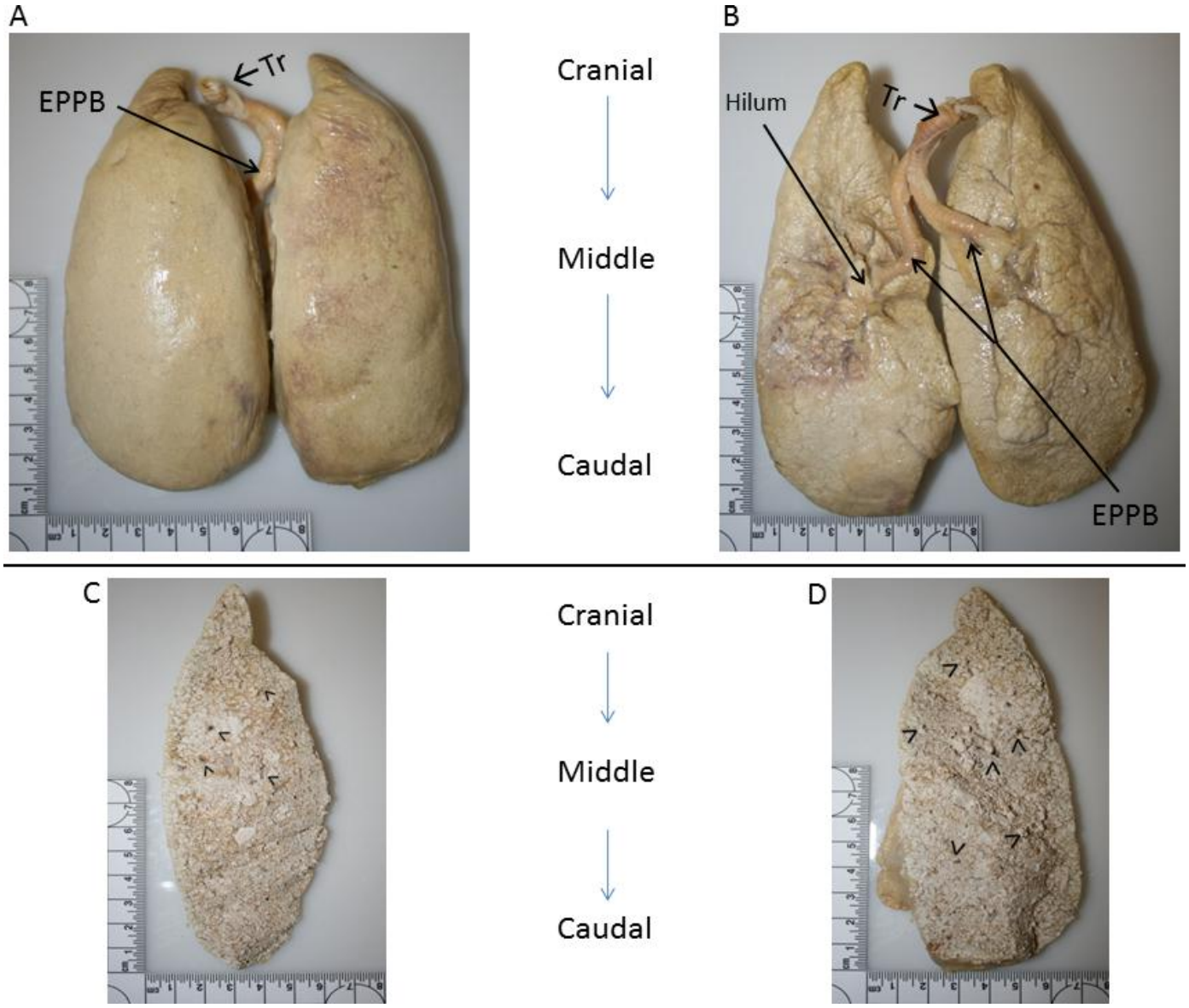
A
EPPB
Tr
Cranial
Middle
Caudal
B
Hilum
Tr
EPPB
C
Cranial
Middle
Caudal
D

### 3.1.2. Light Microscopy

H&E sections of all the sampled regions of the various age group categories illustrated marked heterogeneity. In all specimens, the cranial regions of the lungs appeared more subdivided than the middle and caudal regions respectively (Figures 3.2.1 – 3.5.2). The ventral regions (cranial, middle and caudal) illustrated more partitioning of the parenchyma than their dorsal counterparts (Figures 3.2.1 – 3.5.2).

3 Month Age Group Category

Various structural components were in abundance in certain regions and minimal in the others. The dorsal cranial region of the 3 month age category sample was well subdivided with faveoli surrounding the larger airways, which supply air (Figure 3.2.1 A). The dorsal middle region displayed a less intense division pattern (Figure 3.2.1 B). Larger airways are abundant with fewer faveoli and the appearance of large interfaveolar blood vessels and smooth muscle is apparent (Figure 3.2.1 B). The dorsal caudal region was subdivided but not in the manner of creating numerous faveoli (Figure 3.2.1 C). Large airways, interfaveolar blood vessels and smooth muscle are very prominent in this region (Figure 3.2.1 C).

The ventral cranial region of the 3 month age category was very well subdivided, more than its dorsal counterpart, with numerous faveoli (Figure 3.2.2 A). Smooth muscle and interfaveolar blood vessels were interspersed amongst the parenchyma (Figure 3.2.2 A). The ventral middle region was unevenly subdivided with faveoli radiating from airways (Figure 3.2.2 B). The ventral caudal regions were subdivided in certain areas and had large airways in other parts (Figure 3.2.2 C). Smooth muscle and interfaveolar blood vessels are markedly present in the ventral middle and ventral caudal regions in comparison to the ventral cranial region (Figure 3.2.2).

6 Month Age Group Category

The 6 month age group category samples displayed a similar pattern as the sampled regions of the 3 month age group category (Figures 3.3.1 and 3.3.2). An important observation is the high degree of subdivision of the parenchyma of the cranial ventral region in comparison to the cranial dorsal region (Figures 3.3.1 A and 3.3.2 B). The middle and caudal regions show an increase in the presence of interfaveolar blood vessels and smooth muscle and a decreased level of subdivision respectively (Figures 3.3.1 B, C and 3.3.2 B, C).

12 and 24 Month Age Group Categories

The 12 and 24 month age category samples showed great levels of subdivision of parenchyma in the cranial regions, ventral regions more apparent than the dorsal regions (Figures 3.4.1 A, 3.4.2 A, 3.5.1 A and 3.5.2 A). However, this was in an irregular manner in comparison to the samples from the 3 and 6 month age group categories. In addition, the presence of larger interfaveolar blood vessels and smooth muscles were not restricted to the middle and caudal regions as in the 3 and 6 month age category samples (Figures 3.2.1 – 3.5.2). The middle and caudal regions, of the dorsal and ventral halves of the lung, of the 12 and 24 moth age category samples had an increased presence of smooth muscle and interfaveolar blood vessels with conspicuously larger airways and fewer distinctive faveoli (Figures 3.4.1 B, C, 3.4.2 B, C, 3.5.1 B, C and 3.5.2 B, C).

A review of the observations from the light micrographs of the various sampled regions of the different age groups indicates that the degree of subdivision decreases in a caudal direction. The result of this is a decrease in the number of faveoli in a caudal direction. The dorsal half of the lung is also less subdivided than its cranial counterparts. The thickness of the septa dividing the cranial regions was minimal compared to the thicker ones located in

the caudal regions of the lung. The distribution of smooth muscle was greater in the caudal regions of the lung and hardly occurred or was absent in the cranial regions of the lung.

The 3 month age group category was more highly subdivided in all regions in comparison to the other age group categories. The 6 month age group category displayed lower levels of subdivision compared to the 3 month age group category but had similar subdivision patterns. In comparison, the 12 and 24 month age group categories had markedly lower levels of subdivision with varying degrees of regular symmetrical and asymmetrical subdivision of the respective regions. The younger age group categories tended to have a more symmetrical subdivision throughout the sampled regions. This could be attributed to allometric scaling or it could just be differences in the morphology of the lungs of crocodiles at different ages.

Figure 3.2.1: Light micrographs of the systematically sampled regions of the dorsal half of a 3 month old crocodilian lung. (A) is the dorsal cranial region of the lung which is well and regularly subdivided. (B) is the dorsal middle region of the lung. It is comprised of numerous large airways. (C) is the dorsal caudal region of the lung. The pattern of subdivision is irregular. Smooth muscle and interfaveolar blood vessels are prominent. A = Airways, F = Faveoli, IFBV = Interfaveolar blood vessel, SM = smooth muscle.

A

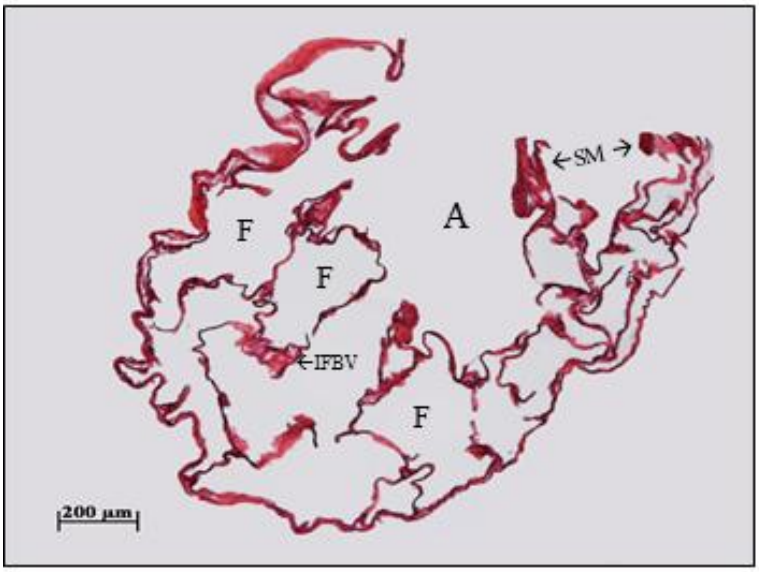
SM
A
F
F
IFBV
F
200 µm

B

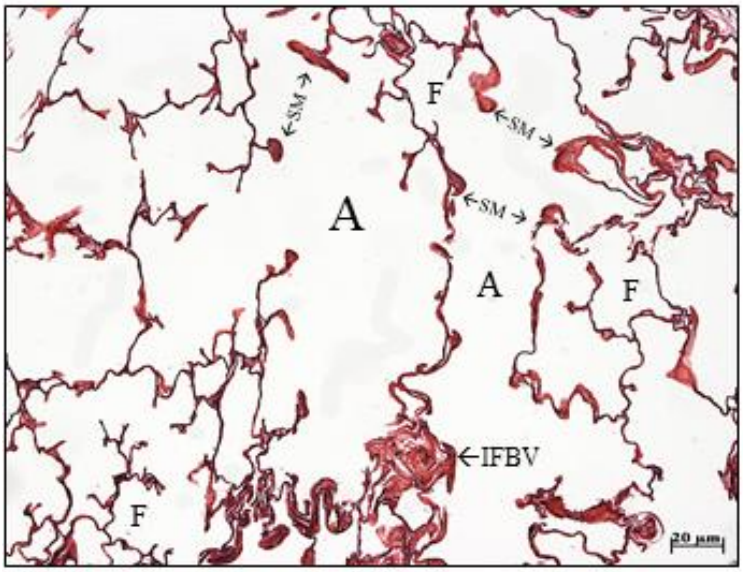
SM
F
SM
SM
A
A
F
IFBV
F
20 µm

C

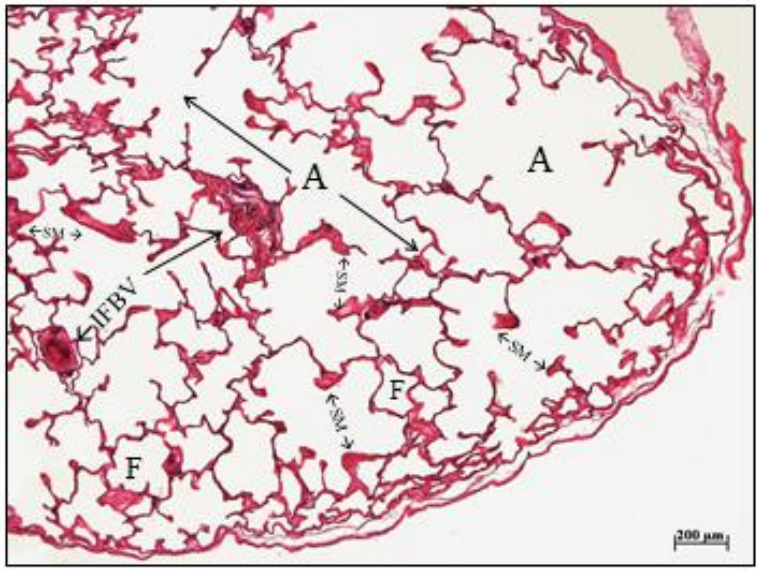
A
A
SM
IFBV
SM
SM
F
SM
F
200 µm

Figure 3.2.2: Light micrographs of the systematically sampled regions of the ventral half of a 3 month old crocodilian lung. (A) is the ventral cranial region. This region is highly subdivided and has a rich air supply. (B) is the ventral middle region of the lung which is irregularly subdivided and has numerous large airways. (C) is the ventral caudal region of the lung. It is has less subdivisions than (A) and (B) respectively. Large airways, smooth muscle and interfaveolar blood vessels are prominent. A = Airways, F = Faveoli, IFBV = Interfaveolar blood vessel, SM = smooth muscle.

A

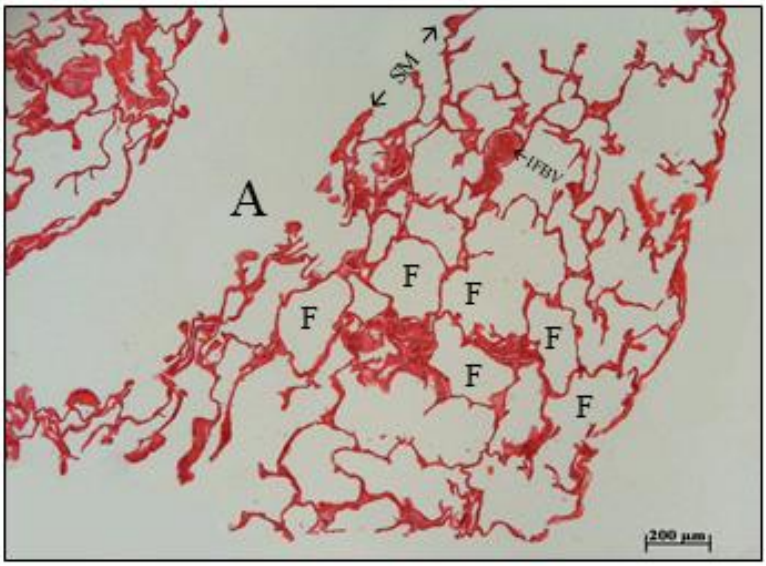
SM
IFBV
A
F
F
F
F
F
F
200 µm

B


F
IFBV
A
A
SM
IFBV
F
F
SM
A
SM
F
20 µm

C

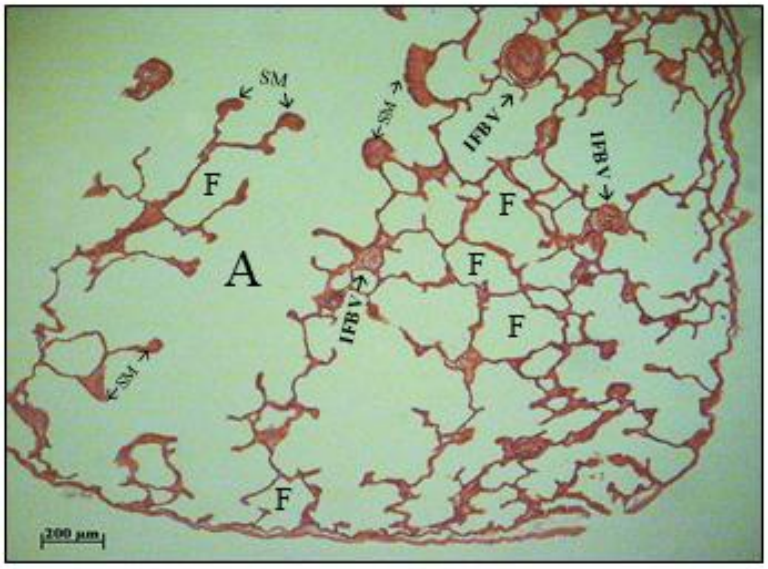
SM
SM
IFBV
IFBV
F
F
A
F
IFBV
F
SM
F
200 µm

Figure 3.3.1: Light micrographs of the systematically sampled regions of the dorsal half of a 6 month old crocodilian lung. (A) is the dorsal cranial region which displays great levels of subdivision with a resultant high density of faveoli. (B) is the dorsal middle region of the lung. It is irregularly subdivided and has numerous interspersed large airways. (C) is the dorsal caudal region of the lung which is has less subdivisions than (A) and (B) respectively. The presence of interfaveolar blood vessels, large airways and smooth muscle is very noticeable. A = Airways, F = Faveoli, IFBV = Interfaveolar blood vessel, SM = smooth muscle.

A

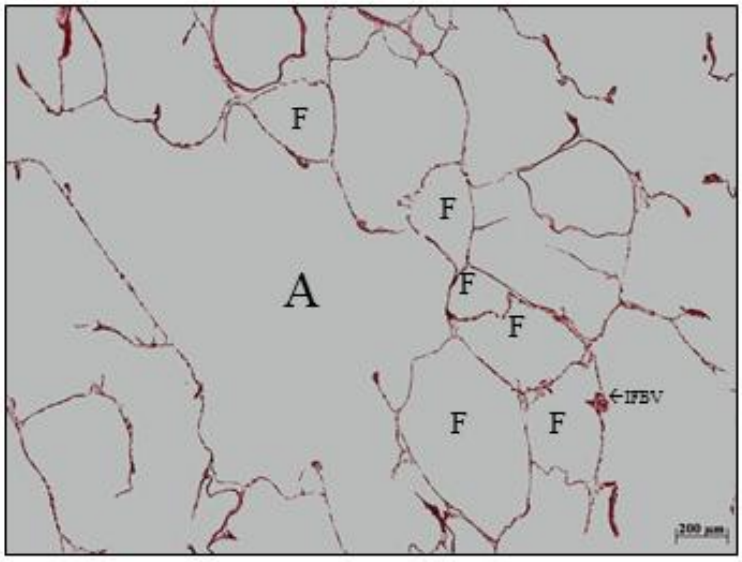
F
F
A
F
F
IFBV
F
F
200 µm

B

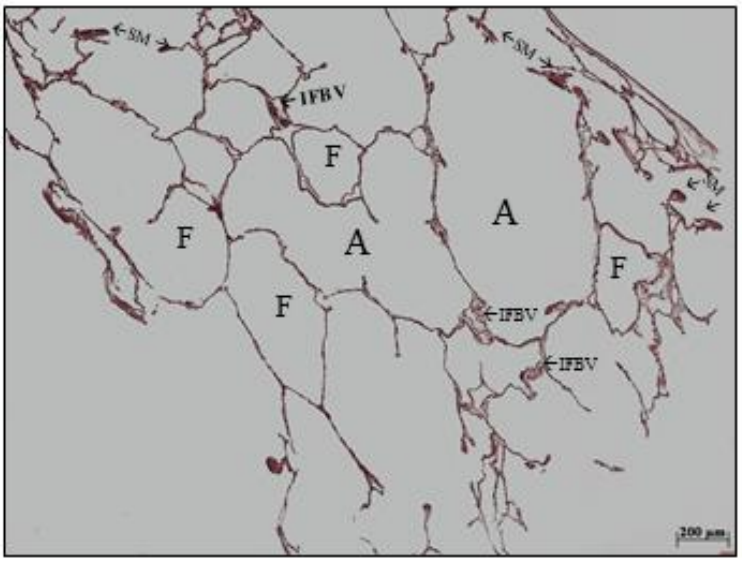
SM
IFBV
SM
F
F
A
A
F
F
IFBV
IFBV
200 µm

C

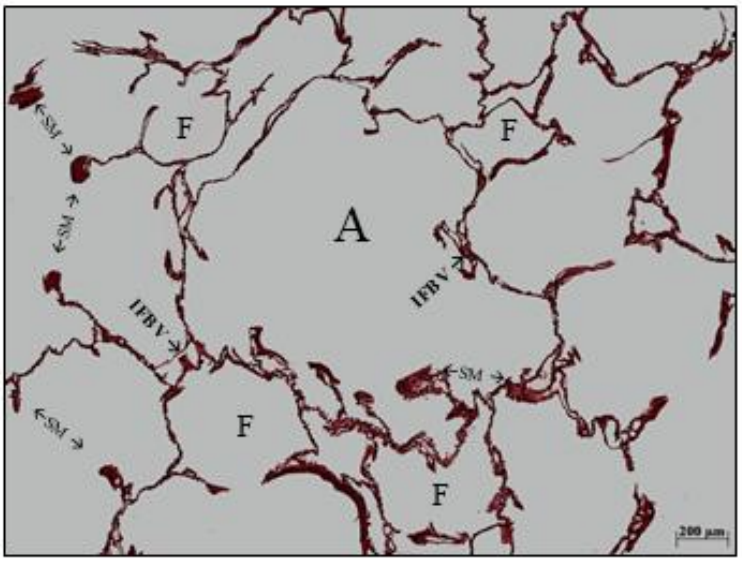
SM
F
F
SM
A
IFBV
IFBV
SM
SM
F
F
200 µm

Figure 3.3.2: Light micrographs of the systematically sampled regions of the ventral half of a 6 month old crocodilian lung. (A) shows the ventral cranial region which is subdivided to a high degree. (B) is the ventral middle region of the lung. It is has a lower degree of subdivision than (A) but have distinct interfaveolar blood vessels. (C) is the ventral caudal region of the lung. In comparison to (A) and (B) it is poorly subdivided. Interfaveolar blood vessels, large airways and smooth muscle are present. A = Airways, F = Faveoli, IFBV = Interfaveolar blood vessel, SM = smooth muscle.

A

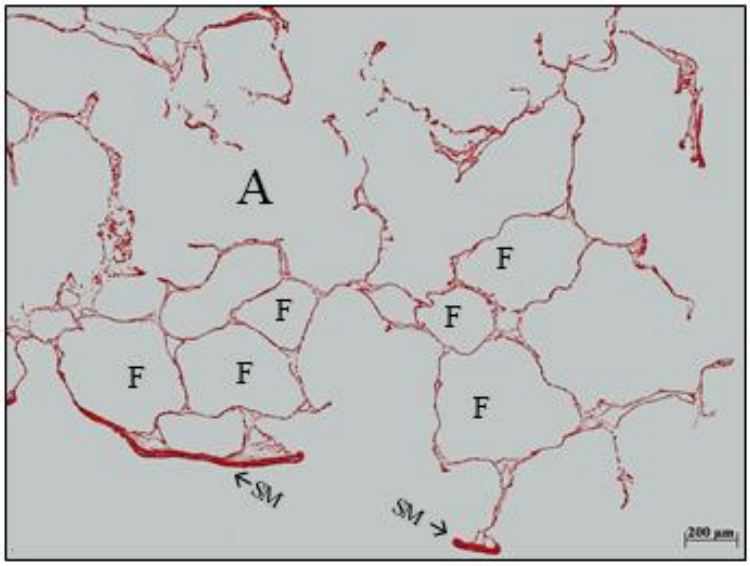
A
F
F
F
F
F
F
SM
SM
200 µm

B

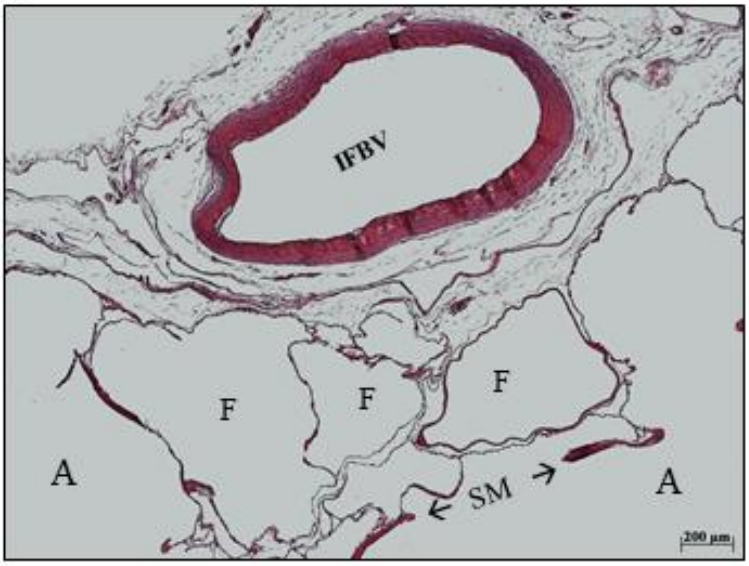
IFBV
F
F
F
A
SM
A
200 µm

C

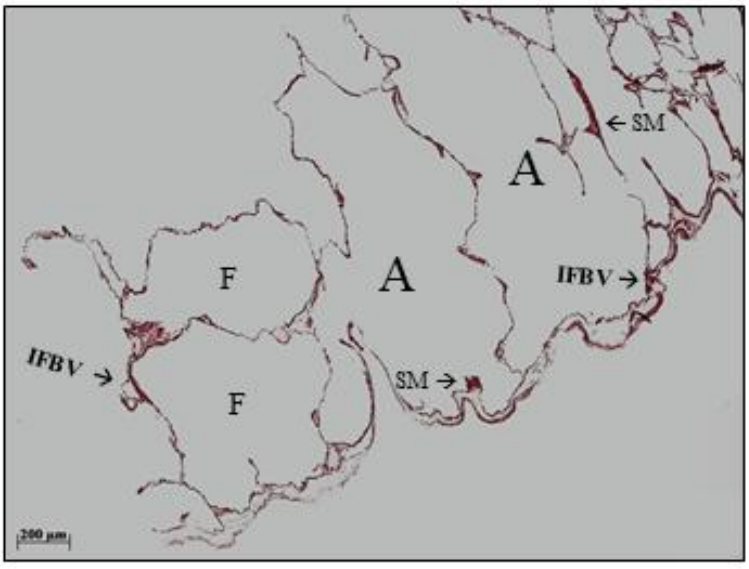
SM
A
F
A
IFBV
IFBV
SM
F
200 µm

Figure 3.4.1: Light micrographs of the systematically sampled regions of the dorsal half of a 12 month old crocodilian lung. (A) is the dorsal cranial region which is subdivided to a high degree. The presence of interfaveolar blood vessels is pronounced. (B) is the dorsal middle region of the lung. It is has a lower degree of subdivision than (A). In addition to the interfaveolar blood vessels, smooth muscle is very conspicuous. (C) is the ventral caudal region of the lung. In comparison to (A) and (B) it is poorly subdivided. Interfaveolar blood vessels, large airways and smooth muscle are ever present. A = Airways, F = Faveoli, IFBV = Interfaveolar blood vessel, SM = smooth muscle

A

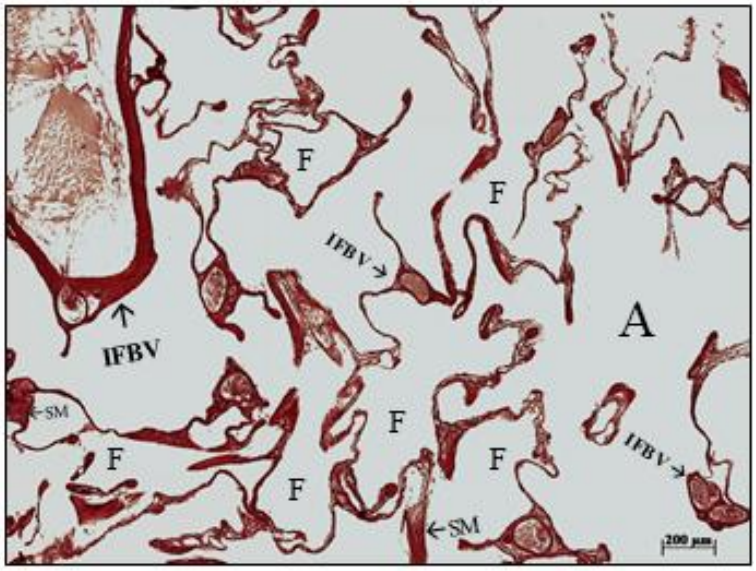
F
F
IFBV
A
IFBV
SM
F
F
F
F
IFBV
SM
200 µm

B

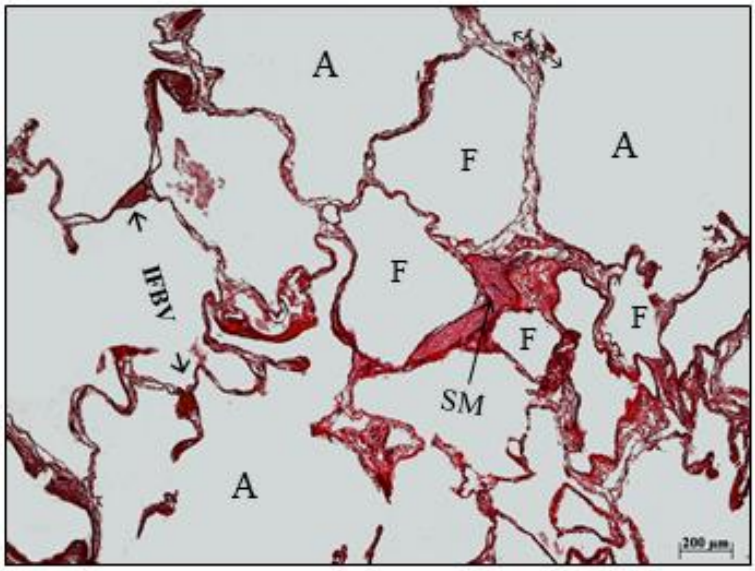
A
F
A
IFBV
F
F
F
SM
A
200 µm

C

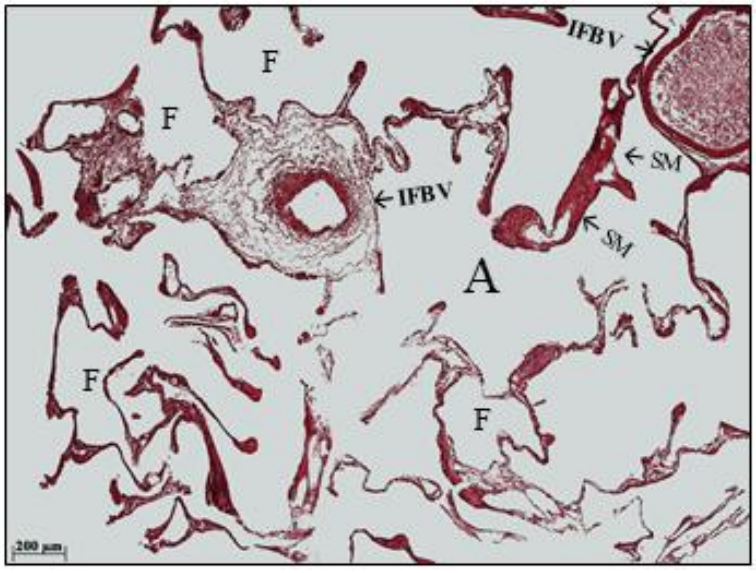
IFBV
F
F
SM
IFBV
SM
A
F
F
200 µm

Figure 3.4.2: Light micrographs of the systematically sampled regions of the ventral half of a 12 month old crocodilian lung. (A) is the ventral cranial region which is highly subdivided and has a good air supply. The presence of interfaveolar blood vessels and smooth muscle is evident. (B) is the ventral middle region of the lung. Large airways are predominant accompanied by interfaveolar blood vessels and smooth muscle. (C) is the ventral caudal region of the lung. This region has low levels of subdivision however the density of large airways interfaveolar blood vessels and smooth muscle is very high. A = Airways, F = Faveoli, IFBV = Interfaveolar blood vessel, SM = smooth muscle.

A

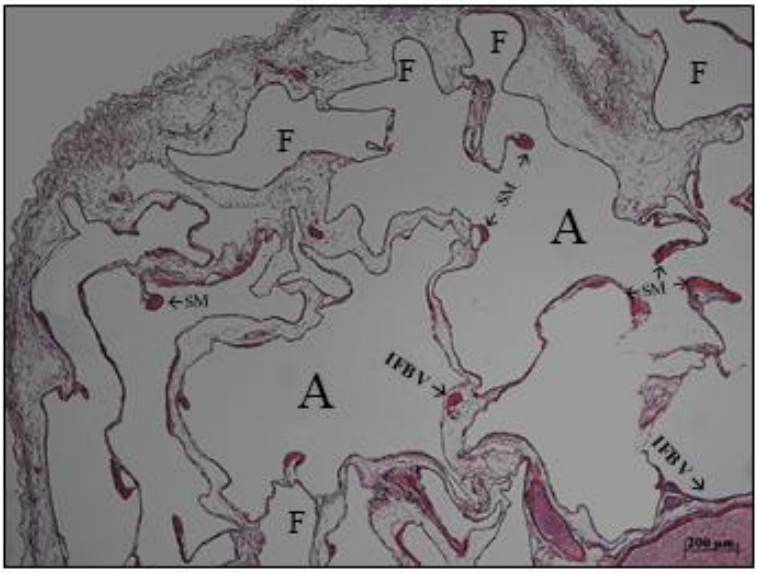
F
F
F
F
F
SM
A
SM
SM
A
IFBV
IFBV
F
200 µm

B

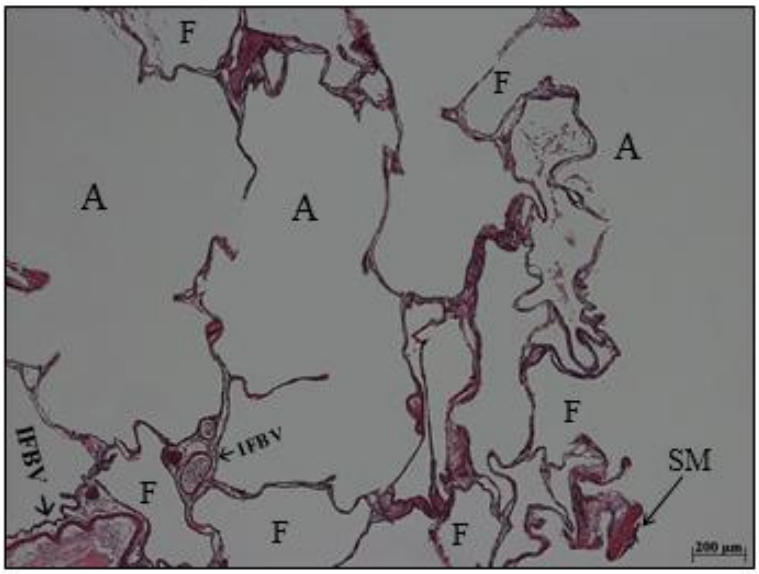
F
F
A
A
A
F
IFBV
IFBV
F
F
F
F
SM
200 µm

C

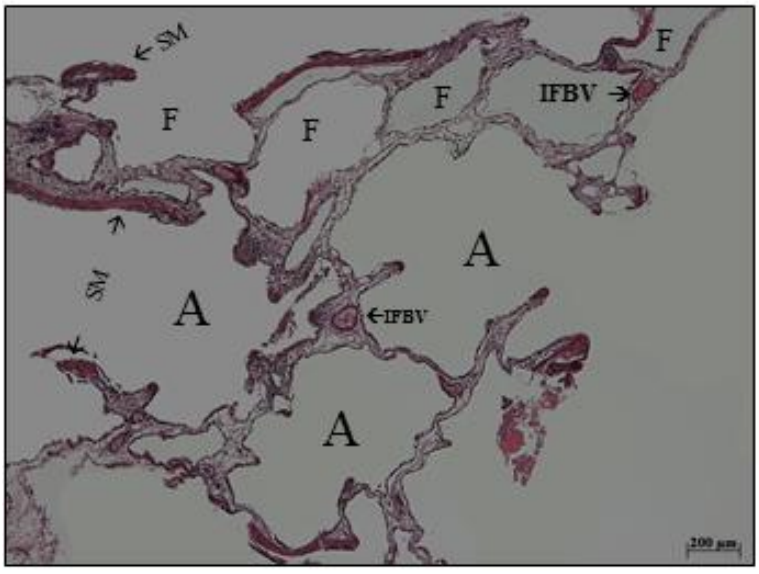
SM
F
F
F
F
IFBV
A
SM
A
IFBV
A
200 µm

Figure 3.5.1: Light micrographs of the systematically sampled regions of the dorsal half of a 24 month old crocodilian lung. (A) is the dorsal cranial region which is subdivided in an irregular manner. The presence of smooth muscle is clearly evident. (B) is the dorsal middle region of the lung. Large airways, interfaveolar blood vessels and smooth muscle are prevalent. (C) is the dorsal caudal region of the lung. This region displays a lower degree of subdivision but possess large amounts of interfaveolar blood vessels and smooth muscle. A = Airways, F = Faveoli, IFBV = Interfaveolar blood vessel, SM = smooth muscle.

A

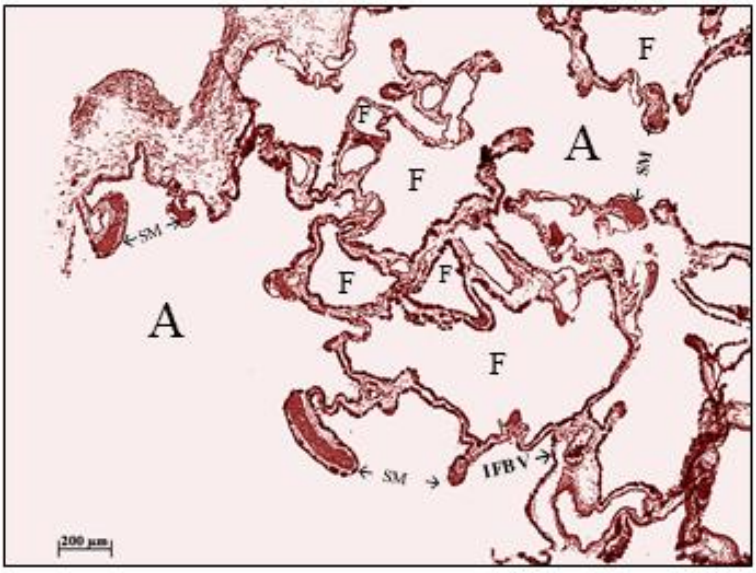


B

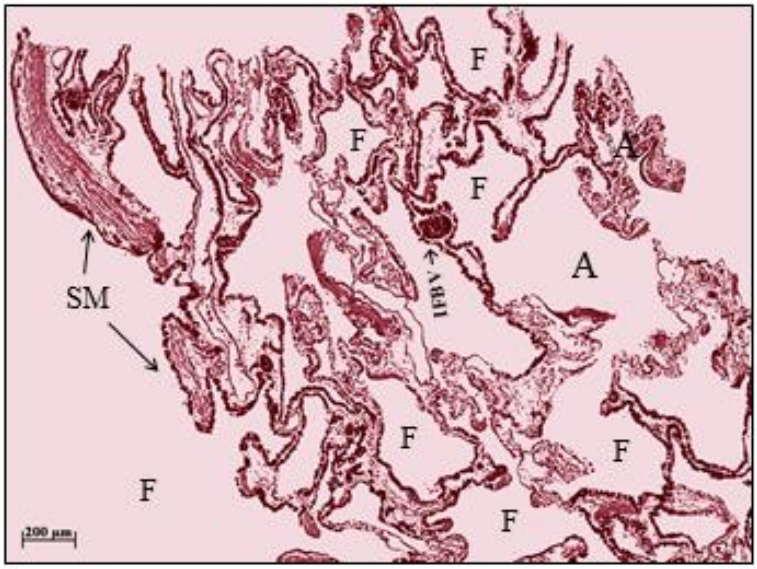


C

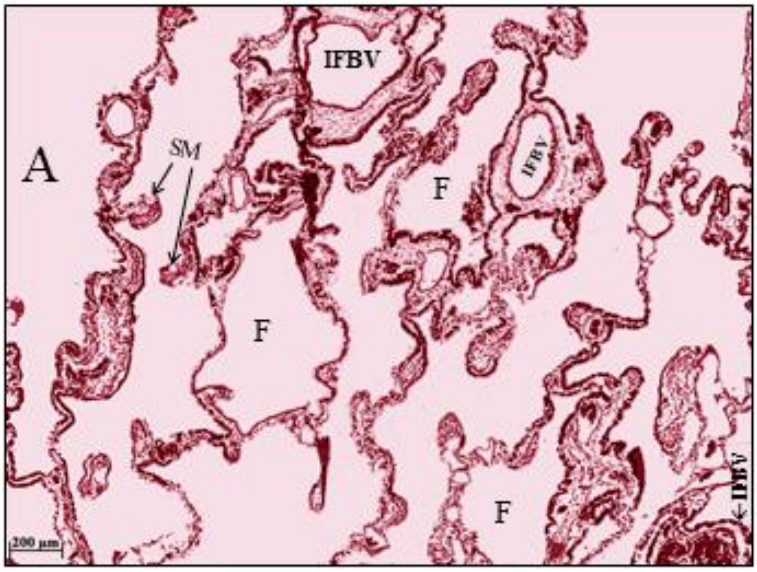

Figure 3.5.2: Light micrographs of the systematically sampled regions of the ventral half of a 24 month old crocodilian lung. (A) is the ventral cranial region which has an asymmetrical pattern of subdivision. (B) is the ventral middle region of the lung. Large airways, interfaveolar blood vessels and smooth muscle are dominant in this region. (C) is the ventral caudal region of the lung. This region is characterised by large airways, interfaveolar blood vessels and smooth muscle. A = airways, F = Faveoli, IFBV = Interfaveolar blood vessel, SM = smooth muscle.

A

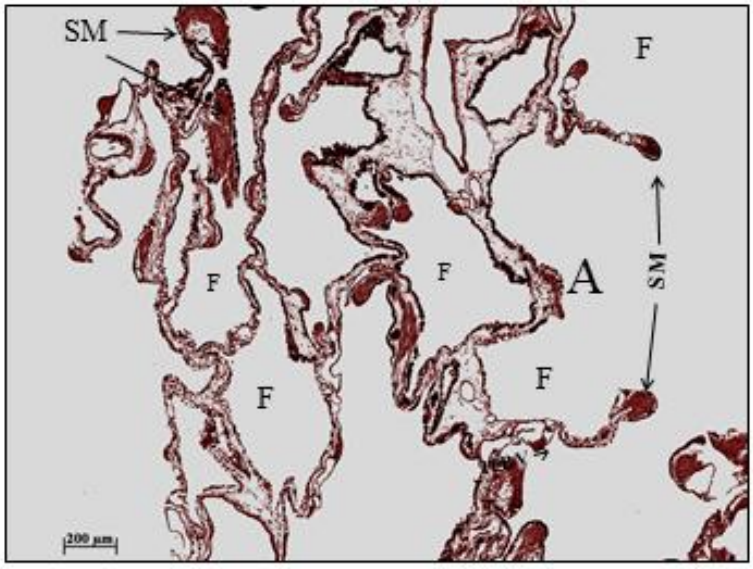
SM
F
F
F
A
SM
F
F
200 µm

B

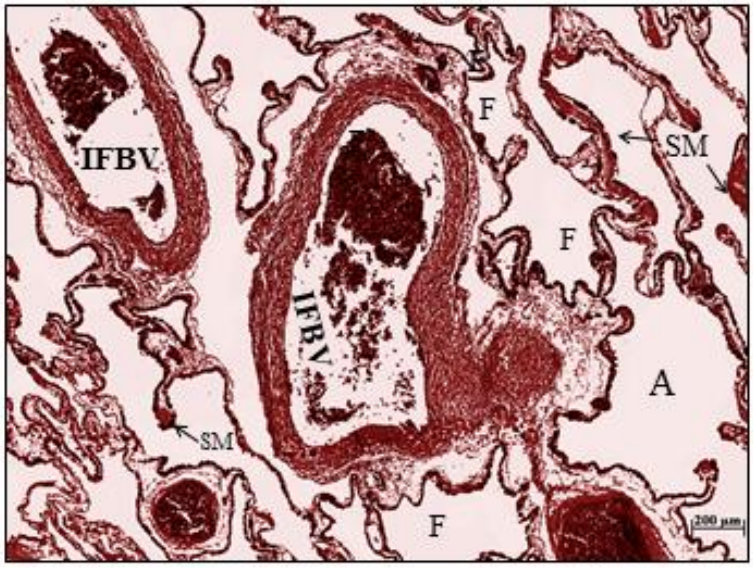
IFBV
IFBV
F
F
SM
SM
F
A
F
200 µm

C

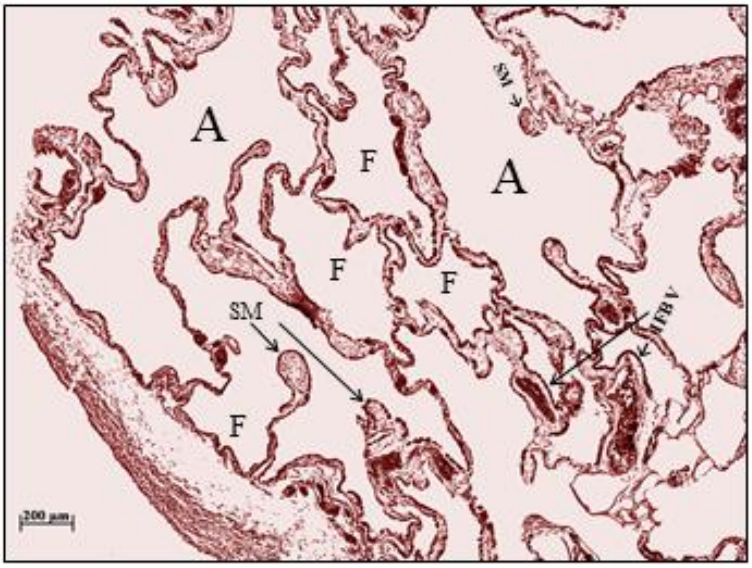
A
F
SM
A
F
F
SM
IFBV
F
200 µm

### 3.1.3. Scanning Electron Microscopy

The scanning electron micrographs of the samples from the various age group categories reinforced the trend observed in the light microscopic sections (Chapter 3.1.2). It is evident that the cranial regions are more subdivided, by means of septa, than the middle and caudal regions respectively (Figures 3.6.1 – 3.6.3). The ventral regions of all the analysed samples were more subdivided than their dorsal counterparts (Figures 3.6.1 – 3.6.3). With an increase in age the degrees of subdivision decreased and size of faveoli increased. Interfaveolar pores, stereocilia and microvilli were observed in different densities through different regions of the lungs in the various age group categories (Figures 3.6.4). An interesting note is that interfaveolar pores haven't been observed / described in scientific literature to date.

Interfaveolar pores in the cranial regions of the lung were high in density; uniform and small (Figure 3.6.4 A, B and C). The middle and caudal regions of the lung had intermediate to low densities of interfaveolar pores respectively. Moving in a caudal direction the size of the interfaveolar pores generally increased and displayed greater variability in size. A higher density of smaller sized interfaveolar pores were more distinct in the cranial ventral regions and middle regions compared to their dorsal counterparts.

The distribution of microvilli was similar to that of the distribution and density of interfaveolar pores in the various regions of the lung (Figure 3.6.4 A, B and C). The density of microvilli was highest in the ventral cranial regions decreasing in a caudal direction. Furthermore, their density was higher in the ventral regions as opposed to their corresponding dorsal counterparts.

Stereocilia occurred throughout the lung but their density and distribution increased in a caudal direction (Figure 3.6.4 D). They occurred on all septa and even covered the

apertures of interfaveolar pores (Figure 3.6.4 D). In the cranial regions they were rarely observed.

3 Month Age Group Category

The dorsal region of the 3 month age category was well subdivided by means of primary (PS), secondary (SS) and tertiary septa (TS) (similar to Figure 3.6.1 A and B). Along the surfaces of the faveoli, microvilli and interfaveolar pores were evenly spread. The dorsal middle region of the 3 month old crocodile lungs had many airways which were divided by septa resulting in faveoli (Figure 3.6.1 C and similar to figure 3.6.1 D). Stereocilia and microvilli were abundant. Interfaveolar pores were also present.

The dorsal caudal region of the 3 month age group category displayed little subdivision resulting in larger but fewer faveoli (Figure 3.6.2 A and similar to 3.6.2 B). The density of stereocilia was high on septa (similar to Figure 3.6.2 B) but the density of microvilli was markedly lower. Interfaveolar pores of varying sizes were easily observed.

The ventral cranial region of the 3 month age group category sample was intensely subdivided resulting in a high density of small faveoli (Figure 3.6.2 C and similar to Figure 3.6.2 D). Fewer stereocilia were observed. Microvilli and interfaveolar pores were abundant and widely spread across the respiratory surface. The ventral middle region of the 3 month lung sample was well subdivided, to a lesser extent than the corresponding cranial region (Figures 3.6.3 A and similar to Figure 3.6.3 B). Stereocilia, microvilli and interfaveolar pores (of varying sizes) were present.

The ventral caudal region of the lung of the 3 month age group category had well delineated faveoli but not as many as the respective cranial and middle regions (similar to Figures 3.6.3 C and D). Stereocilia are plentiful in this region with a lower density of

microvilli. Interfaveolar pores were evenly spread out and more uniform in size in this region.

6 Month Age Group Category

The pattern of subdivision and structural distribution in all sampled regions of the 6 month age group category was similar to that observed in the 3 month age group category. The dorsal cranial region of the 6 month age group category showed high levels of subdivision ranging from primary septa (PS) to secondary septa (SS) to tertiary septa (TS) (Figure 3.6.1 A). Stereocilia and microvilli were present and closely integrated with interfaveolar pores.

The dorsal middle region of the lung of the 6 month age group category has larger faveoli and a lower degree of subdivision than the respective cranial region (similar to Figures 3.6.1 C and D). Stereocilia are in abundance but in the samples viewed no microvilli were observed. Blood vessels are pronounced with interfaveolar pores between the blood vessel networks. The dorsal caudal region of the 6 month age group category had low levels of subdivision. As a result, fewer but larger faveoli were observed (which were notably pronounced) (similar to Figure 3.6.2 A). Stereocilia (similar to Figure 3.6.2 B) and interfaveolar pores were abundant.

The ventral cranial region of the 6 month age group category was very well divided with a high number of faveoli as a result (Figure 3.6.2 D and similar to Figure 3.6.2 C ). Stereocilia were present within the lumina of the vastly distributed interfaveolar pores. Microvilli were present especially in the vicinity of the blood vessels with faveoli. The ventral middle region of the 6 month age group category samples displayed intermediate levels of subdivision of its airways (similar to Figure 3.6.3 A and B). However, the

subdivision was not as ordered as that observed in the respective cranial region. Stereocilia were present on septa and within large interfaveolar pores.

The ventral caudal region of the 6 month age group category had ordered low levels of subdivision (Figure 3.6.3 C). The septa of this region had a medium covering of stereocilia coupled with predominantly large interfaveolar pores. The blood vessels lining the walls of the faveoli were conspicuous with interfaveolar pores interspersed.

12 and 24 Month Age Group Categories

The 12 and 24 month age categories displayed very similar patterns of subdivision, lower than that observed in the respective regions of the 3 and 6 month age group categories. The dorsal cranial region of the 12 month age group was suitably subdivided with a large number of faveoli. (similar to Figure 3.6.1 A and B). Blood vessels were clearly observable lining the walls of the faveoli. Interfaveolar pores were present in abundance in these regions. Stereocilia were present however no microvilli were observed in the viewed samples.

The dorsal middle region is composed of a large number of airways which are divided to form faveoli (similar to Figure 3.6.1 C and D). Interfaveolar pores and stereocilia were present throughout the region. Microvilli were present but very scarce.

The dorsal caudal region of the 12 month age group category had considerably lower levels of subdivision (similar to Figure 3.6.2 A and B, but subdivided to a lesser extent). However, where subdivision occurred it was orderly and intense. Stereocilia and interfaveolar pores were in abundance as opposed to microvilli.

The ventral cranial region of the 12 month age group category was greatly subdivided with a high number of faveoli as a result (similar to Figure 3.6.2 C and D). Interfaveolar pores and microvilli were in abundance with stereocilia interspersed .

The ventral middle region of the 12 month age group category has a large supply of airways which are divided all along resulting in a good distribution of faveoli (Figure 3.6.3 B). An ample number of microvilli and interfaveolar pores are present in this region with stereocilia interspersed.

The ventral caudal region of the 12 month age group category is subdivided in an ordered matter but not to a high extent (similar to Figure 3.6.3 C and D). The resultant faveoli are well delineated. Blood vessels are well pronounced as are the interfaveolar pores interspersed between them . Stereocilia are present and are incorporated with interfaveolar pores.

The dorsal cranial region of the 24 month age group category has high levels of subdivision with its airways (Figure 3.6.1 B). The blood vessel network is pronounced and occupies a large surface area. Interfaveolar pores are interspersed between the blood vessel network and stereocilia, the latter occurring sporadically. Microvilli are present and are distinctive.

The dorsal middle region of the 24 month age group category shows intermediate levels of subdivision (Figure 3.6.1 D and similar to Figure 3.6.1 C). Interfaveolar pores are wide spread through this region. The blood vessels lining the outer surface of faveoli stand out and interfaveolar pores lie between them. Stereocilia and microvilli are also present in this region.

The dorsal caudal region of the 24 month age group category is subdivided to a lesser extent. Faveoli are larger and fewer (similar to Figure 3.6.2 A and B). Interfaveolar pores are widespread through this region and microvilli are found in regions were the interfaveolar pores are larger , otherwise they are few in number or absent. Stereocilia are present in this region mainly on the surface of the larger septa.

The ventral cranial region of the 24 month age group category, as with all the other ventral cranial regions, is thoroughly subdivided which produces numerous faveoli (similar to Figure 3.6.2 C and D but subdivided to a lesser extent). The blood vessel network lining the faveoli is distinctive with interfaveolar pores dispersed through it. Interfaveolar pores in other areas have stereocilia surrounding them. Large numbers of microvilli exist in this region.

The ventral middle region of the 24 month age group age category has numerous airways that are well divided to form faveoli (similar to Figure 3.6.3 C and D). Interfaveolar pores and microvilli are present in high densities in this region. Often associated with interfaveolar pores, the larger ones, are stereocilia.

The ventral caudal region of the 24 month age group category have fewer subdivisions than the respective cranial and middle regions (Figure 3.6.3 D). The blood vessel network of the faveoli is well defined. Numerous interfaveolar pores exist between this network. Stereocilia are present in close association with interfaveolar pores.

Figure 3.6.1: Scanning electron micrographs of the dorsal cranial region (A and B) and dorsal middle region (C and D) of the crocodilian lung. The micrographs displayed here are representative examples of the respective regions for the various age group categories. (A) and (B) are SEM micrographs of the dorsal cranial region of the lung of a 6 and 12 month old crocodile respectively. (A) illustrates the subdivision of this region by various septa. (B) shows how an airway is divided into faveoli by tertiary septa (TS). (C) and (D) are SEM micrographs of the dorsal middle region of a lung of a3 and 24 month old crocodile respectively. (C) demonstrates the subdivision of airways into faveoli. (D) depicts the division of tubular airways into faveoli. F = Faveoli, PS = Primary septum, SS = Secondary Septum, TS = Tertiary Septum, S = Stereocilia, * = Interfaveolar pores, BV = Blood vessels.

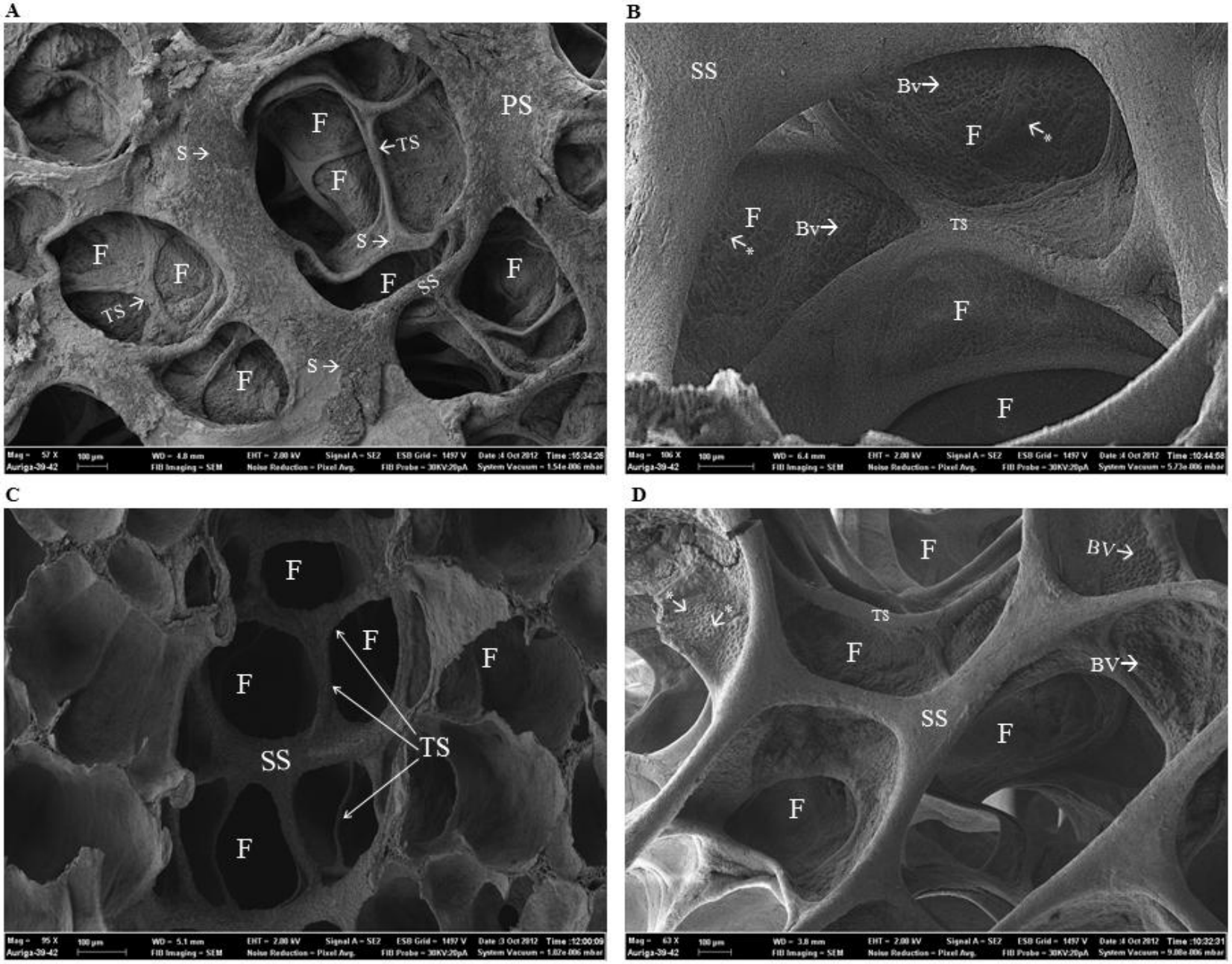
A
PS
F
TS
S
SS
B
SS
Bv
F
TS
C
F
TS
SS
D
BV
TS
SS

Figure 3.6.2: Scanning electron micrographs of the dorsal caudal region (A and B) and ventral cranial region (C and D) of the crocodilian lung. The micrographs displayed here are representative examples of the respective regions for the various age group categories. (A) and (B) are SEM micrographs of the dorsal caudal region of the lung of a 3 and 6 month old crocodile respectively. (A) is a micrograph showing the level of subdivision in this region. (B) is a micrograph of a tertiary septum with stereocilia and interfaveolar pores. (C) and (D) are SEM micrographs of the ventral cranial region of the lung of a 3 and 6 month old crocodile respectively. (C) depicts the high levels of subdivision in this region that results in numerous faveoli. (D) is a micrograph illustrating the delineating of faveoli by tertiary septa. F = Faveoli, SS = Secondary Septum, TS = Tertiary Septum, S = Stereocilia, * = Interfaveolar pores.

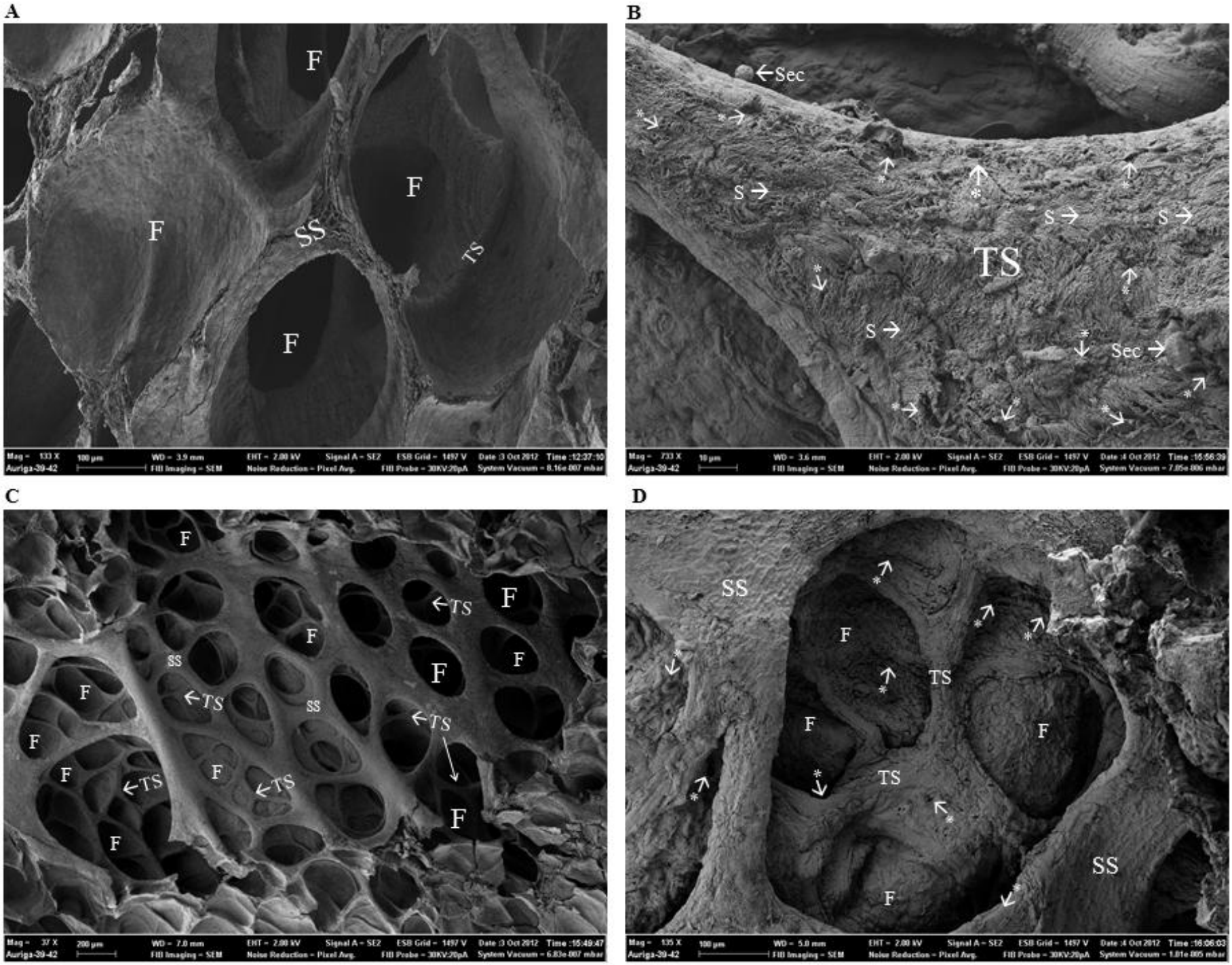
A
F
F
F
F
SS
TS
Mag = 133 X
100 µm
WD = 3.9 mm
EHT = 2.00 kV
Signal A = SE2
ESB Grid = 1497 V
Date :3 Oct 2012
Time :12:37:10
Auriga-39-42
FIB Imaging = SEM
Noise Reduction = Pixel Avg.
FIB Probe = 30KV:20pA
System Vacuum = 8.16e-007 mbar
B
Sec
S
S
S
TS
S
Sec
Mag = 733 X
10 µm
WD = 3.6 mm
EHT = 2.00 kV
Signal A = SE2
ESB Grid = 1497 V
Date :4 Oct 2012
Time :15:56:39
Auriga-39-42
FIB Imaging = SEM
Noise Reduction = Pixel Avg.
FIB Probe = 30KV:20pA
System Vacuum = 7.85e-006 mbar
C
F
F
TS
F
F
SS
F
F
TS
SS
TS
F
F
F
F
TS
F
TS
F
F
Mag = 37 X
200 µm
WD = 7.0 mm
EHT = 2.00 kV
Signal A = SE2
ESB Grid = 1497 V
Date :3 Oct 2012
Time :15:49:47
Auriga-39-42
FIB Imaging = SEM
Noise Reduction = Pixel Avg.
FIB Probe = 30KV:20pA
System Vacuum = 6.83e-007 mbar
D
SS
F
TS
F
F
TS
SS
F
Mag = 135 X
100 µm
WD = 5.0 mm
EHT = 2.00 kV
Signal A = SE2
ESB Grid = 1497 V
Date :4 Oct 2012
Time :16:06:03
Auriga-39-42
FIB Imaging = SEM
Noise Reduction = Pixel Avg.
FIB Probe = 30KV:20pA
System Vacuum = 1.81e-005 mbar

Figure 3.6.3: Scanning electron micrographs of the ventral middle region (A and B) and ventral caudal region (C and D) of the crocodilian lung. The micrographs displayed here are representative examples of the respective regions for the various age group categories. (A) and (B) are SEM micrographs of the ventral middle region of the lung of a 3 and 12 month old crocodile respectively. (A) and (B) illustrate the division of airways into faveoli. (C) shows an ordered subdivision of an airway into faveoli. (D) is an exhibition of airways alongside each other and their subdivision forming faveoli. F = Faveoli, SS = Secondary Septum, TS = Tertiary Septum, S = Stereocilia, * = Interfaveolar pores, A = Airway.

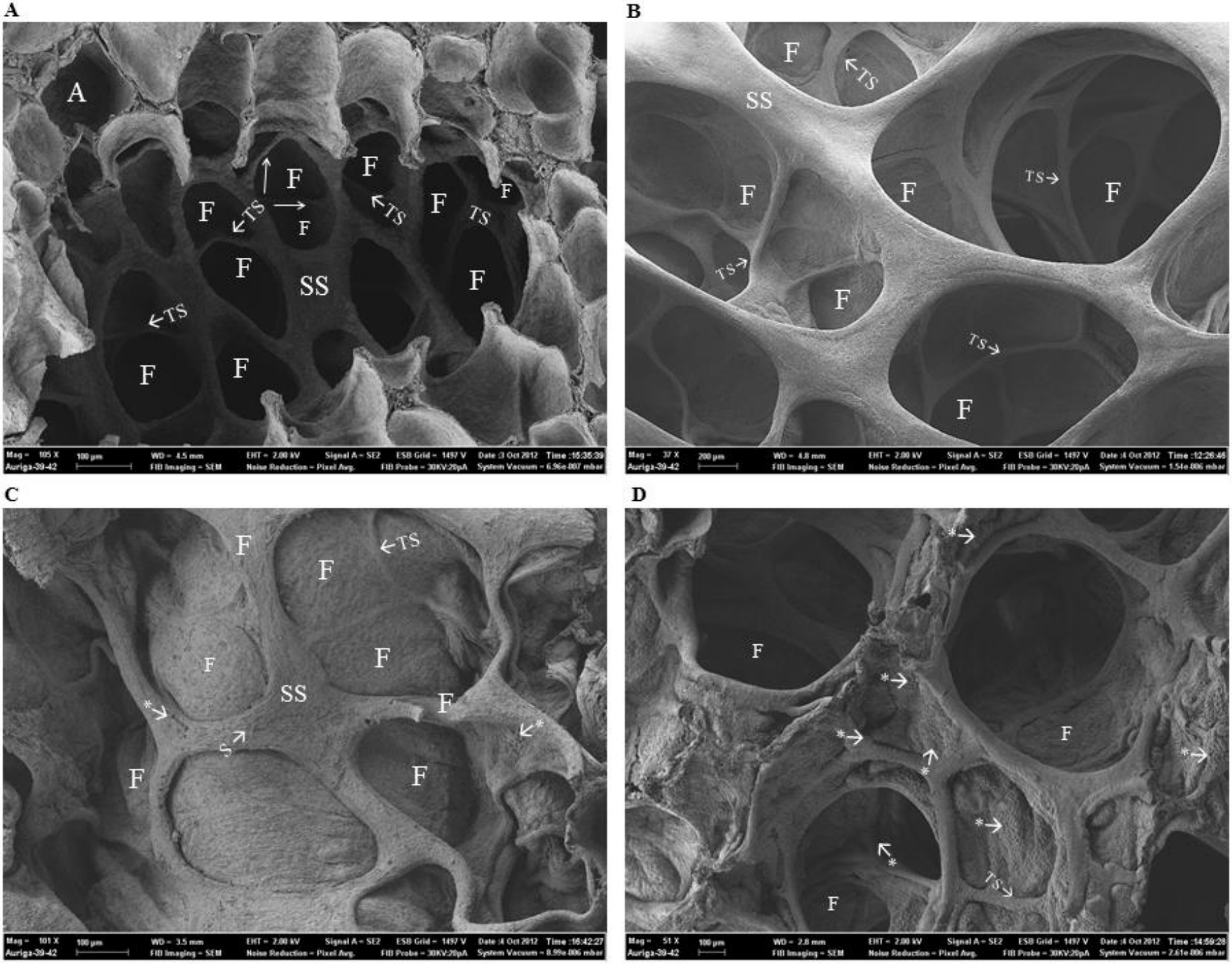
A
A
F
TS
SS
B
F
TS
SS
F
TS
C
F
TS
SS
*
S
D
F
*
TS

Figure 3.6.4: Scanning electron of interfaveolar pores, microvilli and stereocilia. The micrographs depicted here are representatives of the structures observed in the various regions of the lung. They may alter in size and density as discussed in the accompanying text. (A) is a micrograph of the ventral cranial region of a crocodile from the 3 month age group category. The high density of small interfaveolar pores and microvilli are characteristic of this region. (B) is a micrograph of the dorsal middle region of a 3 month old crocodile. The concurrent existence and distribution of stereocilia, microvilli and interfaveolar pores are well displayed. (C) is a micrograph of the dorsal cranial region of a crocodile belonging to the 6 month age group category. The micrograph shows a surface view of faveoli with microvilli and interfaveolar pores being clearly displayed. (D) is a micrograph of stereocilia in the dorsal middle region of a 12 month old crocodile. The high density of stereocilia and their interaction with interfaveolar pores is clearly exhibited. F = Faveoli, S = Stereocilia, * = Interfaveolar pores, Arrow heads (>) = microvilli, Sec = Secretion.

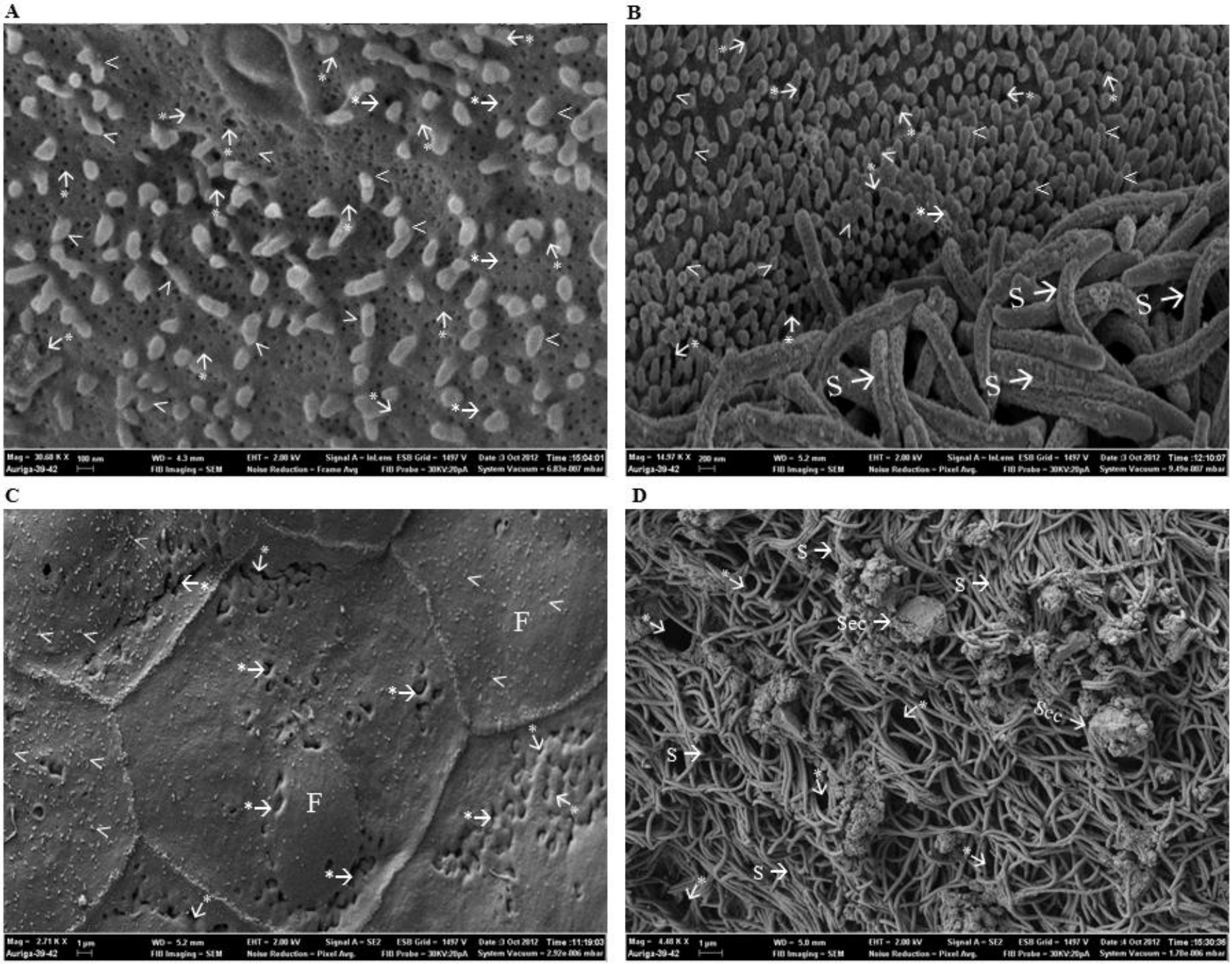
A
B
S
S
S
S
Mag = 30.68 K X 100 nm WD = 4.3 mm EHT = 2.00 kV Signal A = InLens ESB Grid = 1497 V Date :3 Oct 2012 Time :15:04:01
Auriga-39-42 FIB Imaging = SEM Noise Reduction = Frame Avg FIB Probe = 30KV:20pA System Vacuum = 6.83e-007 mbar
Mag = 14.97 K X 200 nm WD = 5.2 mm EHT = 2.00 kV Signal A = InLens ESB Grid = 1497 V Date :3 Oct 2012 Time :12:10:07
Auriga-39-42 FIB Imaging = SEM Noise Reduction = Pixel Avg. FIB Probe = 30KV:20pA System Vacuum = 9.45e-007 mbar
C
D
F
F
S
S
Sec
Sec
S
S
Mag = 2.71 K X 1 µm WD = 5.2 mm EHT = 2.00 kV Signal A = SE2 ESB Grid = 1497 V Date :3 Oct 2012 Time :11:19:03
Auriga-39-42 FIB Imaging = SEM Noise Reduction = Pixel Avg. FIB Probe = 30KV:20pA System Vacuum = 2.92e-006 mbar
Mag = 4.48 K X 1 µm WD = 5.0 mm EHT = 2.00 kV Signal A = SE2 ESB Grid = 1497 V Date :4 Oct 2012 Time :15:30:36
Auriga-39-42 FIB Imaging = SEM Noise Reduction = Pixel Avg. FIB Probe = 30KV:20pA System Vacuum = 1.70e-006 mbar

### 3.1.4. Transmission Electron Microscopy

Only a few samples were processed for transmission electron microscopy and confocal microscopy, essentially to show the structure of stereocilia. Micrographs of sections from various sampling regions illustrate that collagen makes up a large component of interfaveolar septa (Figure 3.7 B, C and D). They also reaffirm that the long "finger like" projections that stem of septa are indeed stereocilia and not cilia as documented by Perry (1988) (Figure 3.7 B, C and D). This further raises a question, have stereocilia been misidentified as cilia in the lungs of the green turtle (Solomon and Purton, 1984) and the central netted dragon (McGregor *et al.,* 1993) amongst others. The structures are identified as stereocilia due to their uniform diameter, length and organisation into bundles (Ross and Pawlina, 2011). Furthermore in cross section they don't exhibit an organised arrangement of microtubules, which is characteristic of cilia (Ross and Pawlina, 2011).

### 3.1.5. Confocal Microscopy

The Phalloidin, Alexa Fluor® 488 Conjugate (Cambrex Bio Science Walkersville Inc, Walkersville, Maryland, USA) / PBS staining solution used for confocal microscopy, stains for filamentous actin (F – Actin) (Lonza product specification documentation, 2008). A core component of cilia is filamentous actin in comparison to stereocilia which has actin filaments cross linked by epsin (Ross and Pawlina, 2011). If cilia were present they would absorb the filamentous actin stain and be visible in the micrographs but they are not. This further reinforces the fact that the long "finger like" projections seen in the scanning electron micrographs are stereocilia. The confocal micrographs also showed that the septa were composed of considerable amounts of actin apart from other connective tissue components (Figure 3.8). Interfaveolar pores are clearly visible and their tubular structural design, in order to facilitate interfaveolar pores, is distinctive (Figures 3.8).

Interfaveolar pores depicted in the micrographs show clear pathways for air to move between airways.

Figure 3.7: A toluidine blue section and transmission electron micrographs of the septa of a 6 month old crocodilian lung. (A) is toluidine blue section of the area where the micrographs (B), (C) and (D) are from. (A) is a toluidine blue section showing interfaveolar septa, blood vessels and capillaries. (B) is a low magnification micrograph of a septum. Collagen fibres that make up the septa are clearly visible and stereocilia are also present. (C) is a higher power micrograph showing stereocilia, cut in cross section, on a septum. (D) is a high power micrograph showing the stereocilia on a septum. Collagen fibres are visible in the top left corner of the image. IFS = Interfaveolar septum, BV = Blood vessel, Capp = Capillary, S = Stereocilia.

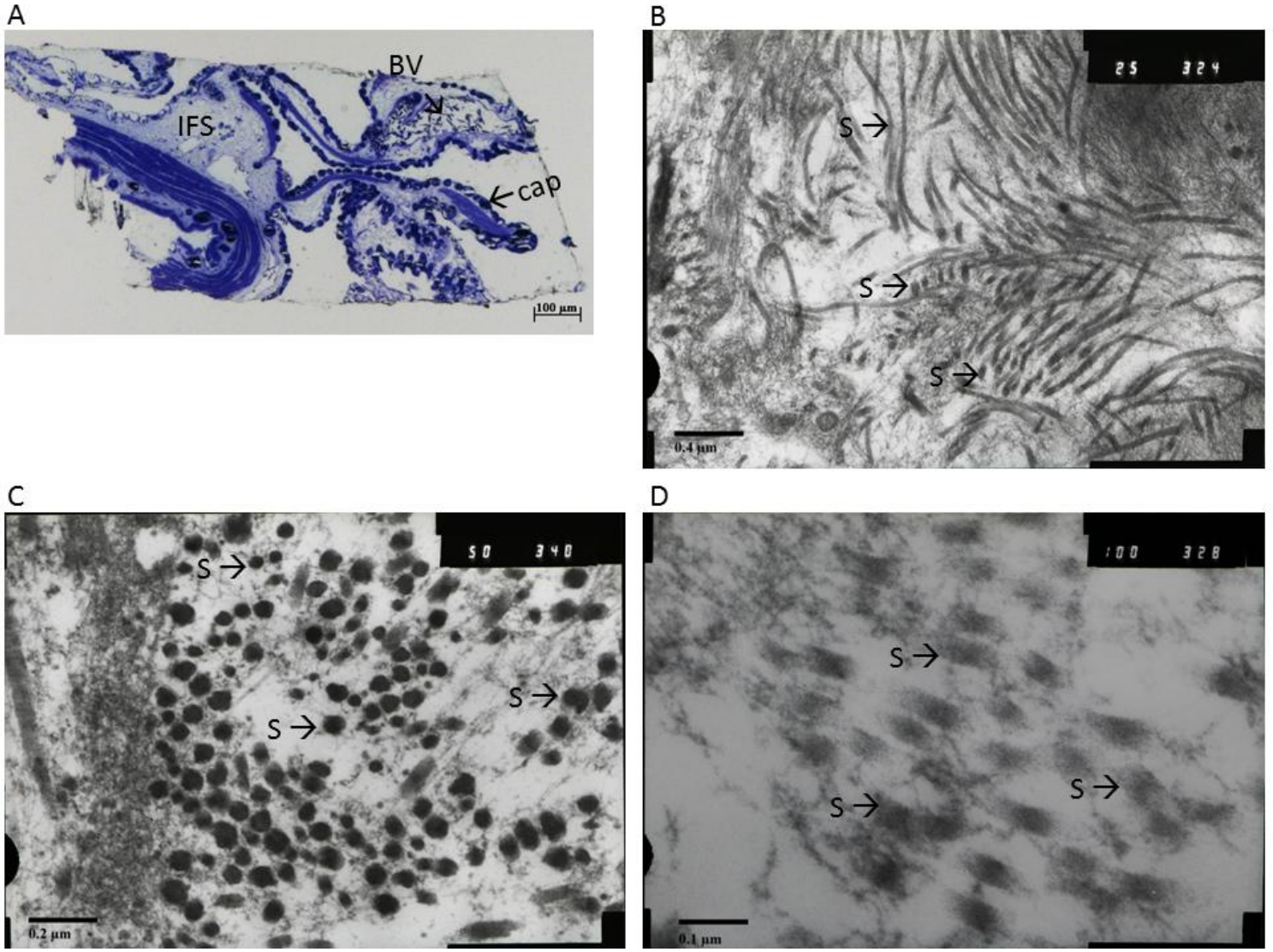
A
BV
IFS
cap
100 µm
B
25 324
S
S
S
0.4 µm
C
50 340
S
S
S
0.2 µm
D
100 328
S
S
S
0.1 µm

Figure 3.8: Confocal images of random sampled regions of the lung of a 6 month old crocodile. (A) is a low magnification micrograph illustrating the actin component of the septa and the presence of interfaveolar pores. (B) is a high magnification micrograph of a tertiary septum showing the unique architecture of septa to facilitate interfaveolar pores. (C) and (D) are low magnification images of septa delineating numerous faveoli, where the interfaveolar pores are clearly observable. F = Faveoli, TS = Tertiary Septum, * = Interfaveolar pores.

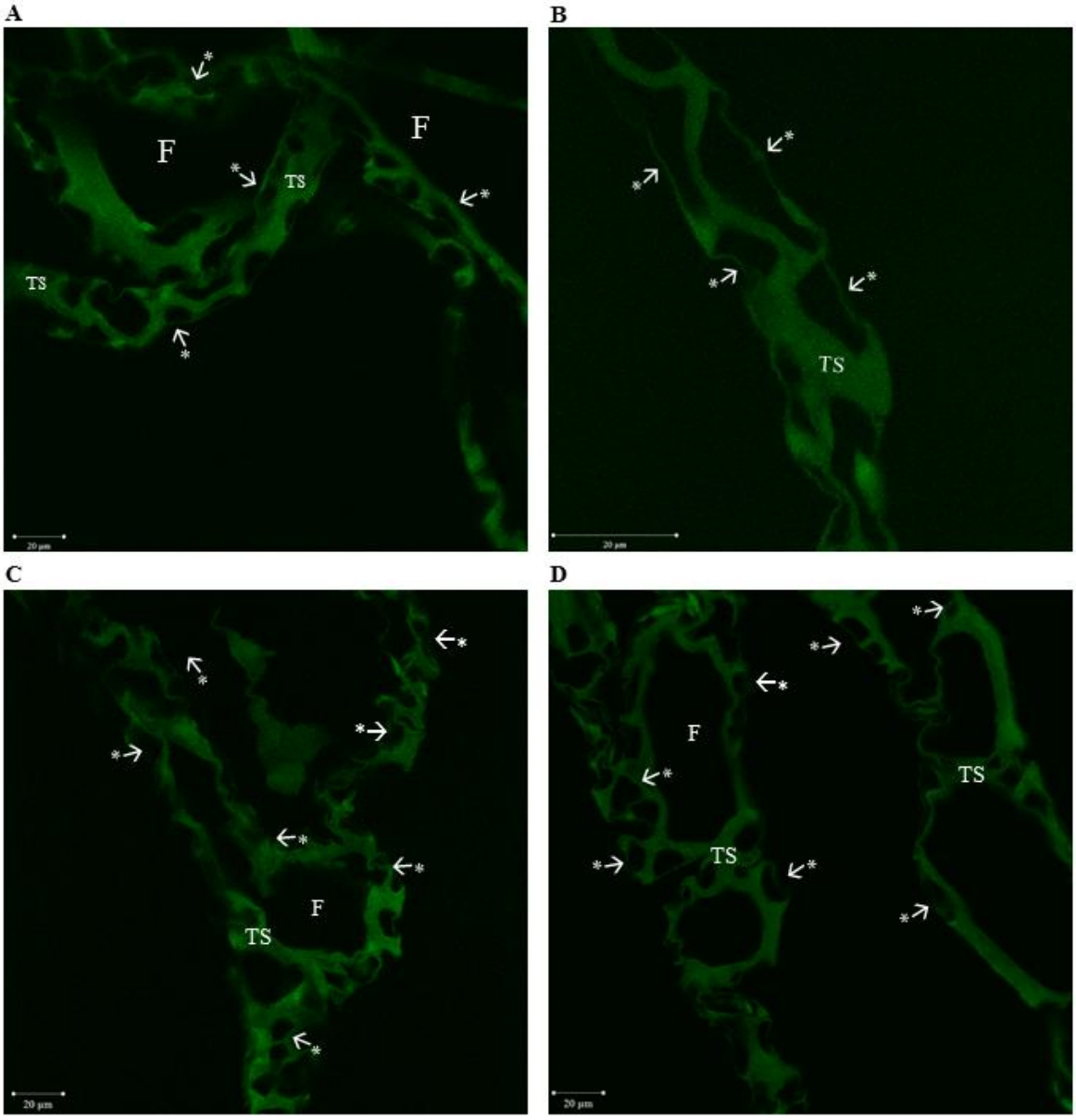
A
F
F
TS
TS
B
TS
C
F
TS
D
F
TS
TS

### 3.1.6. 3 Dimensional Serial Section Computer Reconstruction

**Please Note:** The cd attached to this thesis has the 3 dimensional reconstruction files for each region for age group category copied onto it. Included is the software used to view the 3D reconstructions. The software allows for viewing of the models in 3 dimensional space by manipulating viewing angels and the model as a whole.

All the 3 dimensional models of the different regions from the various age group categories reflected the observations made from the light microscopic sections (Chapter 3.1.2), scanning electron micrographs (Chapter 3.1.3) and confocal microscopy micrographs that were analysed. The cranial regions were all more subdivided than the middle and caudal regions respectively. In addition, the ventral regions of the lung were all more subdivided than their dorsal counterparts. The degree of subdivision of all the regions decreased with an increase in age and the size of faveoli changed allometrically.

The shape of faveoli in the cranial region were consistently oval to circular in shape in comparison to the middle and caudal regions. The 3 dimensional models of all the sampled regions of the various age categories show the intricate networking of the interfaveolar septa; primary, secondary and tertiary septa collectively, to create faveoli in different directions (Figures 3.9.1 – 3.12.6). This observation and notion can't be conceptualised in 2 dimensions

In the 3 month age group category, the 3 dimensional reconstruction model of the dorsal cranial region showed good even subdivision of the area (Figure 3.9.1 A and B). Faveoli were clearly demarcated and the interfaveolar pores are clearly observable and occur at random (Figure 3.9.1 A, B and C). The 3 dimensional reconstruction of the dorsal middle region of the 3 month age group category shows the division of the airways by conspicuously larger interfaveolar septa (Figure 3.9.2 A and B). The faveoli are larger and

interfaveolar pores are clearly observable (Figure 3.9.2 A, B and C). The 3 dimensional model of dorsal caudal region of the 3 month age group category displayed low degrees of subdivision (Figure 3.9.3 A and B). Few faveoli are present in this region but large airways are prominent (Figure 3.9.3 A and B). Interfaveolar pores were present and conspicuous (Figure 3.9.3 C).

The 3 dimensional model of the ventral cranial region of the 3 month age group category displayed high degrees of subdivision (Figure 3.9.4 A and B). Numerous faveoli were seen radiating around airways and interfaveolar pores, in particular, were abundant this region (Figure 3.9.4 A, B and C). The 3 dimensional model of the ventral middle region of the 3 month age group category had conspicuously large airways with a fair number of faveoli (Figure 3.9.5 A and B). Interfaveolar pores were clearly visible (Figure 3.9.5 C). The 3 dimensional model of the ventral caudal region of the 3 month age group category showed the region was well subdivided with considerably larger faveoli (Figure 3.9.6 A and B). Interfaveolar pores were present (Figure 3.9.6 C) but didn't seem as abundant as they were in the ventral cranial and middle regions.

The 3 dimensional models of the cranial dorsal region of the 6 month age group category were well subdivided in an orderly manner (Figure 3.10.1 A and B). Interfaveolar pores were present but were not as pronounced (Figure 3.10.1 C). In the 3 dimensional model of the dorsal middle region of the 6 month age group category larger airways are predominant rather than faveoli (Figure 3.10.2 A and B). Interfaveolar pores are distributed evenly through the interfaveolar septa of this region (Figure 3.10.2 C). The 3 dimensional model of the dorsal caudal region of the 6 month age group category was poorly subdivided with very few faveoli (Figure 3.10.3 A and B). Large interfaveolar pores were very noticeable in this region (Figure 3.10.3 C).

In the ventral cranial region of the 6 month age group category, the area specific 3 dimensional model displayed shows the subdivision of the region in to oval / round faveoli (Figure 3.10.4 A and B). Interfaveolar pores are present in large numbers in this area however they are small in size (Figure 3.10.4 C). The 3 dimensional model of the ventral middle region of the 6 month age group category displayed lower divisions of airways into larger faveoli, than that observed cranially (Figure 3.10.5 A and B). The interfaveolar pores present were also predominantly larger in size (Figure 3.10.5 C). The 3 dimensional reconstruction of the ventral caudal region of the 6 month age group category displayed low levels of subdivision (Figure 3.10.6 A and B). A large airway was predominant with faveoli radiating from it. Interfaveolar pores that were present were consistently large in size (Figure 3.10.6 C).

The 12 month age group category 3 dimensional model of the dorsal cranial region showed lower levels of subdivision but also showed numerous faveoli radiating from an airway (Figure 3.11.1 A and B). Interfaveolar pores of were observed in the interfaveolar septa (Figure 3.11.1 C). The 3 dimensional model of the dorsal middle region of the 6 month age group category displayed low levels of subdivision with large faveoli (Figures 3.11.2 A and B). Interfaveolar pores were present and predominantly larger in size (Figure 3.11.2 C). The 3 dimensional reconstruction of the dorsal caudal region of the 12 month age group category was irregularly and poorly subdivided with an airway being the predominant feature of this area (Figure 3.11.3 A and B). The interfaveolar pores that are present are large in size as in the respective middle region (Figure 3.10.2 C and 3.11.3 C).

The ventral middle region 3 dimensional reconstruction of the 12 month age group category showed a peripheral airway with many smaller faveoli radiating from it (Figure 3.11.4 A and B). Interfaveolar pores are present in large numbers (Figure 3.11.4 C). The 3 dimensional model of the ventral middle region of the 12 month age group illustrates

irregular division of large airways into larger faveoli (Figure 3.11.5 A and B). Numerous interfaveolar pores of different sizes are present (Figure 3.11.5 C). The 3 dimensional reconstruction of the ventral caudal region of the 12 month age group category has a large central airway with faveoli radiating from it (Figure 3.11.6 A and B). Interfaveolar pores, predominantly large are easily observable (Figure 3.11.6 C).

The 3 dimensional model of the dorsal cranial region of the 24 month age group category shows good subdivision of the area around an airway (Figure 3.12.1 A and B). Interfaveolar pores are plentiful, the majority small in size (Figure 3.12.1 C). The 3 dimensional reconstruction of the dorsal middle region of the 24 month age group category is well but irregularly subdivided (Figure 3.12.2 A and B). Uniformly sized interfaveolar pores are present within the interfaveolar septa (Figure 3.12.2 C). The dorsal caudal 3 dimensional model of the 24 month age group category is subdivided in a peculiar manner (Figure 3.12.3 A and B).

The 3 dimensional model of the ventral cranial region of the 24 month age group category has a good central air supply with faveoli regularly and evenly radiating around it (Figure 3.12.4 A and B). The interfaveolar pores present are small in size (Figure 3.12.4 C). The ventral middle 3 dimensional reconstruction of the 24 month age group category is irregularly subdivided with faveoli radiating of a large central airway (Figure 3.12.5 A and B). Interfaveolar pores in this region vary in size (Figure 3.12.5 C). The 3 dimensional reconstruction of the ventral caudal region of the 24 month age group category displays large airways and faveoli (Figure 3.12.6 A and B). Numerous interfaveolar pores of varying sizes exist in this region.

Figure 3.9.1: 3 dimensional reconstruction models of the dorsal cranial region of a 3 month old crocodilian lung. (A) is a 3 dimensional model of the airways and the interfaveolar septa that subdivide the airways into numerous faveoli. (B) is a 3 dimensional model of the interfaveolar septa showing their interaction and how its morphology changes. (C) is a 3 dimensional model showing the presence of interfaveolar pores in the interfaveolar septa. F = Faveoli, IFS = Interfaveolar septa, * = Interfaveolar pores.

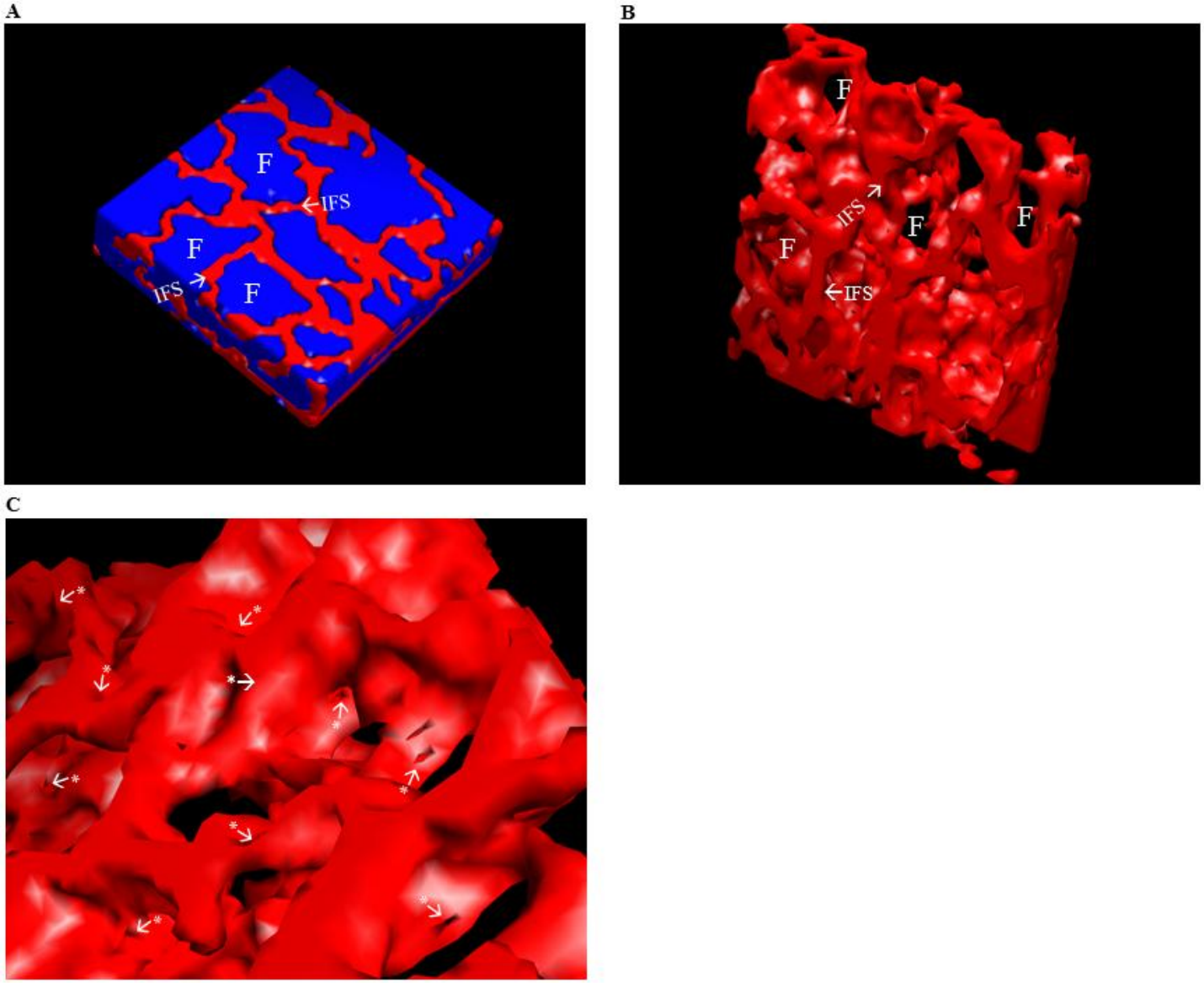
A
F
IFS
F
IFS
F
B
F
IFS
F
F
F
IFS
C

Figure 3.9.2: 3 dimensional reconstruction models of the dorsal middle region of a 3 month old crocodilian lung. (A) is a 3 dimensional model of airways being subdivided by thick and prominent interfaveolar septa. (B) is a 3 dimensional model of the interfaveolar septa showing the arrangement of faveoli. (C) is a 3 dimensional model showing interfaveolar pores and their distribution. F = Faveoli, IFS = Interfaveolar septa, * = Interfaveolar pores.

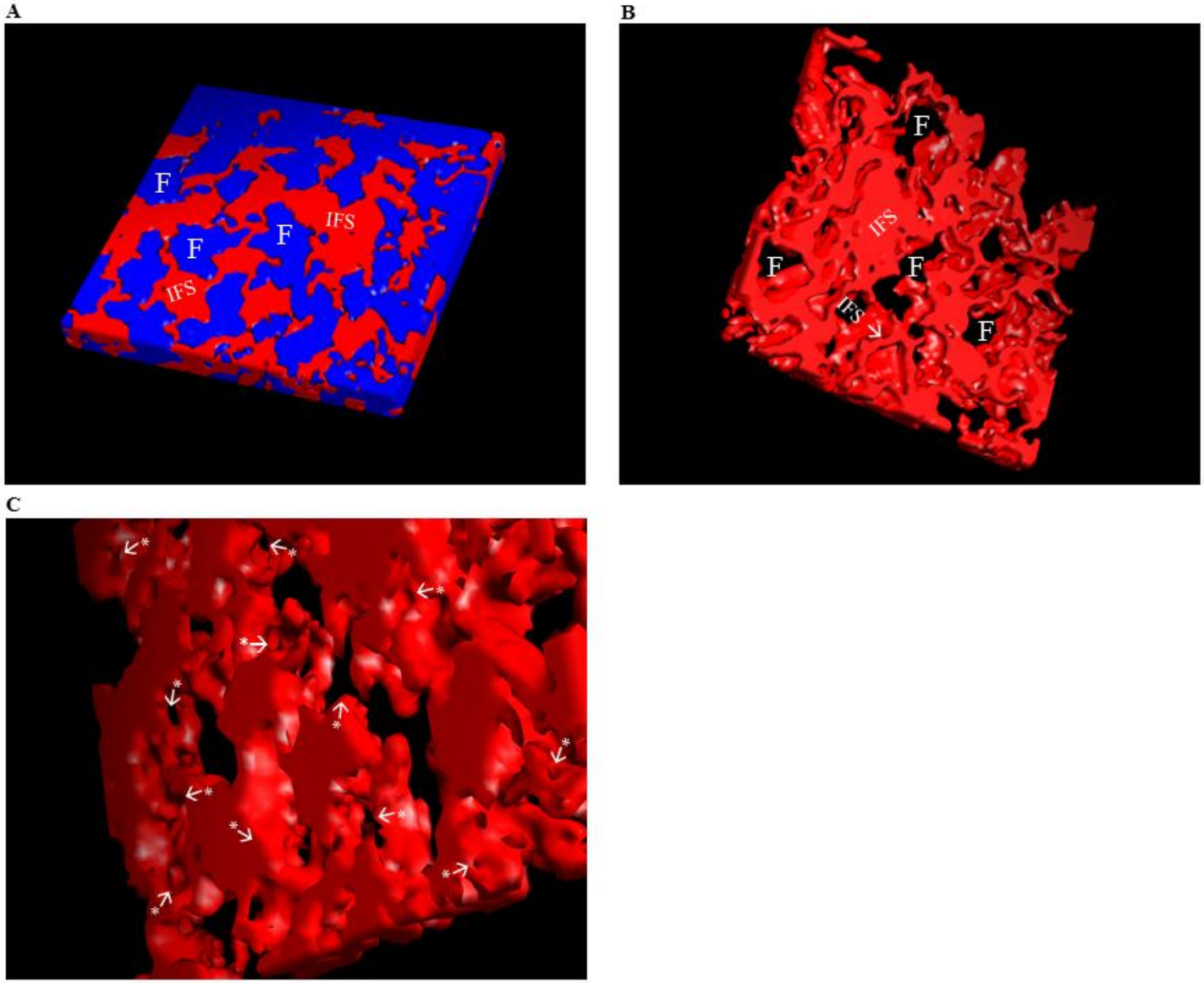
A
F
F
F
IFS
IFS
B
F
IFS
F
F
IFS
F
C

Figure 3.9.3: 3 dimensional reconstruction models of the dorsal caudal region of a 3 month old crocodilian lung. (A) is a 3 dimensional model of the airways and interfaveolar septa of this region. The area has low levels of subdivision and large faveoli. (B) is a 3 dimensional model of the interfaveolar septa that divide this area. (C) is a 3 dimensional model of the interfaveolar pores that are present in this region. A = Airways, F = Faveoli, IFS = Interfaveolar septa, * = Interfaveolar pores.

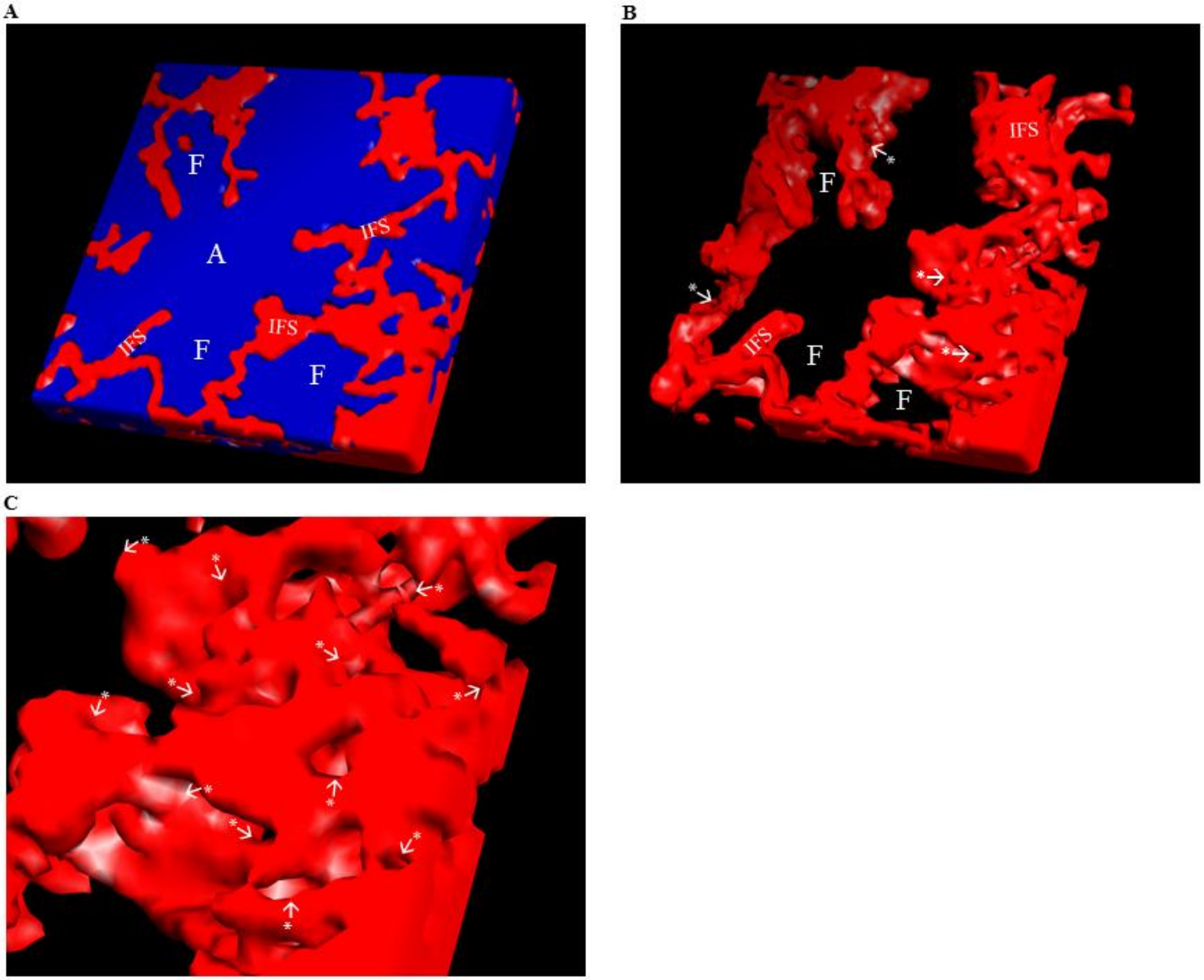
A
F
A
IFS
IFS
F
IFS
F
B
IFS
F
IFS
F
F
C

Figure 3.9.4: 3 dimensional reconstruction models of the ventral cranial region of a 3 month old crocodilian lung. (A) is a 3 dimensional model of the airways and interfaveolar septa. The area is highly subdivided by interfaveolar septa resulting in numerous faveoli. (B) is a 3 dimensional model of the interfaveolar septa that are found in this area. (C) is a 3 dimensional model showing numerous interfaveolar pores with an interfaveolar septum. A = Airways, F = Faveoli, IFS = Interfaveolar septa, * = Interfaveolar pores.

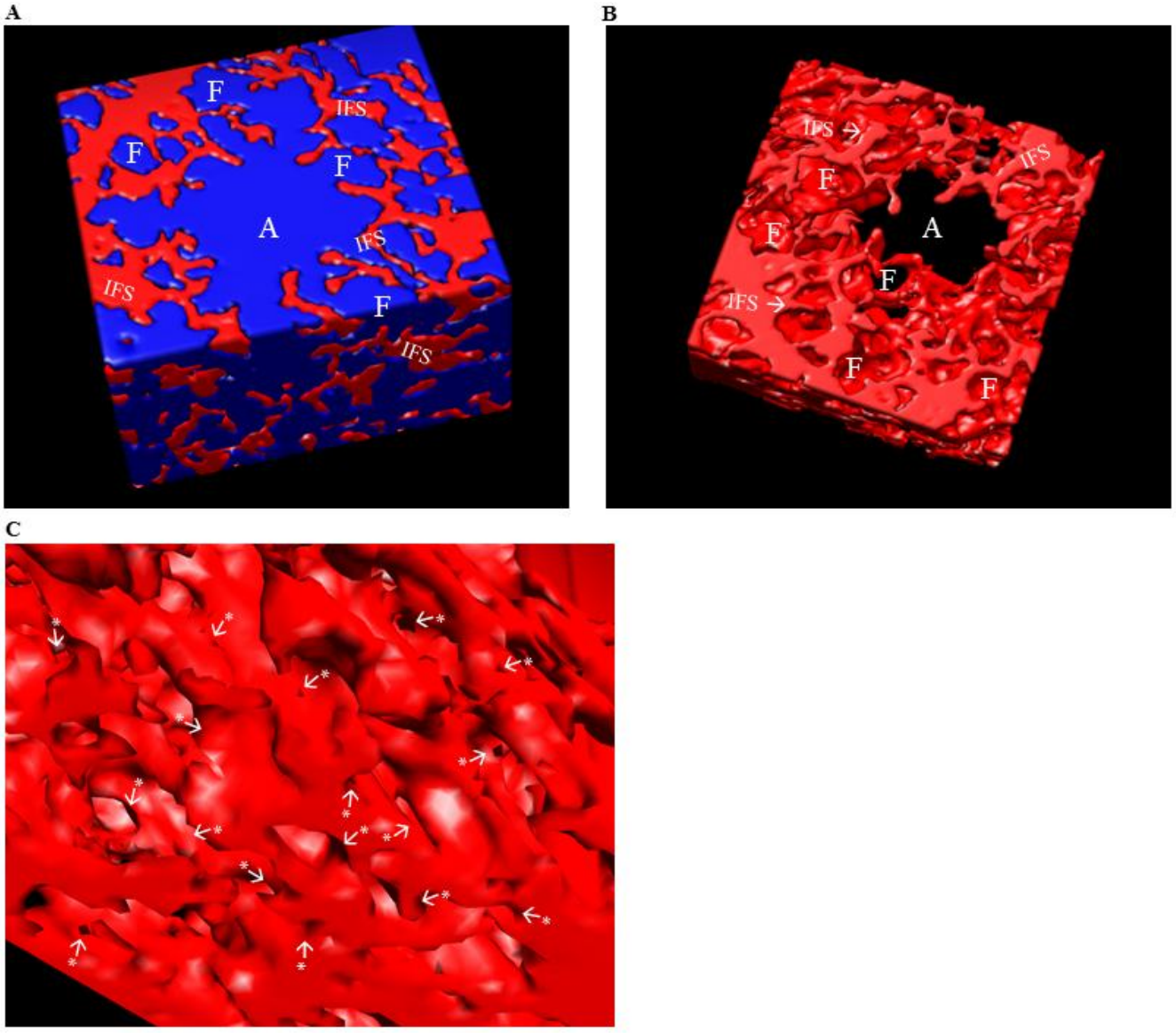
A
F
IFS
F
F
A
IFS
IFS
F
IFS
B
IFS
IFS
F
F
A
F
IFS
F
F
C

Figure 3.9.5: 3 dimensional reconstruction models of the ventral middle region of a 3 month old crocodilian lung. (A) is a 3 dimensional model of the airways and interfaveolar septa of the region. Large airways are present but are subdivided by interfaveolar septa into faveoli. (B) is a 3 dimensional model of the interfaveolar septa that subdivides the airways. (C) is a 3 dimensional model of an interfaveolar septum showing the interfaveolar pores present on it. A = Airways, F = Faveoli, IFS = Interfaveolar septa, * = Interfaveolar pores.

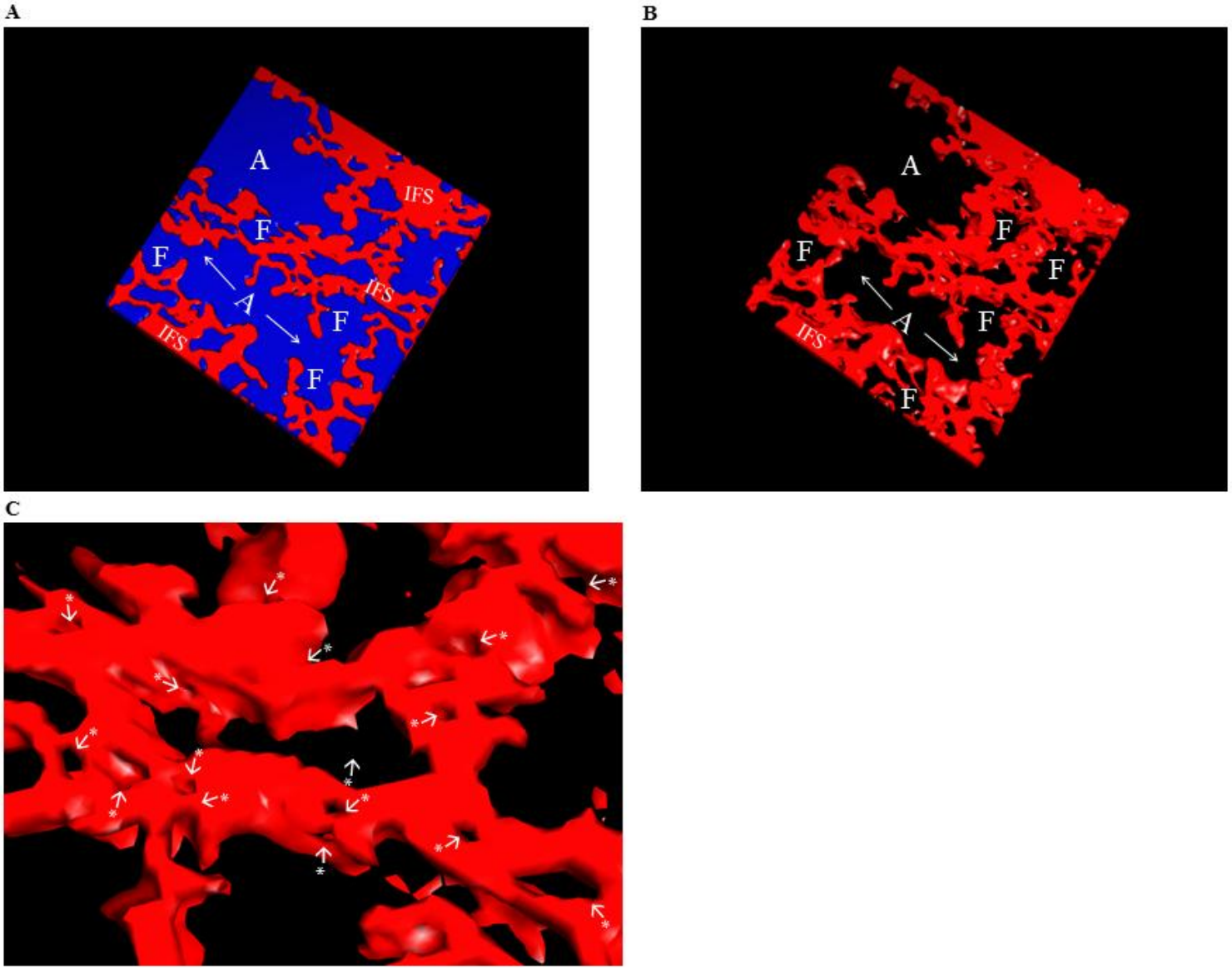
A
A
F
F
IFS
IFS
IFS
F
F
B
A
F
F
F
A
F
IFS
F
C

Figure 3.9.6: 3 dimensional reconstruction models of the ventral caudal region of a 3 month old crocodilian lung. (A) is 3 dimensional reconstruction of the airways and interfaveolar septa found in this area. The interfaveolar septa subdivide the area regularly into various sizes of faveoli. (B) is a 3 dimensional model of the interfaveolar septa representative of this region. (C) is a 3 dimensional reconstruction showing the distribution of interfaveolar pores on interfaveolar septa surrounding a faveolus. F = Faveoli, IFS = Interfaveolar septa, * = Interfaveolar pores.

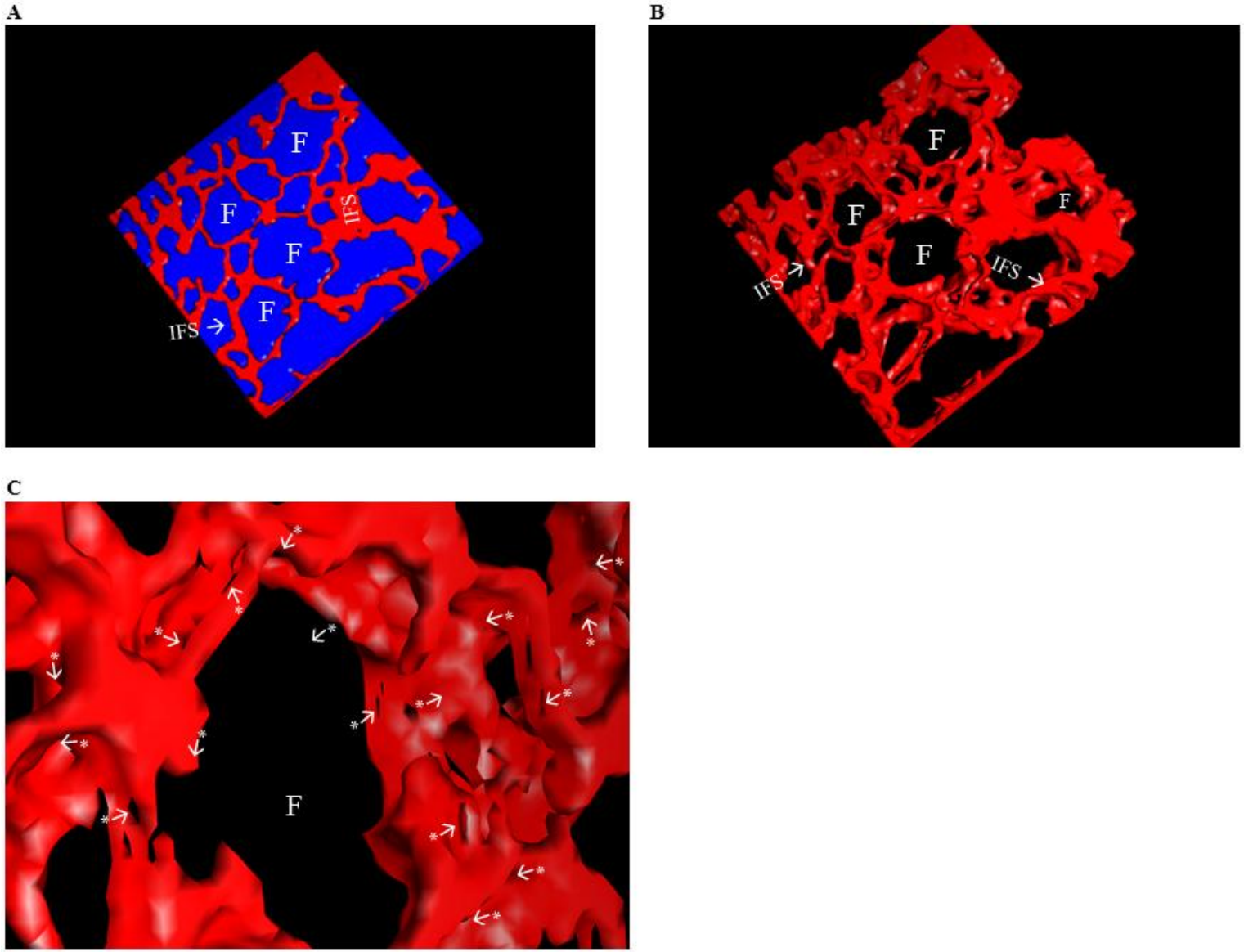
A
F
F
F
F
IFS
B
F
F
F
F
IFS
IFS
C
F

Figure 3.10.1: 3 dimensional reconstruction models of the dorsal cranial region of a 6 month old crocodilian lung. (A) is a 3 dimensional reconstruction showing a regular subdivision of the airways of this region by interfaveolar septa. (B) is a 3 dimensional model of the interfaveolar septa that subdivide the airways. (C) is 3 dimensional model that displays the interfaveolar pores present in the interfaveolar septa of this region. F = Faveoli, IFS = Interfaveolar septa, * = Interfaveolar pores.

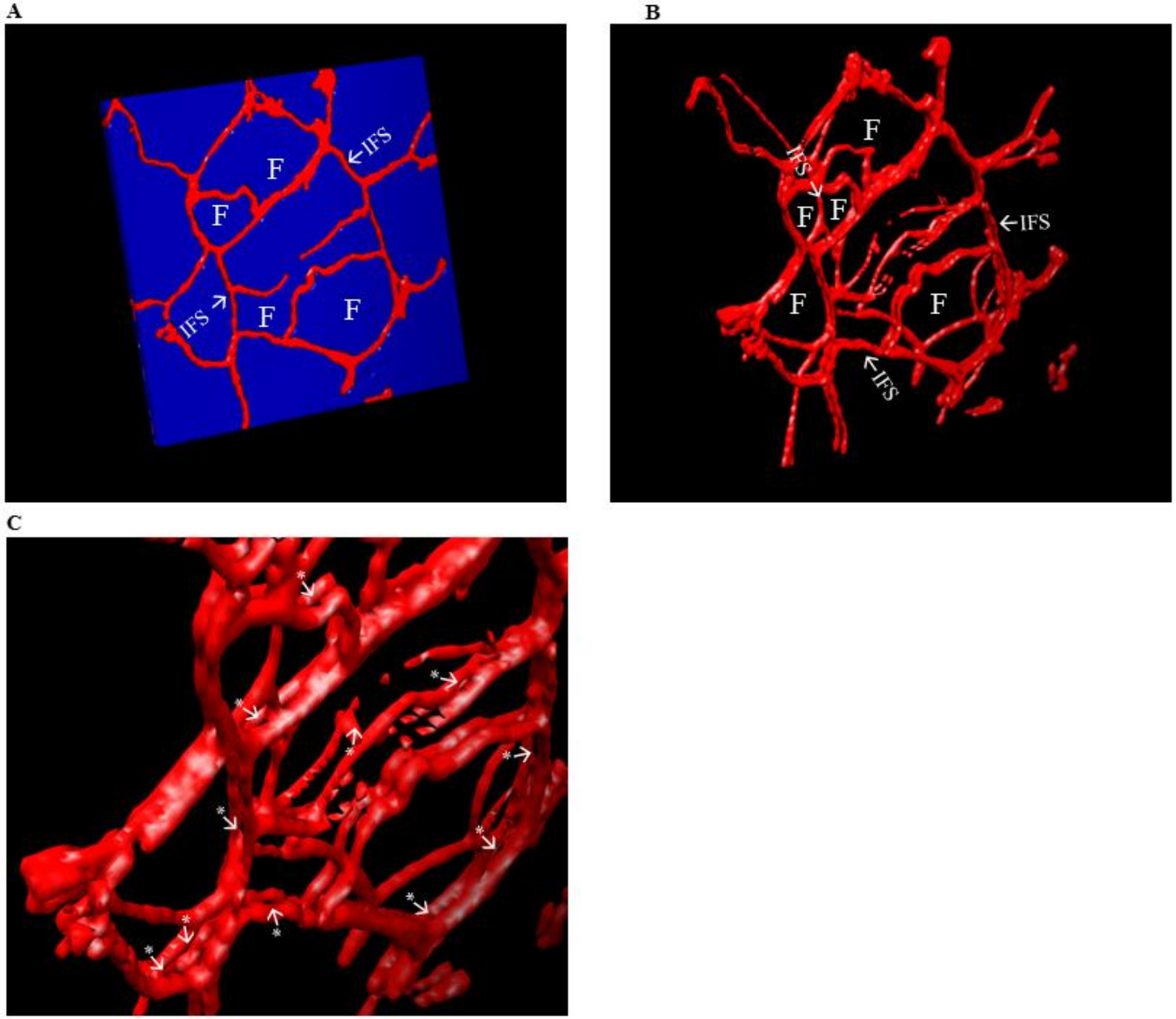
A
F
F
IFS
IFS
F
F
B
F
IFS
F
F
IFS
F
F
IFS
C

Figure 3.10.2: 3 dimensional reconstruction models of the dorsal middle region of a 6 month old crocodilian lung. (A) is a 3 dimensional model illustrating lower degrees of subdivision of airways by interfaveolar septa. (B) is a 3 dimensional model showing the arrangement of interfaveolar septa of this area. (C) is a 3 dimensional model showing the distribution and size of interfaveolar pores in this region. A = Airways, F = Faveoli, IFS = Interfaveolar septa, * = Interfaveolar pores.

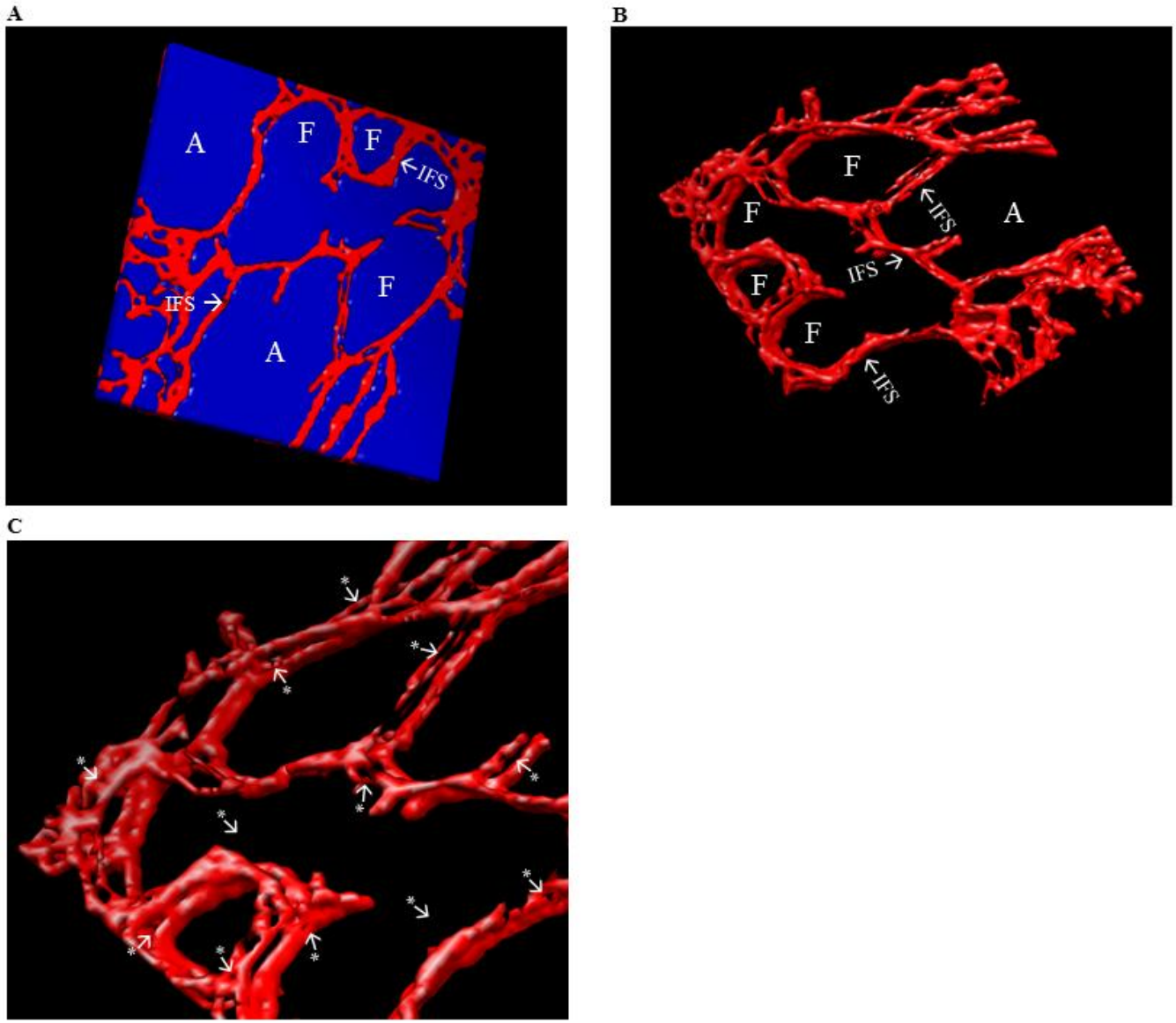
A
A
F
F
IFS
IFS
F
A
B
F
F
IFS
A
IFS
F
F
IFS
C

Figure 3.10.3: 3 dimensional reconstruction models of the dorsal caudal region of a 6 month old crocodilian lung. (A) is 3 dimensional model showing the low subdivision of the airways by interfaveolar septa. (B) is a 3 dimensional model of the interfaveolar septa that divide the airways of this region. (C) is a 3 dimensional model highlighting the interfaveolar pores present in this area. A = Airways, F = Faveoli, IFS = Interfaveolar septa, * = Interfaveolar pores.

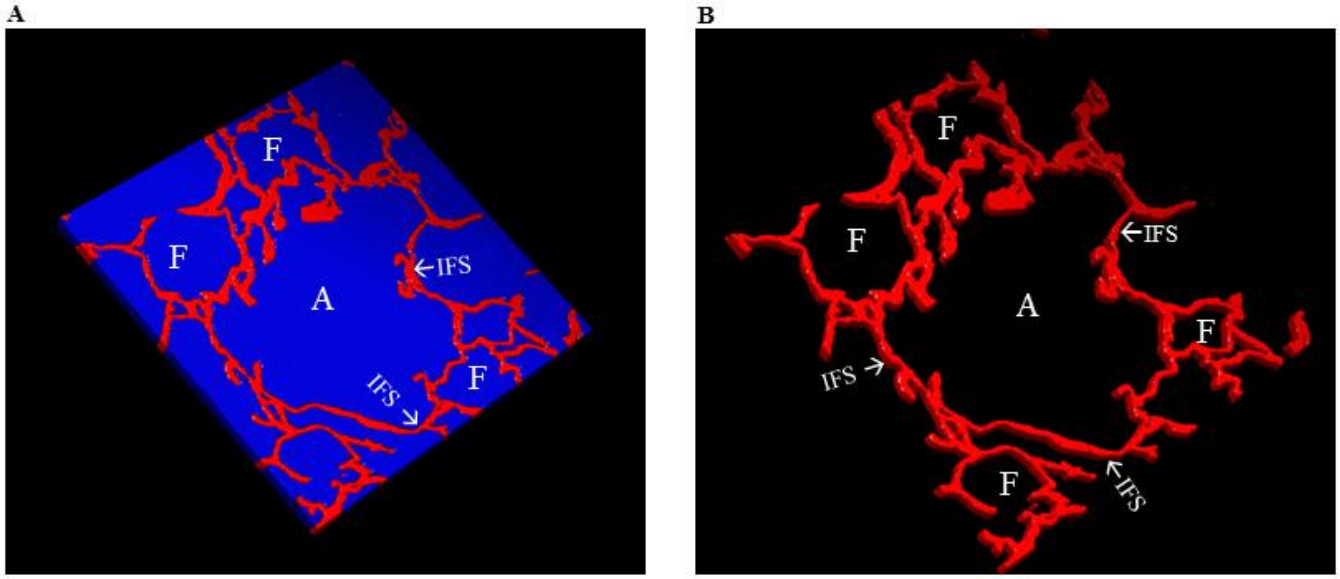
A
F
F
A
IFS
IFS
F
B
F
F
IFS
A
F
IFS
F
IFS
C

Figure 3.10.4: 3 dimensional reconstruction models of the ventral cranial region of a 6 month old crocodilian lung. (A) is a 3 dimensional model showing the regular subdivision of a localised airway into faveoli. (B) is a 3 dimensional model of the interfaveolar septa that divide airways in this region. (C) is a 3 dimensional model showing the small size of the numerous interfaveolar pores that exist in this region. F = Faveoli, IFS = Interfaveolar septa, * = Interfaveolar pores.

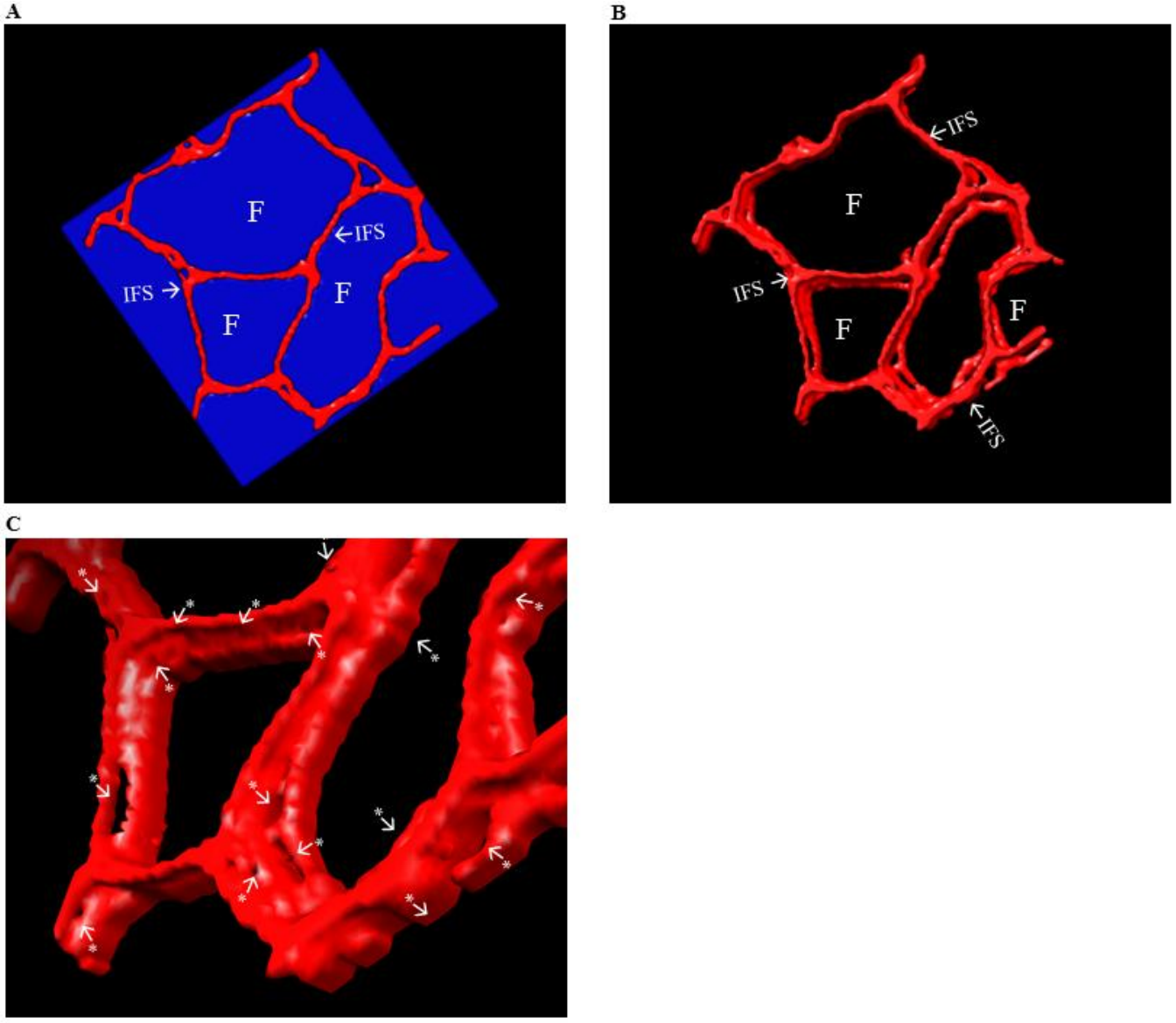
A
F
IFS
IFS
F
F
B
IFS
F
IFS
F
F
IFS
C

Figure 3.10.5: 3 dimensional reconstruction models of the ventral middle region of a 6 month old crocodilian lung. (A) is a 3 dimensional model of the irregularly subdivided airways of this region by interfaveolar septa. (B) is a 3 dimensional model of the interfaveolar septa that divide the airways of this region. (C) is a 3 dimensional model showing the distribution and various sizes of interfaveolar pores on interfaveolar septa in this region. F = Faveoli, IFS = Interfaveolar septa, * = Interfaveolar pores.

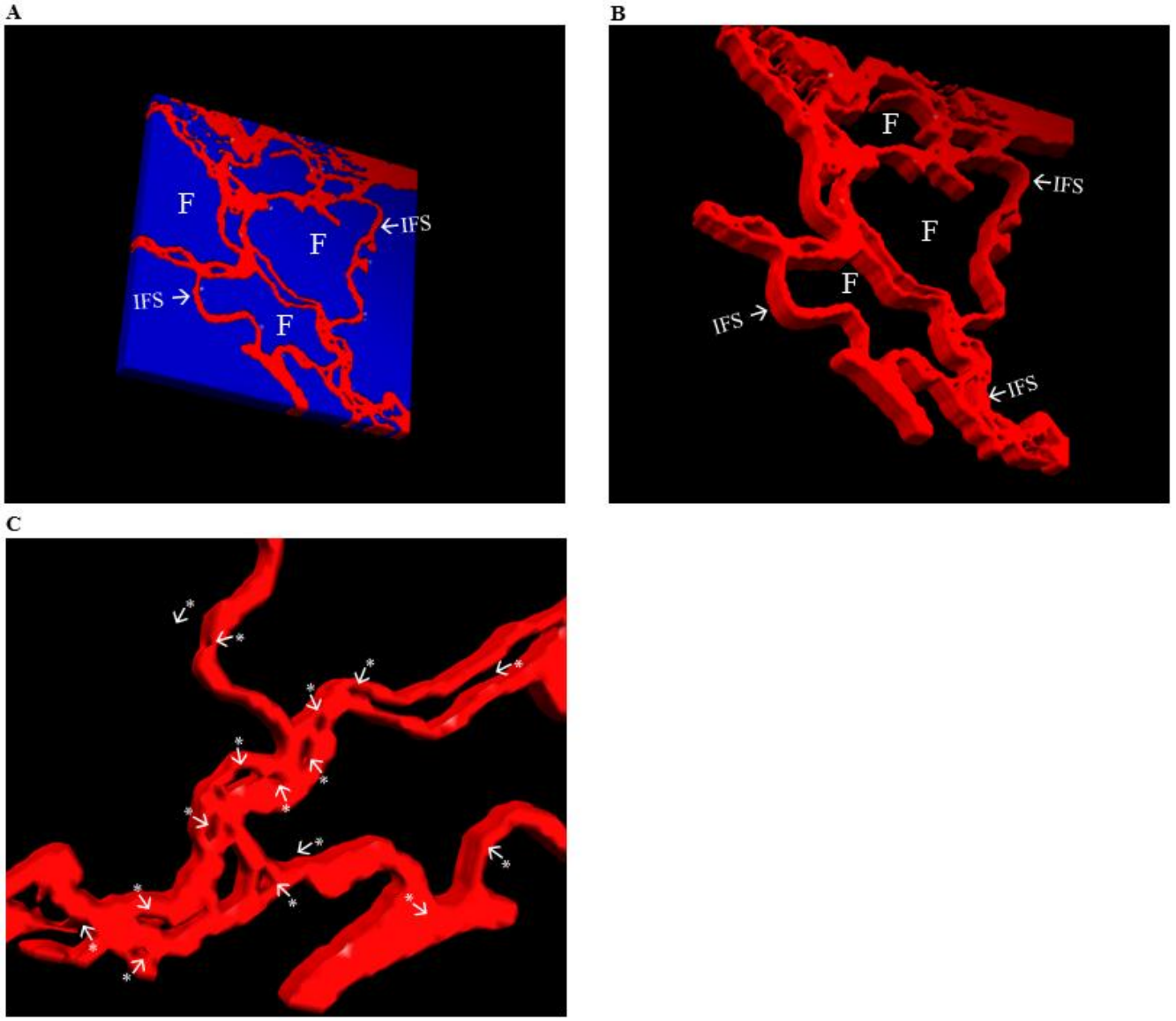
A
F
F
F
IFS
IFS
B
F
F
F
IFS
IFS
IFS
C

Figure 3.10.6: 3 dimensional reconstruction models of the ventral caudal region of a 6 month old crocodilian lung. (A) is a 3 dimensional model of an airway with faveoli radiating from it. (B) is a 3 dimensional model displaying the interfaveolar septa that subdivides the area. (C) is a 3 dimensional model of the numerous interfaveolar pores which are variable in size. A= Airways, F = Faveoli, IFS = Interfaveolar septa, * = Interfaveolar pores.

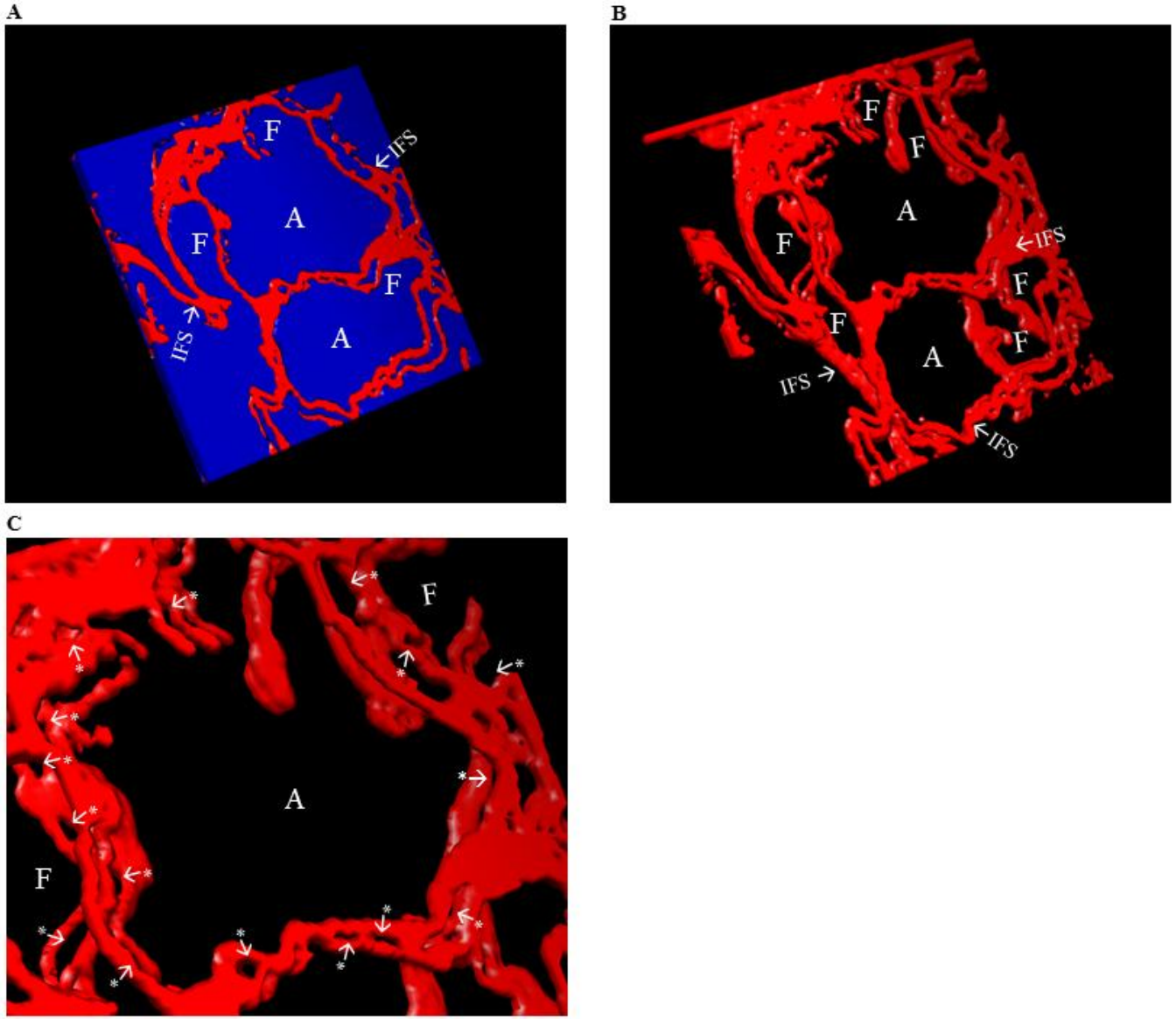
A
F
IFS
A
F
F
IFS
A
B
F
F
A
F
IFS
F
F
A
IFS
IFS
C
F
A
F

Figure 3.11.1: 3 dimensional reconstruction models of the dorsal cranial region of a 12 month old crocodilian lung. (A) is a 3 dimensional model showing the subdivision of airways into faveoli by interfaveolar septa. (B) is a 3 dimensional model of the interfaveolar septa showing their arrangement. (C) is a 3 dimensional model of interfaveolar septa, delineating airways and faveoli, with interfaveolar pores within them. A= Airways, F = Faveoli, IFS = Interfaveolar septa, * = Interfaveolar pores.

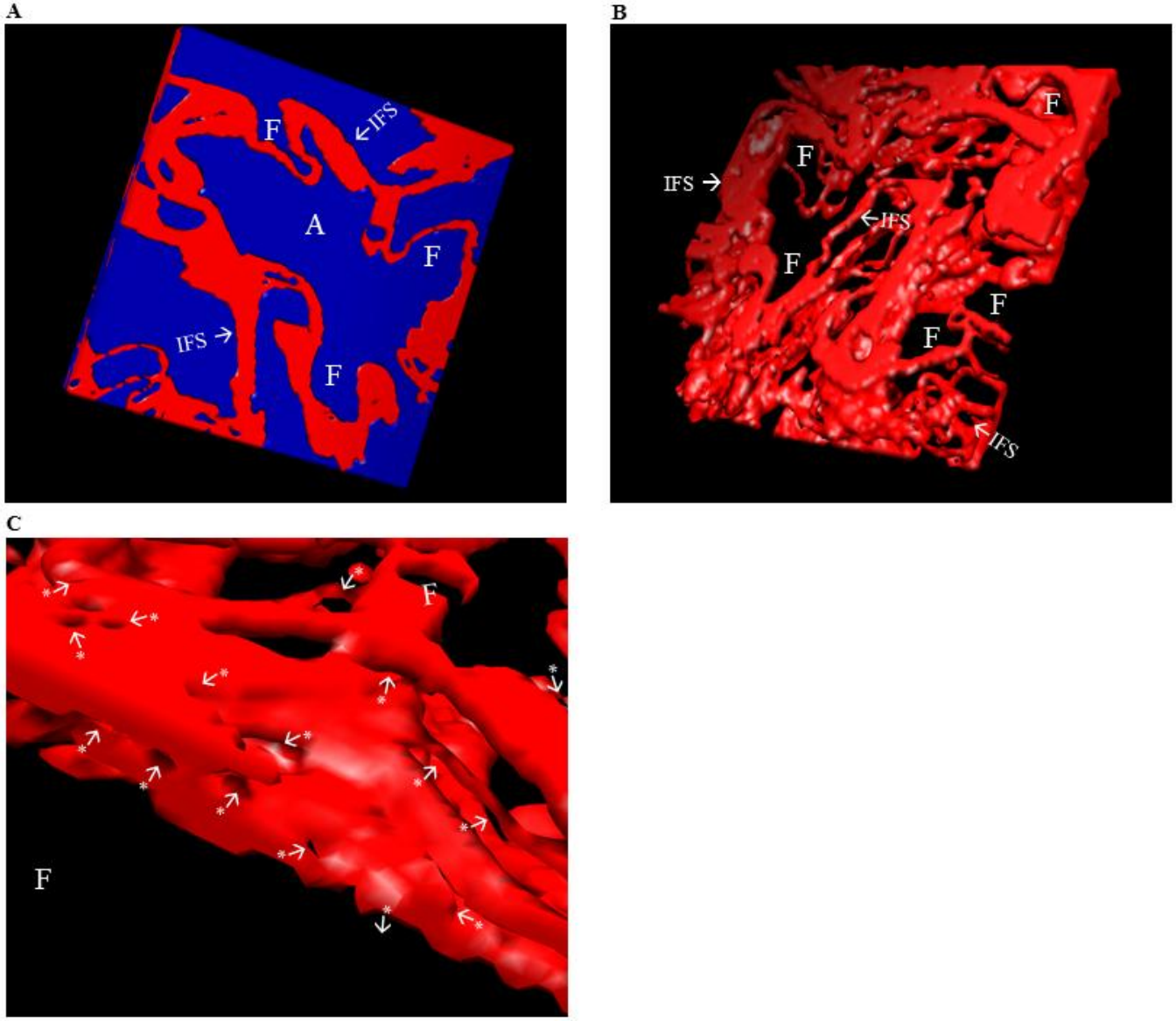
A
F
IFS
A
F
IFS
F
B
F
F
IFS
IFS
F
F
F
IFS
C
F
F

Figure 3.11.2: 3 dimensional reconstruction models of the dorsal middle region of a 12 month old crocodilian lung. (A) is a 3 dimensional model of the region illustrating a low degree of subdivision of the airways. The faveoli that are delineated are large in size. (B) is a 3 dimensional model showing the arrangement of the interfaveolar septa in this region. (C) is a 3 dimensional reconstruction showing the density and variable size of interfaveolar pores in this region. F = Faveoli, IFS = Interfaveolar septa, * = Interfaveolar pores.

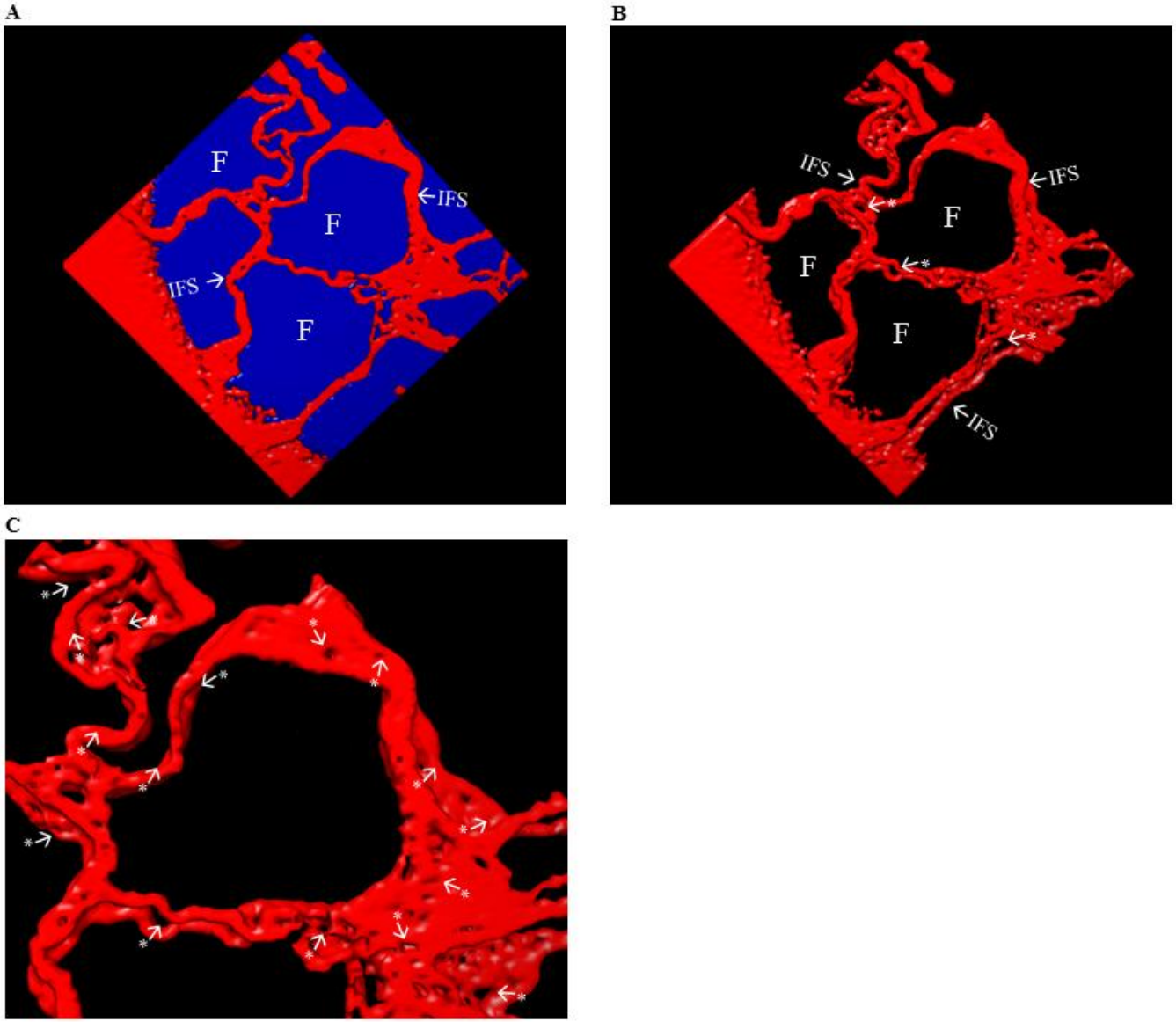
A
F
F
F
IFS
IFS
B
IFS
IFS
F
F
F
IFS
C

Figure 3.11.3: 3 dimensional reconstruction models of the dorsal caudal region of a 12 month old crocodilian lung. (A) is a 3 dimensional model showing the irregular and low level of subdivision of this region. (B) is a 3 dimensional model of the interfaveolar septa present in this area. (C) is a 3 dimensional model showing large interfaveolar pores around a faveolus. A = Airways, F = Faveoli, IFS = Interfaveolar septa, * = Interfaveolar pores.

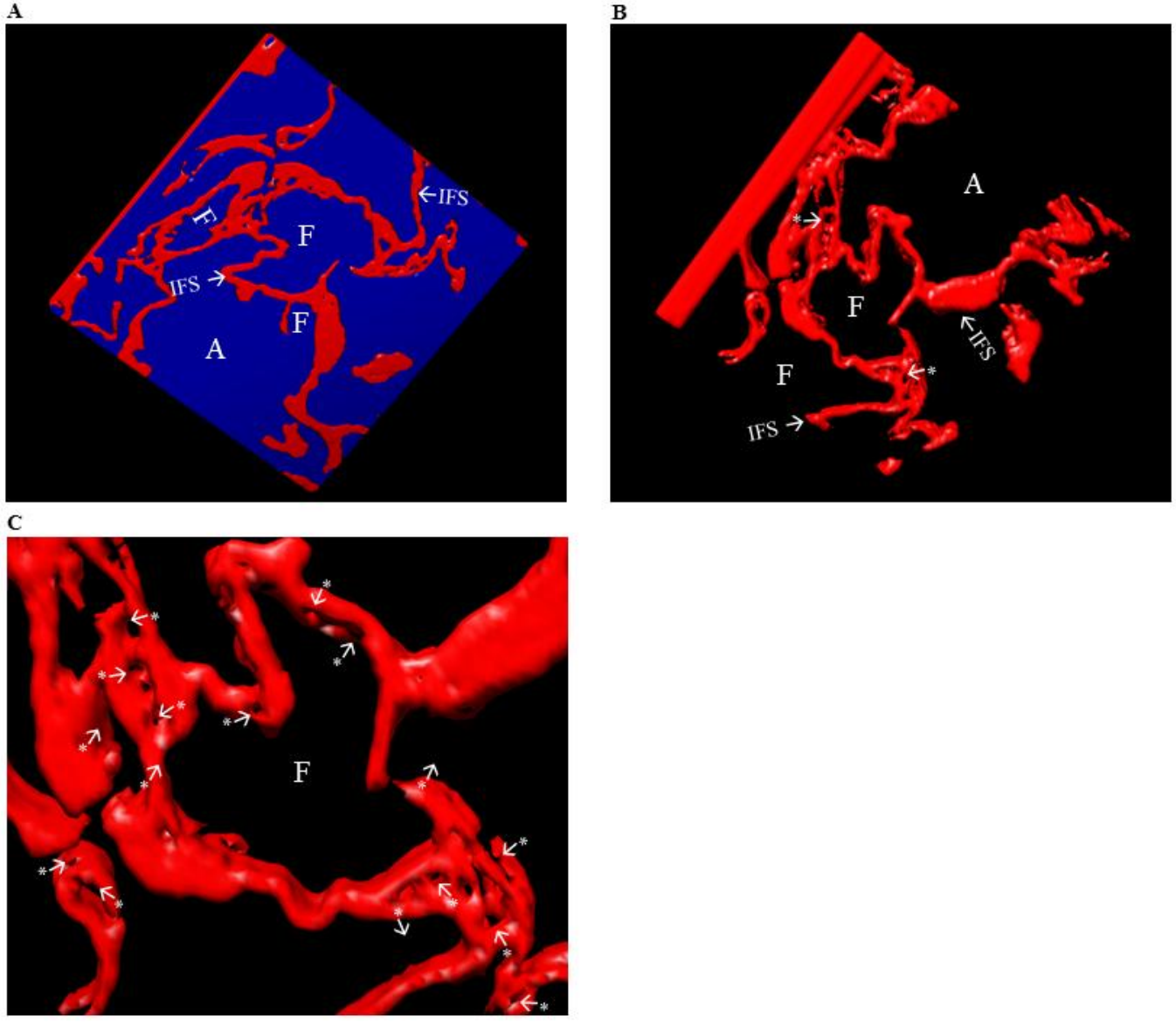
A
F
IFS
F
IFS
F
A
B
A
F
IFS
F
IFS
C
F

Figure 3.11.4: 3 dimensional reconstruction models of the ventral cranial region of a 12 month old crocodilian lung. (A) is a 3 dimensional model showing a large peripheral airway with faveoli radiating from it. (B) is a 3 dimensional model of the interfaveolar septa that facilitates the division. (C) is a 3 dimensional model of the numerous interfaveolar pores that occur on interfaveolar septa in this region. A= Airways, F = Faveoli, IFS = Interfaveolar septa, * = Interfaveolar pores.

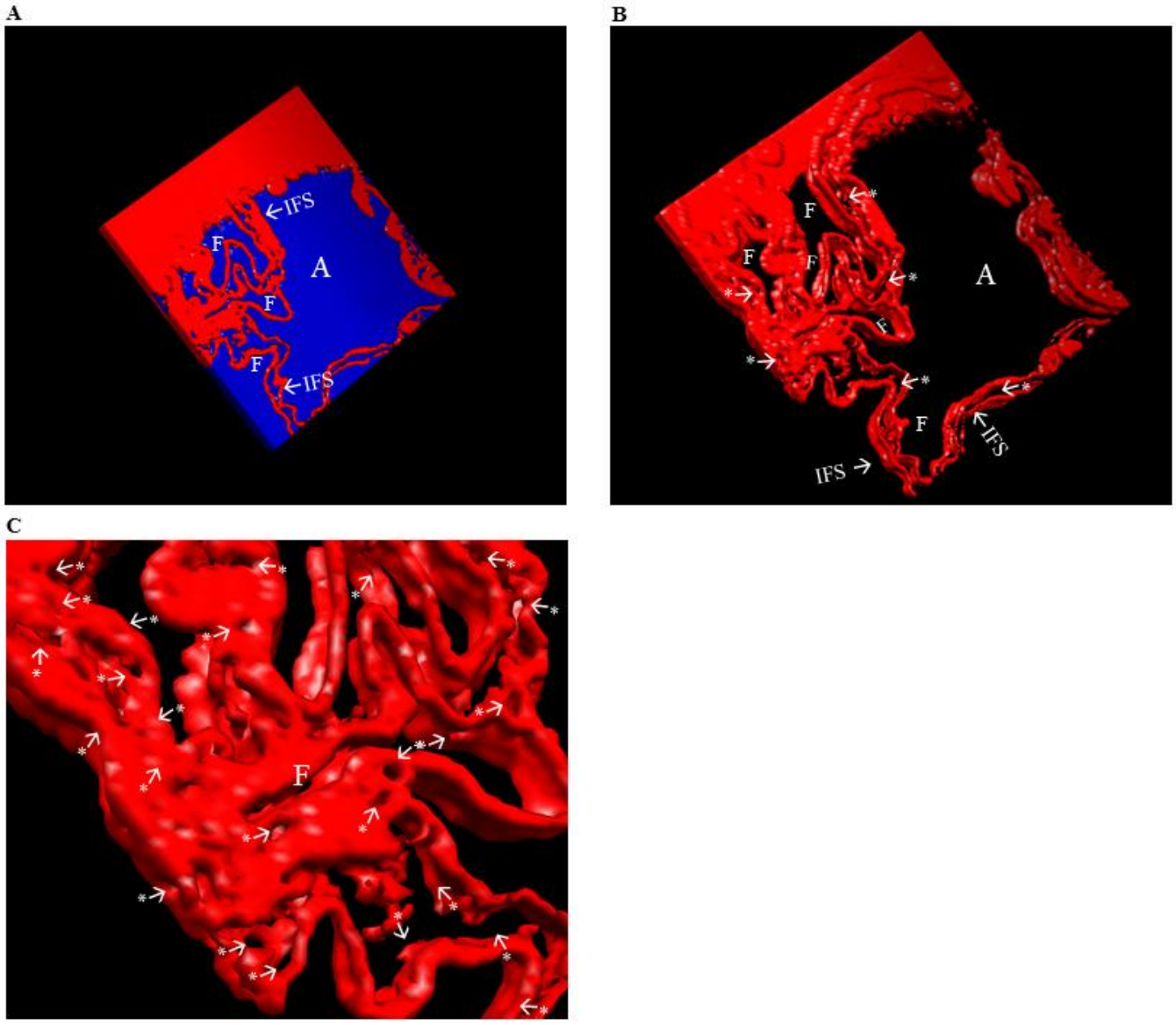
A
IFS
F
A
F
F
IFS
B
F
F
F
A
F
IFS
IFS
C
F

Figure 3.11.5: 3 dimensional reconstruction models of the ventral middle region of a 12 month old crocodilian lung. (A) is a 3 dimensional model showing the asymmetrical subdivision of airways into faveoli. (B) is a 3 dimensional model of the arrangement of the interfaveolar septa. (C) is a 3 dimensional model showing the distribution of various sizes of interfaveolar pores on interfaveolar septa in this region. F = Faveoli, IFS = Interfaveolar septa, * = Interfaveolar pores.

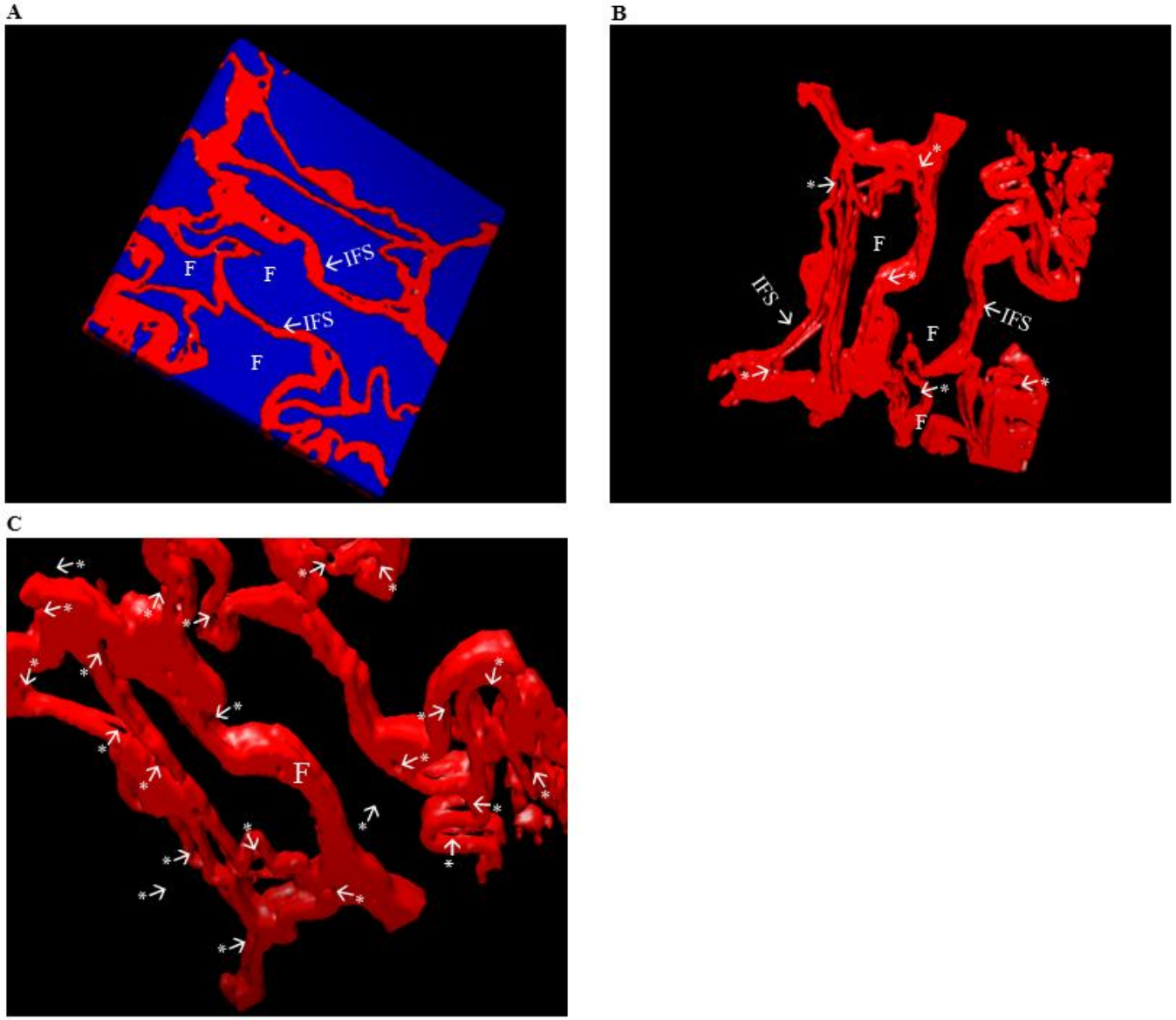
A
F
F
IFS
IFS
F
B
IFS
F
IFS
F
F
C
F

Figure 3.11.6: 3 dimensional reconstruction models of the ventral caudal region of a 12 month old crocodilian lung. (A) is a 3 dimensional model of depicting low levels of subdivision of airways into faveoli. (B) is a 3 dimensional model of the structure of the interfaveolar septa of this area. (C) is a 3 dimensional model of numerous interfaveolar pores, which vary in size, within interfaveolar septa of this region. A = Airways, F = Faveoli, IFS = Interfaveolar septa, * = Interfaveolar pores.

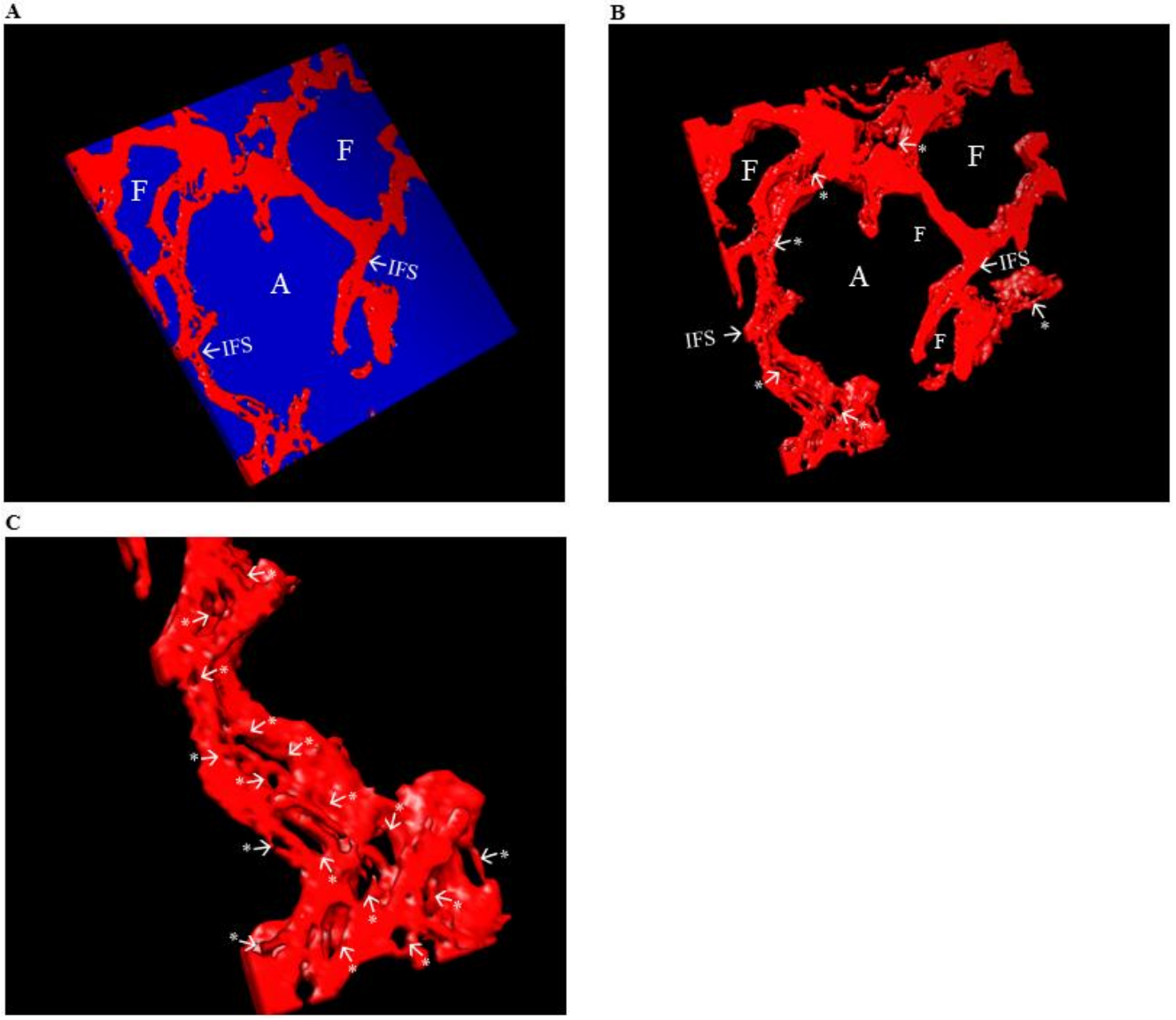
A
F
F
A
IFS
IFS
B
F
F
F
A
IFS
IFS
F
C

Figure 3.12.1: 3 dimensional reconstruction models of the dorsal cranial region of a 24 month old crocodilian lung. (A) is a 3 dimensional model showing the division of airways into various sizes of faveoli. (B) is a 3 dimensional model showing the assembly of interfaveolar septa in this region. (C) is a 3 dimensional model of the high density of interfaveolar pores present in this area. A = Airways, F = Faveoli, IFS = Interfaveolar septa, * = Interfaveolar pores.

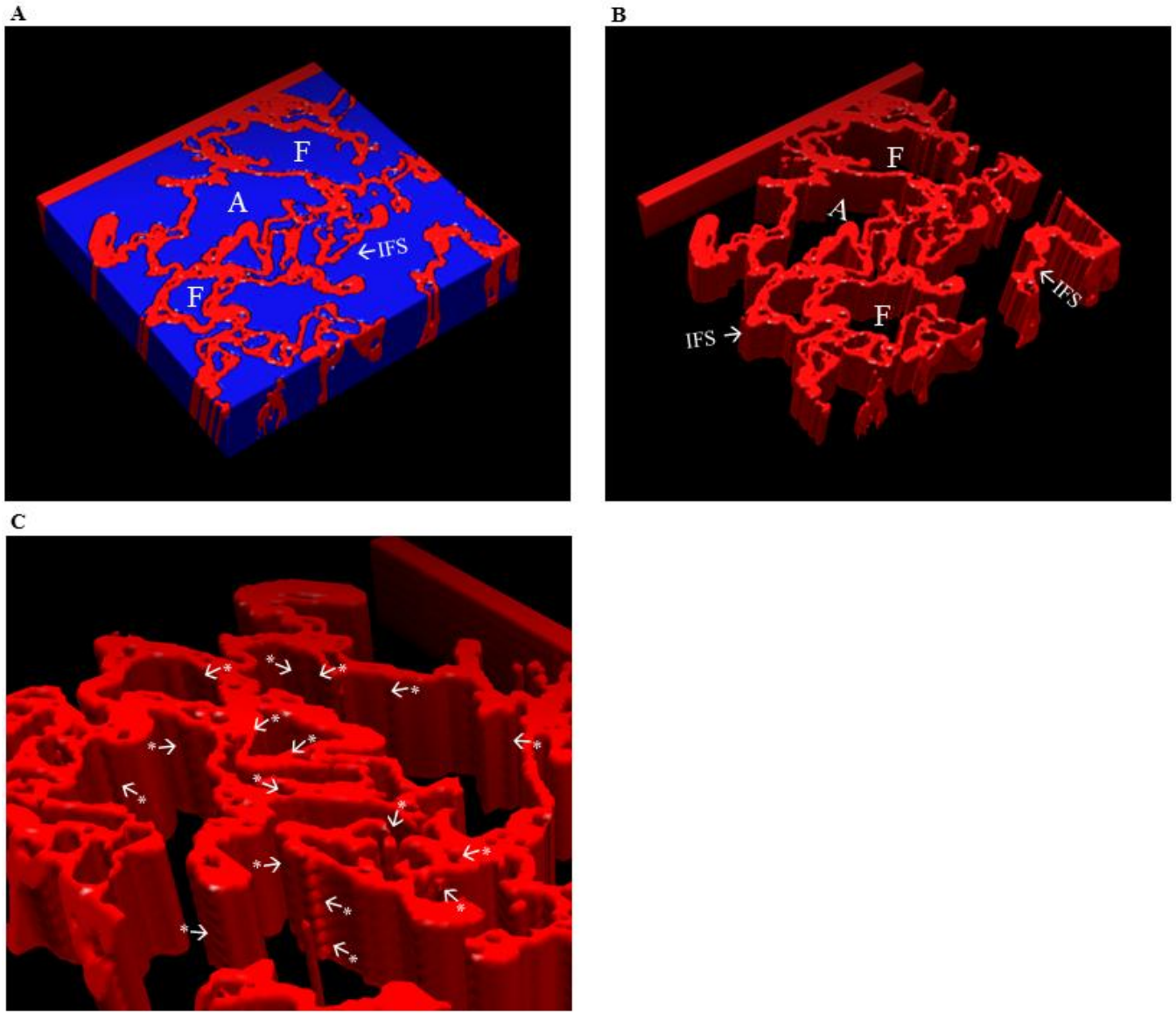
A
F
A
IFS
F
B
F
A
IFS
F
IFS
C

Figure 3.12.2: 3 dimensional reconstruction models of the dorsal middle region of a 24 month old crocodilian lung. (A) is a 3 dimensional model of the irregularly subdivided airways of this region. (B) is a 3 dimensional model showing the structure of the interfaveolar septa found in this area. (C) is a 3 dimensional model of the interfaveolar pores present with the interfaveolar septa of this region. A = Airways, F = Faveoli, IFS = Interfaveolar septa, * = Interfaveolar pores.

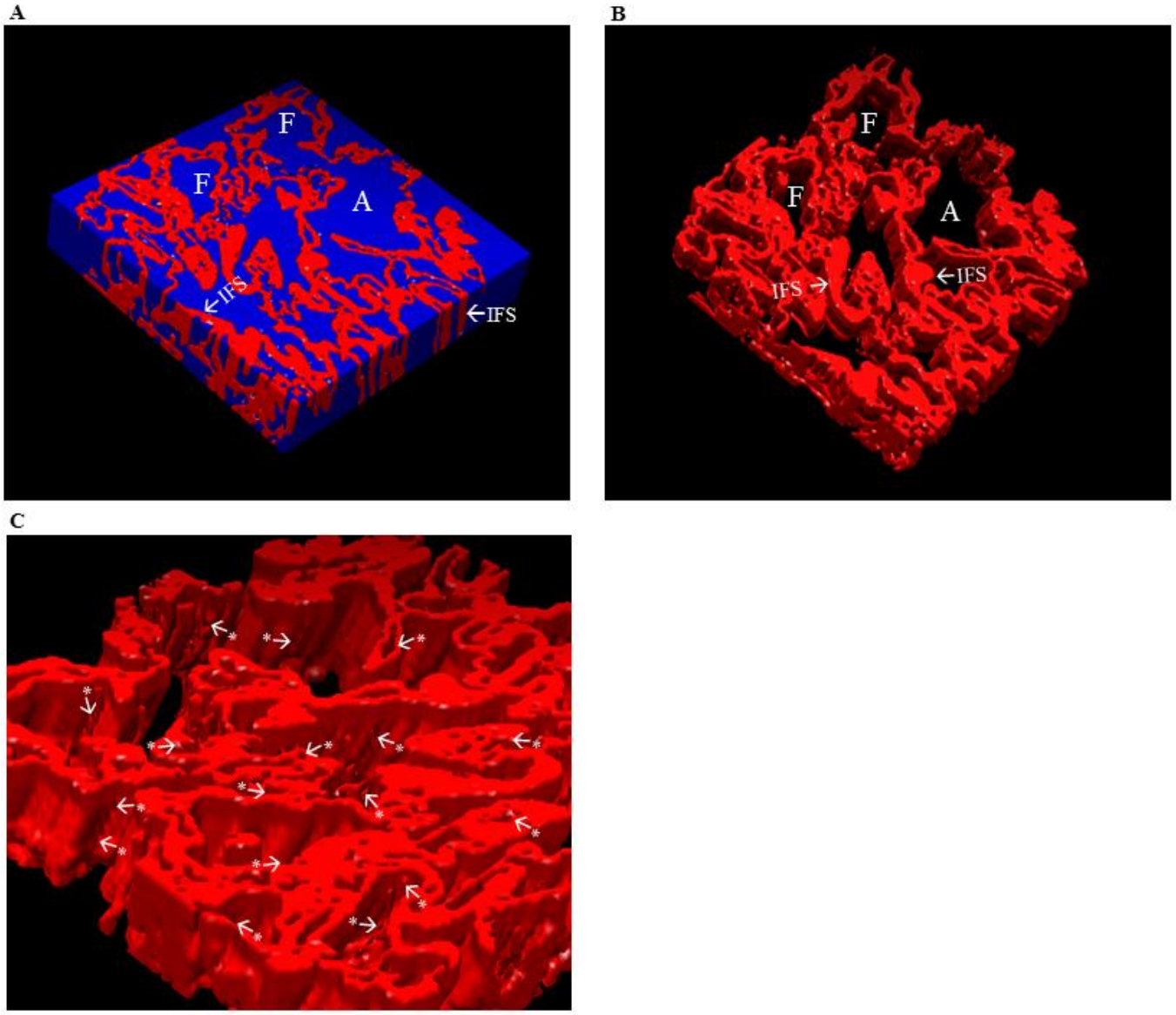
A
F
F
A
IFS
IFS
B
F
F
A
IFS
IFS
C

Figure 3.12.3: 3 dimensional reconstruction models of the dorsal caudal region of a 24 month old crocodilian lung (A) is a 3 dimensional model showing the odd subdivision of the airways of this region. (B) is a 3 dimensional model of the interfaveolar septa that subdivides this region. (C) is a 3 dimensional model of the interfaveolar pores within the interfaveolar septa of this region. A = Airways, F = Faveoli, IFS = Interfaveolar septa, * = Interfaveolar pores.

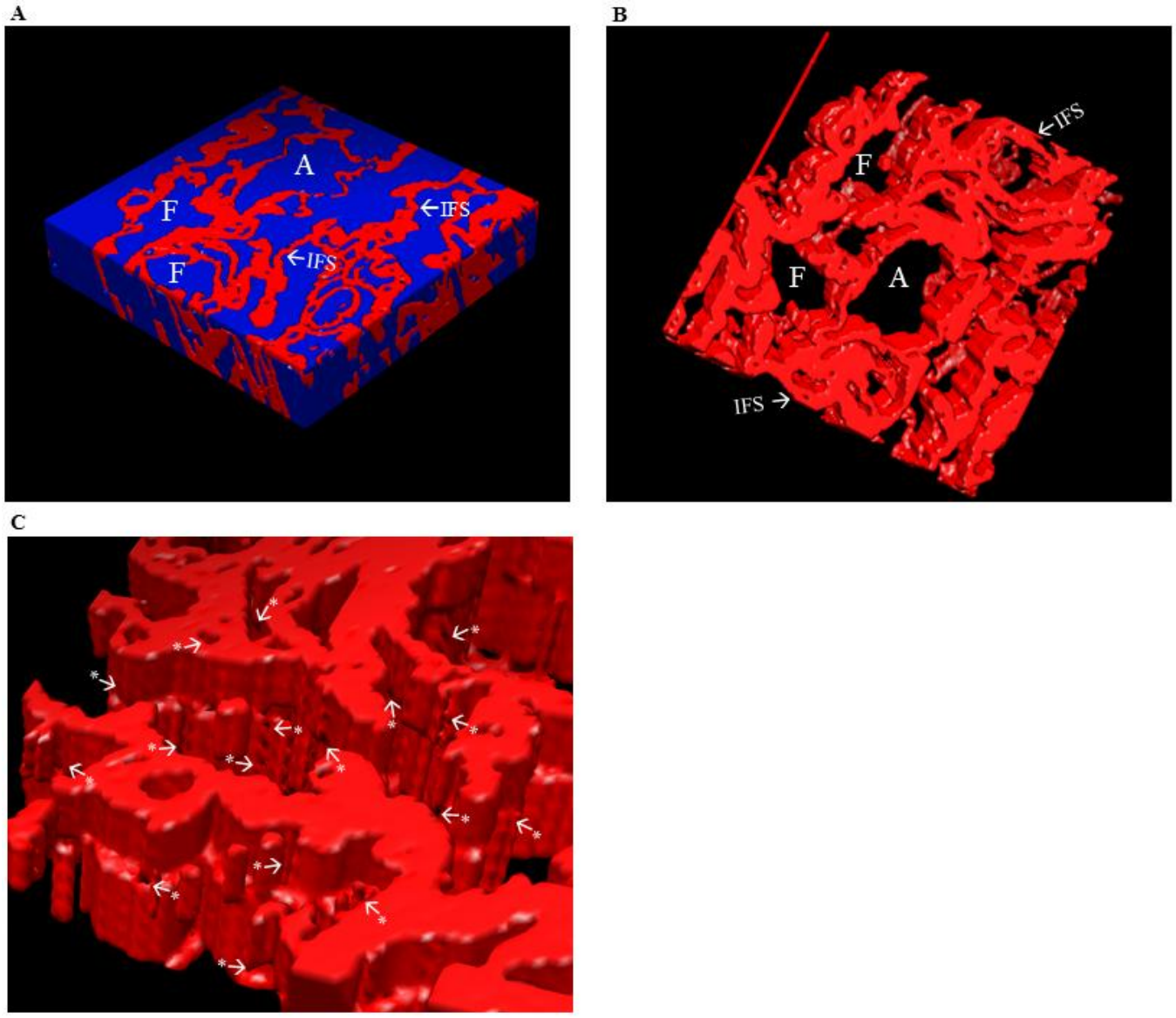
A
A
F
F
IFS
IFS
B
F
F
A
IFS
IFS
C

Figure 3.12.4: 3 dimensional reconstruction models of the ventral cranial region of a 24 month old crocodilian lung. (A) is a 3 dimensional model illustrating a rich air supply that is well subdivided. Two airways are central and faveoli radiate from them. (B) is a 3 dimensional reconstruction of the layout of the interfaveolar septa in (A). (C) is a 3 dimensional reconstruction illustrating the numerous interfaveolar pores in the wall of the interfaveolar septa. A = Airways, F = Faveoli, IFS = Interfaveolar septa, * = Interfaveolar pores.

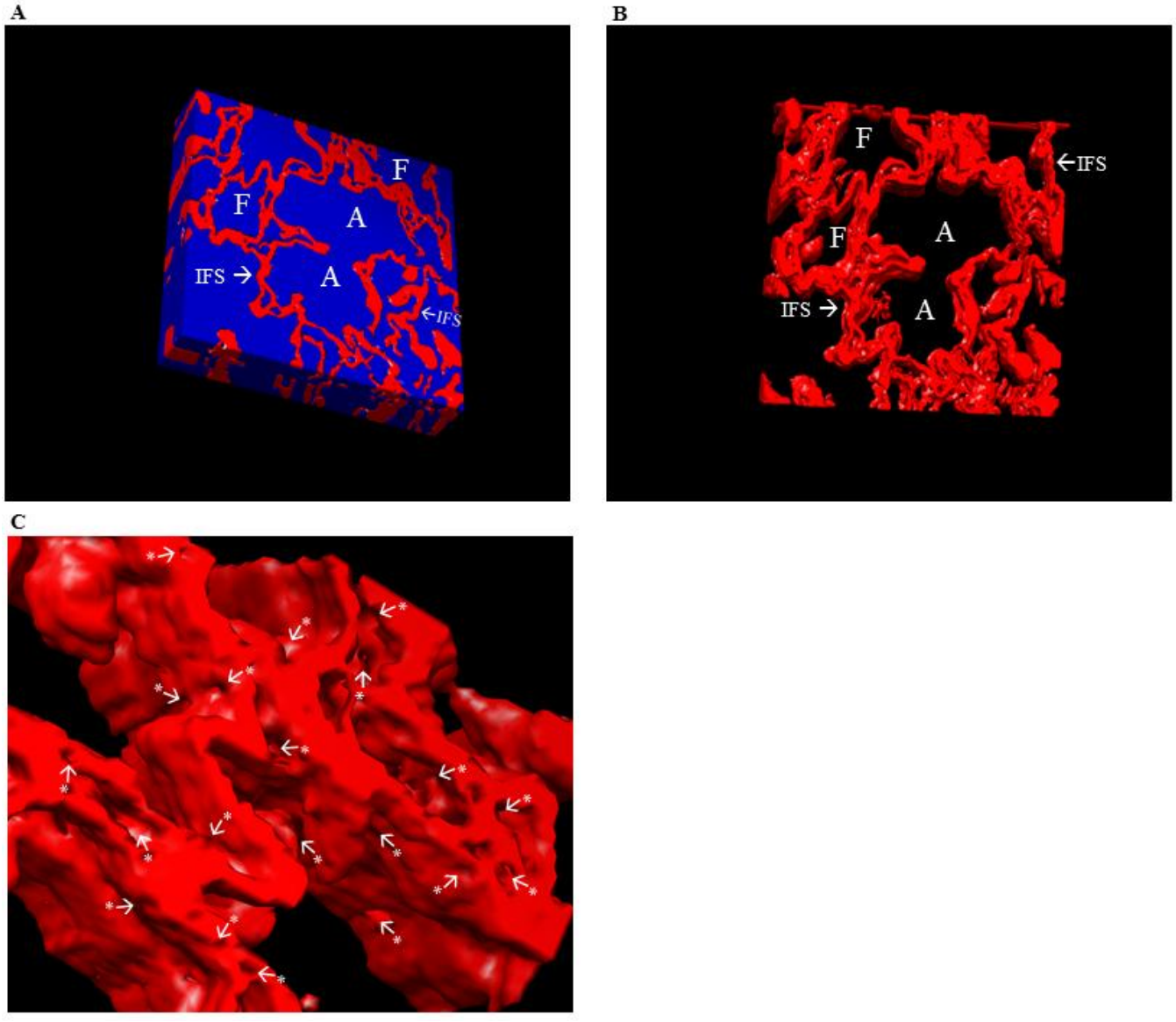
A
F
F
A
IFS →
A
←IFS
B
F
←IFS
F
A
IFS →
A
C

Figure 3.12.5: 3 dimensional reconstruction models of the ventral middle region of a 24 month old crocodilian lung. (A) is a 3 dimensional reconstruction showing an aberrant subdivision of airways. Faveoli can also be seen radiating from the large central airway. (B) is a 3 dimensional model of the interfaveolar septa that subdivides this region. (C) is a 3 dimensional model that displays numerous interfaveolar pores which vary in size. A = Airways, F = Faveoli, IFS = Interfaveolar septa, * = Interfaveolar pores.

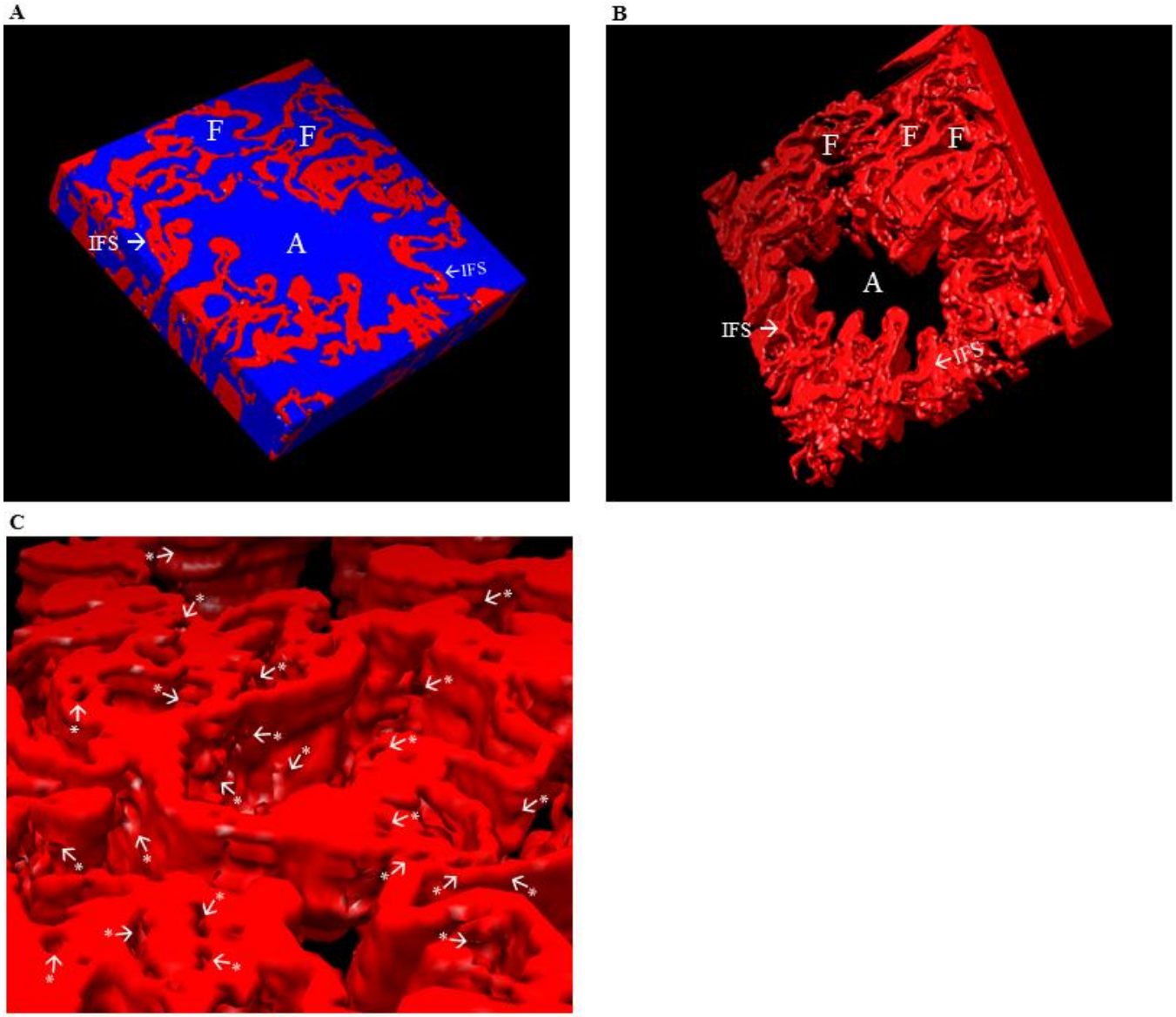
A
F
F
A
IFS →
←IFS
B
F
F
F
A
IFS →
←IFS
C

Figure 3.12.6: 3 dimensional reconstruction models of the ventral caudal region of a 24 month old crocodilian lung. (A) is a 3 dimensional model showing a simple subdivision of airways into larger faveoli. (B) is 3 dimensional model illustrating the structure of the interfaveolar septa of this region. (C) is a 3 dimensional model of interfaveolar septa showing a large number of interfaveolar pores of different sizes within them. A = Airways, F = Faveoli, IFS = Interfaveolar septa, * = Interfaveolar pores.

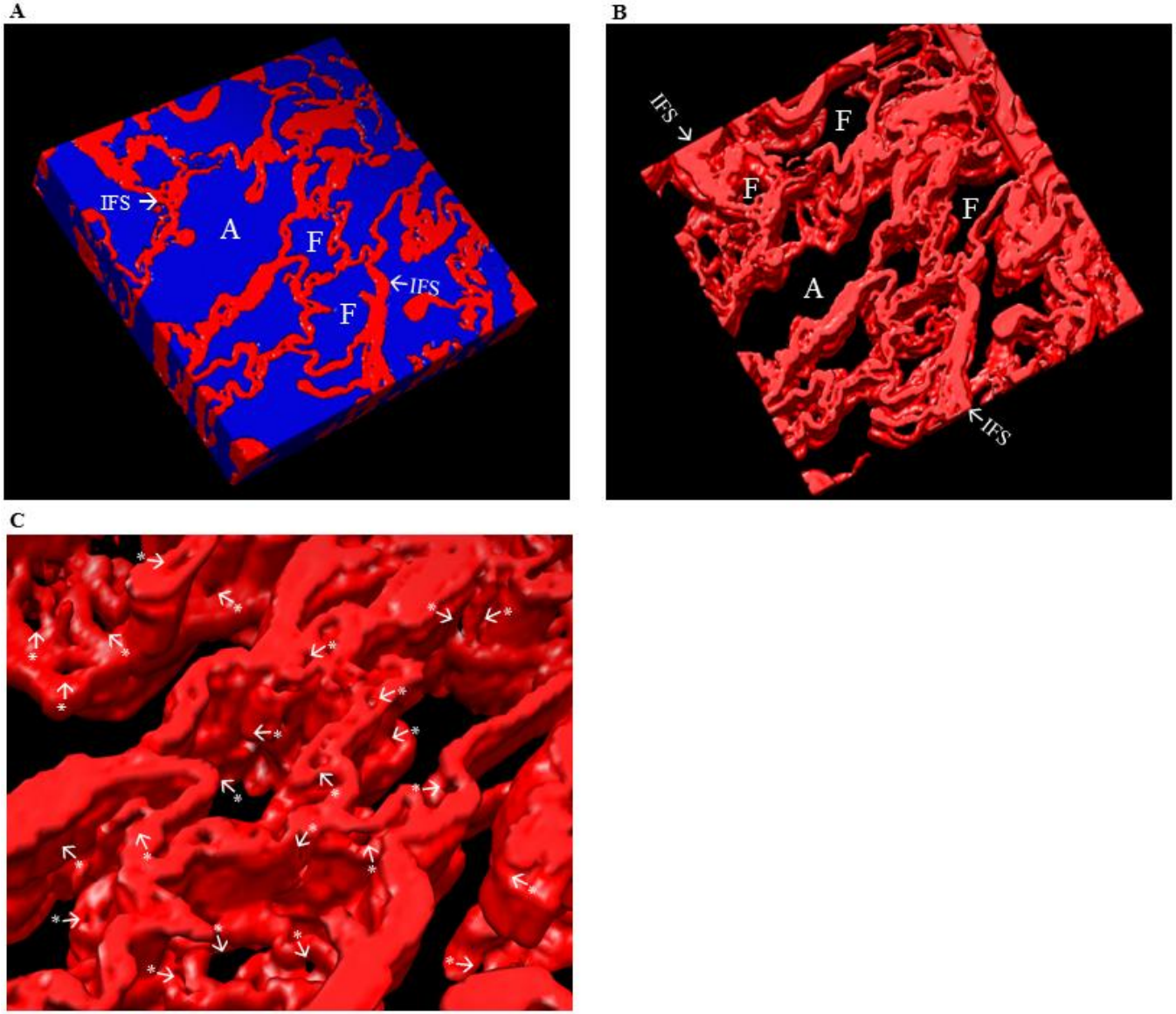
A
IFS
A
F
IFS
F
B
IFS
F
F
F
A
IFS
C

## 3.2. Morphometry

The cumulative summation average graph that was plotted (Figure 3.13) indicated that every 10$^{th}$ section was adequate for the analysis at the specific stratum chosen. This was due to the volume density of the parenchyma ($Vv_{par}$) and volume density of the non-parenchyma ($Vv_{non-par}$) levelling out at the 8$^{th}$ section on the cumulative summation graph and remaining consistent for three sections (the 10$^{th}$ section).

The morphometric analyses indicated that the $Vv_{par}$ of all regions is highest in the 3 month age group category and decreased with an increase in age (Figure 3.14.1) and vice versa for the $Vv_{non-par}$ (Figure 3.14.2). The only exception was the $Vv_{par}$ of the ventral caudal region of the 3 month age group category. This difference could be attributed to a large number of sections of a few samples being analysed.

The cranial regions of all age group categories had the highest $Vv_{par}$ with the middle and caudal regions following respectively (Figure 3.14.1). The opposite trend was observed for the $Vv_{non-par}$ (Figure 3.14.2). The ventral regions, of all age group categories, had a higher $Vv_{par}$ than their dorsal counterparts and vice versa for the $Vv_{non-par}$ (Figures 3.14.1 and 3.14.2).

The $Vv_{par}$ of the all the sampled regions decrease with an increase in age (Figure 3.14.1). A marked decrease in $Vv_{par}$ occurs from the 3 month age group category and becomes more subtle toward the 12 and 24 month age group categories (Figure 3.14.1). The $Vv_{non-par}$ of all the regions of the older age group categories (12 and 24 months) was noticeably higher in comparison to the younger age group categories (3 and 6 months) (Figure 3.14.2).

Figure 3.13: The cumulative summation average graph which is indicative that every $10^{th}$ section is sufficient for the morphometric analysis.

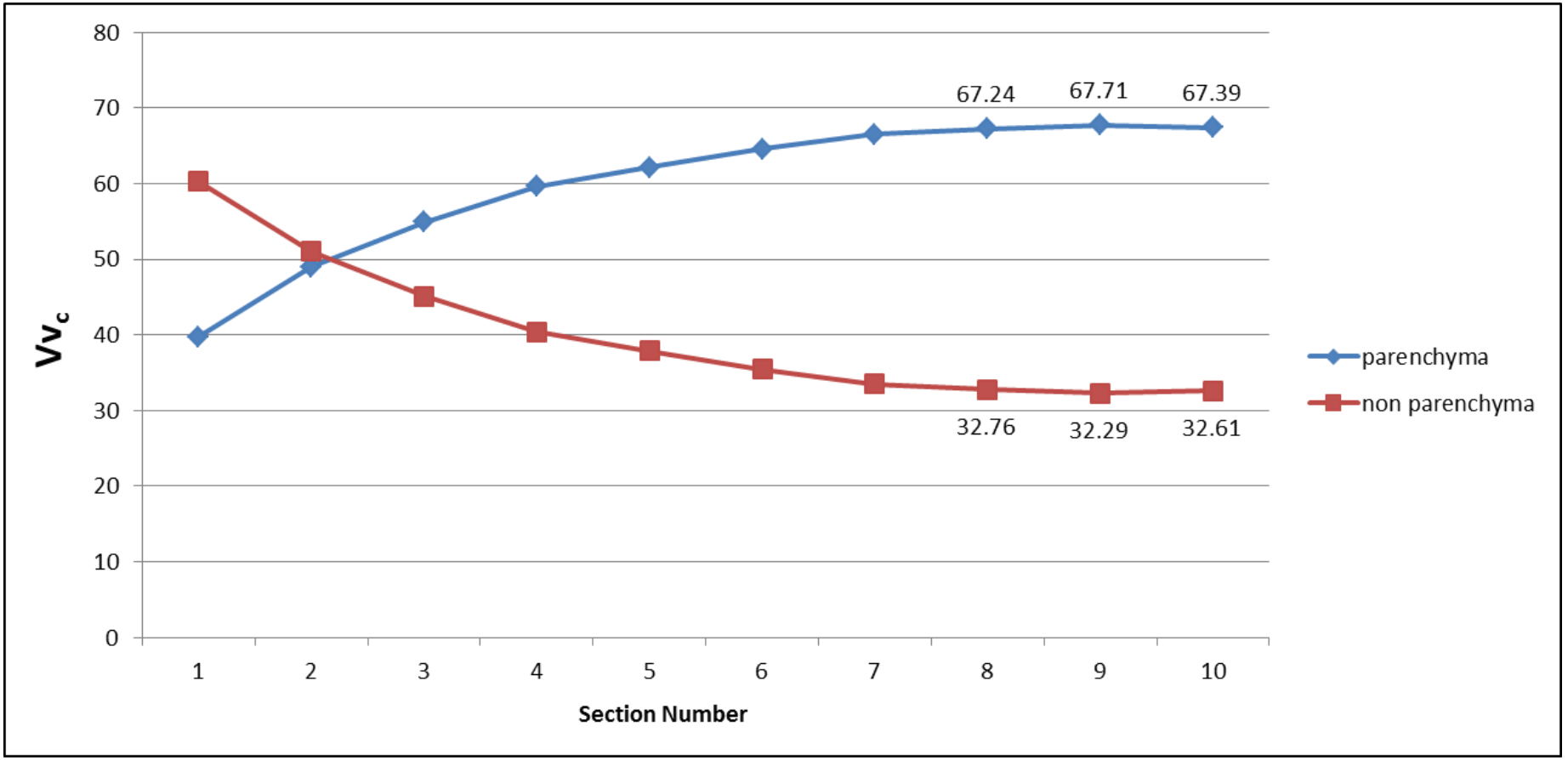
80
70
60
50
40
30
20
10
0
Vvc
67.24
67.71
67.39
32.76
32.29
32.61
1
2
3
4
5
6
7
8
9
10
Section Number
parenchyma
non parenchyma

Figure 3.14.1: A graph of the volume density of the parenchyma ($Vv_{par}$) of the various sampling regions of the different age group categories. The cranial regions of all age group categories have the highest $Vv_{par}$ decreasing in the middle and caudal regions respectively. All the ventral regions of the different age group categories have a higher $Vv_{par}$ than their dorsal counterparts. The younger age group categories have higher $Vv_{par}$ in all regions compared to the older age group categories.

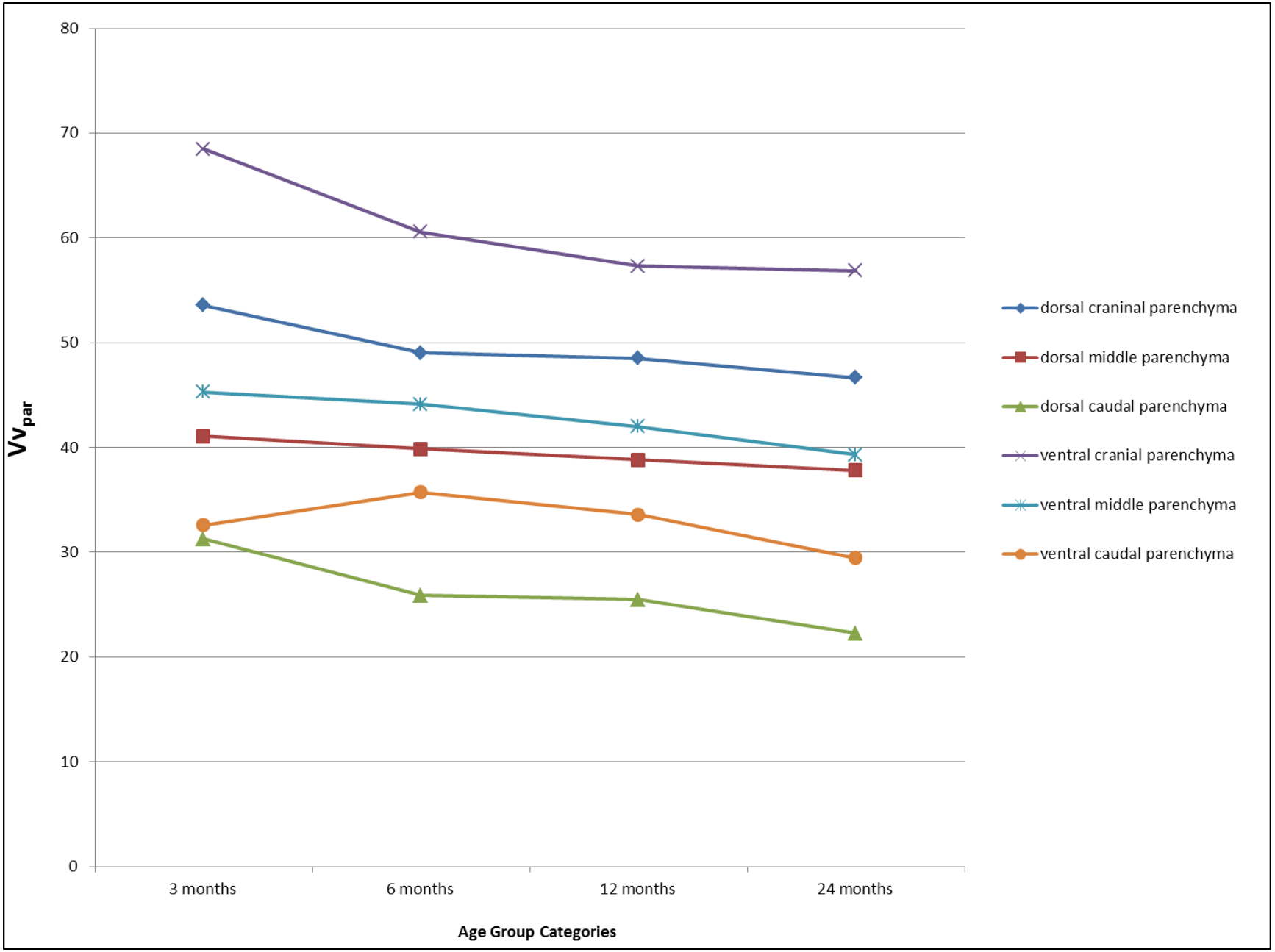
80
70
60
50
40
30
20
10
0
$Vv_{par}$
3 months
6 months
12 months
24 months
Age Group Categories
dorsal craninal parenchyma
dorsal middle parenchyma
dorsal caudal parenchyma
ventral cranial parenchyma
ventral middle parenchyma
ventral caudal parenchyma

Figure 3.14.2: A graph illustrating the volume density of the non-parenchyma ($Vv_{non\text{-}par}$) of the various sampling regions of the different age group categories. In all age group categories, the cranial regions have the lowest $Vv_{non\text{-}par}$ but this increases in a caudal direction. Also, the dorsal regions have a higher $Vv_{non\text{-}par}$ than all their ventral counterparts. With an increase in age, all the sampled regions increase in $Vv_{non\text{-}par}$.

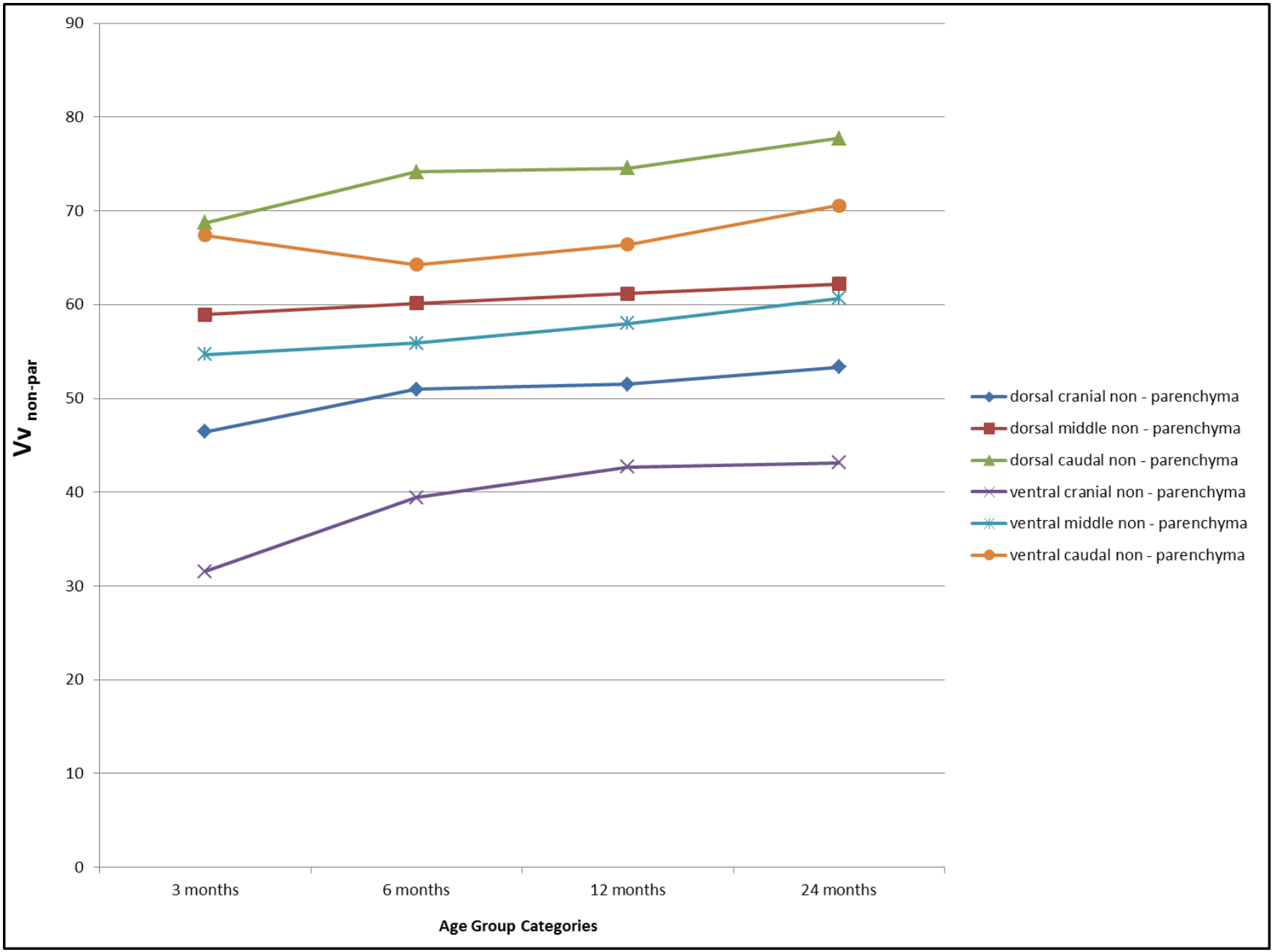
90
80
70
60
50
40
30
20
10
0
Vv non-par
3 months
6 months
12 months
24 months
Age Group Categories
dorsal cranial non - parenchyma
dorsal middle non - parenchyma
dorsal caudal non - parenchyma
ventral cranial non - parenchyma
ventral middle non - parenchyma
ventral caudal non - parenchyma

One way ANOVA's were conducted to test if there were any significant differences in the $Vv_{par}$ and $Vv_{non\text{-}par}$ of the different regions across the age group categories. The $Vv_{par}$ and $Vv_{non\text{-}par}$ of all the various regions across the different age group categories were not significantly different ($P > 0.05$) with the exception of the $Vv_{par}$ and $Vv_{non\text{-}par}$ of the ventral middle region ($P = 0.031$*), which was barely significant (Table 3.1). Appendix D provides the full statistical outputs of the tests. This could, again, be attributed to a large number of sections of limited samples being analysed.

Table 3.1: A summary of the statistical outputs of the One way ANOVA's conducted on the various regions across the age group categories.

| **$Vv_c$ Dorsal Regions** | **P Values** | **Vv Ventral Region** | **P Values** |
|---|---|---|---|
| Dorsal Cranial $Vv_{par}$ | 0.2579 | Ventral Cranial $Vv_{par}$ | 0.2422 |
| Dorsal Cranial $Vv_{non\text{-}par}$ | 0.2579 | Ventral Cranial $Vv_{non\text{-}par}$ | 0.2422 |
| Dorsal Middle $Vv_{par}$ | 0.1986 | Ventral Middle $Vv_{par}$ | 0.0311 |
| Dorsal Middle $Vv_{non\text{-}par}$ | 0.1986 | Ventral Middle $Vv_{non\text{-}par}$ | 0.0311 |
| Dorsal Caudal $Vv_{par}$ | 0.0546 | Ventral Caudal $Vv_{par}$ | 0.2199 |
| Dorsal Caudal $Vv_{non\text{-}par}$ | 0.0546 | Ventral Caudal $Vv_{non\text{-}par}$ | 0.2199 |

The absolute volumes of the parenchyma and non-parenchyma of the various regions of the different age group categories correlated exactly with the trends of the $Vv_{par\ and}$ $Vv_{non\text{-}par}$. This was expected as the absolute volume calculations are dependent on the $Vv_{par\ and}$ $Vv_{non\text{-}par}$ of each region of the different age group categories (Chapter 2.5.1). Table 3.2 summarises the average $Vv_{par}$, average $Vv_{non\text{-}par}$ , average absolute volume of parenchyma and average absolute volume of non-parenchyma of the respective regions across the various age group categories.

Table 3.2: A tabulation of the averages of $Vv_{par,}$ $Vv_{non\text{-}par,}$ the absolute volume of parenchyma and absolute volume of non-parenchyma of the different regions across all age group categories.

| age group | Region | Average Lung Volume | Average $Vv_{par}$ | Average $Vv_{non\text{-}par}$ | Avergae Absolute $Volume_{par}$ | Average Absolute Volume $_{non\text{-}par}$ |
|---|---|---|---|---|---|---|
| 3 months | dorsal cranial | 1.495 | 53.57365 | 46.42635 | 0.799088215 | 0.695911785 |
| | dorsal middle | | 41.05779762 | 58.94220238 | 0.612505958 | 0.882494042 |
| | dorsal caudal | | 31.262 | 68.738 | 0.4663142 | 1.0286858 |
| | ventral cranial | | 68.46868333 | 31.53131667 | 1.024855893 | 0.470144107 |
| | ventral middle | | 45.31268063 | 54.68731937 | 0.675625282 | 0.819374718 |
| | ventral caudal | | 32.58988889 | 67.41011111 | 0.488063822 | 1.006936178 |
| 6 months | dorsal cranial | 8.08 | 49.02185588 | 50.97814412 | 3.969776704 | 4.110223296 |
| | dorsal middle | | 39.86406857 | 60.13593143 | 3.224905644 | 4.855094356 |
| | dorsal caudal | | 25.86715907 | 74.13284093 | 2.102879325 | 5.977120675 |
| | ventral cranial | | 60.56886952 | 39.43113048 | 4.91482642 | 3.16517358 |
| | ventral middle | | 44.11747516 | 55.88252484 | 3.593468104 | 4.486531896 |
| | ventral caudal | | 35.72743667 | 64.27256333 | 2.89120739 | 5.18879261 |
| 12 months | dorsal cranial | 43.575 | 48.50302632 | 51.49697368 | 21.13903659 | 22.43596341 |
| | dorsal middle | | 38.81575 | 61.18425 | 16.9069314 | 26.6680686 |
| | dorsal caudal | | 25.46021309 | 74.53978691 | 11.07197451 | 32.50302549 |
| | ventral cranial | | 57.32688995 | 42.67311005 | 24.9801923 | 18.5948077 |
| | ventral middle | | 42.34771364 | 57.65228636 | 18.43783905 | 25.13716095 |
| | ventral caudal | | 33.60603551 | 66.39396449 | 14.66730692 | 28.90769308 |
| 24 months | dorsal cranial | 62.545 | 46.677 | 53.323 | 29.17430505 | 33.37069495 |
| | dorsal middle | | 37.8025 | 62.1975 | 23.63694785 | 38.90805215 |
| | dorsal caudal | | 22.2804 | 77.7196 | 13.93335699 | 48.61164301 |
| | ventral cranial | | 56.8855 | 43.1145 | 35.5776827 | 26.9673173 |
| | ventral middle | | 40.565 | 59.435 | 25.3816079 | 37.1633921 |
| | ventral caudal | | 29.4475 | 70.5525 | 18.41465235 | 44.13034765 |

Table 3.3: A summary of results obtained from all the experiments conducted, for all age group categories combined

| Dorsal Half of the Lung | | Ventral Half of the Lung |
|---|---|---|
| | | |
| Cranial Region | | Cranial Region |
| Apex of Lung | | Apex of Lung |
| Highly Subdivided | | Highly Subdivided |
| Predominantly Small Blood Vessels or Cappilaries | | Predominantly Small Blood Vessels or Cappilaries |
| High Density of Small Interfaveolar Pores | | High Density of Small Interfaveolar Pores |
| High Density of Microvilli | | High Density of Microvilli |
| Few Stereocilia | | Few Stereocilia |
| High Volume Density of Parenchyma ($Vv_{par}$) | | High Volume Density of Parenchyma ($Vv_{par}$) |
| | | |
| Middle Region | | Middle Region |
| Long and Tubular | | Long and Tubular |
| Intermediate Subdivision | | Intermediate Subdivision |
| Mixture of small blood vessels and large interfaveolar blood vessels | | Mixture of small blood vessels and large interfaveolar blood vessels |
| Varying Sizes of Interfaveolar Pores | | Varying Sizes of Interfaveolar Pores |
| Varying Densities of Microvilli | | Varying Densities of Microvilli |
| Intermediate Number of Stereocilia | | Intermediate Number of Stereocilia |
| Higher Volume Density of Non-Parenchyma ($Vv_{non\text{-}par}$) to Volume Density of Parenchyma ($Vv_{par}$) | | Higher Volume Density of Non-Parenchyma ($Vv_{non\text{-}par}$) to Volume Density of Parenchyma ($Vv_{par}$) |
| | | |
| Caudal Region | | Caudal Region |
| Broad Sac - Like | | Broad Sac - Like |
| Poorly Subdivided | | Poorly Subdivided |
| Predominantly Large Interfaveolar Blood Vessels | | Predominantly Large Interfaveolar Blood Vessels |
| Predominantly Large Interfaveolar Pores | | Predominantly Large Interfaveolar Pores |
| Low Density of Microvilli | | Low Density of Microvilli |
| Large Number of Stereocilia | | Large Number of Stereocilia |
| High Volume Density of Non-Parenchyma ($Vv_{non\text{-}par}$) | | High Volume Density of Non-Parenchyma ($Vv_{non\text{-}par}$) |
| | | |
| **All Ventral Regions of the Lung are more subdivided than their Dorsal counterparts** | | |
| **Regional Levels of Subdivision Decrease with Age** | | |
| **Density of Structural Components Change According to Age / Allometrically** | | |
| **Overall, the 3 month age group category was best suited for gas exchange. This level of efficiency decreased with an increase in age** | | |

# Discussion

The latex casts of all the samples illustrated that the shape of the lung of the Nile crocodile is conical. The broad caudal base is sac like and can receive large volumes of air. Moving in a cranial direction the area available to store air decreases as the lung becomes smaller and ends in an apex. This leads to the assumption that the middle regions are best suited for air conduction and the cranial regions for efficient gas exchange. The broad caudal region could potentially store air or act as a compressor feeding air to the middle and cranial regions of the lung.

The rationale for this is that the volume of an inspired bolus of air must pass through all regions of the lung. If the cranial areas are smaller than the caudal areas they must have a larger respiratory surface area to volume ratio than the larger caudal regions to facilitate the same bolus of air.

Following the normal principle of surface area to volume ratio, an area of the lung which has a high respiratory surface area to volume ratio will have the most efficient gas exchange and vice versa (Massaro and Massaro, 1996). Based on this the cranial regions of the lung should be more conducive to efficient gas exchange decreasing in a caudal direction. As the shape of the lung remains constant with an increase in size as individuals' age, no change in the structural morphology is to be expected. As a result of this patterns of gas exchange efficiency in the different regions should remain the same across individuals of different ages.

The light microscopy sections revealed that the structural morphology of the lungs differed both regionally and between the dorsal and ventral halves, across all age group categories. The cranial regions are well subdivided decreasing in a caudal manner. This reinforces the

supposition previously made about respiratory surface area to volume ratios and that the cranial regions are more suited to gas exchange than the other regions. The cranial regions are divided by thin septa into smaller regular circular / oval shaped faveoli. The regular oval / circular shape of the faveoli in this the region increases the respiratory surface area to volume ratio for gas exchange to occur. Further aiding the gas exchange efficiency are the thin septa subdividing the area. As the septa are thin, the blood gas barrier thickness is decreased and so rapid unaided diffusion occurs.

The presence of large interfaveolar blood vessels, smooth muscle, a loss in a regular oval / circular shape of faveoli and thicker septa in the middle regions leads to the conclusion that a lower surface area to volume ratio exists in this region. This has implications in that gas exchange efficiency of this region is decreased. However, due to the presence of large airways and numerous faveoli in this region it can be postulated that this is a transition zone of air supply to the more gas exchange efficient area, cranial regions, of the lung.

The caudal regions of the lung have an abundance of smooth muscle, large interfaveolar blood vessels and thick subdividing septa which effectively causes a large decrease in respiratory surface area to volume ratio. This makes the area an inefficient gas exchange region. Further compounding this is the fact that the thick septa hardly divide the region into faveoli. Thus it can be postulated that the caudal region of the lung holds received air and distributes it by means of the numerous large airways present.

The ventral regions of the lung are all more subdivided than their dorsal counterparts which increases their gas exchange efficiency. This questions the region at which air is delivered into the lung. The EPPB enters at the ventral middle region of the lung. If air is delivered at this point this region should logically have less faveoli than its dorsal counterpart as it needs to function as a conduit at that immediate point and not as a

functional gas exchange region. The EPPB becomes the intrapulmonary primary bronchus (IPPB) when it is fully within in the lung. It can thus be assumed that the IPPB delivers air principally to the dorsal middle region of the lung and that a branch of the IPPB may directly deliver air to the ventral middle region.

The scanning electron micrographs gave another unique insight into the levels of subdivision of the various sampling regions of the dorsal and ventral halves of the lung. The results of the scanning electron micrographs support the assumption made based on the shape of the lung and the trends observed in the light microscopic section.

The cranial regions of the lung exhibited the highest levels of subdivision. This was done via means of primary, secondary and tertiary septa which delineated large airways, airways or large faveoli and faveoli respectively. The high degree of subdivision of the cranial region was attributed by the tertiary septa. As the cranial regions were highly subdivided into small round / oval faveoli it could thought that they would be the most efficient gas exchange regions.

Adding to this was the presence of numerous small interfaveolar pores and microvilli. Interfaveolar pores are pores within septa allowing air to move / shunt to adjacent faveoli. This should allow other faveoli the opportunity to absorb oxygen from a bolus of air in which oxygen hasn't yet been absorbed thus increasing the efficiency of gas exchange. The small size of the interfaveolar pores and high density of microvilli further increases the surface area to volume ratio of the respiratory surface to increase the efficiency of gas exchange. Small numbers of stereocilia are observed in the cranial regions. They are often associated with microvilli and most probably function to trap any foreign particles, that weren't captured earlier, that may affect the gas exchange process.

At first glance, the stereocilia in the crocodilian lung it may be mistaken for cilia. In order to remove the ambiguity transmission electron microscopy and confocal microscopy was used to determine and confirm the identity of the structure. Transmission electron micrographs illustrate that the structure in question doesn't have the cross sectional morphology of cilia (Ross and Pawlina, 2011). In addition, they are longer in length than "normal" cilia (Ross and Pawlina, 2011). Confocal microscopy micrographs, stained for filamentous actin – a component present in cilia and absent in stereocilia (Ross and Pawlina, 2011), did not highlight any structures fitting the morphology of cilia. It is therefore concluded that these structures are stereocilia.

The middle regions of the lung exhibited large airways with larger faveoli. They were predominantly subdivided by numerous primary and secondary septa with a lower number of tertiary septa than that seen in the cranial regions. This allows the region to be an air conduit and a transition zone from poorly subdivided caudal regions to highly subdivided cranial regions. The faveoli are larger in size and vary in shape, in most cases they are oblong. As a result of the division of the region and the shape and size of the faveoli, the respiratory surface area to volume ratio is lower than that in the cranial regions.

In certain parts of the middle regions, the respiratory surface area is increased by microvilli and small interfaveolar pores. Interfaveolar pores however vary in size and may be used for shunting air in this area. Larger interfaveolar pores and high densities of stereocilia in other parts of the middle regions will decrease the respiratory surface area but they will help in air control and cleaning of the air respectively.

Besides trapping foreign particles, in combination with secretions and surfactant (McGregor *et al*., 1993), for "cleaner" air for the more cranially located efficient gas exchange regions, stereocilia may have other functions in the crocodilian lung. In the

middle regions and caudal regions of the lung they may act as mechano-sensing structures which detect pressure changes and air motion. As mechano-electrical transducers, e.g. the ear (Tilney *et al*., 1980; Ross and Pawlina, 2011), they may then directly or indirectly affect a change to suit the respiratory requirements of the crocodile at that moment in time.

The caudal regions of the lung are poorly subdivided, mainly by primary and secondary septa. Areas within the caudal regions are subdivided by tertiary septa forming model (small round / oval) faveoli. However, in a majority of the areas of the caudal region faveoli delineated by tertiary septa are large, asymmetrical and oblong. Various sizes of interfaveolar pores, predominantly large, and an abundance of stereocilia are observed in this region. The large interfaveolar pores and stereocilia can most likely be assumed to serve as a means of air shunting, trapping foreign particles (in combination with secretions and surfactant) and detecting stimuli. This is because they reduce the respiratory surface area to volume ratio and are not beneficial to gas exchange.

All the ventral regions of all the age group categories were more subdivided than their dorsal counterparts. The distribution of smaller interfaveolar pores and higher densities of microvilli were observed in this region. This suggests that the majority of gas exchange occurs in the ventral regions of the lung.

The 3 dimensional reconstruction models reaffirmed the observations made on the latex casts and in the light micrographs and scanning electron micrographs. The ventral regions were more subdivided than their cranial counterparts in all age groups. The degree of subdivision of the lung also decreased in a caudal direction, resulting in areas of different gas exchange efficiency.

An important observation made from the 3 dimensional reconstruction models is that the interfaveolar septa subdividing the airways have a complex architecture which alters in the

spatial scale that it occupies. They may often form a convoluted labyrinth which doesn't conform to the representations of 2 dimensional images. This structural arrangement can help in altering the respiratory surface area to volume ratio. It can also help in the aerodynamic channelling and sharing of air for inspiration and expiration.

The networking of the high density of small interfaveolar pores in the interfaveolar septa of the cranial regions demonstrate the other mechanisms, other than subdivision of the lung into favourable faveoli shapes and sizes, used to increase the respiratory surface area to volume ratio for gas exchange.

The varying interfaveolar pore networking, size and density in combination with the various sizes and shapes of airways and faveoli in the middle and caudal regions of the lung confirm that these regions play an important role in the supply of air to the cranial gas exchange efficient regions of the lung.

The stereological analyses of the lung, for all age group categories, illustrates that the cranial regions of the lung have the highest $Vv_{par}$ decreasing in a caudal direction and vice versa for $Vv_{non\text{-}par}$. This morphometrically confirms the observations and postulations made on the structural morphology of the lung using morphological experimental techniques.

As the ventral cranial region of the lung has the highest $Vv_{par}$ and structural morphology that has the highest respiratory surface area to volume ratio it is evident it is the most efficient gas exchange region in the lung. In descending order, this is followed by the dorsal cranial region, ventral middle region, ventral caudal region and dorsal caudal region.

This pattern of regional lung efficiency doesn't fit the pattern of tidal ventilation. Tidal ventilation entails breathing a bolus of air in and out (Maina, 2002a). For this type of ventilation the $Vv_{par}$ and $Vv_{non\text{-}par}$ of all the respective regions should be closely matched to one another to maximise gas exchange but are not, e.g. the $Vv_{par}$ and $Vv_{non\text{-}par}$ of the ventral caudal region is more closely correlated to the dorsal middle region, with the exception of the 3 month age group category. Furthermore large disparities in the $Vv_{par}$ and $Vv_{non\text{-}par}$ of the dorsal and ventral regions of the lung should exist.

All these points considered, the model of unidirectional airflow in the lung of alligator (Farmer and Sanders, 2010) is plausible in the Nile crocodile lung. The aforementioned postulations, the gross and structural morphology of the components comprising the lung and the distribution of the parenchyma and non-parenchyma in the lung make it plausible.

Air would be delivered to the lung by the EPPB which enters the hilum of the lung in the ventral middle region of the lung. The IPPB would then transport the bulk of the air to the dorsal middle region of the lung with branches of it delivering air to the other regions. Most of the air would then move to the dorsal caudal region of the lung.

There are hardly any faveoli here (high $Vv_{non\text{-}par}$) and the respiratory surface area to volume ratio is low so less gas exchange would occur. The presence of stereocilia in this region would allow for "cleaning of the air" that would later be used for efficient gas exchange. The interfaveolar septa in this region vary in size thus allowing for optimization of gas exchange that occurs here (small interfaveolar pores) and allows for air to be shunted between the airways of this region.

The air flow control to the ventral caudal region of the lung would be controlled by the large amounts of smooth muscle present in the dorsal caudal region. It would do this by either contracting or dilating thus closing or opening the airways respectively. The smooth

muscle mechanism in the ventral caudal region of the lung would then also meter out the amounts of air that would move cranially by contraction or dilation. The higher degree of subdivision and a higher $Vv_{par}$ than the dorsal caudal region would make it more conducive to gas exchange. The smaller interfaveolar pores present would also help with increasing the efficiency of gas exchange and the larger ones would help shunting air to keep it within the region.

Ultimately the air would be passed to the ventral middle region of the lung. In this region, the $Vv_{par}$ is higher and more conducive to gas exchange. Smooth muscle and varying sizes of interfaveolar pores exist here which would provide the same functions as previously mentioned. The density of microvilli, increasing gas exchange efficiency, is also markedly higher than the previously mentioned regions.

A noticeable observation in this region is that, while it may be an area where effective gas exchange can occur, its morphology is conspicuously conduit orientated. This is indicative that it is a transition zone where effective gas exchange begins but it functions more to pass air to the cranial region of the lung.

Air then moves to the cranial regions which are highly subdivided and more efficient gas exchange occurs. The high respiratory surface area to volume ratio, small round / oval faveoli, small interfaveolar pores, microvilli, thin septa, minimal stereocilia and very rare presence of interfaveolar blood vessels ensures this occurs. Air also moves to the dorsal cranial region from the ventral middle region concurrently and or from the ventral cranial region. The dorsal cranial region has a similar architecture of the ventral cranial region except it is less subdivided (lower $Vv_{par}$).

In these regions the maximum levels of gas exchange occurs. The rate at which this occurs is governed by the amount of air supplied to the region by the caudally located regions,

which could use smooth muscle mechanisms and or air shunting to either increase or decrease the supply of air.

After completing a full cycle, air enters the middle dorsal region where gas exchange will continuously occur before expiration. The smooth muscle and interfaveolar pore mechanisms would function in the same manner as the other regions. Upon expiration not all the air that went through the cycle will be expired. An amount will remain to maintain the residual volume of the lung.

The flow of air in the crocodilian lung could thus be hypothesised to be similar to birds. Upon inspiration air enters the lung, caudal air sacs in birds, and moves the necessary amount of air forward displacing air in front of it into the next region of the cycle which causes a knock on effect (Maina, 1998, 2000a, b 2002a). This would cause the corresponding or necessary amounts of air in the other regions to move forward.

Air movement thus becomes unidirectional as air would enter the dorsal middle region of the lung and cause a corresponding movement in the other regions but at the same time would receive “spent” air from the cranial regions. In birds the air would be moved to cranial air sacs (Maina, 1998, 2000a, b 2002a). Thus for every inspiration in the crocodilian lung there is an expiration, air being forced to be moved from the cranial regions due to the knock on effect. Similarly, for every expiration there is an inspiration, air exiting the lung would cause air to move cranially from the caudal regions. This inspiratory and expiratory cycle is very similar to the well documented lung air sac system in birds (Maina, 1998, 2000a, b 2002a).

It is also likely that the branches of the IPPB deliver air to the different regions in different proportions. This should ensure that there is enough air in the respective regions

preventing the lung from collapsing but at the same time not altering the rate of gas exchange.

Whilst this system exists, why does regional heterogeneity occur in the lung of the Nile crocodile? Birds have lungs that are highly subdivided throughout and are a successful class. The answer is chiefly due to the fact that Nile crocodiles are ectotherms whose metabolisms are governed by the external environment (Hawkins, 1995). If they had a lung such as that possessed by birds they would need to have a higher constant metabolism to facilitate their respiratory system and vice versa. Absolute volume calculations of the various regions show how much parenchyma and non-parenchyma would comprise the entire lung if it had a homogenous architecture as the respective regions.

If it had a uniform design of the ventral cranial region, with ectothermy the animal would be in a constant state of physiological stress. Conversely, if the structure of the lung was the same of the dorsal caudal region, the animal would survive but its pace of life would be slow and would not match its lifestyle. By having a heterogeneous lung the crocodile can alter its respiratory behaviour in accordance with its activities.

This structural morphology of the crocodilian lung and the hypothesis of unidirectional air flow strengthens the current reptile – avian pulmonary theory, that is lungs of birds did evolve from reptiles (archosaurs – principally crocodilians). This coincides with the conclusions made by Schachner *et al*., (2013) which state that unidirectional airflow is ancestral for archosaurs. However, this study  Furthermore it answers a question posed by Schied (1990) (Chapter 1.7.2) to an extent. In order to maintain a high metabolic rate (endothermy) and fly (in certain families), a fully functional and efficient lung / respiratory system is required. Therefore the altered elaborate homogenously subdivided respiratory pattern that birds adapted may well have been evolved out of functional needs. This has

assisted in making aves a very successful vertebrate class as unidirectional airflow in the lung suits the high metabolic requirements of birds to bypass most biogeographical barriers. This has allowed allopatric populations to create sympatric distributions over different habitat types, each benefitting the organisms in its own particular manner with regard to ethology, ecology, ontogeny, and reproduction.

The $Vv_{par}$ of the more gas exchange efficient ventral regions of the lung, particularly ventral cranial, was much higher in the lungs of juveniles than the other sampled age group categories. This was true for all regions of the juvenile in comparison to the other age groups, except for the ventral caudal region explained in Chapter 3.2. This correlates well with the growth rates of individuals.

Juveniles, in their first year, grow rapidly. This requires lots of food resources, readily obtained in the environment, but equally important a good respiratory system. If oxygen requirements aren't met, the metabolism of the organisms will decrease retarding growth, alternatively they will experience physiological stress. This makes them vulnerable to predators and decreases the assimilation efficiency of meals which reduces their capacity for growth. A seeming disadvantage of having such an efficient lung is that they can't dive and submerge for long periods of time. This may hamper hunting techniques (once they're able to hunt small prey independently) and anti-predatory behaviour. They curb this problem by maintaining a diet which consists primarily of invertebrates, crustaceans and amphibians. To minimise predation, they remain in crèches close to adults and due to their size and efficient lung, they are nimble and quick making it hard for a predator to capture them out in the open or once they have entered a refuge (e.g. reeds). Having a lung developed in this manner could thus be a key component of the young crocodiles being precocial.

As individuals age their growth rate decreases and a corresponding change in the $Vv_{par\ and}$ $Vv_{non\text{-}par}$ of the lung is observed. This could possibly be due to numerous factors, which include food availability, thermoregulation and longevity. A lung with the same composition as a 3 or 6 month old crocodile in an older individual would require the individual to feed more often, actively practice thermoregulatory behaviours or search for more thermoregulatory refugia and increase its baseline metabolism. This increases competition, for food and refugia, risk of injury and shorter longevity, due to combat and a higher metabolism. The composition of the lungs of all the individuals' suits their lifestyle adequately.

For reproduction, apart from other intrinsic and extrinsic factors a Nile crocodiles utilise their respiratory system to good effect. Courtship behaviour requires individuals to bark roar, cough and blow bubbles in water. In order for this the lung needs to be fully functional. Nasal geysering and posture inflation to see off rival males and enemies alike requires a refined lung which is adaptive.

This could be done by controlling rates of expiration without compromising the integrity of the lung. It could also be facilitated by shunting and the air storage mechanism causing the broad base of the lung to increase which causes the body to inflate in size. The young crocodile also bark or vocalise in response to threats or stress. In order for these sounds to be produced juveniles have to control their rates of expiration whilst remaining vigilant and active. The composition of their lungs allows them to meet oxygen requirements to do this and to speedily pass air out to vocalise.

The phenotypic plasticity of the Nile crocodile lung is well exhibited during terrestrial locomotion. The lungs have to change position or levels of inflation according to a particular gait but still remain functional to the extent of providing enough oxygen for

particular behaviours to be conducted. An example is when the crocodile belly runs to the water. Lungs have to alter their shape so as to prevent damage from the nature of the motion but still meet the oxygen requirements for the activity.

For aquatic locomotion and dwelling the uniqueness and structural complexity of the crocodilian lung can be appreciated. Over time the lung of the Nile crocodile has been controversially been hypothesised to allow submergence of the crocodile (Graham *et al.,* 1975, Henderson, 2003). Nile crocodiles feed, thermoregulate and reproduce etc. in water thus stating that one organ system has the greatest bearing over this is a sensitive topic.

From the evidence gathered, it is hypothesised that the lung of the Nile crocodile is central to its aquatic lifestyle. When the crocodiles float in water the dorsal caudal region of the lung could be holding air in creating a swim bladder effect. This keeps the crocodile afloat and normal respiration, as previously hypothesised, occurs according to activity.

When the crocodile submerges itself, it stays under water for long periods of time. This should entail the caudal regions taking in as much air as possible in order to provide adequate air for gas exchange while submerged. This is feasible however if only the dorsal caudal region stores air, the crocodile will float. Therefore the ventral caudal region should also stores air causing the crocodile to sink. The air has to be rationed in order for the crocodile to remain under water for a period of time. The smooth muscle of the ventral caudal region constricts and as a consequence the air supply to the middle and cranial regions decreases. Shunting of air using large interfaveolar pores will also keep air in the region. The lower $Vv_{par}$ and reduced respiratory surface area to volume ration of the ventral caudal region will also ensure that the air is not spent in that region. In tandem, the ventral middle region, the conduit region, will also constrict smooth muscle closing airways and decreasing the flow of air accordingly. The large interfaveolar pores of this

region will function to the same effect as that in the ventral caudal region. All the $CO_2$ that enters the caudal regions of the lung, from gas exchange and or that which was inspired, also helps the crocodile to sink and prevents the lung collapsing due to the effects of pressure (Wright and Kirshner, 1987)

The degree of constriction of airways and consequently the air flow rate will be governed by the depth of submergence of the crocodile. An increase in diving depth increases pressure which changes the amount of air required for efficient gas exchange. The change in pressure and flow rates of air is detected by the stereocilia. These structures possibly function to directly or indirectly alter the structural arrangements of the lung, size of airways and air shunting. They may also alter the cardiac output (Wright and Kirshner, 1987) which would retard the gas exchange process which further facilitates the saving of air.

When hunting prey on banks crocodiles rely on this system to move into favourable positions of attack while being unnoticed. When the crocodiles have to strike prey, the lung would be required to provide sufficient amounts of oxygen for energy to perform the task adequately. It does this by dilating smooth muscle and reducing shunting of air. This results in air rapidly moving into the cranial regions for gas exchange to occur. Crocodiles then latch onto prey and dead roll them in the water until they are dead (Cott, 1961).

Not limiting to but due to hunting and submergence (and the pressure associated with it) the disparity of dorsal and ventral region heterogeneity can be explained. When the crocodile strikes prey from water it is vulnerable to trauma on its dorsal surface, despite its toughness, from kicking or anti predatory behaviours. If this happens the lung of the organism gets damaged. If the dorsal surface was the area of greatest gas exchange the aquatic lifestyle and basic respiration is compromised putting the animal at risk. If the

dorsal surface of the lung does sustain trauma that isn't fatal, the crocodile would still be able to pass air to the more gas exchange efficient area and survive hence it is the less subdivided half of the two.

The ventral regions of the lung are required to be plastic and adapt to pressure changes to facilitate the primarily aquatic lifestyle of the crocodile. An inverse model to the one proposed here would not be feasible as submergence would not be as effective. Also, the effects of pressure on gas exchange based on the regional composition of the lung would not favour gas exchange in the dorsal half of the lung.

In conclusion, the lung of the Nile crocodile is a multifaceted heterogeneous structure that exhibits immense architectural and compositional complexity. In many cases, the seemingly simple lifestyle of the Nile crocodile has been associated with an uncomplicated respiratory system both being misconceptions. The dexterity of the lung of the Nile crocodile highlights its importance in the organism. It also elucidates to the fact that it is as important or even more important as any other organ / organ system that comprises the Nile crocodile. It is with no doubt that the lung of the crocodile is nothing short of a marvel. Due to this it is no wonder they have outlived the dinosaurs and are referred to as the living ones.

# References

Allen, D. 1998. Nile crocodiles in Zimbabwe. Reptile & Amphibian Magazine **52**:18-22.

Anderson, G., and Bancroft, J., 2002. Tissue processing and microtomy. In: *Theory and practice of histological techniques, 5th edition*: 85 - 99. Bancroft, J. D., and Gamble, M. (Eds). Churchill Livingstone, London.

Bakhle, Y. S., 1975. Pharmacokinetic function of the lung. In: *Lung Metabolism*. Junod, A. F. and Haller, R. (Eds).

Blake, D. K., 1982. Crocodile ranching in Zimbabwe. *The Zimbabwe Science News*. **26**: 208 – 209.

Blake, D. K. and Loveridge, J. P., 1975. The role of commercial crocodile farming in crocodile conservation. *Biol Conserv*. **8(4)**: 261 – 272.

Blomberg, G. E. D., 1976. Feeding and nesting ecology and habitat preferences of Okavango crocodiles. Proceedings of the Symposium: Okavango Delta and its future utilisation, Botswana Society, Gaborone, Botswana.

Branch, B., 1993. Southern African Snakes and other Reptiles. A photographic guide. New Holland (Publishers) Ltd, London.

Branch, B., 1998. Field guide to Snakes and Other Reptiles of Southern Africa. Third Revised Edition. Ralph Curtis Books Publishing, Sanibel Island, Florida.

Brander, D., 1925. Stones in crocodile's stomach. *Field* **146**: 537.

Brinkman, D., 1980. The hind limb step cycle of *Caiman sclerops* and the mechanics of crocodilian tarsus and metatarsus. *Can J Zool.* **58**: 2187 – 2200.

Buffetaud, E., 1982. The evolution of crocodilians. *American Science*. **241**: 124 – 132.

Busbey, A. B., 2005. Form and function of feeding apparatus of *Alligator mississippiensis*. *J Morph*. **202(1)**: 99 – 127.

Cansdale, G., 1955. Reptiles of West Africa. Penguin Books Ltd, Harmondsworth, England.

Carrier, D. R., 1984. The energetic paradox of human running and hominid evolution. *Curr Antropol*. **25**: 483 – 495.

Carrier, D. R., 1987. The evolution of locomotor stamina in tetrapods: circumventing a mechanical constraint. *Paleobiology*. **13**: 326 – 341.

Carroll, R. L., 1988. Vertebrate palaeontology and evolution. Freeman, New York.

Claessens, L. P. A. M., 2002. Analysis of the kinematics of lung ventilation in crocodylians. *Integr Comp Biol.* **42**: 1208.

Claessens, L. P. A. M., 2004. Archosaurian respiration and the pelvic girdle aspiration breathing of crocodyliforms. *Proc R Soc Lond B.* **2004 271**: 1461 – 1465.

Cope, E. D. (1894). On the lungs of the Ophidia. Proc. Am. Phil. Soc. 33, 217-224.

Corbett, P. S., 1959a. The food of a sample of crocodiles (*Crocodylus niloticus l*) from Lake Victoria. *Proceedings of the Zoological Society of London*. **133(4)**: 561 – 572.

Corbett, P. S., 1959b. Notes on the insect food of the Nile crocodile in Uganda. *Proceedings of the Royal Entomological Society of London.* **Series A Gen 34:** 17 -22.

Cott, H. B., 1954. The status of the Nile crocodile in Uganda. *Uganda Journal*. **18(1)**: 1 – 12.

Cott, H. B., 1961. Scientific results of an enquiry into the ecology and economic status of the Nile crocodile (*Crocodylus niloticus*) in Uganda and Northern Rhodesia. *Trans Zool Soc Lond.* **29(4)**: 211 – 356, plates 1 – 9.

Cott, H. B., 1975. Looking at animals: A zoologist in Africa. Scribner's Sons, New York.

Crawford, E. C., Gatz, R. N., Magnussen, H., Perry, S. F. and Pipper, J., 1976. Lung volumes, pulmonary blood flow and carbon monoxide diffusing capacity of turtles. *J Comp Physiol*. **107**: 169 – 178.

Davenport, J., Grove, D. J., Cannon, J., Ellis, T. R. and Stables, R., 1990. Food capture, appetite, digestion rate and efficiency in hatchling and juvenile *Crocodylus porosus*. *J Zool*. **220**: 569 – 592.

Diefenbach, C. O. DA. C., 1973. Integumentary permeability to water in Caiman Crocodiles and Crocodylus Niloticus (Crocodilia: Reptilia). *Phys Zool*. **46(1)**: 72 - 78.

Dodson, P., 2003. Allure of El Lagarto – Why do dinosaur palaeontologists love alligators, crocodiles and their kin? *Anat Rec.* **274A**: 887 – 890.

Dunson, W. A., 1982. Salinity relations of crocodiles in Florida Bay. *Copeia*. **2**: 374–385

Duncker, H. R., 1978. General morphological principles of amniotic lungs. In: *Respiratory Function in Birds, Adult and Embryonic*. Piiper, J. (Ed.). Springer-Verlag, Berlin.

Duncker, H. R., 1991. The evolutionary biology of homeothermic vertebrates: the analysis of complexity as a specific task of morphology. *Verh Dtsch Zool Ges*. **84**: 39 – 60.

Duncker, H. R., 2004. Vertebrate lungs: Structure, topography and mechanics. A comparative perspective of the progress integration of respiratory system, locomotor apparatus and ontogenetic development. *Resp Physiol Neurobi*. **144(2004)** 111 – 124.

Farmer, C. G., 2006. On the origin of avian air sacs. *Resp Physiol Neurobi*. **154(2006)**: 89 -106

Farmer, C. G. and Carrier, D. R., 2000. Pelvic aspiration in the American alligator (Alligator *mississippiensis*). *J Exp Biol.* **203**: 1679 – 1687.

Fedde, M. R., 1980. The structure and gas flow pattern in the avian lung. *Poultry Science*, **59**: 2642 – 2653

Fergusson, R. A., 2010. Nile crocodile, *Crocodylus niloticus*. In: *Crocodiles. Status survey and conservation action plan. Third edition*. Manolis, S. C. and Stevenson, C., (Eds.). Crocodile Specialist Group, Darwin.

Fleishman, L. J., Howland, H. C., Hownland, M. J., Rand, A. S. and Davenport, M. L., 1988. Crocodiles don't focus underwater. *J Comp Physiol*. **163A**: 441 – 443.

Frank, J., Radermacher, M., Penczek, P., Zhu, J., Li, Y., Ladjadj, M. and Leith, A., 1996. SPIDER and WEB: processing and visualisation of images in 3D electron microscopy and related fields. *J Struct Biol.* **116**: 190 – 199.

Frasca, J. M., Carter, H. W. and Schaffer, W. A., 1978**.** An improved latex injection media for replicating the pulmonary microvasculature. Scanning Electron Microsc. **2485-490.**

Ludke, S. J., Baldwin, P. R. and Chiu, W., 1999. EMAN: Semiautomated software for high-resolution single-particle reconstructions. *J Struct Biol*. **128**: 82 – 97.

Gans, C., 1969. Comments on inertial feeding. *Copiea*. **1969**: 855 - 857

Gans, C. and Clark, B., 1976 Studies on ventilation in Caiman *crocodilus*. *Resp Physiol.* **26**: 285 – 301.

Gans, C. and Maderson, P. F. A., 1973. Sound producing mechanisms in recent reptiles: review and comment. *Am Zool*. **13**: 1195 – 1203.

Garrick, L. D. and Lang, J. W., 1977. Social signals and behaviours of adult alligators and crocodiles. *Am Zool.* **17**: 225 – 239

Glass, M. L. and Johansen, K., 1979. Periodic breathing in the Crocodile, *Crocodylus niloticus*: Consequences for the gas exchange ratio and control of breathing. *J Exp Zool*. **208**: 319 – 326.

Glass, M. L. and Johansen, K., 1981. Pulmonary diffusing capacity in reptiles (relations to temperature and oxygen uptake). *J Comp Physiol*. **107**: 169 – 178.

Graham, A., 1990. Eyelids of Morning. The mingled destinies of Crocodiles and Men. First Chronicle Books Edition. Chronicle Books, San Francisco.

Graham, A., 1968. The Lake Rudolf crocodile (*Crocodylus niloticus laurenti*) population. Report to Kenya Game Department (Mimeo).

Graham, J. B., Gee, J. H. and Robinson, F. S., 1975. Hydrostatic and gas exchange functions of the lung of the sea snake, *Pelamis platurus*. *Comp Biochem Phys A*. **50**: 477 – 482.

Grenard, S. 1991. Handbook of Alligators and Crocodiles. Krieger Publishing Company, Malabar, Florida.

Grigg, G. C., Seebacher, F., Beard, L. A. and Morris, D., 1998. Thermal relations of large crocodiles, *Crocodylus porosus*, free ranging in an naturalistic situation. *Proc R Soc Lond B*. **265**: 1793 – 1799.

Groombridge, B. 1987. The distribution and status of world crocodilians. In: *Wildlife management: Crocodiles and Alligators*. Webb, J. W., Manolis, S. C. and P. J. Whitehead, P. J., (Eds). Surrey Beatty & Sons Pty Limited, Chipping Norton, Australia.

Guggisberg, C. A. W., 1972. Crocodiles. Their Natural History, Folklore and Conservation. Stackpole Books, Harrisburg, Pennsylvania.

Guntheroth, W. G., Luchtel, D. L. and Kawabori, I., 1982. Pulmonary microcirculation: Tubules rather than sheet and post. *J Appl Physiol*. **53510 - 515.**

Hadley, D. 1969. Breeding of crocodile in Livingstone Game Park. Puku (Chilange, Zambia). **5:** 226-228.

Hawkins, A. J. S., 1995. Effects of temperature change on ectotherm metabolism and evolution: Metabolic and physiological inter-relations underlying the superiority of multilocus heterozygotes in heterogeneous environments. *J Therm Biol*. **22 (1/2)**: 22 - 33.

Heatwole, H., 1981. Role of the saccular lung in the diving of the sea krait, *Laticuda colubrine*, (Serpentes: Laticaudidae). *Australian Journal of Herpetology.* **1**: 11 – 16.

Henderson, D. M., 2003. Effects of stomach stones on the buoyancy and equilibrium of a floating crocodilian: a computational analysis. *Can J Zool*. **81**: 1346 – 1357.

Hippel, E. V., 1946. Stomach contents of crocodiles. *Uganda J.* **10**: 148 – 149.

Hlastala, M. P., Standaert, T. A., Pierson, D. J. and Lutchel, D. L., 1985. The matching of ventilation and perfusion in the lung of the Tegu, *Tupinambis nigropunctus*. *Respir Physiol*. **60**: 277 – 294.

Hunt, R. H., 1974. Hatching and rearing of Morelet's Crocodile, C. *moreletii*. *Conf Am Ass Zool Parks and Aquaria* Arlington, Texas.

Hutton, J. M., 1987. Growth and feeding ecology of the Nile crocodile, *Crocodylus niloticus*, at Ngezi, Zimbabwe. *J Anim Ecol*. **56**: 25 – 38.

Hutton, J. M., 1989. Movements, home range, dispersal and separation of size classes in Nile crocodiles. *Am Zool*. **29**: 1033 – 1049.

Ihle, J. E. W., van Kampen, P. N., Nierstrasz, N. F. and Versluys, J. Vergleichende., 1971. Anatomie der wirbeltiere. Springer – Verlag, Berlin

Jackson, S. and Ryan, P. G., 1986. Differential digestion rates of White chinned Petrels (Procellaria *aequinoctialis*). *Auk*. **103**: 617 – 619.

Janke, A., Gullberg, A., Hughes, S., Aggarwal, R. K. and Arnason, U., 2005. Mitogenomic analyses place the gharial (*Gavialis gangeticus*) on the crocodile tree and provide Pre-K/T Divergence times for most crocodilians. *J Mol Evol.* **61**:620–626.

Jewell, P. A., 1966. The concept of home range in mammals. *Symp Zool Soc London*. **18**: 85 – 109.

Jones, A. 1998. Croc adventures in retrospect, forty years later. Reptile & Amphibian Magazine. **53**:54-63.

Jones, J. H., Effmannn, E. L. and Schmidt-Nielsen, K., 1985. Lung volume changes in during respiration in ducks. *Respir Physiol*. **559**: 15 – 25.

King, F. W., 1989. *Crocodylus niloticus* Laurenti 1768. In: *Crocodilian, Tuatara, and Turtle species of the world. A Taxonomic and Geographic Reference*. King, F. W. and Burke, R. L., (Eds). The Association of Systematics Collections, Washington, DC.

King, J. R. and Farner, D. A., 1969. Energy metabolism, thermoregulation and body temperature. In*: Biology and comparative physiology of birds, Vol. 2*, Marshall, A. J. (Ed). Academic press, London.

Kleiber, M., 1961. *The Fire of Life: An introduction to Animal Energetics*. Wiley, New York.

Klein, W. and Codd, J. R., 2010. Breathing and locomotion: Comparative anatomy, morphology and function. *Resp Physiol Neurobi.* **173S (2010):** S26 – S32.

Klemm, R. D., Gatz, R. N., Westfall, J. A. and Fedde, M. R., 1979. Microanatomy of the lung parenchyma of a Teju lizard, *Tupinambis nigropunctatus*. *J Morphol*. **161**: 257 – 280.

Krogh, A., 1941. The comparative physiology of respiratory mechanisms. University of Pennsylvania Press, Philadelphia, PA, USA

Kushlan, J. A., 1973. Observations on maternal behaviour in the American alligator, *Alligator mississippiensis*. *Herpetologica*. **29**: 256 – 257.

Kyalo, S., 2008. Non –detriment finding studies on Nile crocodile (*Crocodylus niloticus*): The status of and trade in the Nile crocodile in Kenya. NDF workshop case studies, WG 7 – Reptiles and Amphibians.

Laitman, T. J., Reidenberg, J. S., Marquez, S. and Gannon, P. J., 1996. What the nose knows: new understandings of the Neanderthal upper respiratory tract. *Proc Natl Acad Sci., USA*. **93**: 10543 – 10545.

Lamar, W. W. 1997. The world's most spectacular Reptiles & Amphibians. World Publications, Tampa.

Lang, J. W. 1987. Crocodilian behaviour: Implications for management. In: *Wildlife Management: Crocodiles and Alligators*. Webb, G. J. W., Manolis, S. C. and Whitehead, P. J. (Eds). Surrey Beatty & Sons Pty Ltd, Chipping Norton, Australia.

Lang, J. W. 1989. Social behaviour. In: *Crocodiles and Alligators*. Ross, C. A. (Ed). Facts on File, Inc., New York.

Leslie, A. J., 1997. The ecology and physiology of the Nile crocodile*, Crocodylu*s *niloticus*, in St Lucia, Kwazulu Natal, South Africa. PhD Thesis, Drexel University, USA.

Lonza product specification sheet, 2008. Lonza Walkersville Inc, Walkersville, Maryland, USA.

Loveridge, J. P., 1984. Thermoregulation in the Nile crocodile, *Crocodylus niltoicus*, *Symposium of the Zoological Society of London*. **52**: 443 – 467.

Luchtel, D. L., and Kardong, K. V., 1981.Ultrastructure of the lung of the rattlesnake, *Crotalus viridus oreganos*. *J Morphol*. **169**: 267 – 275.

Lutz, P. L., Bentley, T. B., Harrison, K. E. and Marszalek, S., 1980. Oxygen and water vapour conductance in the shell and shell membrane of the American crocodile egg. *Comp Biochem Physiol.* **66A**: 335 – 338.

Magnussen, H., Wilmer, H. and Scheid, P., 1976. Gas exchange in the air sacs: contribution to respiratory gas exchange in ducks. *Respir Physiol*. **26**: 129 – 146.

Magnusson, W. E., 1980. Hatching and crèche formation by *Crocodylus porsus*. *Copeia*. **1980**: 359 – 362.

Magnusson, W. E., Da Silva, E. V. and Lima, A. P., 1987. Diets of Amazonian crocodilians. *J Herpetol* **21**: 85–95.

Magnusson, W. E., Vliet, K. A, Pooley, A. C. and Whitaker, R., 1989. Reproduction. In: *Crocodiles and Alligators*. Ross, C. A., (Ed). Facts on File, Inc., New York.

Maina, J. N., 1982. **A** scanning electron microscopic study of the air and blood capillaries of the lung of the domestic fowl ***(Gallus domesticus).*** *Experientia.* **38**: 614-616.

Maina, J. N., 1984. Morphometrics of the avian lung III. The structural design of the passerine lung. *Respir Physiol*. **55**: 291 – 309.

Maina, J. N., 1987. The morphology and morphometry of the adult normal baboon lung ***(Pupio anubis).*** *J. Anat*. **150**: 229-245.

Maina, J. N., 1988. Scanning electron microscope study of the spatial organization of the air and blood conducting components of the avian lung (*Gallus gallus* variant *domesticus*). *Anat Rec*. **222**: 145 – 153.

Maina, J. N., 1989. The morphometry of the avian lung. In: *Form and function of birds, Vol. 4*. King, A.S. and Mclelland, J. (Eds). Academic press, London.

Maina, J. N., 1998. The Gas Exchangers: Structure, Function, and Evolution of the Respiratory Process. Springer-Verlag, Heidelberg

Maina, J. N., 2000a. Comparative respiratory morphology: Themes and principles in the design and construction of the gas exchangers. *Anat Rec (New Anat.)*. **261**: 25 -44.

Maina, J.N., 2000b. What it takes to fly: The structural and functional respiratory refinements in birds and bats. *J Exp Biol*. **203**: 3045 – 3064.

Maina, J. N., 2002a. Functional Morphology of the Vertebrate Respiratory Systems. Dutta, H. M. and Kline, D. W. (Eds). Science Publishers, Inc., Enfield, USA.

Maina, J. N., 2002b. Structure, function and evolution of the gas exchangers: comparative perspectives. *J Anat*. **201**: 281 – 304.

Maina, J. N., 2002c. Comparative morphology of the gas exchangers. *J Anat*. **200**: 201 – 202.

Maina, J. N., 2003. Structure and function of non-mammalian vertebrate lungs. In: *Lung Development and Regeneration*. Marcel Dekker, New York.

Maina, J. N., *pers comm.* University of Johannesburg, Auckland Park, South Africa. Contact address: University of Johannesburg, Kingsway Campus: 233 D3 Lab. Contact: jmaina@uj.ac.za.

Maina, J. N., King, A. S. and Settle, G., 1989a. An allometric study of pulmonary morphometric parameters in birds, with mammalian comparisons. *Philosophical Trans Zool Soc Lond*. **326B (1231)**: 1 – 57.

Maina, J. N., Maloiy, G. M. O., Warui, C. N., Njogu, E. K. and Kokwaro, E. D., 1989b. Scanning Electron Microscope Study of the Morphology of the Reptilian Lung: The Savanna Monitor Lizard *Varanus exanthematicus* and the Pancake Tortoise *Malacochersus tornieri. Anat Rec* **224**: 514-522.

Maina, J. N., Veltcamp, C. J. and Henry, J., 1999. Study of the spatial organization of the gas exchange components of a snake lung - the sandboa Eryx colubrinus (Reptilia: Ophidia: Colubridae) - by latex casting. *J Zool Lond.* **247 (1999)**: 81 – 90.

Maina, J. N. and Woodward, J. D., 2009. Three-dimensional serial section computer reconstruction of the arrangement of the structural components of the parabronchus of the ostrich, *Struthio camelus* lung. *Anat Rec*. **292**: 1685 – 1698.

Marcellini, D., 1977. Acoustic and visual display of Gekkonid lizards. *Amer Zool*. **17(1)**: 251 – 260.

Marcus, H Lungen, 1937. In*: Handbuch der vergleichenden anatomie der wirbeltiere, III*. Bolk, L., Göppert, E., Kallius, E., Lubosch, W. (Eds). Urban and Schwarzenberg, Berlin – Wien.

Martin, S., 2008. Global diversity of crocodiles (Crocodilia, Reptilia) in freshwater. *Hydrobiologia*. **595**: 587–591.

Massaro, G. D. and Massaro, D., 1996. Formation of pulmonary alveoli and gas-exchange surface area: quantitation and regulation. *Annual review of physiology* **58(1)**: 73-92.

Mazzotti, J. and Dunson, W. A., 1984. Adaptations of *Crocodylus acutus* and Alligator for life in saline water. *Comp Biochem Phys* **79**: 641–646.

McGregor, L. K., Daniels, C. B. and Nicholas, T. E., 1993. Lung Ultrastructure and the Surfactant-Like System of the Central Netted Dragon*, Ctenophorus nuchalis*. *Copeia*. **1993(2)**: 326 -333.

Mclelland, J. 1989. Anatomy of the lungs and air sacs. In: *Form and function in birds Vol. 4*, King, A.S. and Mclelland, J. (Eds). Academic Press, London.

Meban, C., 1977. Ultrastructure of the respiratory epithelium in the lungs of the tortoise, *Testudo graeca*. *Cell Tissue Res*. **181**: 267 – 275.

Meban, C., 1978. Functional anatomy of the lungs of the green lizard, *Lacerta viridis*. *J Anat*. **125**: 421 – 431.

Messsel, H. and Vorlicek, G., 1987. A population model for *Crocodylus porosus* in the tidal waterways of Northern Australia: Management implications. In: *Wildlife management: Crocodiles and alligators*. Webb, G. J. W., Manolis, S. C. and White, P. J. (Eds). Surrey Beatty and Sons, Australia.

Milani, A., 1894. Beiträge zur kenntniss der reptilienlunge. Fischer, Germany.

Milsom, W. K., 1984. The interrelationship between pulmonary mechanics and spontaneous breathing in the tokay lizard, *Gekko gecko*. *J Exp Biol*. **113**: 203 – 214.

Modha, M. L., 1967. The ecology of the Nile crocodile (*Crocodylus niloticus* Laurenti) on Central Island, Lake Rudolf. *East Afr Wild J.* **5**: 74 – 95.

Modha, M. L., 1968. Basking behaviour of the Nile crocodile (*Crocodylus niloticus*) on Central Island, Lake Rudolf. *East Afr Wild J.* **6**: 81 – 88.

Murphy, C. R., Rogers, P. A. W., Kovacs, G., Hosie, M. and Beaton, L., 1990. Early evaluation of post – menopausal hormonal steroid therapy by scanning electron microscopy of the uterine epithelium. *Acta Anatomica*. **138**: 364 – 366.

Neckvasil, N. P. and Olson, K. R., 1986. Extraction and metabolism of circulating catecholamines by the trout gill. *Am J Physiol*. **19**: R5276 – 5287.

Neill, W. T., 1971. The Last of the Ruling Reptiles: Alligators, Crocodiles, and their kin. Columbia University Press, New York and London.

O'Connor, P. M. O. and Claessens, L. P. A. M., 2005. Basic avian pulmonary design and flow through ventilation in non – avian theropod dinosaurs. *Nature*. **436**: 253 – 256.

Ogden, J. C. and Singletary, C., 1973. Night of the crocodile. *Audubon*. **75(3)**: 32 – 37.

Owen-Smith, N. E., 1977. On territoriality in ungulates and an evolutionary model. *Q Rev Biol.* **52**: 1 – 38.

Owerkowicz, T. and Brainerd, E. L., 1997. How to circumvent a mechanical constraint: Ventilatory strategy of *Varanus exanthematicus* during locomotion. *J Morphol.* **232**: 305.

Parrish, J. M., 1987. The origin of crocodilian locomotion. *Paleobiology*. **13(4)**: 396 – 414.

Pauwels, O. S. G., Branch, W. R. and Burger, M., 2004. Les reptiles du Gabon. Smithsonian Institution and Shell – Gabon, New York.

Perry, S. F., 1978. Quantitative anatomy of the lungs of the red eared turtle, *Pseudemys scripta elegans*. *Respir Physiol.* **35**: 245 – 262.

Perry, S. F., 1981. Morphometric analysis of the pulmonary structure: methods for evaluation and comparison of unicameral lungs. *Mikroscopie.* **38**: 278 – 293

Perry, S. F., 1988. Functional morphology of the lungs of the Nile crocodile, *Crocodylus niloticus*: Non respiratory parameters. *J Exp Biol.* **134**: 99 – 117.

Perry, S. F., 1989a. Mainstreams in the evolution of vertebrate respiratory structures. In: *Form and Function in Birds, Vol. 4*, King, A.S. and McLelland, J. (Eds.). Academic Press, London.

Perry, S. F., 1989b. Structure and function of the reptilian respiratory system. In: *Comparative Pulmonary Physiology: Current concepts*, Wood, S. C. (Ed.). Marcel Dekker, New York.

Perry, S. F., 1990. Gas exchange strategy in the Nile crocodile: A morphometric study. *J Comp Physiol B*: Biochemical, Systemic, and Environmental Physiology, **159(6)**: 761 – 769.

Perry, S. F., 1998. Lungs: Comparative anatomy, functional morphology and evolution. In: *Biology of Reptilia, Vol. 19, Morphology G: Visceral Organs*. Gans, C. and Gaunt, S. C. (Eds). Society for the study of Amphibians and Reptiles. Ithaca, New York.

Perry, S. F. and Duncker, H. R., 1978. Lung architecture, volume and static mechanical factors in five species of lizards. *Respir Physiol*. **34**: 61 – 81

Perry, S. F. and Duncker, H. R., 1980.Interrelationships of static mechanical factors and anatomical structures in lung evolution. *J Comp Physiol*. **138**: 321 – 334.

Peters, R. H. and Wassenberg, K., 1983. The effect of body size on animal abundance. *Oecologia* (Berlin) **60**: 89-96.

Pettersen, E. F., Goddard, T. D., Huang, C. C., Couch, G. S., Greenblatt, D. M., Meng, E. C. and Ferrin, T. E., 2004. USCF Chimera – a visualization system for exploratory research and analysis. *J Comput Chem*. **25**: 1605 – 1612.

Pooley, A. C., 1962. The Nile crocodile, *Crocodylus niloticus*. Notes on the incubation period and growth rates of juveniles. *Lammergeyer*. **2**: 1 -55.

Pooley, A. C., 1969. Preliminary studies on the breeding of the Nile crocodile, *Crocodylus niloticus*, in Zululand. *Lammergeyer*. **10**: 22 – 24.

Pooley, A. C. 1974a. Parental care in the Nile crocodile: A preliminary report on behaviour in a captive female. Lammergeyer (Pietermaritzburg) **3**: 43-45.

Pooley, A. C. 1974b. How does a baby crocodile get to water? African Wildlife **28(4)**: 8-11.

Pooley, A. C., 1977. Nest opening response of the Nile crocodile, *Crocodylus niloticus. J Zool*. **182**: 17 -26.

Pooley, A. C., (1982). Discoveries of a crocodile man. William Collins Sons and Co. Ltd, Johannesburg.

Pooley, A. C. and Gans, C., 1976. The Nile crocodile. *Sci Am*. **234(4)**: 114-124.

Pooley, A. C., Hines, T. C. and Shield, J., 1989. Attacks on humans. In: *Crocodiles and Alligators*. Ross, C. A., (Ed). Facts on File, Inc., New York.

Powell, F. L., 2000. Respiration. In: *Sturkie's Avian Physiology, fifth edition*. Academic Press, San Diego.

Powell, F. L. and Hopkins, S. R., 2004. Comparitive physiology of lung complexity: Implications for gas exchange. *News Physiol Sci*. **19**: 55 – 60.

Powell, F. L. and Scheid, P., 1989. Physiology of gas exchange in the avian respiratory system. In: *Form and Function in Birds, Vol. 4,* King, A. S. and McLelland, J. (Eds.). Academic Press, London.

Putteril, J. F. and Soley, J. T., 2003. General morphology of the oral cavity of the Nile crocodile, *Crocodylus niloticus* (Laurenti, 1768). I. Palate and gingivae. *Onderstepoort Journal of Vetinary Research*. **70(4)**: 281 – 297.

Putteril, J. F. and Soley, J. T., 2006. Morphology of the gular valve of the Nile crocodile, *Crocodylus niloticus* (Laurenti, 1768). *J Morph*. **267(8)**: 924 – 939.

Rauther, M., 1937. Die Schwimmblase. In: *Handbuch der vergleichenden anatomie der wirbeltiere, Bd III*. Bolk, L., Göppert, E., Kallius, E. and Lubosch, W. (Eds). Urban and Schwarzenberg, Berlin.

Roseman, A. M., 2003. Particle finding in electron micrographs using a fast local correlation algorithm. *Ultramicroscopy*. **94**: 225 – 236.

Roosevelt, T. 1909. African Game Trails. An account of the African wanderings of an American hunter-naturalist. Vols. I-II. Charles Scribner's Sons, New York.

Ross, C. A. and Magnusson, W. E., 1989. Living crocodilians. In: *Crocodiles and Alligators*. Ross, C. A. (Ed.). Facts on File, Inc., New York.

Ross, M. H. and Pawlina, W., 2011. Histology, Text and Atlas 6th Edition. Wolters Kluwer Health; Lippincott, Williams and Wilkins, Baltimore.

Ruben, J. A., Dal Sasso, C., Geist, N. R., Hillenius, W. J., Jones, T. D. and Signore, M., 1999. Pulmonary function and metabolic physiology of theropod dinosaurs. *Science*. **283**: 514 – 516.

Saalfeld, E von, 1934a. Die mechkanik der atmung bei *Uromastix* (Lacertilia). *Pflügers Arch Ges Physiol.* **233**: 431 – 438.

Saalfeld, E von, 1934b. Die nervöse regulierung der atembewegung bei *Uromastix* (Lacertilia). *Pflügers Arch Ges Physiol.* **233**: 439 – 448.

SANS, 2008. South African National Standards. *The care and use of animals for scientific purposes, 1st edition*. SABS Standards Division, Pretoria, South Africa.

Schachner, E. R., Hutchinson, J. R. and Farmer, C. G., 2013. Pulmonary anatomy in the Nile crocodile and the evolution of unidirectional airflow in archosaurian. *Peer J PrePrints*.

Schaeffer, B., 1941. The morphological and functional evolution of the tarsus in amphibians and reptiles. *Bull Am Mus Nat Hist.* **78**: 395 – 472.

Scheid, P., 1979. Mechanisms of gas exchange in bird lungs. *Rev Physiol Biochem Pharmacol*. **86**: 137 – 186.

Scheid, P. and Piiper, J. 1985. Gas exchange in the avian parabronchial lung. In: *Bird flight BIONA Report 3*. Nachtigall, W. (Ed). Gustav Fischer, Stuttgart, New York.

Scheid, P. and Piiper, J., 1989. Respiratory mechanics and airflow in birds. In: *Form and Function in Birds, Vol. 4*, King, A.S. and McLelland, J. (Eds.). Academic Press, London.

Scheid, P., 1990. Avian respiratory system and gas exchange. In: *Hypoxia: The Adaptations*. Sutton, J. R., Coates, G. and Remmers, J. E. (Eds.).BC Decker Inc., Burlington, Ontario.

Scheid, P. and Shams, H., 1995. Höhenflug von Vögeln. *Naturwiss Rdsch*. **48**: 413 – 418.

Scherle, W. S., 1970. A simple method for volumetry of organs in quantitative stereology. *Mikroskopie*. **26**: 57 – 60.

Shine, R. 1988. Parental care in reptiles. In: *Biology of the Reptilia. Ecology B. Defence and Life History. Vol. 16.* Gans, C. and Huey, R. B. (Eds). Alan R. Liss, New York.

Shine, T., Böhme, H., Nickel, D. F. T. and Wilms, T., 2001. Rediscovery of relict populations of Nile crocodile, *Crocodylus niloticus*, in South Eastern Mauritania, with observations on their natural history. *Oryx*. **35**: 260 – 262.

Solomon, S. E. and Purton, M., 1984. The respiratory epithelium of the lung in the green turtle (*Chelonia mydas L.*). *J Anat*. **139(2)**: 353 – 370.

Staton, M. A. and Dixon, J. A., 1975. Studies on the dry season biology of Caiman *crocodilus crocodilus* from the Venezuelan Llanos. *Mem Soc Cienc Nat La Salle*. **35**: 237 – 265.

Staton, M. A., 1978. "Distress Calls" of crocodilians. Whom do they benefit? *Am Nat.* **112**: 327 – 332.

Taplin, L. E., 1984. Evolution and Zoogeopgraphy of eusuchian crocodilians In: *Vertebrate evolution and zoogeography in Australia*. Archer, M. and Clayton, G. (Eds). Hesperian Press, Perth.

Taplin, L. E. and Grigg, G. C., 1989. Historical zoogeography of the eusuchian crocodilians: a physiological perspective. *Am Zool.* **29**: 885 – 901.

Taylor, G. W., 1973. Nile crocodile in the Okavango Delta. A report on a wildlife population for Botswana Game Industries.

Taylor, C. R. and Weibel, E. R., 1981. Design of the mammalian respiratory system. I. Problem and strategy. *Respir Physiol*. **44**: 1 -10.

Tenney, S. M. and Tenney, J. B., 1970. Quantitative morphology of cold blooded lungs: Amphibia and Reptilia. *Respir Physiol.* **9**: 197 – 215.

Tilney, L. G., Derosier, D. J. and Mulroy, M. J., 1980. The organization of actin filaments in the stereocilia of cochlear hair cells. *JCB*. **86(1)**: 244 – 259.

Torday, J. S. Rehan, V. K., Hicks, J. W., Wang, T., Maina, J. N., Weibel, E. R., Hsia, C. C., Sommer, R. J. and Perry, S. F., 2007. Deconvoluting lung evolution: from phenotypes to gene regulatory networks. *Integr Comp Biol*. **47(4)**: 601 – 609.

Toro, A del M., 1969. Breeding the Spectacled Caiman, Caiman *Crocodylus*, at Tuxtla Guttierrez Zoo. *Int Zoo Yb*. **9**: 35 – 36.

Voeltzkow, A., 1893. Ueber Biologie und Embryonalentwickelung der Krokodile. *Sitzber. Akad. Berlin.* **1893**: 347 – 353.

Wagner, G., 1998. Complexity matters. *Science*. **279**: 1158 – 1159.

Walker, A. D., 1972. New light on the origin of birds and crocodiles. *Nature*. **237**: 257 – 263.

Wallace, K. M. and Leslie, A. J., 2008. Diet of the Crocodile (*Crocodylus niloticus*) in the Okavango Delta, Botswana. *J Herpetol*. **42**: 361 – 368.

Walls, G. L., 1942. *The vertebrate eye*. Cranbrook Institute of Science, Bllomfield Hills, Michigan.

Webb, G. J. W. and Gans, C., 1982. Galloping in *Crocodylus johnstoni,* a reflection of terrestrial activity. *Rec Austr Mus*. **34**: 607 – 618.

Weibel, E.R., 1979. *Stereological Methods, Vol. 1: Practical Methods for Biological Morphometry*. Academic Press, London.

Weibel, E. R. 2000. Symmorphosis. *On form and function in shaping life*. Harvard University Press, London, England.

Whitfield, A. K. and Blaber, S. J. M., 1979. Predation on Striped Mullet (Mugel *cephalus*) by *Crocodilus niloticus* at St. Lucia, South Africa. *Copeia*. **2**: 266 – 269.

Woodward, J. D. and Maina, J. N., 2008. Study of the structure of the air and blood capillaries of the gas exchange tissue of the avian lung by serial section three-dimensional reconstruction. *J Microsc*. **230**: 84 – 93.

Wright, J. C. and Kirshner, D. S., 1987. Allometry of lung volume during voluntary submergence in the saltwater crocodile *Crocodylus porosus*. *J Exp Biol.* **130**: 433 – 436.

Zug, G., 1974. Crocodilian galloping, a unique gait for reptiles. *Copeia.* **1974**: 550 – 552.

# Appendix A

## 6. Preparation of Solutions and Buffers

### 0.1M Sodium Phosphate buffer (pH 7.4)

| | |
|---|---|
| Phosphate buffer Part A = 15.6g/l | 0.1M $NaH_2PO_4$ (ACE, Southdale, Gauteng, South Africa) |
| Phosphate buffer Part B = 14.2g/l | 0.1M $Na_2HPO_4$ (ACE, Southdale, Gauteng, South Africa) |

| | |
|---|---|
| 140ml | Phosphate buffer Part A |
| 360ml | Phospahte buffer Part B |
| To 500ml | Distilled water |

### 2.5% Glutaraldehyde

| | |
|---|---|
| 10ml | 25% Glutaraldehyde (Merck KGaA, Damstadt, Germany) |
| To 100ml | 0.1M Sodium phosphate buffer (pH 7.4) |

### Haematoxylin (Mayer's)

| | |
|---|---|
| 1g | Haematoxylin (Merck KGaA, Damstadt, Germany) |
| 0.2g | Sodium Iodate (BDH chemicals LTD, Poole, England) |
| 50g | Potassium Alum (Merck KGaA, Damstadt, Germany) |
| 20ml | Glacial Acetic Acid |
| To 1000ml | Distilled water |

**Eosin (Working Solution)**

| | |
|---|---|
| 250ml | Eosin Y Stock Solution (Merck KGaA, Damstadt, Germany) |
| 750ml | 80% Alcohol |
| 5ml | Glacial Acetic Acid |

**Method of Staining, Haematoxylin and Eosin (H&E)**

Dewax slides in two changes of xylene (2 x 10 minutes).

Pass through a change of 100 %, 95% and 70% alcohol (5 minutes each).

Run slides in gently running water.

Stain in Haematoxylin for 5 minutes. Wash slides in gently running water to “blue”.

**If necessary differentiate by dipping slides 2 -3 times in 1% Acid Alcohol**

Counter stain in Eosin for a minute.

Wash slides in gently running water to wash out excess eosin.

Pass slides through an ascending series of alcohols, 70%, 95% and 100% (10 dips in each).

Then pass slides to two changes of xylene (2 x 10 minutes).

Coverslip slides and store in slide boxes.

**1% Aqueous Osmium Tetroxide**

| | |
|---|---|
| 2ml | 4% Osmium tetroxide (Agar Scientific Ltd., Essex, England) |
| 6ml | 0.1M Sodium phosphate buffer |

**Embed 812 Araldite Resin**

| | |
|---|---|
| 25ml | Embed 812 (Electron Microscopy Sciences, Hatfield, Pennsylvania, USA) |
| 15ml | Araldite 502 (Electron Microscopy Sciences, Hatfield, Pennsylvania, USA) |
| 55ml | DDSA (Electron Microscopy Sciences, Hatfield, Pennsylvania, USA) |
| 1.5ml | DMP – 30 (Electron Microscopy Sciences, Hatfield, Pennsylvania, USA) |

**Toluidine blue and Pyronin Y solution**

| | |
|---|---|
| 1g | Sodium borate (Saarchem Merck Chemicals, Gauteng, South Africa) |
| 100ml | Distilled water |

| | | |
|---|---|---|
| Solution A: | 1g | Pyronin Y (Spi-Chem, West Chester, Pennsylvania, USA) |
| | 100ml | Distilled water |
| Solution B: | 1g | Toluidine blue (Spi-Chem, West Chester, Pennsylvania, USA) |
| | 100ml | 1% Sodium borate |

Mix 1 part Solution A with 4 parts of Solution B.

**Filter before use**

**5% Aqueous Uranyl acetate**

| | |
|---|---|
| 5g | Uranyl acetate (Electron Microscopy Sciences, Hatfield, Pennsylvania, USA) |
| 100ml | Double distilled water |
| 1 Drop | 100% ethanol (to preserve solution) |

Stored in a light resistant tight tube at 4$^{o}$C

**1% Aqueous Lead citrate**

| | |
|---|---|
| 0.66g | Lead nitrate (Electron Microscopy Sciences, Hatfield, Pennsylvania, USA) |
| 0.88g | Sodium citrate (ACE, Southdale, Gauteng, South Africa) |
| 15ml | Boiled distilled water |

Stored at 4$^{o}$C

**Phosphate Buffer Saline (PBS) (pH 7.4)**

| | |
|---|---|
| 8g | NaCl (ACE, Southdale, Gauteng, South Africa) |
| 1.15g | $Na_2HPO_4$ (ACE, Southdale, Gauteng, South Africa) |
| 0.2g | KCl (ACE, Southdale, Gauteng, South Africa) |
| 0.2g | $KH_2PO_4$ (Saarchem (Pty) LTD, Johannesburg, South Africa) |
| To 1000ml | Distilled water |

**0.1% Bovine Serum Albumin (BSA)/PBS**

| | |
|---|---|
| 2g | Bovine Serum Albumin (BSA) (Sigma-Aldrich, St Louis, Missouri, USA) |
| 2000ml | Phosphate buffer saline (PBS) |

**Stir on a magnetic stirrer until completely dissolved.**

**0.1% Triton® X – 100 in 0.1% BSA/PBS**

| | |
|---|---|
| 50µl | Triton ® X – 100 (Sigma-Aldrich Chemie, GmbH, Germany) |
| 50ml | 0.1% BSA/PBS |

**2.5% Phalloidin, Alexa Flour® 488 conjugate in 0.1% BSA/PBS Staining Solution**

| | |
|---|---|
| 25µl | Phalloidin, Alexa Fluor® 488 conjugate (Cambrex Bio Science Walkersville Inc, Walkersville, Maryland, USA) in 1000µl PBS |
| 1000µl | 0.1% BSA / PBS |

# Appendix B

## 7. Equipment and Software Used

### 7.1. Euthanasia, Intratracheal Instillation and Latex Casting

- **Casting Apparatus**

Cannula, Disposable Syringes, Unit with independent valves.

### 7.2. Volume Determination

- **Weigh Balance**

Adams PGW 753e weigh balance (Adams equipment, Kempton Park, South Africa)

### 7.3. Morphology

#### 7.3.1. Gross Morphology

- **Camera**

Canon EOS 400D (Canon, Japan)

- **Camera Lens**

Canon 70 – 300mm lens

- **Camera Flash**

Canon Ring Flash (Canon, Japan)

## 7.3.2. Light Microscopy

**Processing and Sectioning of the Sampled Lung Tissue**

- **Automated Tissue Processor**

Shanon Citadel ™ 1000 automated tissue processor (Thermo Scientific, USA)

- **Embedding Console**

Miles Scientific Tissue Tec® Cryo-console (Miles Scientific, Princeton, Minnesota, USA)

- **Microtome**

Leica 2035 Biocut rotary microtome (Leica Instruments GmbH, Germany)

- **Microtome Blades**

Feather S35 disposable microtome blades (FEATHER Safety Razor Co., Ltd, Japan)

- **Light Microscope**

Zeiss Montagesatz T-UL research microscope (Zeiss Instruments, Jena, Germany)

- **Photographic Microscope**

Zeiss AXIOSKOP 2 plus microscope (Zeiss Instruments, Jena, Germany).

Zeiss AxioCam HRc, Carl Zeiss, Oberkochen, Germany

- **Photographic Microscope Image Rendering and Analysis Software**

AxioVision software 40 Version 4.8.0.0 (Carl Zeiss Imaging Solution GmbH, Carl Zeiss, Oberkochen, Germany)

## 7.3.3. Scanning Electron Microscopy

**Critical Point Drying**

- **Critical Point Drier**

Hitachi HCP – 2 – critical point drier (Hitachi, Tokyo, Japan)

**Mounting, Sputter Coating and Viewing of Samples**

- **Dissecting Microscope**

Leica Wild M3B dissecting microscope (Leica, Heerbrugg, Switzerland)

- **Sputter Coater**

EMITECH K550 X (Emitech Ltd., Kent, England)

- **Scanning Electron Microscopes**

FEI QUANTA 400 E SEM (FEI Company, USA)

ZEISS, FIB / SEM cross beam, Auriga (Zeiss, Oberkoden, Germany)

### 7.3.4. Transmission Electron Microscopy

- **Resin Oven**

Memmert 854 resin oven (Memmert, Schwabach, West Germany)

- **Ultra-microtome**

Leica Ultracut UCT ultra-microtome (Leica Microsystems, Bannockburn, Illinois, USA)

- **Glass Knife Maker**

LKB knife maker Type7801A (LKB produkter, Stockholm, Sweden)

- **Transmission Electron Microscope**

Jeol JEM – 100S transmission electron microscope (Jeol, Tokyo, Japan)

### 7.3.5. Confocal Microscopy

**Confocal Microscope**

Zeiss LSM 780 confocal microscope (Zeiss, Heidelberg, Germany)

### 7.3.6. Dimensional Serial Section Computer Reconstruction

- **Photographic Microscope**

Zeiss AXIOSKOP 2 plus microscope (Zeiss Instruments, Jena, Germany).

Zeiss AxioCam HRc, Carl Zeiss, Oberkochen, Germany

- **Photographic Microscope Image Rendering and Analysis Software**

AxioVision software 40 Version 4.8.0.0 (Carl Zeiss Imaging Solution GmbH, Carl Zeiss, Oberkochen, Germany)

- **Graphic Software**

Adobe Photoshop® CS5, Version 12.1 x64 (1990 – 2011, Adobe Systems Incorporated)

IrfanView, Version 4.20 (1996 – 2008, Irfan Skiljan©)

Spider, Version UNIX 17.05 (Spider © Health Research Inc., Albany, New York)

BOXER (1999, Boxer©, Steve Ludke)

UCSF Chimera package (Resource for Biocomputing, Visualization and Informatics at the University of California supported by NIH P41 RR-01081), Version 1.3 (build2577) (2000 – 2008, Regents of the University of California©)

- **Computer and Operating System**

Intel® Duo™ 2 Core processor, CPU E8400 with 2GB RAM at 3.00 GHz (Model No: Hp Compaq dx 7400 Microtower)

Ubuntu Linux Version. 8.10 operating system (open source license)

## 7.4. Morphometry

**Techniques, Parameters and Processes**

- **Microscope**

Zeiss Montagesatz T-UL research microscope (Zeiss Instruments, Jena, Germany)

- **Graticule and Eye Piece**

100 point quadratic lattice integrating graticule (Zeiss Instruments, Jena, Germany)

Interchangeable graticule holder eye piece (Zeiss Instruments, Jena, Germany)

- **Software**

Microsoft Excel 2010 (2011, Microsoft Corporation ©)

JMP® 10.0.0 (2012, SAS Institute Inc. ©)

# Appendix C

## 8. Scanning Electron Microscopy Pilot Study

### 8.1. The "O method"

This method is a traditional processing methodology and the protocol that is used is from Murphy *et al*. (1990). Samples were incubated, at room temperature, in a 1% aqueous osmium tetroxide (Agar Scientific Ltd., Essex, England) solution (Appendix A) for an hour. This was followed by 5 washes with double distilled water ($ddH_2O$) over 10 minutes. For ease of comparison to the other method, this method of infiltration is referred to as termed the **"O method"**.

### 8.2. The "OTO method"

This method is adapted from Kelly *et al*. (1973). The first step of the OTO method was the same as the O method tissue preparation. Following this, samples were incubated, at room temperature, in a 1% aqueous osmium tetroxide (Agar Scientific Ltd., Essex, England) solution (Appendix A) for an hour. This was followed by 5 washes with double distilled water ($ddH_2O$) over 10 minutes. Following this, the samples were incubated (at normal room temperature) in a 1% aqueous thiosemicarbazide (The British Drug Houses Ltd., Poole, England) solution (Appendix A) for 10 minutes. This was followed by a further 5 washes of the samples with $ddH_2O$ over 10 minutes. The samples were incubated (at room temperature) in a 1% osmium tetroxide aqueous solution (Agar Scientific Ltd., Essex, England) (Appendix A) and washed in $ddH_2O$, as in the first step of this method. This method of tissue preparation is called the **"OTO method"** (Kelley *et al.,* 1973).

## 8.3. Critical Point Drying

When using the CPD method for drying, the samples in the critical point drier [Hitachi HCP – 2 – critical point drier (Hitachi, Tokyo, Japan)] chamber were flooded with liquid carbon dioxide (Afrox, Johannesburg, South Africa) at $5^{o}$ C. The critical point drier chamber was flushed until there was no evidence of any ethanol at the exhaust valve. The temperature of the liquid carbon dioxide was raised to above its critical point ($31^{0}$ C) and stopped at $42^{o}$ C. The dried specimens were then returned to atmospheric pressure by exhausting the carbon dioxide gas while maintaining a temperature of $32^{o}$ C or above so as to prevent any condensation.

## 8.4. Chemical Drying using Hexamethyldisilazane (HMDS)

For drying using the HMDS method, the samples were immersed in 100% HMDS (Sigma-Aldrich CHEMIE, GmbH, Germany) for 3 minutes and quickly removed to a desiccator containing silica gel for 24 hours to allow for further drying and to prevent water contamination

Figure 4.1: An organogram summarising the processing of samples by the respective infiltration and drying techniques.

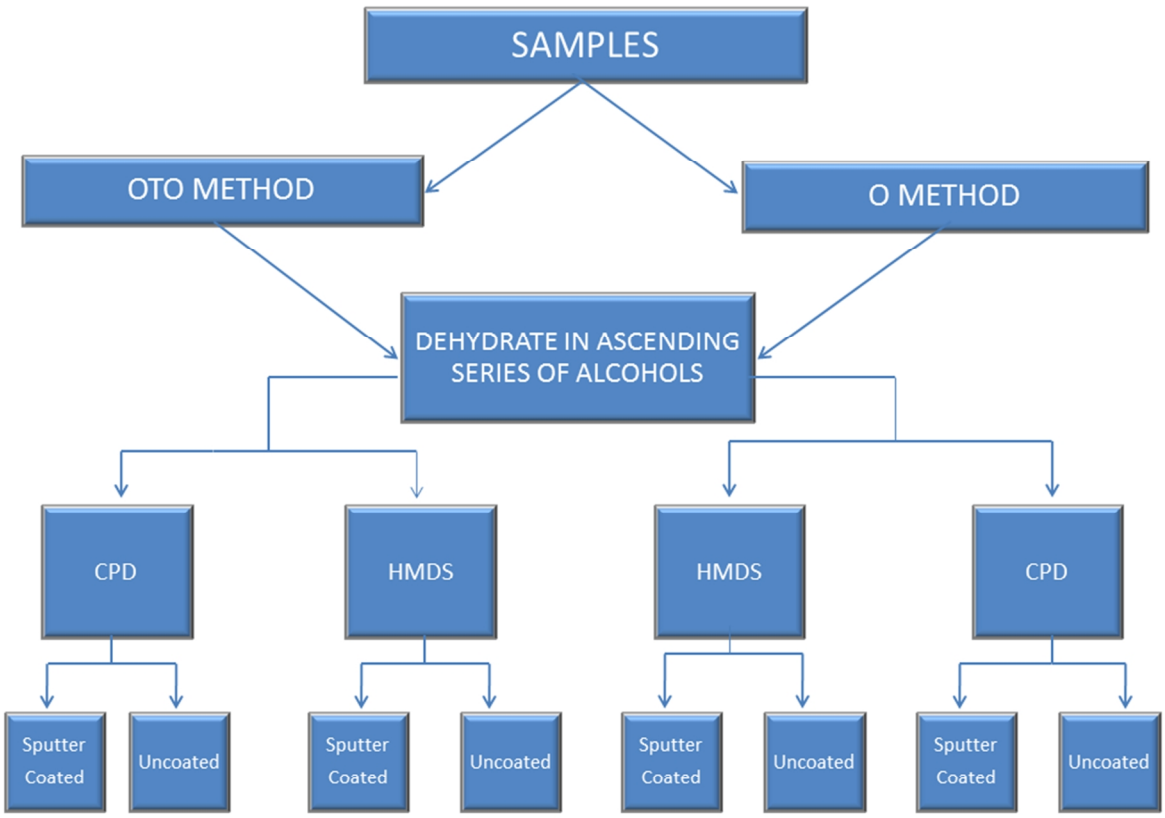
SAMPLES
OTO METHOD
O METHOD
DEHYDRATE IN ASCENDING SERIES OF ALCOHOLS
CPD
HMDS
HMDS
CPD
Sputter Coated
Uncoated
Sputter Coated
Uncoated
Sputter Coated
Uncoated
Sputter Coated
Uncoated

## 8.5. Mounting, Sputter Coating and Viewing of Samples

Following the drying procedures, the samples were mounted onto aluminium stubs under a Leica Wild M3B dissecting microscope (Leica, Heerbrugg, Switzerland) using double sided carbon tape. All the samples were sputter coated with gold palladium using an EMITECH K550 X (Emitech Ltd., Kent, England) sputter coater to a thickness of 15nm. The samples were then examined and photographed using a FEI QUANTA 400 E SEM (FEI Company, USA).

## 8.6. Results of the Pilot Study

When comparing CPD and HMDS dried samples prepared using the O method, it is observed that the HMDS dried samples preserve more surface detail than the CPD dried samples. Furthermore, the HMDS dried samples do not charge as much as the CPD dried specimens when viewed in the SEM.

All the samples prepared using the OTO method illustrated an excellent preservation of surface morphology. The OTO prepared samples dried either by CPD or HMDS exhibited no / minimal charging. Additionally, they did not appear as brittle (gross view of specimen) as the samples prepared using the O method.

The HMDS samples prepared using the OTO sample preparation method showed good preservation of the sample. Furthermore, these samples could be viewed at various depths without any charging (Figure 4.2 A).

When evaluating CPD and HMDS dried samples prepared using the OTO method, it is evident that both drying techniques preserve the sample well but the HMDS prepared samples, have a greater degree of surface detail preservation.

Altogether, samples that were prepared by the OTO method, dried with HMDS and sputter coated yielded the best results. This conclusion was reached due to the fact that samples did not charge and exhibited greater surface detail than the rest of the viewed samples (Figure 4.2 B). In addition, tensegrity of samples were maintained which allowed for clear depth perception (Figure 4.2 A and B). Those samples prepared using the O method and dried via CPD produced the worst results from all the tested methods. This was attributed to the high levels of charging and comparatively poor preservation of surface detail.

Due to the results obtained from the pilot study the sampled tissue was prepared using the OTO method, dried using HMDS and sputter coated to view on the scanning electron microscope.

Figure 4.2 A: A micrograph illustrating the arrangement of faveoli along a large tubular airway. The perception of depth is clear along the entire length of the airway. These samples of crocodilian lung were prepared using the OTO method, dried via HMDS and sputter coated. F = Faveolus, White Arrows = Secondary septa.

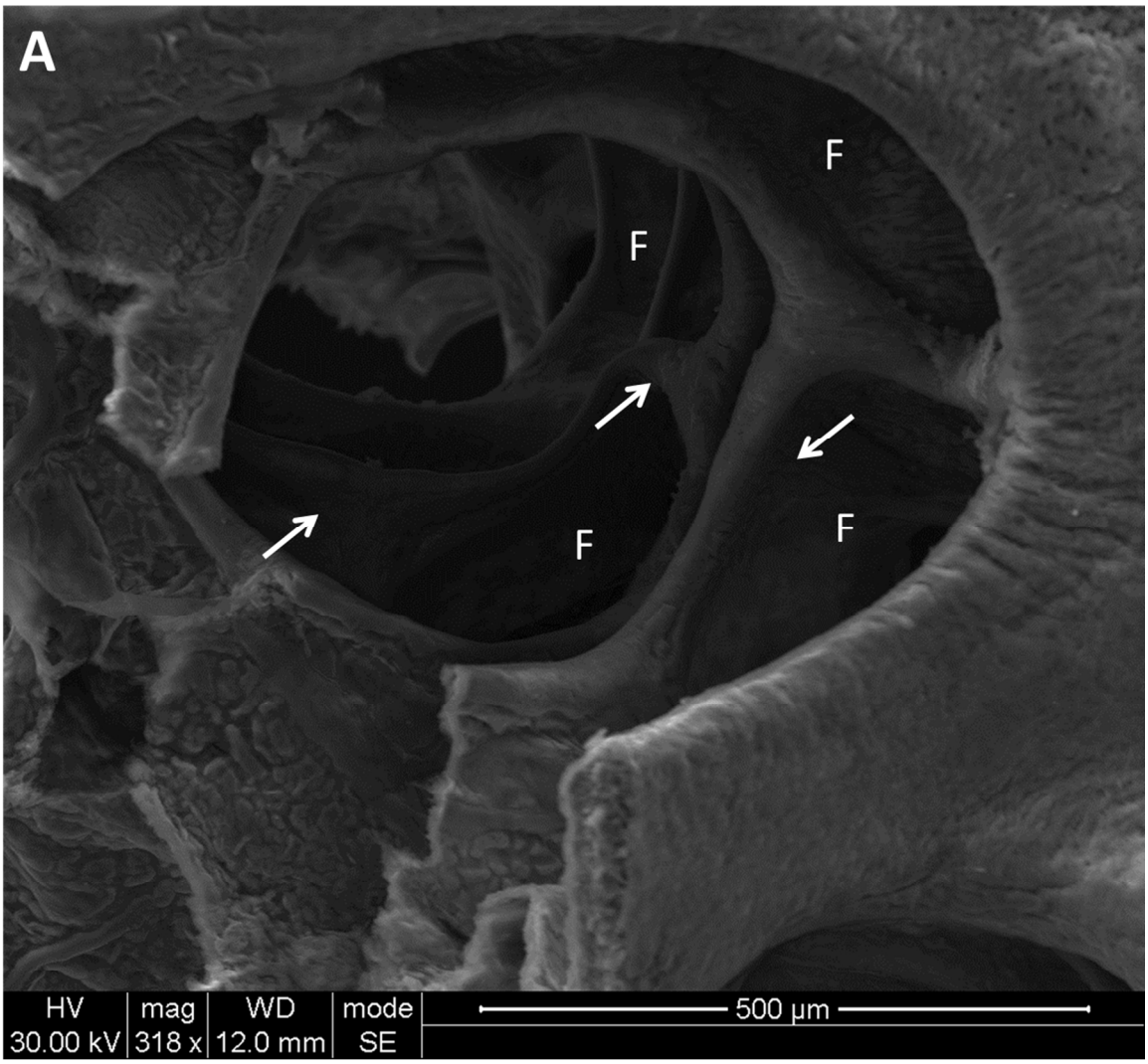
A
F
F
F
F
HV
30.00 kV
mag
318 x
WD
12.0 mm
mode
SE
500 µm

Figure 4.2 B: A high magnification micrograph of a secondary septum, dividing the parenchyma of a crocodilian lung. The sample was prepared in the same manner as Figure 4.2 A

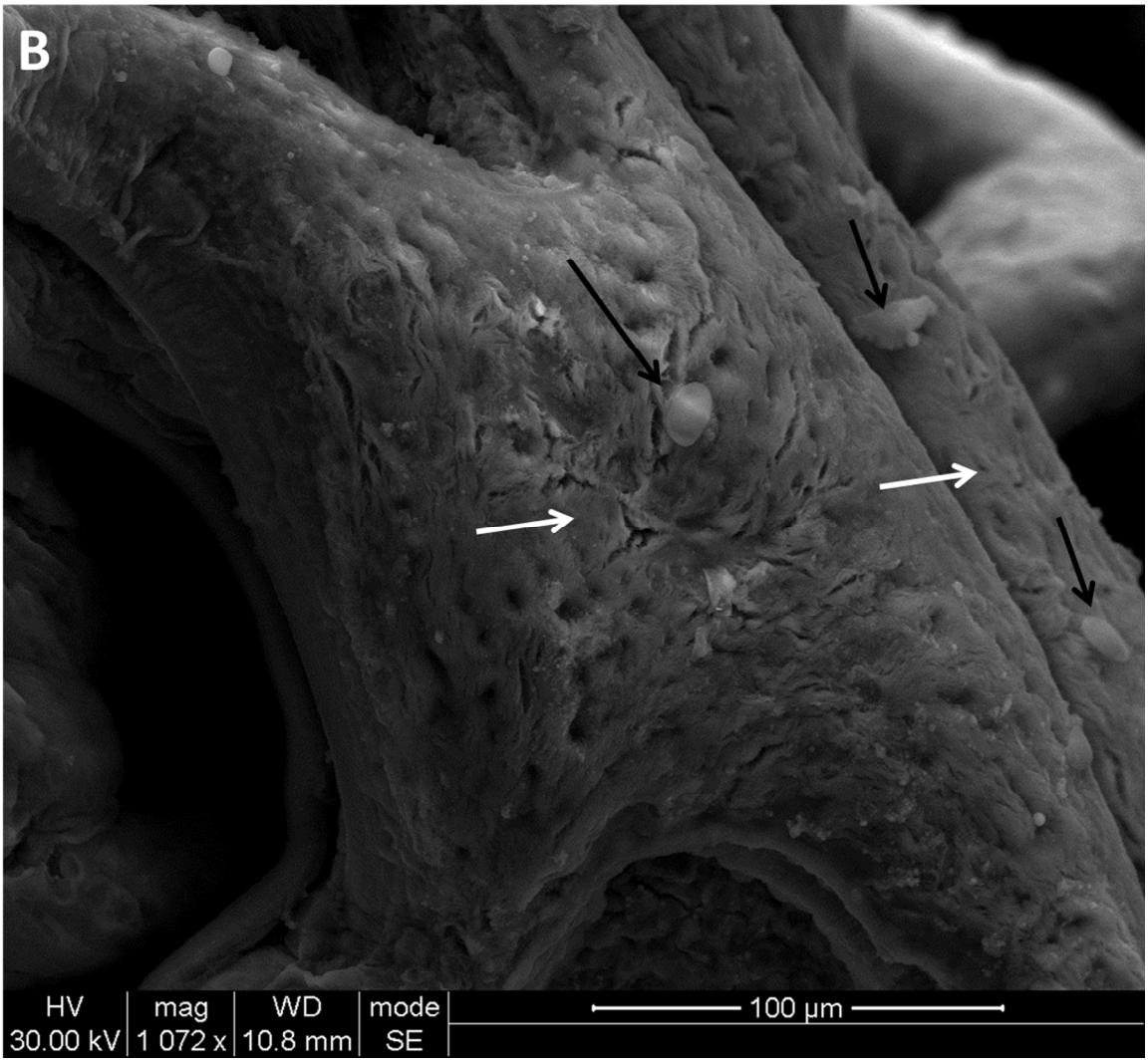
B
HV
30.00 kV
mag
1 072 x
WD
10.8 mm
mode
SE
100 µm

## 9. 3 Dimensional Serial Section Computer Reconstruction Algorithms

A calculated set of algorithms used to create the 3 dimensional reconstructions are as follows. They are to be done sequentially and run in a terminal window.

9.1.File format conversion

All picture files must be converted into a *. RAW file format.

2.2. Convert to Spider

This algorithm converts *. RAW files into a file format (*. SPI) that allows for accurate cross correlation. The script of the algorithm is as follows:

*x10=11*
*x11=1388*
*x12=1040;*
*x10 is the number of images ;*
*x11 is the width;*
*x12 is height;*
*do lb1 x55=1, x10*
*cp from raw*
*5times_lowest_res_{****x55}.raw ;*
*change name! (8) (x11,x12) (0) image{****x55} lb1*

9.2.Boxer

Boxer is opened in a new terminal and the first image in the newly created file format (*.SPI) is opened. The dimensions of the image are then set and saved. The file is in a stack and is converted to a single file by means of the following command in a terminal window: *proc2d windowed0001.spi windowed0001.spi spider-single.*

9.3. Pad Boxed Area to be Reconstructed

This algorithm is run on the single stack image created in 2.2. It is used to define the area of reconstruction removing any “noise”.

The script of the algorithm is as follows:

```
pd
windowed0001 ;Name of boxed area of interest, single stack file
padded_aligned001 ;
(1388,1040) ;original image dimensions
b
(495,321) ; This is the coordinate of the top left corner
```

9.4. Align Images Of Area to be Reconstructed

With the use of this algorithm all the cross correlation images are aligned to one another for a reconstructed volume to be created. The script of the algorithm is as follows:

```
; perfect.jer;
; define dimensions:;
x20=400 ;length of reconstructed volume (also number of images) (123)
x21=1388 ;width of images (200)
x22=1040 ;height of images (200)
x23=-15 ;greatest rotation in negative range (multiple of 1)
x24=31  ;number of 1 degree increments
x25=199  ;half the reconstructed volume length (minus 1);
do lb1 x50=2,x20 ;loop through each image
do lb2 x51=1,x24 ;loop through each angle
x78=x50-1 ;template number;
rt
image{****x50}
rotate{***x51}
x23+(x51*1)-1
;
; normalised cross-correlation
cc n
rotate{***x51}
padded_aligned{***x78}
ccn{***x51}
;
;find highest correlating angle and displacement
pk m x11,x12,x13,x14,x15 ;x15: max, x11: x, x12: y
ccn{***x51}
(1,1)
;
sd x51,x11,x12,x13,x14,x15,x51; save coordinates and coefficients in document
document{***x50}
lb2
;
;apply angle and displacement
doc sort ;sort coefficients from small to big
document{***x50}
```

```
sorted_doc{***x50}
(5)
y
;
ud x24,x70,x71,x13,x14,x15,x16
sorted_doc{***x50}
;rotate image
rt
image{****x50}
rotated
x23+(x16*1)-1
;
;window image
wi
rotated
lekker{***x50}
(400 400) ;the new image dimensions
x70-x25,x71-x25
;
;pad image
pd
lekker{***x50}
padded_aligned{***x50}
x21,x22
b
(495,321); This is the coordinate of the top left corner
;
lb1
;
de a
document001
;
de a
sorted_doc001
```

9.5.Create Volumes from the Aligned Images

The 3 Dimensional volumes of the interfaveolar septa and airways are then constructed from the aligned images. It is done via the following algorithm with the following script:

```
;NORMALISE FILES TO COMMON AVE AND STD, filter and decimate
;msd=0,1
X10=0
X11=1

;x10 = ave
;x11 = sd

FS x30,x31,x32,x33,x34
```

```
volume
x34=x6
if (x6.ne.0) goto lb3
x34=1
lb3
X12=X33
X13=X11/X34
AR
volume
_6
((P1-X12)*X13)
;
fq
_6
volumecorrect
3
0.2 ;filter radius  ;
dc s ;decimate the volume
volumecorrect
volumecorrect_small
2,2                    ;
2                      ;
;
pd ;pad the volume up
volumecorrect_small
trans_2
202,202,8 ; new volume dimensions, old dimensions + 2
y
2,2,2 ; top left coordinates!;
ar
trans_2
trans_2_interfaveolar septa
P1*(-1)

RE
```

The two volume files trans_ 2.spi and trans_ 2_interfaveolar septa can then be opened in USCF Chimera (Resource for Biocomputing, Visualization and Informatics at the University of California supported by NIH P41 RR-01081), Version 1.3 (build 5277) (Regents of the University of California©) and viewed separately or together.

# Appendix D

## Anova Summary Tables for Morphometry

Table 4.1: Analysis of variance summary table for the $Vv_{par}$ of the dorsal cranial region of all age group categories.

| Source | Degrees of Freedom | Sum of Squares | Mean Square | F Ratio | Prob > F |
|---|---|---|---|---|---|
| | 3 | 898.27 | 299.423 | 1.3482 | 0.2579 |
| Error | 530 | 117705.88 | 222.087 | | |
| C. Total | 533 | 118604.15 | | | |

Table 4.2: Analysis of variance summary table for the $Vv_{non\text{-}par}$ of the dorsal cranial region of all age group categories.

| Source | Degrees of Freedom | Sum of Squares | Mean Square | F Ratio | Prob > F |
|---|---|---|---|---|---|
| | 3 | 898.27 | 299.423 | 1.3482 | 0.2579 |
| Error | 530 | 117705.88 | 222.087 | | |
| C. Total | 533 | 118604.15 | | | |

Table 4.3: Analysis of variance summary table for the $Vv_{par}$ of the dorsal middle region of all age group categories.

| Source | Degrees of Freedom | Sum of Squares | Mean Square | F Ratio | Prob > F |
|---|---|---|---|---|---|
| | 3 | 641.516 | 213.839 | 1.5569 | 0.1986 |
| Error | 693 | 95185.6 | 137.353 | | |
| C. Total | 696 | 95827.116 | | | |

Table 4.4: Analysis of variance summary table for the $Vv_{non\text{-}par}$ of the dorsal middle region of all age group categories.

| Source | Degrees of Freedom | Sum of Squares | Mean Square | F Ratio | Prob > F |
|---|---|---|---|---|---|
| | 3 | 641.516 | 213.839 | 1.5569 | 0.1986 |
| Error | 693 | 95185.6 | 137.353 | | |
| C. Total | 696 | 95827.116 | | | |

Table 4.5: Analysis of variance summary table for the $Vv_{par}$ of the dorsal caudal region of all age group categories.

| Source | Degrees of Freedom | Sum of Squares | Mean Square | F Ratio | Prob > F |
|---|---|---|---|---|---|
| | 3 | 1322.37 | 440.788 | 2.5493 | 0.0546 |
| Error | 832 | 143859.07 | 172.908 | | |
| C. Total | 835 | 145181.44 | | | |

Table 4.6: Analysis of variance summary table for the $Vv_{non\text{-}par}$ of dorsal caudal region of all age group categories.

| Source | Degrees of Freedom | Sum of Squares | Mean Square | F Ratio | Prob > F |
|---|---|---|---|---|---|
| | 3 | 1322.37 | 440.788 | 2.5493 | 0.0546 |
| Error | 832 | 143859.07 | 172.908 | | |
| C. Total | 835 | 145181.44 | | | |

Table 4.7: Analysis of variance summary table for the $Vv_{par}$ of the ventral cranial regions of all age group categories.

| Source | Degrees of Freedom | Sum of Squares | Mean Square | F Ratio | Prob > F |
|---|---|---|---|---|---|
| | 3 | 1073.73 | 357.91 | 1.3983 | 0.2422 |
| Error | 620 | 158691.33 | 255.954 | | |
| C. Total | 623 | 159765.06 | | | |

Table 4.8: Analysis of variance summary table for the $Vv_{non\text{-}par}$ of the ventral cranial regions of all age group categories.

| Source | Degrees of Freedom | Sum of Squares | Mean Square | F Ratio | Prob > F |
|---|---|---|---|---|---|
| | 3 | 1073.73 | 357.91 | 1.3983 | 0.2422 |
| Error | 620 | 158691.33 | 255.954 | | |
| C. Total | 623 | 159765.06 | | | |

Table 4.9: Analysis of variance summary table for the $Vv_{par}$ of the ventral middle regions of all age group categories.

| Source | Degrees of Freedom | Sum of Squares | Mean Square | F Ratio | Prob > F |
|---|---|---|---|---|---|
| | 3 | 1462.587 | 487.529 | 2.9793 | 0.0311 |
| Error | 501 | 81983.889 | 163.64 | | |
| C. Total | 504 | 83446.476 | | | |

Table 4.10: Analysis of variance summary table for the $Vv_{non\text{-}par}$ of the ventral middle regions of all age group categories.

| Source | Degrees of Freedom | Sum of Squares | Mean Square | F Ratio | Prob > F |
|---|---|---|---|---|---|
| | 3 | 1462.587 | 487.529 | 2.9793 | 0.0311 |
| Error | 501 | 81983.889 | 163.64 | | |
| C. Total | 504 | 83446.476 | | | |

Table 4.11: Analysis of variance summary table for the $Vv_{par}$ of the ventral caudal regions of all age group categories.

| Source | Degrees of Freedom | Sum of Squares | Mean Square | F Ratio | Prob > F |
|---|---|---|---|---|---|
| | 3 | 836.7 | 278.9 | 1.4758 | 0.2199 |
| Error | 685 | 129455.87 | 188.987 | | |
| C. Total | 688 | 130292.57 | | | |

Table 4.12: Analysis of variance summary table for the $Vv_{non\text{-}par}$ of the ventral caudal regions of all age group categories.

| Source | Degrees of Freedom | Sum of Squares | Mean Square | F Ratio | Prob > F |
|---|---|---|---|---|---|
| | 3 | 836.7 | 278.9 | 1.4758 | 0.2199 |
| Error | 685 | 129455.87 | 188.987 | | |
| C. Total | 688 | 130292.57 | | | |